frontiers | Research Topics

Bone cell differentiation in health and disease

Edited by
Chandi C. Mandal and Michaela Tencerova

Published in
Frontiers in Endocrinology

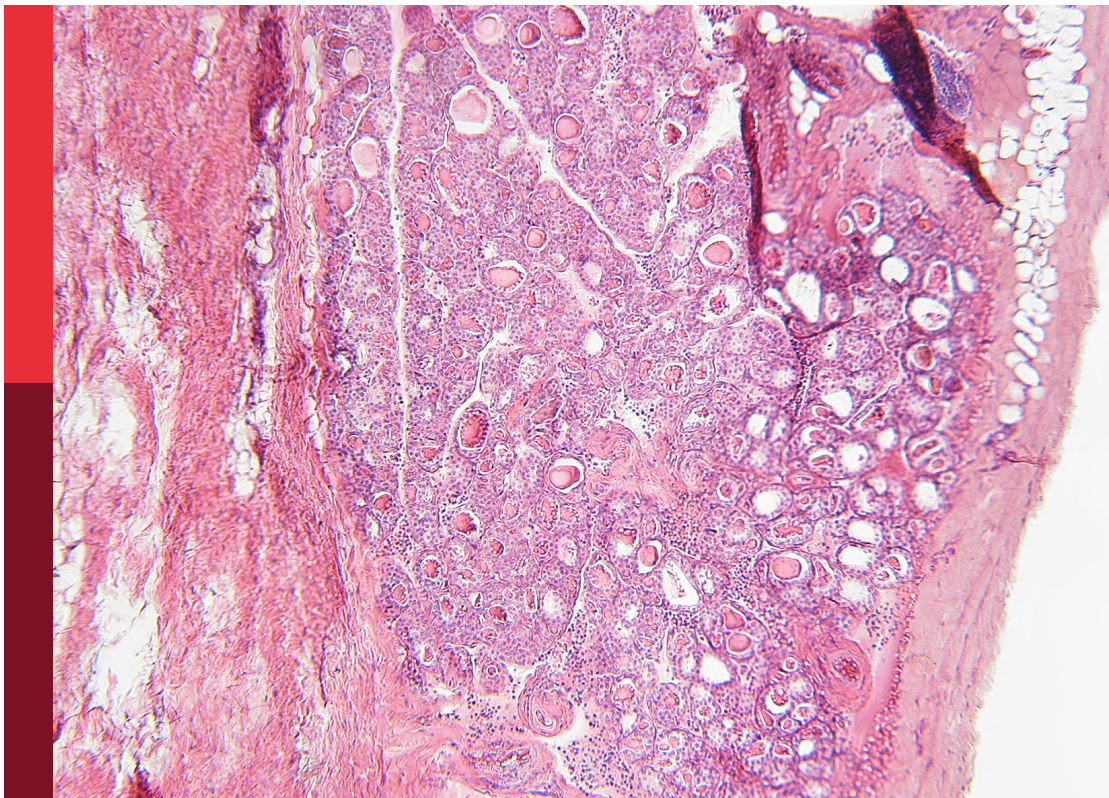

ISSN 1664-8714
ISBN 978-2-83251-192-3
DOI 10.3389/978-2-83251-192-3

About Frontiers

Frontiers is more than just an open access publisher of scholarly articles: it is a pioneering approach to the world of academia, radically improving the way scholarly research is managed. The grand vision of Frontiers is a world where all people have an equal opportunity to seek, share and generate knowledge. Frontiers provides immediate and permanent online open access to all its publications, but this alone is not enough to realize our grand goals.

Frontiers journal series

The Frontiers journal series is a multi-tier and interdisciplinary set of open-access, online journals, promising a paradigm shift from the current review, selection and dissemination processes in academic publishing. All Frontiers journals are driven by researchers for researchers; therefore, they constitute a service to the scholarly community. At the same time, the *Frontiers journal series* operates on a revolutionary invention, the tiered publishing system, initially addressing specific communities of scholars, and gradually climbing up to broader public understanding, thus serving the interests of the lay society, too.

Dedication to quality

Each Frontiers article is a landmark of the highest quality, thanks to genuinely collaborative interactions between authors and review editors, who include some of the world's best academicians. Research must be certified by peers before entering a stream of knowledge that may eventually reach the public - and shape society; therefore, Frontiers only applies the most rigorous and unbiased reviews. Frontiers revolutionizes research publishing by freely delivering the most outstanding research, evaluated with no bias from both the academic and social point of view. By applying the most advanced information technologies, Frontiers is catapulting scholarly publishing into a new generation.

What are Frontiers Research Topics?

Frontiers Research Topics are very popular trademarks of the *Frontiers journals series*: they are collections of at least ten articles, all centered on a particular subject. With their unique mix of varied contributions from Original Research to Review Articles, Frontiers Research Topics unify the most influential researchers, the latest key findings and historical advances in a hot research area.

Find out more on how to host your own Frontiers Research Topic or contribute to one as an author by contacting the Frontiers editorial office: frontiersin.org/about/contact

Bone cell differentiation in health and disease

Topic editors

Chandi C. Mandal — Central University of Rajasthan, India

Michaela Tencerova — Institute of Physiology, Academy of Sciences of the Czech Republic (ASCR), Czechia

Citation

Mandal, C. C., Tencerova, M., eds. (2023). *Bone cell differentiation in health and disease*. Lausanne: Frontiers Media SA. doi: 10.3389/978-2-83251-192-3

Table of contents

frontiers | Frontiers in Endocrinology

TYPE Editorial
PUBLISHED 16 December 2022
DOI 10.3389/fendo.2022.1115444

OPEN ACCESS

EDITED AND REVIEWED BY
Jonathan H. Tobias,
University of Bristol,
United Kingdom

*CORRESPONDENCE
Chandi C. Mandal
chandicmandal@gmail.com
Michaela Tencerova
michaela.tencerova@fgu.cas.cz

SPECIALTY SECTION
This article was submitted to Bone Research, a section of the journal Frontiers in Endocrinology

RECEIVED 04 December 2022
ACCEPTED 08 December 2022
PUBLISHED 16 December 2022

CITATION
Tencerova M and Mandal CC (2022) Editorial: Bone cell differentiation in health and disease.
Front. Endocrinol. 13:1115444.
doi: 10.3389/fendo.2022.1115444

Editorial: Bone cell differentiation in health and disease

Michaela Tencerova[1]* and Chandi C. Mandal[2]*

[1]Laboratory of Molecular Physiology of Bone, Institute of Physiology of the Czech Academy of Sciences, Prague, Czechia, [2]Department of Biochemistry, School of Life Sciences, Central University of Rajasthan, Ajmer, India

KEYWORDS

osteoblast differentiation, osteoclast differentiation, metabolic and rare bone disease, inflammatory disease, molecular mechanism

Editorial on Research Topic
Bone cell differentiation in health and disease

Bone is a dynamic organ that undergoes remodeling processes throughout life which require precise regulation. The bone remodeling consists of bone formation performed by osteoblasts and bone resorption performed by osteoclasts. The balance between these processes maintains bone homeostasis and bone renewal. However, in pathophysiological conditions including osteoporosis, diabetes, obesity, aging and rare bone diseases, bone remodeling is impaired causing poor bone quality and higher risk of fractures. Therefore, it is important to understand the molecular mechanism regulating bone cell differentiation in health and disease. This Special Issue focused on the topic of osteoblast and osteoclast differentiation in bone physiology in context of different bone diseases. It collected several original research articles presenting novel findings regarding the regulation of bone homeostasis.

Impact of various bioactive molecules on osteoclastogenesis and osteogenesis

The study by Zhu et al., found that peiminine, an alkaloid obtained from the bulb of *Fritillaria thunbergii Miq* prevented osteoclast differentiation and function. *In vitro* treatment with peiminine reduced the number of osteoclast cells in a dose dependent manner and suppressed fusion of osteoclast cells *via* inhibition of M-CSF and GST-rRANKL and decreased activation of NF-κB. Further, peiminine treament in ovariectomized mice (OVX) slowed down bone resorption and prevented bone loss.

Thus, this study showed that peiminine affects osteoclast function, which makes it a potential candidate molecule to prevent osteoporosis.

Next, Yu et al., investigated whether glucagon-like peptide-1 receptor (GLP-IR) agonists such as liraglutide could prevent bone loss in type 1 diabetes (T1D). Using female streptozotocin-induced diabetic C57BL/6J mice, liraglutide treatment for 8 weeks improved glucose metabolism in comparison to placebo treatment, which was accompanied by improved trabecular and cortical bone parameters. Further, molecular analysis using RNA-sequencing showed that liraglutide treatment in T1D mice decreased osteoclastogenesis and inflammation. Thus, this study demonstrates that liraglutide prevents T1D-induced bone fagility by suppression of osteoclastogenesis.

Further, Zheng et al. explored the effect of melatonin on osteogenesis and angiogenesis in osteoporotic fracture healing. In this study, bilateral ovariectomy was done in rat model followed by monocortical tibia defect. The animals were treated with melatonin for 4 weeks, resulting in improvement of bone healing and bone strength compared to control group. Further, immunohistochemical staining indicated higher expression levels of osteogenesis-related marker (OCN) and angiogenesis-related markers (VEGF and CD31) in the melatonin-treated OVX rats. Thus, these findings suggest a positive effect of melatonin on fracture healing in osteoporotic condition.

The study by Goodnough et al., compared the response of mouse and human SSCs to Non-Steroidal Anti-Inflammatory Drugs (NSAIDs) in fracture healing, as NSAIDs are used in the early inflammatory responses during bone fracture. Using primary SSCs from fractures the authors found that the mouse SSCs treated with NSAIDs were impaired in osteochondrogenic differentiation, while human SSCs were not affected. These findings point out the cross-species differences in response to NSAID and its sensitivity during fracture healing.

Different angles on signaling pathways involved in osteogenesis

The bone remodeling is an active dynamic process by coordinating action of bone resident osteoblasts and osteoclasts, which is dysregulated in diseases with high bone turnover rates and transforming growth factor beta 1 (TGF-β1). The study by Chen et al. reported the role of TGF-β1 signaling in bone resorption in patients with Camurati-Engelmann disease (CED). This study reported a higher level of active Rho GTPases and migration-related proteins Integrin β1and β3 in peripheral blood in this disease patients. TGF-β1 activates Rho to increase osteoclast formation and bone resorption, with simulatenous enhancment of migration of pre-osteoclasts and mature osteoclasts. Whereas hyperactive TGF-β1-stimulated osteoclastogenesis was rescued by inhibition of Rho GTPases *in vitro*. Thus, these data assume that crosstalk between Rho and TGF-β1 leads to increase bone turnover in CED. A complex multifactorial disorder osteoporosis is associated with various risk factors and medical conditions, with bone marrow-derived mesenchymal stem cell dysfunction being a crutial factor. The study by Li et al. identified upregulation of miR-4739 in BMSC of osteoporotic subjects. Further, cell viability, osteoblast differentiation, and heterotopic bone formation were diminished by overexpression of miR-4739, whereas miR-4739 inhibition showed opposite effects. Thus, this study presented a novel signaling pathway regulating osteoblast differentiation in osteoporosis.

The study by Cheng et al. identified a role of neural cell adhesion molecule (NCAM) in osteoblast differentation, Downregulation of NCAM in MC3T3-E1 resulted in decreased expression of osteogenic markers *RunX2* and *Osterix*, and decreased deposition of calcium, hence diminishing osteoblast differentiation. Similarly β-catenin levels and Akt phosphorylation levels were reduced. Thus these findings assumed that NCAM plays a pivotal role in the regulation of signaling pathways involved in osteoblast differentiation.

Gu et al. determined the role of super-enhancer-associated LINC01485/miR-619-5p/RUNX2 signaling in osteogenic differentiation. During osteogenic induction expression level of LINC01485 was increased along with osteogenic genes including RUNX2, and OCN. Over-expression of LINC01485 *in vitro* induced up-regulation of osteogenic genes and ALP activity, while knockdown caused an opposite effect on osteoblast differentiation. The RAP assay identified miR-619-5p as a candidate binding partner. Further data showed that LINC01485 competes with miR-619-5p to promote expression of RUNX2. Thus, this study points out that osteogenesis is promoted by LINC01485 whose activation is controled by miR-619-5p.

Link between bone resident cells and diabetes

Obesity and diabetes impair bone remodeling and slow down bone turnover causing increased risk of fractures. In their study, Ballato et al. investigated the presence of circulating osteoblast progenitors (COP) and circulating osteoclast progenitors (OCP) in relation to type 2 diabetes (T2D) and bone turnover. This clinical study reported that patients with poor glycemic control had higher percentage of COP in the circulation comparison to healthy controls suggesting a copying mechanism to increased osteoblast apoptosis in the hyperglycemic condition in diabetes. The authors suggested that high COP could be a marker of a poor glycemic control and predictor of disturbances of bone homeostasis.

Further study by Phimphilai et al. reported that T2D patients showed impaired osteoblast differentiation in peripheral blood derived mononuclear cells (PBMC) due to increased expression of receptor of advance glycation end products (RAGE). They found that younger age of T2D patients had a protective effect on osteoblast differentiation, while chronic exposure to T2D caused higher RAGE activation in PMBC of T2D patients associated with impaired osteoblast differentiation. These patients had increased BAX/BCL2 ratio, which was negatively correlated with osteoblast markers. Thus, these data suggest that, RAGE activation and age contributed to the diminished osteogenic differentiation potential of PBMC in T2D patients.

In fact, this especial issue provides new insights on the bone cell differentiation in different conditions and experimental settings. We believe that this Issue opens new questions which will be followed in future by basic and translational studies.

Author contributions

All authors listed have made a substantial, direct, and intellectual contribution to the work and approved it for publication.

Acknowledgments

We appreciate all Authors who submitted their research articles and all Reviewers for their great contributions to this Research Topic.

Conflict of interest

The authors declare that the research was conducted in the absence of any commercial or financial relationships that could be construed as a potential conflict of interest.

Publisher's note

frontiers in Endocrinology

ORIGINAL RESEARCH
published: 12 May 2021
doi: 10.3389/fendo.2021.657953

Neural Cell Adhesion Molecule Regulates Osteoblastic Differentiation Through Wnt/β-Catenin and PI3K-Akt Signaling Pathways in MC3T3-E1 Cells

Bin-Feng Cheng[1], Xiao Feng[1], Yao-Xin Gao[1], Shao-Qin Jian[1], Shi-Rao Liu[1], Mian Wang[1], Yun-Fei Xie[1], Lei Wang[1], Zhi-Wei Feng[2] and Hai-Jie Yang[1,3]**

[1] School of Life Sciences and Technology, Xinxiang Medical University, Xinxiang, China, [2] Institute of Precision Medicine, Xinxiang Medical University, Xinxiang, China, [3] Henan Children's Hospital, Zhengzhou, China

OPEN ACCESS

Edited by:
Toru Hosoi,
Sanyo-Onoda City University, Japan

Reviewed by:
Guillermo Romero,
University of Pittsburgh, United States
Deborah Schechtman,
University of São Paulo, Brazil

***Correspondence:**
Bin-Feng Cheng
chbinfeng@163.com
Hai-Jie Yang
hjyang_wmd@hotmail.com

Specialty section:
This article was submitted to Cellular Endocrinology, a section of the journal Frontiers in Endocrinology

Received: 24 January 2021
Accepted: 26 April 2021
Published: 12 May 2021

Citation:
Cheng B-F, Feng X, Gao Y-X, Jian S-Q, Liu S-R, Wang M, Xie Y-F, Wang L, Feng Z-W and Yang H-J (2021) Neural Cell Adhesion Molecule Regulates Osteoblastic Differentiation Through Wnt/β-Catenin and PI3K-Akt Signaling Pathways in MC3T3-E1 Cells. Front. Endocrinol. 12:657953. doi: 10.3389/fendo.2021.657953

Neural cell adhesion molecule (NCAM) is involved in cell multi-directional differentiation, but its role in osteoblast differentiation is still poorly understood. In the present study, we investigated whether and how NCAM regulates osteoblastic differentiation. We found that NCAM silencing inhibited osteoblast differentiation in pre-osteoblastic MC3T3-E1 cells. The function of NCAM was further confirmed in NCAM-deficient mesenchymal stem cells (MSCs), which also had a phenotype with reduced osteoblastic potential. Moreover, NCAM silencing induced decrease of Wnt/β-catenin and Akt activation. The Wnt inhibitor blocked osteoblast differentiation, and the Wnt activator recovered osteoblast differentiation in NCAM-silenced MC3T3-E1 cells. We lastly demonstrated that osteoblast differentiation of MC3T3-E1 cells was inhibited by the PI3K-Akt inhibitor. In conclusion, these results demonstrate that NCAM silencing inhibited osteoblastic differentiation through inactivation of Wnt/β-catenin and PI3K-Akt signaling pathways.

Keywords: NCAM, osteoblast differentiation, Wnt/β-catenin signaling, PI3K-Akt signaling, MC3T3-E1 cells

INTRODUCTION

Osteoporosis (OP) is one of the most common bone disorders in human beings, its incidence increases with age, especially in postmenopausal women because of the decrease in estrogen (1, 2). With the growth of the aging population in the world, the prevalence of OP is increasing dramatically, bringing a huge economic burden to the society and families (3, 4).

OP is characterized by a reduction in bone mineral density, which is mainly due to the imbalance of bone tissue formation and absorption (5, 6). Bone homeostasis depends on the balance between osteoblasts and osteoclasts, OP occurs as a result of the decrease of osteoblast-induced bone formation and the increase of osteoclast-induced bone absorption. Bone weakness and fracture are common in patients with OP because of their low bone mass and quality. Abnormal proliferation and differentiation of osteoblasts were shown involved in reduction of bone mass (7, 8). Study on the molecular mechanisms of osteoblastic differentiation is helpful to understand the pathogenesis of OP and develop new strategies for OP treatment.

Neural cell adhesion molecule (NCAM, CD56), a member of the immunoglobulin (IgG) superfamily, is widely expressed in the nervous system and plays multi-functional roles in neural regeneration, cell to cell adhesion, signal transduction and modulation of learning and memory (9–11). NCAM has been found to be expressed in other cell types such as epithelial cells, natural killer cells, skeletal muscle and mesenchymal stem cells (MSCs) (12, 13). In our previous studies, we demonstrated that NCAM enhances insulin sensitivity and promotes adipocyte differentiation, and we further found that NCAM inhibits hypertrophic chondrocyte differentiation and reduces chondrocyte hypertrophy in experimental osteoarthritis model (14, 15). Our results indicate that NCAM plays a key role in cell multi-directional differentiation, however, the function of NCAM in osteoblastic differentiation remains largely unknown.

In the present study, we evaluated the effects of NCAM on osteoblastic differentiation in mouse preosteoblast-like cells (MC3T3-E1) and in mouse MSCs. We also investigated the underlying mechanism involved in NCAM-regulated osteoblastic differentiation.

MATERIALS AND METHODS

Materials

LY294002, β-glycerophosphate, ascorbic acid-2-phosphate, and dexamethasone were obtained Sigma-Aldrich (St. Louis, MO, USA). XAV939 was obtained from EMD Millipore (Darmstadt, Germany). Lithium Chloride (LiCl) was purchased from Nacalai Tesque, Inc. (Kyoto, Japan). Fetal bovine serum (FBS) was purchased from Gibco (Grand Island, NY, USA). The mammalian expression vector pcDNA4/Myc was obtained from Invitrogen (Carlsbad, CA, USA). siRNA expression vectors pSilencer 4.1-CMV neo was obtained from Ambion (Austin, TX, USA). Lipofectamine 2000, G418 and puromycin were purchased from Invitrogen (Carlsbad, CA, USA). Antibodies against RunX2, Osterix, β-catenin, phospho-Akt, and β-actin were purchased from Cell Signaling Technology, Inc. (Beverly, MD, USA). The secondary antibodies were purchased from Santa Cruz Biotechnology (Santa Cruz, CA, USA). TRIzol regent was purchased from Invitrogen (Carlsbad, CA, USA). QuantiTect Reverse Transcription kit was purchased from Qiagen (Valencia, CA, USA). SYBR Green Master Mix was purchased from Bio-Rad Laboratories (Richmond, CA, USA). Other chemicals were purchased from Sigma-Aldrich.

NCAM-Deficient Mice and MSCs

The *Ncam*$^{-/-}$ (knockout; KO) mice were generated on a C57/BL6 background as previously described (16). Wild-type (WT) and KO MSCs were obtained from 8-week-old male mice as previously described (14). Briefly, cells were harvested from mouse bone marrow and cultured in low glucose Dulbecco's modified Eagle's medium (DMEM-LG, with 1 g/L glucose; Hyclone, Logan, UT, USA) containing 10% fetal bovine serum (FBS), 100 IU/mL penicillin and 100 g/mL streptomycin. Non-adherent hematopoietic cells were discarded after incubation for 7 days, and the adhered MSCs were purified by repeated passaging. MSCs with fibroblast-like morphology from passage 6 to 9 was used in this study.

Cell Culture and Osteogenic Differentiation

The mouse osteoblastic cell line MC3T3-E1 was purchased from American Type Culture Collection (ATCC; Rockville, MD, USA). Cells were cultured in α-modified Eagle's medium (α-MEM; Hyclone, Logan, UT, USA) supplemented with 10% FBS, penicillin (100 U/mL), and streptomycin (100 g/mL).

WT and KO MSCs were cultured in DMEM-LG containing 10% FBS, 100 IU/mL penicillin and 100 g/mL streptomycin as previously described (14).

Cells were seeded in 12-well plates at a concentration of 1×10^5 cells/mL. The MC3T3-E1 cells and MSCs were respectively incubated in a-MEM and DMEM with 10 mM β-glycerophosphate, 25 μM ascorbic acid-2-phosphate and 10 nM dexamethasone.

Plasmids and Transfection

siRNA vectors silencing NCAM and plasmids expressing full-length mouse NCAM were designed and constructed as previously described (14). Transfection was conducted using Lipofectamine 2000 following manufacturer's instructions. To obtain stable mixed cell lines, cells were selected with puromycin at 1 μg/mL and G418 at 800 μg/mL for 14 days. Gene silencing or overexpression of NCAM was validated by Western blotting with anti-NCAM antibody.

Real-Time PCR

Total RNA was extracted with TRIzol (Invitrogen) according to the manufacturer's instructions, and cDNA was synthesized using a High-Capacity cDNA Reverse Transcription Kit (Applied Biosystems, Foster City, CA). The mRNA levels were measured using an ABI Prism 7500 Sequence detection system (Applied Biosystems) and SYBR Green qPCR Master Mix (KAPA Biosystems). The expression levels of *RunX2* and *Osterix* were normalized using the internal reference gene *GAPDH*. The PCR primers were shown in **Table 1**.

Western Blot

Cells were lysed with radio immuno-precipitation (RIPA) buffer and lysed on ice supplemented with proteinase and phosphatase inhibitors cocktail (Sigma). Protein concentrations were determined using BCA Protein Assay Kit (Pierce). Equal amounts of protein were separated by sodium dodecyl sulfate-polyacrylamide gel electrophoresis and transferred to polyvinylidene difluoride (PVDF) membrane. After blocking with 3% bovine serum albumin (BSA; Sigma) for 1 h, the membranes were incubated with primary

TABLE 1 | Primers for real-time PCR.

Gene	Forward primer (5'-3')	Reverse primer (5'-3')
RunX2	CGAAATGCCTCCGCTGTTAT	TGAGGAATGCGCCCTAAATC
Osterix	TGACTACCCACCCTTCCCTC	GCCTTGTACCACGAGCCATA
GAPDH	CTTCAACAGCAACTCCCACT	GTCCAGGGTTTCTTACTCCT

antibodies against RunX2, Osterix, β-catenin, p-Akt, or β-actin overnight at 4°C. The membranes subsequently were washed three times with TBST and incubated with the secondary antibodies for 40 min at room temperature. The band density was scanned by ImageQuant LAS 4000 system (GE Healthcare) and analysed by ImageJ software.

Alizarin Red Staining and Quantification

The alizarin red staining was performed at 0, 7, or 14 days. Cells were fixed in 4% paraformaldehyde (PFA) for 30 min followed by staining with 40 mM Alizarin Red S (ARS; pH 4.2) for 30 min and then washed three times with deionized water. For the quantitative analysis of ARS, the stained wells were incubated with 10% cetyl pyridinium chloride monohydrate for 30 min at room temperature and then measured at 562 nm using a Molecular Devices microplate reader (15).

Statistical Analysis

All data are expressed as the mean ± SEM. Statistical analysis was performed using one-way ANOVA followed by Tukey's test. Differences were regarded as statistically significant at $P < 0.05$. Each experiment was performed at least in triplicate.

RESULTS

NCAM Silencing Inhibits Osteoblast Differentiation of MC3T3-E1 Cells

To explore the function of NCAM in osteoblast differentiation, stable NCAM down-regulated MC3T3-E1 cells were developed using plasmid-based small interfering RNA (siRNA). The expression level of NCAM was determined using western blot. The result showed that NCAM expression in the Sh-NCAM cells was much lower compared with that of Sh-ctl cells and the interference rate reached 70% (**Figures 1A, B**). The gene expressions of osteogenic markers *RunX2* and *Osterix* were examined by quantitative real-time PCR, down-regulation of NCAM inhibited expressions of *RunX2* and *Osterix* during osteogenic differentiation (**Figures 1C, D**). Western blotting analysis showed that the protein levels of RunX2 and Osterix were also decreased in Sh-NCAM MC3T3-E1 cells (**Figures 1E–G**). In addition, calcium deposition was visualized by Alizarin Red staining and quantitative analysis, the calcium content was significantly decreased in Sh-NCAM cells as compared to Sh-ctl MC3T3-E1 cells (**Figures 1H, I**). These results demonstrated that gene silencing of NCAM inhibits osteoblast differentiation of MC3T3-E1 cells.

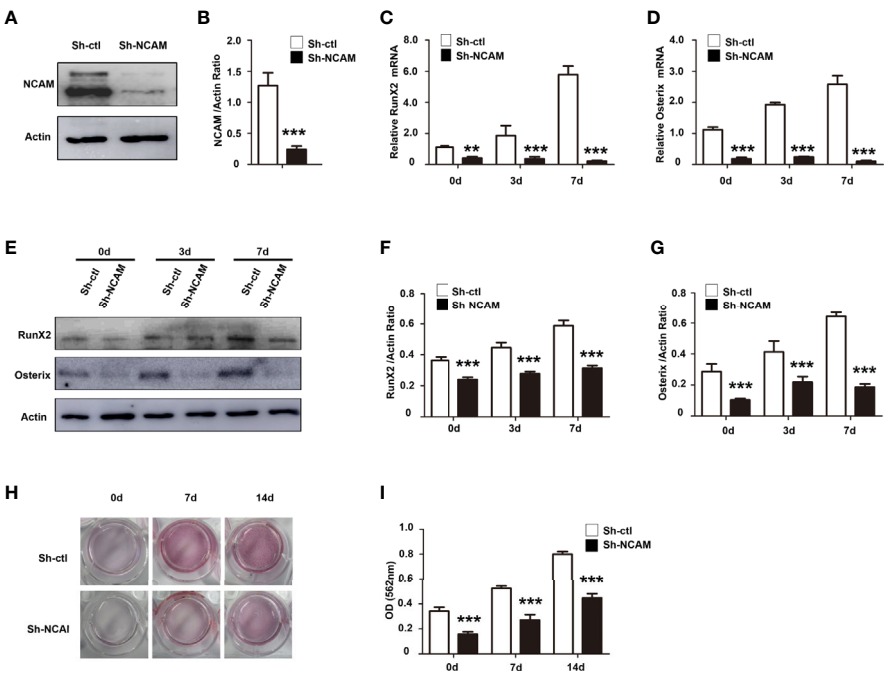

FIGURE 1 | NCAM silencing inhibits osteoblast differentiation of preosteoblast-like MC3T3-E1 cells. **(A)** Cells were transfected with pSilencer-4.1-based plasmid containing a scrambled sequence (control; Sh-ctl) or a 19-bp oligonucleotide insert targeting mouse NCAM (Sh-NCAM), and analysed by immunoblotting with anti-NCAM antibody. **(B)** Level of NCAM was quantified by densitometry and normalized to β-actin (n=3; mean ± SEM; ***$p < 0.001$, compared with control siRNA group). The expression of RunX2 **(C)** and Osterix **(D)** was analysed by real-time PCR (The results are expressed as the mean ± SEM of three independent experiments. **$p < 0.01$, ***$p < 0.001$, compared with control siRNA-transfected cells). **(E)** The expression of RunX2 and Osterix was analysed by immunoblotting, β-actin was detected as a loading control. Levels of **(F)** RunX2 and **(G)** Osterixwere quantified by densitometry and normalized to β-actin (Data are representative of three independent experiments and values are means ± SEM. ***$p < 0.001$, compared with control siRNA-transfected cells). **(H)** Cells transfected with control or NCAM siRNA were induced with osteoblastic media and stained with Alizarin red. **(I)** The Alizarin red staining was extracted and quantified, the wavelength was measured at 562 nm (Data are representative of three independent experiments and values are means ± SEM. ***$p < 0.001$, compared with control siRNA-transfected cells).

NCAM Deficiency Impairs Osteoblast Differentiation of Mouse MSCs

To further confirm the role of NCAM in osteoblast differentiation, we isolated bone marrow derived MSCs from wild-type (WT) and *Ncam*$^{-/-}$ (KO) mice. The Western blot results confirmed the expression of NCAM in wild-type MSCs but not in *Ncam*$^{-/-}$ cells (**Figure 2A**). To investigate whether NCAM deficiency affects osteoblast differentiation of MSCs, wild-type and *Ncam*$^{-/-}$ MSCs were treated with osteogenic differentiation medium. The mRNA expressions of *RunX2* and *Osterix* were down-regulated in *Ncam*$^{-/-}$ MSCs as compared to WT cells (**Figures 2B, C**). The protein levels of RunX2 and Osterix were detected by Western blotting. As shown in **Figures 2D–F**, the induction of RunX2 and Osterix in *Ncam*$^{-/-}$ MSCs was also lower than that in wild-type cells. Alizarin red staining and quantitative analysis of the calcium content in *Ncam*$^{-/-}$ MSCs showed decreased calcium deposition as compared to wild-type cells (**Figures 2G, H**). The results further confirmed the NCAM level involved in osteoblast differentiation of MSCs, suggesting that NCAM might play a key role in osteogenesis of various cell lines.

Wnt/β-catenin Signaling Contributes to NCAM-Mediated Osteoblast Differentiation

It has been shown that the Wnt/β-catenin signaling pathway plays an important role in osteogenic lineage (17). To investigate the mechanism of osteoblast differentiation mediated by NCAM, the expression of β-catenin was examined in Sh-ctl and Sh-NCAM MC3T3-E1 cells. The Western blotting results showed that β-catenin level was significantly decreased in Sh-NCAM cells (**Figures 3A, B**). To determine the role of β-catenin, we applied the Wnt signaling inhibitor XAV939 during osteogenic differentiation in MC3T3-E1 cells. The β-catenin expression was almost completely inhibited by XAV939 (≥ 5 μM) (**Figures 3C, D**). As a result of β-catenin suppression, the mRNA expressions of *RunX2* and *Osterix* were down-regulated (**Figures 3E, F**). Accordingly, XAV939 at 5 μM totally inhibited the protein levels of RunX2 and Osterix in MC3T3-E1 cells (**Figures 3G–I**). In addition, calcium deposition was also significantly blocked by XAV939 (**Figures 3J, K**). These results indicate that Wnt/β-catenin signaling is involved in NCAM-mediated osteoblast differentiation.

To further determine the contribution of Wnt/β-catenin signaling to NCAM-mediated osteoblast differentiation, the β-catenin level was increased by the Wnt pathway activator LiCl during osteogenic differentiation in Sh-NCAM MC3T3-E1 cells (**Figures 4A, B**). As shown in **Figures 4C, D**, inducing of β-catenin restored the mRNA expressions of *RunX2* and *Osterix* down-regulated by NCAM silencing. The protein levels of RunX2 and Osterix were also recovered in LiCl-treated Sh-NCAM MC3T3-E1 cells, compared with that in control cells (**Figures 4E–G**). Besides, Alizarin red staining and quantitative

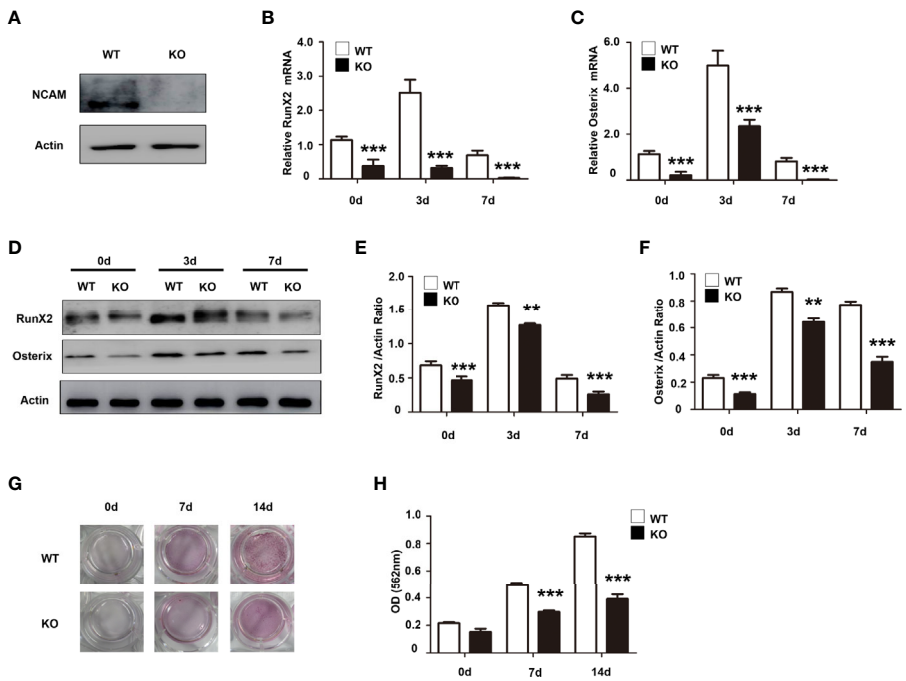

FIGURE 2 | NCAM deficiency inhibits osteoblast differentiation of mouse MSCs. **(A)** Wild-type (WT) and *Ncam*$^{-/-}$ (KO) MSCs were examined with anti-NCAM antibody. β-actin was detected as a loading control. The expression of RunX2 **(B)** and Osterix **(C)** was analysed by real-time PCR (The data are expressed as the mean ± SEM of three independent experiments. ***$p < 0.001$, compared with WT MSCs). **(D)** The expression of RunX2 and Osterix was analysed by immunoblotting, β-actin was detected as a loading control. Levels of RunX2 **(E)** and Osterix **(F)** were quantified by densitometry and normalized to β-actin (Data are representative of three independent experiments and values are means ± SEM. **$p < 0.01$, ***$p < 0.001$, compared with WT MSCs). **(G)** Calcium deposition of differentiated WT and KO MSCs was assessed by Alizarin red staining. **(H)** The Alizarin red staining was extracted and quantified, the wavelength was measured at 562 nm (Data are representative of three independent experiments and values are means ± SEM. ***$p < 0.001$, compared with WT MSCs).

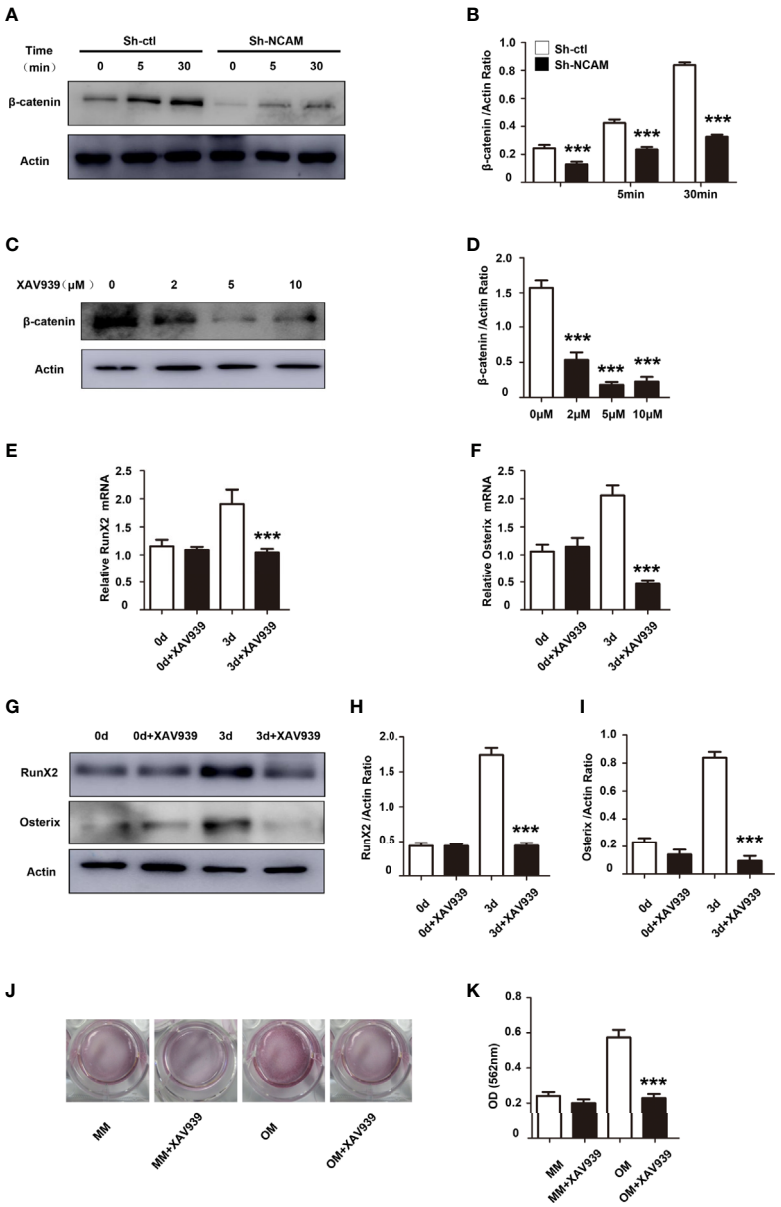

FIGURE 3 | Inhibition of Wnt/β-catenin signaling inhibits osteoblast differentiation. **(A)** Sh-ctl and Sh-NCAM MC3T3-E1 cells were treated with differentiation media for 0, 5, and 30 min, the expression of β-catenin was analysed by immunoblotting. β-actin was detected as a loading control. **(B)** Level of β-catenin was quantified by densitometry and normalized to β-actin (n=3; mean ± SEM; ***$p < 0.001$, compared with control siRNA group). MC3T3-E1 cells were pretreated with the Wnt inhibitor XAV939. **(C)** The expression of β-catenin was analysed and **(D)** quantified by densitometry and normalized to β-actin (n=3; mean ± SEM; ***$p < 0.001$, compared with cells without XAV939). The expressions of **(E)** RunX2 and **(F)** Osterix were examined by real-time PCR (The results are expressed as the mean ± SEM of three independent experiments. ***$p < 0.001$, compared with cells without XAV939). **(G)** The expressions of RunX2 and Osterix were analysed by immunoblotting, β-actin was detected as a loading control. Levels of **(H)** RunX2 and **(I)** Osterix were quantified by densitometry and normalized to β-actin (Data are representative of three independent experiments and values are means ± SEM. ***$p < 0.001$, compared with cells without XAV939). **(J)** Calcium deposition was assessed by Alizarin red staining. **(K)** The Alizarin red staining was extracted and quantified, the wavelength was measured at 562 nm (Data are representative of three independent experiments and values are means ± SEM. ***$p < 0.001$, compared with cells without XAV939).

analysis revealed that β-catenin up-regulation reversed the lower accumulation of calcium content induced by NCAM silencing in Sh-NCAM MC3T3-E1 cells (**Figures 4H, I**). The results further confirmed the contribution of Wnt/β-catenin signaling to NCAM-mediated osteoblast differentiation.

PI3K-Akt Signaling Contributes to NCAM-Mediated Osteoblast Differentiation

The phosphatidylinositol 3'-kinase (PI3K)-Akt signaling plays a significant role in the osteoblast differentiation (18). To investigate the role of PI3K-Akt signaling in NCAM-mediated osteoblast

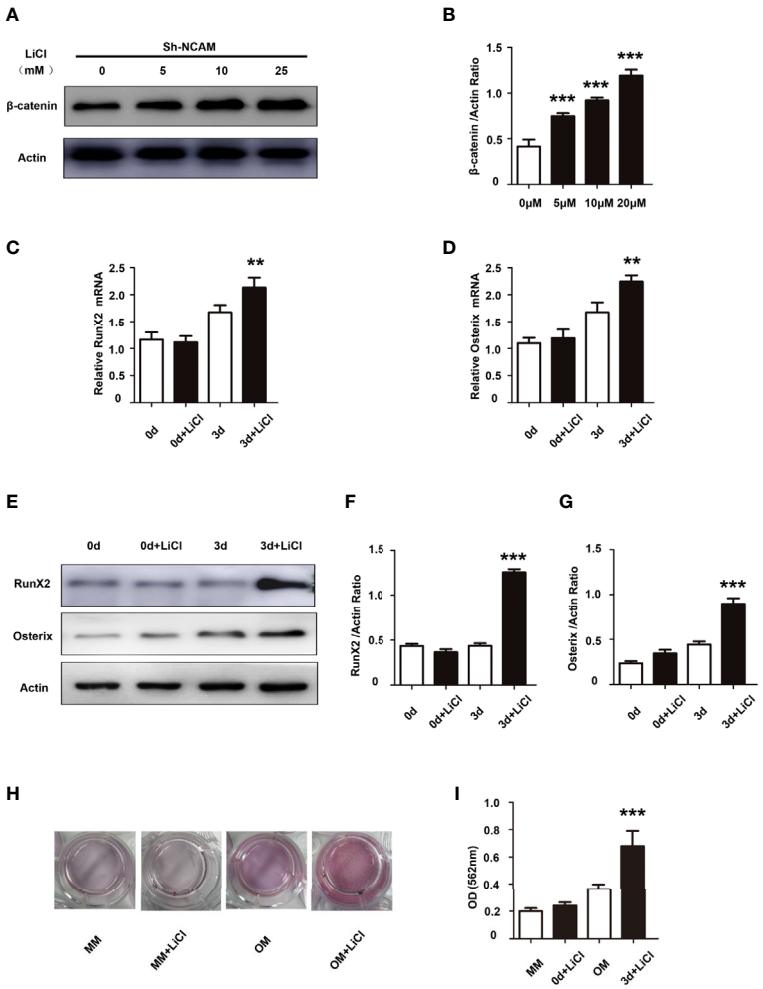

FIGURE 4 | Activation of Wnt/β-catenin signaling recovers osteoblast differentiation inhibited by NCAM silencing. Sh-NCAM MC3T3-E1 cells were pretreated with the Wnt agonist LiCl. **(A)** the expression of β-catenin was analysed by immunoblotting at 0, 5, 10 and 25 min, β-actin was detected as a loading control. **(B)** Level of β-catenin was quantified by densitometry and normalized to β-actin (n=3; mean ± SEM; ***$p < 0.001$, compared with cells without LiCl). The expressions of **(C)** RunX2 and **(D)** Osterix were examined by real-time PCR (The results are expressed as the mean ± SEM of three independent experiments. **$p < 0.01$, compared with cells without LiCl). **(E)** The expressions of RunX2 and Osterix were analysed by immunoblotting, β-actin was detected as a loading control. Levels of **(F)** RunX2 and **(G)** Osterix were quantified by densitometry and normalized to β-actin (Data are representative of three independent experiments and values are means ± SEM. ***$p < 0.001$, compared with cells without LiCl). **(H)** Calcium deposition was assessed by Alizarin red staining. **(I)** The Alizarin red staining was extracted and quantified, the wavelength was measured at 562 nm (Data are representative of three independent experiments and values are means ± SEM. ***$p < 0.001$, compared with cells without LiCl).

differentiation, the phosphorylation of Akt was examined during osteogenic differentiation. The results showed that the Akt phosphorylation was significantly decreased in Sh-NCAM MC3T3-E1 cells as compared to Sh-ctl cells (**Figures 5A, B**). The Akt inhibitor LY294002 was applied to determine whether the NCAM-mediated Akt inhibition is involved in osteoblast differentiation. The data revealed that 10 μM of LY294002 was almost completely inhibited the phosphorylation of Akt (**Figures 5C, D**), and the levels of RunX2 and Osterix were significantly reduced in both mRNA expression (**Figures 5E, F**) and protein production (**Figures 5G–I**) during osteogenic differentiation in MC3T3-E1 cells. Alizarin red staining and quantitative analysis showed that the calcium deposition was also significantly decreased in LY294002-treated MC3T3-E1 cells (**Figures 5J, K**). These results indicated that Akt signaling is involved in NCAM-mediated osteoblast differentiation.

DISCUSSION

OP is a systemic skeletal disease characterized by low bone mineral density (19). Recent studies have shown that abnormality of osteoblast differentiation is one of the key factors leading to decreased bone mass (8, 20). In the present study, we revealed a novel role of NCAM in osteoblast differentiation. NCAM deficiency inhibits osteoblast differentiation in both mouse pre-osteoblast cells and mouse adult stem cells, in which Wnt/β-catenin and Akt signaling pathways play important roles.

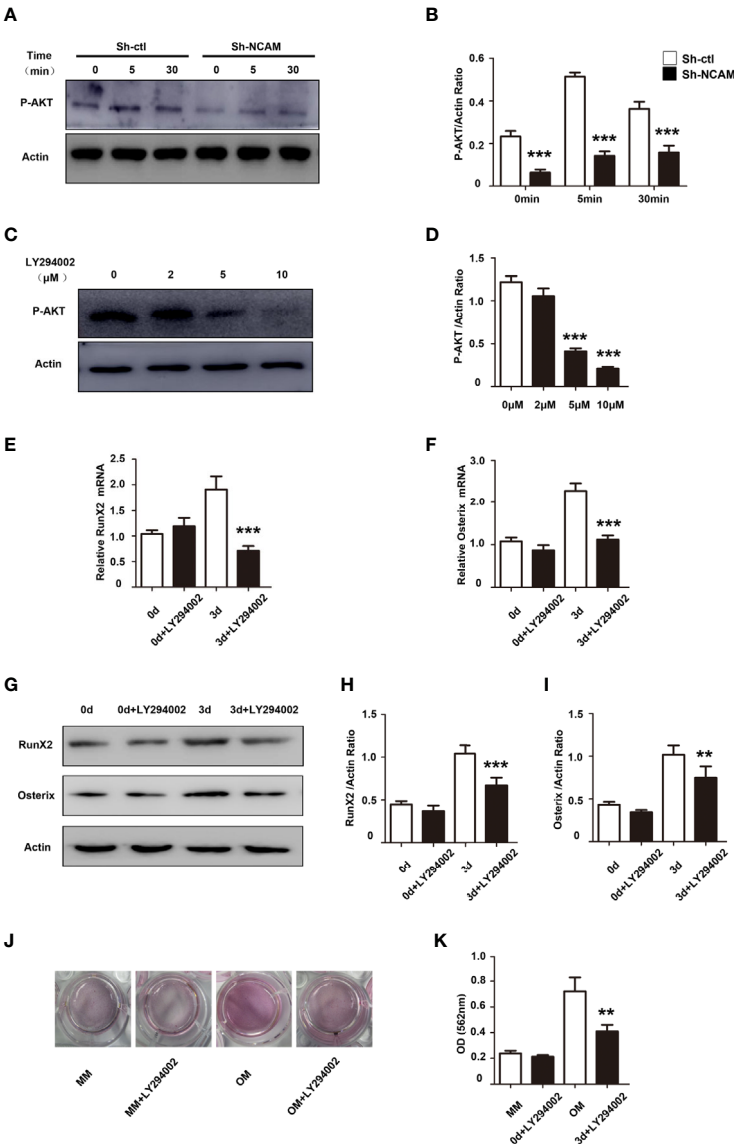

FIGURE 5 | PI3K-Akt signaling contribute to NCAM-mediated osteoblast differentiation. **(A)** Sh-ctl and Sh-NCAM MC3T3-E1 cells were treated with differentiation media for 0, 5, and 30 min, the phosphorylation of Akt was analysed by immunoblotting. β-actin was detected as a loading control. **(B)** Level of phosphorylated Akt was quantified by densitometry and normalized to β-actin (n=3; mean ± SEM; ***$p < 0.001$, compared with control siRNA group). MC3T3-E1 cells were pretreated with the PI3K-Akt inhibitor LY294002. **(C)** The expression of phosphorylated Akt was analysed and **(D)** quantified by densitometry and normalized to β-actin (n=3; mean ± SEM; ***$p < 0.001$, compared with cells without LY294002).The expressions of **(E)** RunX2 and **(F)** Osterix were examined by real-time PCR (The results are expressed as the mean ± SEM of three independent experiments. ***$p < 0.001$, compared with cells without LY294002). **(G)** The expressions of RunX2 and Osterix were analysed by immunoblotting, β-actin was detected as a loading control. Levels of **(H)** RunX2 and **(I)** Osterix were quantified by densitometry and normalized to β-actin (Data are representative of three independent experiments and values are means ± SEM. **$p < 0.01$, ***$p < 0.001$, compared with cells without LY294002). **(J)** Calcium deposition was assessed by Alizarin red staining. **(K)** The Alizarin red staining was extracted and quantified, the wavelength was measured at 562 nm (Data are representative of three independent experiments and values are means ± SEM. **$p < 0.01$, compared with cells without LY294002).

MC3T3–E1, an osteoblast precursor cell line derived from mouse calvaria, has been widely used as a useful model for osteoblast differentiation research (21). Here, we explored the function of NCAM in osteoblast differentiation in MC3T3–E1 cells. During the process of osteoblast differentiation, *RunX2* and *Osterix* are key genes required for osteoblasts. Previous studies reported that Runx2-deficient (*Runx2*$^{-/-}$) mice lack osteoblasts and bone formation (22, 23). Knockout of *Osterix* study in mice also demonstrated a complete lack of osteoblasts (24). Osterix and Runx2 initiate osteoblast differentiation by regulating the expression levels of various specific genes that characterize the osteogenic lineage, such as osteopontin, osteocalcin, bone sialoprotein, and alkaline phosphatase (25–28). In our study, we showed that NCAM silencing inhibited osteoblast differentiation

as demonstrated by decreased induction of RunX2 and Osterix, and decreased calcium deposition in MC3T3−E1 cells. This novel role of NCAM was further corroborated in mouse MSCs, the differentiation of osteoblast was also inhibited in *Ncam*$^{-/-}$ MSCs. Our results demonstrated that either NCAM down-regulation in preosteoblast-like cells or NCAM deficiency in MSCs impaired osteoblast differentiation, indicating that NCAM plays a pivotal role in osteogenesis.

Wnt/β-catenin signaling, as the canonical Wnt pathway, is crucial for osteogenic lineage at early stages of osteogenic differentiation (29). Activation of Wnt/β-catenin signaling involves the binding of Wnt to surface receptors low-density lipoprotein receptor related protein 5/6 (LRP5/6) and Frizzled (30). In this study, we demonstrated that the β-catenin expression is decreased whereas the osteogenic markers and calcium deposition are recovered by Wnt activator in NCAM-silenced MC3T3−E1 cells. NCAM induces activation of FGFR and is an important interaction partner (31). Previous study (32) showed that NCAM-silencing represses β-catenin signaling *via* fibroblast growth factor receptor (FGFR) and glycogen synthase kinase-3β (GSK-3β). Other report has demonstrated that Wnt/β-catenin pathway reduces expression of NCAM through miR-30a-5p (33). These findings suggest that the effect of NCAM on Wnt signaling appears to bidirectional and indirect, which might be mediated by FGFR, GSK-3β or miR-30a-5p. PI3K/Akt signaling pathway was also found to play central role in osteoblast differentiation (34). We showed here that Akt activation is decreased in NCAM-silenced MC3T3−E1 cells and contributes to NCAM-mediated osteoblast differentiation. A previous study demonstrated that the critical osteogenic gene Runx2 is a target of β-catenin/TCF1 for the regulation of osteoblast differentiation and bone formation (35). Runx2 is also involved in Akt pathway activation, Runx2 and PI3K-Akt signaling are dependent on each other in the control of osteoblast differentiation, PI3K inhibitor inhibits DNA binding of Runx2 and Runx2-dependent transcription, and Runx2 also up-regulates expression of Akt and p85 and p110b subunits of PI3K (36). Another key osteogenic gene Osterix is a downstream osteoblastic gene of Runx2 (24, 37). These previous studies are consistent with our results indicating that NCAM silencing inhibits the expressions of osteogenic genes *Runx2* and Osterix by regulation of Wnt/β-catenin and PI3K-Akt signaling pathways.

OP and osteoarthritis (OA) are the two most common disorders of bone related to aging worldwide. OA is characterized by degeneration of cartilage and damage in subchondral and periarticular bone (38). Although some studies reported that OP may aggravates the degree of cartilage destruction in OA knee (39–41), the relationship between them is complex. In the present study, we found that NCAM silencing inhibits osteoblast differentiation, indicating that NCAM plays a key role in OP. We also previously demonstrated that NCAM deficiency increases the severity of cartilage damage in experimental OA (15). Our data provide NCAM as a novel target insight into the relationship between OA and OP, suggesting that overexpression of NACM can be used as a new potential strategy for the treatment of patients with OP and OA.

However, there are some limitations to the study, for example that it neither take into the role of NCAM in osteoblastogenesis *in vivo* studies, nor relates to further research on in-depth mechanism that how NCAM triggers the signaling pathways.

In conclusion, we demonstrate a novel role of NCAM in osteoblast differentiation in both pre-osteoblasts and MSCs. Wnt/β-catenin and PI3K-Akt signaling pathways contribute to NCAM-mediated osteoblast differentiation. The results support NCAM as a new regulator of osteoblast differentiation and a potential therapeutic target for OP treatment.

DATA AVAILABILITY STATEMENT

The original contributions presented in the study are included in the article/supplementary material. Further inquiries can be directed to the corresponding authors.

ETHICS STATEMENT

The animal study was reviewed and approved by The Ethics Committee of Xinxiang Medical University.

AUTHOR CONTRIBUTIONS

H-JY and B-FC conceived and designed the experiments. B-FC, XF, Y-XG, LW, Y-FX, S-RL, and MW performed the experiments. XF, Y-XG, S-QJ and Z-WF analyzed the data. B-FC and H-JY wrote the manuscript. All authors contributed to the article and approved the submitted version.

FUNDING

This work was supported by the grants from the National Natural Science Foundation of China (No. U1704186, 81771336 and 81671226), Key Scientific Research Project of Colleges and Universities in Henan Province (No. 19A310020), and Henan Neural Development Engineering Research Center for Children Foundation (SG201909).

REFERENCES

1. van der Spoel E, van Vliet NA, van Heemst D. Viewpoint on the Role of Tissue Maintenance in Ageing: Focus on Biomarkers of Bone, Cartilage, Muscle, and Brain Tissue Maintenance. *Ageing Res Rev* (2019) 56:100964. doi: 10.1016/j.arr.2019.100964
2. Gennari L, Rotatori S, Bianciardi S, Nuti R, Merlotti D. Treatment Needs and Current Options for Postmenopausal Osteoporosis. *Expert Opin Pharmacother* (2016) 17(8):1141–52. doi: 10.1080/14656566.2016.1176147
3. Awasthi H, Mani D, Singh D, Gupta A. The Underlying Pathophysiology and Therapeutic Approaches for Osteoporosis. *Med Res Rev* (2018) 38(6):2024–57. doi: 10.1002/med.21504
4. Wang Y, Tao Y, Hyman ME, Li J, Chen Y. Osteoporosis in China. *Osteoporos Int* (2009) 20(10):1651–62. doi: 10.1007/s00198-009-0925-y
5. Yang TL, Shen H, Liu A, Dong SS, Zhang L, Deng FY, et al. A Road Map for Understanding Molecular and Genetic Determinants of Osteoporosis. *Nat Rev Endocrinol* (2020) 16(2):91–103. doi: 10.1038/s41574-019-0282-7

6. Takayanagi H. Osteoimmunology: Shared Mechanisms and Crosstalk Between the Immune and Bone Systems. *Nat Rev Immunol* (2007) 7 (4):292–304. doi: 10.1038/nri2062
7. Xie Y, Zhang L, Xiong Q, Gao Y, Ge W, Tang P. Bench-to-Bedside Strategies for Osteoporotic Fracture: From Osteoimmunology to Mechanosensation. *Bone Res* (2019) 7:25. doi: 10.1038/s41413-019-0066-7
8. Qu H, Li T, Jin H, Zhang S, He B. Silent Mating Type Information Regulation 2 Homolog (SIRT1) Influences Osteogenic Proliferation and Differentiation of MC3T3-E1 Cells Via Regulation of Mir-132-3p. *Med Sci Monit* (2019) 25:2289–95. doi: 10.12659/MSM.912392
9. Ronn LC, Hartz BP, Bock E. The Neural Cell Adhesion Molecule (NCAM) in Development and Plasticity of the Nervous System. *Exp Gerontol* (1998) 33(7-8):853–64. doi: 10.1016/S0531-5565(98)00040-0
10. Ronn LC, Berezin V, Bock E. The Neural Cell Adhesion Molecule in Synaptic Plasticity and Ageing. *Int J Dev Neurosci* (2000) 18(2-3):193–9. doi: 10.1016/S0736-5748(99)00088-X
11. Weinhold B, Seidenfaden R, Rockle I, Muhlenhoff M, Schertzinger F, Conzelmann S, et al. Genetic Ablation of Polysialic Acid Causes Severe Neurodevelopmental Defects Rescued by Deletion of the Neural Cell Adhesion Molecule. *J Biol Chem* (2005) 280(52):42971–7. doi: 10.1074/jbc.M511097200
12. Buhring HJ, Treml S, Cerabona F, de Zwart P, Kanz L, Sobiesiak M. Phenotypic Characterization of Distinct Human Bone Marrow-Derived MSC Subsets. *Ann N Y Acad Sci* (2009) 1176:124–34. doi: 10.1111/j.1749-6632.2009.04564.x
13. Crigler L, Robey RC, Asawachaicharn A, Gaupp D, Phinney DG. Human Mesenchymal Stem Cell Subpopulations Express a Variety of Neuro-Regulatory Molecules and Promote Neuronal Cell Survival and Neuritogenesis. *Exp Neurol* (2006) 198(1):54–64. doi: 10.1016/j.expneurol.2005.10.029
14. Yang HJ, Xia YY, Wang L, Liu R, Goh KJ, Ju PJ, et al. A Novel Role for Neural Cell Adhesion Molecule in Modulating Insulin Signaling and Adipocyte Differentiation of Mouse Mesenchymal Stem Cells. *J Cell Sci* (2011) 124(Pt 15):2552–60. doi: 10.1242/jcs.085340
15. Cheng BF, Lian JJ, Yang HJ, Wang L, Yu HH, Bi JJ, et al. Neural Cell Adhesion Molecule Regulates Chondrocyte Hypertrophy in Chondrogenic Differentiation and Experimental Osteoarthritis. *Stem Cells Transl Med* (2020) 9(2):273–83. doi: 10.1002/sctm.19-0190
16. Olofsson CS, Hakansson J, Salehi A, Bengtsson M, Galvanovskis J, Partridge C, et al. Impaired Insulin Exocytosis in Neural Cell Adhesion Molecule-/- Mice Due to Defective Reorganization of the Submembrane F-actin Network. *Endocrinology* (2009) 150(7):3067–75. doi: 10.1210/en.2008-0475
17. Etheridge SL, Spencer GJ, Heath DJ, Genever PG. Expression Profiling and Functional Analysis of Wnt Signaling Mechanisms in Mesenchymal Stem Cells. *Stem Cells* (2004) 22(5):849–60. doi: 10.1634/stemcells.22-5-849
18. Ghosh-Choudhury N, Abboud SL, Nishimura R, Celeste A, Mahimainathan L, Choudhury GG. Requirement of BMP-2-induced Phosphatidylinositol 3-Kinase and Akt Serine/Threonine Kinase in Osteoblast Differentiation and Smad-dependent BMP-2 Gene Transcription. *J Biol Chem* (2002) 277 (36):33361–8. doi: 10.1074/jbc.M205053200
19. Kanis JA. Diagnosis of Osteoporosis. *Osteoporos Int* (1997) 7 Suppl 3:S108–16. doi: 10.1007/BF03194355
20. Armas LA, Recker RR. Pathophysiology of Osteoporosis: New Mechanistic Insights. *Endocrinol Metab Clin North Am* (2012) 41(3):475–86. doi: 10.1016/j.ecl.2012.04.006
21. Xu CP, Sun HT, Yang YJ, Cui Z, Wang J, Yu B, et al. ELP2 Negatively Regulates Osteoblastic Differentiation Impaired by Tumor Necrosis Factor Alpha in MC3T3-E1 Cells Through STAT3 Activation. *J Cell Physiol* (2019) 234(10):18075–85. doi: 10.1002/jcp.28440
22. Komori T, Yagi H, Nomura S, Yamaguchi A, Sasaki K, Deguchi K, et al. Targeted Disruption of Cbfa1 Results in a Complete Lack of Bone Formation Owing to Maturational Arrest of Osteoblasts. *Cell* (1997) 89(5):755–64. doi: 10.1016/s0092-8674(00)80258-5
23. Otto F, Thornell AP, Crompton T, Denzel A, Gilmour KC, Rosewell IR, et al. Cbfa1, a Candidate Gene for Cleidocranial Dysplasia Syndrome, is Essential for Osteoblast Differentiation and Bone Development. *Cell* (1997) 89(5):765–71. doi: 10.1016/s0092-8674(00)80259-7
24. Nakashima K, Zhou X, Kunkel G, Zhang Z, Deng JM, Behringer RR, et al. The Novel Zinc Finger-Containing Transcription Factor Osterix is Required for Osteoblast Differentiation and Bone Formation. *Cell* (2002) 108(1):17–29. doi: 10.1016/s0092-8674(01)00622-5
25. Cheng A, Genever PG. SOX9 Determines RUNX2 Transactivity by Directing Intracellular Degradation. *J Bone Miner Res* (2010) 25(12):2680–9. doi: 10.1002/jbmr.174
26. Fu H, Doll B, McNelis T, Hollinger JO. Osteoblast Differentiation In Vitro and In Vivo Promoted by Osterix. *J BioMed Mater Res A* (2007) 83(3):770–8. doi: 10.1002/jbm.a.31356
27. Choi YH, Han Y, Jin SW, Lee GH, Kim GS, Lee DY, et al. Pseudoshikonin I Enhances Osteoblast Differentiation by Stimulating Runx2 and Osterix. *J Cell Biochem* (2018) 119(1):748–57. doi: 10.1002/jcb.26238
28. Komori T. Regulation of Proliferation, Differentiation and Functions of Osteoblasts by Runx2. *Int J Mol Sci* (2019) 20(7):1694. doi: 10.3390/ijms20071694
29. Maupin KA, Droscha CJ, Williams BO. A Comprehensive Overview of Skeletal Phenotypes Associated With Alterations in Wnt/beta-catenin Signaling in Humans and Mice. *Bone Res* (2013) 1(1):27–71. doi: 10.4248/BR201301004
30. Krishnan V, Bryant HU, Macdougald OA. Regulation of Bone Mass by Wnt Signaling. *J Clin Invest* (2006) 116(5):1202–9. doi: 10.1172/JCI28551
31. Kiselyov VV, Skladchikova G, Hinsby AM, Jensen PH, Kulahin N, Soroka V, et al. Structural Basis for a Direct Interaction Between FGFR1 and NCAM and Evidence for a Regulatory Role of ATP. *Structure* (2003) 11(6):691–701. doi: 10.1016/s0969-2126(03)00096-0
32. Liu R, Shi Y, Yang HJ, Wang L, Zhang S, Xia YY, et al. Neural Cell Adhesion Molecule Potentiates the Growth of Murine Melanoma Via β-Catenin Signaling by Association With Fibroblast Growth Factor Receptor and Glycogen Synthase Kinase-3β. *J Biol Chem* (2011) 286(29):26127–37. doi: 10.1074/jbc.M111.237297
33. Wang Z, Dai X, Chen Y, Sun C, Zhu Q, Zhao H, et al. MiR-30a-5p is Induced by Wnt/beta-catenin Pathway and Promotes Glioma Cell Invasion by Repressing NCAM. *Biochem Biophys Res Commun* (2015) 465(3):374–80. doi: 10.1016/j.bbrc.2015.08.007
34. Guntur AR, Rosen CJ. The Skeleton: A Multi-Functional Complex Organ: New Insights Into Osteoblasts and Their Role in Bone Formation: The Central Role of PI3Kinase. *J Endocrinol* (2011) 211(2):123–30. doi: 10.1530/JOE-11-0175
35. Gaur T, Lengner CJ, Hovhannisyan H, Bhat RA, Bodine PV, Komm BS, et al. Canonical WNT Signaling Promotes Osteogenesis by Directly Stimulating Runx2 Gene Expression. *J Biol Chem* (2005) 280(39):33132–40. doi: 10.1074/jbc.M500608200
36. Fujita T, Azuma Y, Fukuyama R, Hattori Y, Yoshida C, Koida M, et al. Runx2 Induces Osteoblast and Chondrocyte Differentiation and Enhances Their Migration by Coupling With PI3K-Akt Signaling. *J Cell Biol* (2004) 166(1):85–95. doi: 10.1083/jcb.200401138
37. Nishio Y, Dong Y, Paris M, O'Keefe RJ, Schwarz EM, Drissi H. Runx2-mediated Regulation of the Zinc Finger Osterix/Sp7 Gene. *Gene* (2006) 372:62–70. doi: 10.1016/j.gene.2005.12.022
38. Goldring SR, Goldring MB. Changes in the Osteochondral Unit During Osteoarthritis: Structure, Function and Cartilage-Bone Crosstalk. *Nat Rev Rheumatol* (2016) 12(11):632–44. doi: 10.1038/nrrheum.2016.148
39. Wang CJ, Huang CY, Hsu SL, Chen JH, Cheng JH. Extracorporeal Shockwave Therapy in Osteoporotic Osteoarthritis of the Knee in Rats: An Experiment in Animals. *Arthritis Res Ther* (2014) 16(4):R139. doi: 10.1186/ar4601
40. Calvo E, Castaneda S, Largo R, Fernandez-Valle ME, Rodriguez-Salvanes F, Herrero-Beaumont G. Osteoporosis Increases the Severity of Cartilage Damage in an Experimental Model of Osteoarthritis in Rabbits. *Osteoarthr Cartil* (2007) 15(1):69–77. doi: 10.1016/j.joca.2006.06.006
41. Stewart A, Black A, Robins SP, Reid DM. Bone Density and Bone Turnover in Patients With Osteoarthritis and Osteoporosis. *J Rheumatol* (1999) 26(3):622–6.

Conflict of Interest: The authors declare that the research was conducted in the absence of any commercial or financial relationships that could be construed as a potential conflict of interest.

frontiers in Endocrinology

ORIGINAL RESEARCH
published: 26 August 2021
doi: 10.3389/fendo.2021.726182

Age-Influenced Receptors of Advanced Glycation End Product Overexpression Associated With Osteogenic Differentiation Impairment in Patients With Type 2 Diabetes

Mattabhorn Phimphilai[1]*, *Peraphan Pothacharoen*[2] *and Prachya Kongtawelert*[2]

[1] Division of Endocrinology, Department of Internal Medicine, Faculty of Medicine, Chiang Mai University, Chiang Mai, Thailand, [2] Thailand Excellence Center for Tissue Engineering and Stem Cells, Department of Biochemistry, Faculty of Medicine, Chiang Mai University, Chiang Mai, Thailand

OPEN ACCESS

Edited by:
Guillaume Mabilleau,
Université d'Angers, France

Reviewed by:
Philip C. Trackman,
The Forsyth Institute, United States
Armando Rojas,
Catholic University of the Maule, Chile

***Correspondence:**
Mattabhorn Phimphilai
mphimphi@hotmail.com

Specialty section:
This article was submitted to Bone Research, a section of the journal Frontiers in Endocrinology

Received: 16 June 2021
Accepted: 10 August 2021
Published: 26 August 2021

Citation:
Phimphilai M, Pothacharoen P and Kongtawelert P (2021) Age-Influenced Receptors of Advanced Glycation End Product Overexpression Associated With Osteogenic Differentiation Impairment in Patients With Type 2 Diabetes. Front. Endocrinol. 12:726182. doi: 10.3389/fendo.2021.726182

Preclinical studies have found impaired osteogenic differentiation to be associated with type 2 diabetes (T2DM), which is related to skeletal accumulation of advanced glycation end products (AGEs). Our previous study also showed impaired osteogenic differentiation in peripheral blood-derived mononuclear cells (PBMC) isolated from patients with long-standing T2DM, which is conceivably due to the overexpression of receptor of advance glycation end products (RAGE) and the enhancement of cellular apoptosis. However, the existence of RAGE overexpression in earlier stages of diabetes remains unclear, as do the factors influencing that RAGE overexpression. This cross-sectional study enrolled 40 patients with T2DM treated with metformin monotherapy and 30 age-matched non-diabetic controls (NDM) to investigate the overexpression of RAGE in PBMC derived from patients with earlier stage diabetes, as well as to explore its determining factors. Almost all (90%) PBMC-isolated from NDM (NDM-pD) expressed osteoblast-specific genes including *ALPL*, *BGLAP*, *COL1A1*, and *RUNX2/PPAR* while only 40% of PBMC-derived from diabetic patients (DM-pD) expressed those genes. By using age- and pentosidine-matched NDM-pD as a reference, *AGER* and *BAX/BCL2* expression in PBMC isolated from diabetic patients showing impaired osteoblast-specific gene expression (DM-iD) were 6.6 and 5 folds higher than the reference while *AGER* and *BAX/BCL2* expression in DM-pD were comparable to the reference. *AGER* expression showed a significant positive correlation with age (r=0.470, p=0.003). The multivariate analysis demonstrated that both age and *AGER* expression correlated with the potential for osteogenic differentiation in the PBMC isolated from patients with diabetes. In conclusion, this study showed osteogenic differentiation impairment in approximately half of PBMC derived from type 2 diabetic patients receiving metformin monotherapy. Both *AGER* and *BAX/BCL2* overexpression were demonstrated only in PBMC-isolated from diabetic patients with poor osteogenic differentiation. Therefore, this study not only illustrated the existence of RAGE

overexpression in PBMC derived from patients with early stages of T2DM but also strengthened the linkage between that RAGE overexpression and the retardation of osteogenic differentiation. Age was also shown to be a positive influencing factor for RAGE overexpression. Furthermore, both age and RAGE overexpression were demonstrated as independent risk factors for determining osteogenic differentiation potential of the PBMC-isolated from T2DM.

Keywords: advanced glycation end products, receptor of advanced glycation end products, osteogenic differentiation, peripheral blood derived mononuclear cells, type 2 diabetes

INTRODUCTION

Type 2 diabetes (T2DM) is a major health issue worldwide. It is a metabolic disorder characterized by insulin resistance and chronic hyperglycemia, contributing to multiple devastating microvascular and macrovascular complications. It is well documented that chronic hyperglycemia accelerates the accumulation of advanced glycation end products (AGEs) (1–3). These are non-enzymatic modifications of proteins which usually slowly accumulate in long-lived substrates in aging animals (4) and humans (5, 6). The accumulation of AGEs is one of the main mechanisms linking hyperglycemia and the chronic microvascular and macrovascular complications which develop in cases of diabetes (7–9).

T2DM is associated with a decrease in bone turnover (10, 11), changes in bone microarchitecture (12) and increases in the risk of fragility fractures (13–18) with a preserved bone mineral density (15, 16, 18). These indicate an adverse effect of diabetes on bone quality. Furthermore, the risk of fragility fractures increases with poorer glycemic control (19–21), suggesting an impact of hyperglycemia on fragility fractures, the most serious complication of osteoporosis. The skeletal accumulation of AGEs, which is accelerated in the presence of hyperglycemia, may contribute to those phenomena in diabetic patients. The non-enzymatic glycation of type 1 collagen of the bone competes with the enzymatic collagen crosslinking, yielding a skeletal accumulation of AGEs such as pentosidine. Multiple preclinical studies have demonstrated that the accumulation of AGEs altered the mechanical properties of bone (22–24) and interferes with the functions of bone cells including osteoblasts (25–30). In clinical studies Furst and colleagues (31) demonstrated an inverse correlation between skin AGE accumulation and bone material strength in patients with T2DM. Furthermore, a positive correlation has been shown between serum pentosidine and vertebral fractures (32–34). In contrast, an endogenous secretory receptor of AGE (esRAGE), a neutralizing molecule of AGE, showed a negative correlation with vertebral fractures in T2DM (34, 35).

AGEs act *via* binding to their specific receptor, the receptor of AGE (RAGE). Following binding with AGEs, RAGEs initiate multiple signal cascades including inflammatory and apoptotic pathways. Several *in vitro* studies in osteoblast lineage cells have demonstrated that AGEs-dependent RAGE activation inhibited osteoblast differentiation (36–39) and enhanced osteoblast apoptosis (25, 28, 39, 40). In our previous study in human subjects with T2DM, impaired osteogenic differentiation and enhanced cellular apoptotic signals were demonstrated, both of which are possibly linked to cellular RAGE overexpression in individuals with T2DM (41).

Our previous study illustrated higher *AGER* expression in peripheral-blood derived mononuclear cells (PBMC)-isolated from patients with long-standing T2DM compared to those in a matched non-diabetic control group, suggesting higher cellular RAGE activation in individuals with long-standing T2DM (41). Moreover, the cellular RAGE overexpression was positively associated with enhanced cellular apoptotic signals and then was potentially involved in the impairment of osteogenic differentiation potential of the cells (41). However, the existence of cellular RAGE overexpression in earlier stages of diabetes remains to be elucidated, as do the factors influencing that RAGE overexpression. It is known that the peripheral blood-derived mesenchymal stem cells can differentiate into multiple cell types, including adipocytes, chondrocytes and osteoblasts (42–44). Our previous study also showed the osteogenic differentiation potential of the PBMC-isolated from both healthy volunteers and patients with T2DM (41). To determine osteogenic differentiation of stem cells using the least invasive measures, this study was conducted using PBMC-derived from participants to investigate: 1) the osteogenic differentiation potential of PBMC-isolated from T2DM patients receiving metformin monotherapy, 2) the existence of cellular RAGE overexpression and the effects of that RAGE overexpression on osteogenic differentiation and cellular apoptotic signals, and 3) factors influencing that cellular RAGE overexpression.

MATERIALS AND METHODS

Ethical Statements

This study was a cross-sectional study, performed at Maharaj Nakorn Chiang Mai Hospital, Chiang Mai University, Chiang Mai, Thailand. The study was approved by the Research Ethics Committee of the Faculty of Medicine, Chiang Mai University (MED-2557-02609). All participants signed an informed consent agreement before they were enrolled on the study.

Study Population and Sample Collection

Metformin is the first-line medication recommended for treatment of T2DM by the majority of international guidelines. In Thailand, metformin monotherapy is mostly used as initial therapy for

patients with T2DM. Therefore, in this study, T2DM patients taking metformin monotherapy were enrolled to be representative of early-stage diabetes. Age-matched non-diabetic individuals were enrolled as a control group. The exclusion criteria were as follows: females with serum creatinine higher than 1.4 mg/dL or males with serum creatinine above 1.5 mg/dL; individuals who use thiazolidinedione, steroids, immunosuppressive agents, anti-resorptive agents or anabolic agents for osteoporosis, and individuals with metastatic or hematologic malignancy. Venous blood (35-40 mL) was collected from all enrolled participants to isolate the PBMC, and to determine serum levels of pentosidine (Elabscience Biotechnology, WuHan, Hubei, China) and sRAGE (R&D, Minneapolis, MN, USA). Fasting plasma glucose (FPG), glycated hemoglobin (HbA1c), low-density lipoprotein cholesterol (LDL-C) and serum creatinine were assessed using standardized procedures at a central laboratory of the Faculty of Medicine, Chiang Mai University. Glomerular filtration rate (eGFR) was calculated using the Chronic Kidney Disease Epidemiology Collaboration (CKD-EPI) method. Fracture risk estimation was estimated from The Fracture Risk Assessment Tool (FRAX®) using the Thailand database (45).

Isolation and Culture of Human Peripheral Blood-Derived Mononuclear Cells (PBMC)

PBMC were isolated from the 35-40 mL of peripheral venous blood using density gradient centrifugation as described in our previous study (41). In brief, the venous blood was centrifuged at 1500 rpm for 5 minutes. After plasma was removed, the remaining fraction was first diluted with an equal volume of DMEM (Gibco, Grand Islands, NY, USA) and then overlaid on Histopaque (specific gravity 1.077 g/mL; Sigma-Aldrich, St Louis, MO, USA) and finally centrifuged at 4000 rpm for 30 minutes. The PBMC were isolated from the mononuclear cell layer and plated in 24-well culture plates. These were then cultured in RPMI supplemented with 10% (v/v) fetal bovine serum (Gibco, Grand Islands, NY, USA). After removing the floating cells, the plastic-adhered cells were cultured in DMEM supplemented with 10% (v/v) fetal bovine serum (Gibco, Grand Islands, NY, USA), called non-osteogenic-inducing medium in the present study, for 7-10 days until confluence. To induce osteogenic differentiation, the plastic-adhered cells were cultured in non-osteogenic-inducing medium until reaching 50% confluence. They were then changed to an osteogenic-inducing medium (DMEM supplemented with 10^{-7} M dexamethasone, 60 μM ascorbic acid and 10 mM β-glycerophosphate) and cultured for a further 21 days.

Analysis for the Expression of Osteoblast-Specific Genes, *AGER*, and Cellular Apoptotic-Associated Genes

To examine gene expression total RNA was extracted using the illutraRNA spin Mini Kit (GE Healthcare Life Science, Buckinghamshire, UK) in accordance with the manufacturer's instructions. Total RNA (500 ng) of each sample was used for reverse transcription into cDNA using an iScript™cDNA Synthesis Kit (Bio-Rad, Hercules, CA, USA) in accordance with the manufacturer's protocol. Afterwards, the cDNA was analyzed by real-time quantitative polymerase chain reaction (real-time qPCR)(SsoFast EvaGreen Supremixes; Bio-Rad, Hercules, CA, USA). The reaction took place at 45 cycles of 5 seconds at 95°C, 10 seconds at 60°C and 30 seconds at 72°C using the Applied Biosystems 7500/7500 Fast Real-Time PCR system. The total RNA extracted from the PBMC, cultured both in non-osteogenic and osteogenic-inducing media, was used to determine: 1) osteoblast-specific genes including *ALPL, BGLAP, COL1A1* and *RUNX2* for representing osteoblast differentiation and 2) *PPAR-γ* which is a transcription factor driving towards adipocytes for evaluating signals against osteoblast differentiation. Differentiation towards osteoblasts was defined by the increment of expression of all osteoblast-specific marker genes including *ALPL*, *BGLAP* and *COL1A1*, as well as the increment of the *RUNX2/PPARγ*ratio. In contrast, the total RNA extracted only from the PBMC cultured in the non-osteogenic-inducing medium was used to determine: 1) *AGER* expression to elucidate cellular RAGE overexpression, and 2) *BAX* and *BCL2* expression for the evaluation of cellular apoptotic signals. The primers were purchased from Invitrogen (**Table 1**). In the real-time qPCR, the *GAPDH* gene was used for normalization of the relative expression levels for each primer set by the $2^{(-\Delta\Delta CT)}$ method.

Statistical Analysis

All descriptive data are reported as mean ± standard deviation. An independent *t*-test was used to compare all continuous parameters while a Chi square test was used to compare binary parameters. Linear regression analysis was used to demonstrate factors

TABLE 1 | Sequences of real-time qPCR primers.

Genes	Primer sequence (5'-3')	
	Forward	Reverse
ALPL	CATGGCTTTGGGCAGAAGGA	CTAGCCCCAAAAAGAGTTGCAA
AGER	GCTGGAATGGAAACTGAACACAGG	TTCCCAGGAATCTGGTAGACACG
BAX	TGGAGCTGCAGAGGATGATTG	GAAGTTGCCGTCAGAAAACATG
BCL2	CATGCTGGGGCCGTACAG	GAA CCGGCACCTGCACAC
BGLAP	GAAGCCCAGCGGTGCA	CACTACCTCGCTGCCCTCC
COL1A1	CAGCCGCTTCACCTACAGC	TTTTGTATTCAATCACTGTCTTGCC
GAPDH	CCCTTCATTGACCTCAACTA	AGATGATGACCCTTTTGGCT
PPARγ	AAAGAAGCCAACACTAAACC	CTTCCATTACGGAGAGATCC
RUNX2	TCTTAGAACAAATTCTGCCCTTT	TGCTTTGGTCTTGAAATCACA

correlating with osteoblast differentiation. Pearson's correlation was used to identify the correlation between parameters, the exception being the correlation between *AGER* expression and other parameters which was done using Spearman's correlation. A *p*-value of less than 0.05 was used as a measure of statistical significance. All statistical analyses were done with SPSS version 23.0.

RESULTS

Demographic Data and Clinical Characters of Study Participants

The study included 40 patients with T2DM treated with metformin monotherapy (DM) and 30 age-matched participants without diabetes (NDM). All patients with T2DM were diagnosed as DM using the FPG criteria with a cut-off value of 126 mg/dL as recommended by the American Diabetes Association. Age, gender, body mass index (BMI), systolic blood pressure (SBP), diastolic blood pressure (DBP), LDL-C, eGFR, and 10-year fracture risk as determined by FRAX® were comparable in both NDM and DM groups (**Table 2**). With comparable levels of blood pressure in both DM and NDM groups, the usage rates of anti-hypertensive agents, including angiotensin-converting enzyme inhibitors (ACEI), angiotensin II receptor blockers (ARB), dihydropyridine calcium channel blockers (DHP-CCB) and thiazide-like diuretics, were higher in DM group than in NDM group. With comparable levels of LDL-C in both groups, the rate of statin use was higher in DM group than in NDM group. However, the difference in anti-hypertensive drugs and statins usage rates did not reach statistical significance (**Table 2**). Metformin was not applicable to NDM group. In the group with diabetes, the duration of diabetes was 5.5 ± 4.1 years with a 47.5% prevalence of microvascular complications and 10% prevalence of macrovascular complications. Metformin was the only anti-hyperglycemic agent used in all diabetic participants with a dosage of 1652.5 ± 627.4 mg/day. Both FPG and HbA1c levels were significantly higher in the DM group than those in NDM (**Table 2**). Serum pentosidine was significantly elevated in DM compared to that in NDM (6.1 ± 3.6 ng/mL vs 4.0 ± 2.1 ng/mL, p=0.03), suggesting accelerated AGEs accumulation in T2DM (**Table 2**). In contrast to pentosidine, serum sRAGE, a decoy receptor of AGEs, was comparable in both DM and NDM groups (527.1 ± 249.7 pg/mL vs 599.4 ± 422.1 pg/mL, p=0.374). Even though FPG, HbA1c and serum pentosidine levels were significantly higher in DM than in NDM group, serum pentosidine level showed no correlation with either FPG (r=0.065, p =0.598) or HbA1c (r=0.062, p=0.668). In addition, serum pentosidine level showed no correlation with other parameters, including age, BMI, eGFR and sRAGE level. Fracture risk as estimated by FRAX using the Thailand database was comparable between DM and NDM groups (**Table 2**).

Age Was an Independent Risk Factor for Preserving Osteogenic Differentiation Potential in Type 2 Diabetes

The PBMC-derived from diabetic patients showed a reduced potential to differentiate towards osteoblasts compared with those from non-diabetic controls. By using osteoblast-specific

TABLE 2 | Clinical characteristics of the study participants.

Parameter	NDM (n = 30)	DM (n = 40)	*p*-value
Demographic data			
Age (years)	59.7 ± 7.7	58.1 ± 6.8	0.355
Gender (% female)	63.3	60.0	0.487
BMI (kg/m²)	24.6 ± 3.9	25.8 ± 4.3	0.269
SBP (mmHg)	130.8 ± 13.1	129.1 ± 11.8	0.553
DBP (mmHg)	78.9 ± 9.8	75.5 ± 9.4	0.150
FPG (mg/dL)	95.8 ± 9.6	138.6 ± 26.0	<0.0001
HbA1c (%)	5.9 ± 0.50	7.5 ± 0.9	<0.0001
LDL-C* (mg/dL)	111.4 ± 31.3	100.5 ± 42.4	0.222
DM duration (years)	–	5.5 ± 4.1	–
Metformin dosage (mg/day)	–	1652.5 ± 627.4	–
Other drugs (% use)			
•ACEI or ARB**	44.8	67.5	0.084
•DHP-CCB#	51.7	57.5	0.807
•Thiazide-like diuretic	13.8	20.0	0.749
•Statins	66.7	79.5	0.275
Microvascular complications (%)	–	47.5	–
eGFR (ml/min)	86.8 ± 14.3	85.5 ± 17.0	0.745
Macrovascular complications (%)	–	10.0	–
FRAX: 10-year risk of hip fractures (%)	0.7 ± 0.9	0.5 ± 0.9	0.399
FRAX: 10-year risk of osteoporotic fractures (%)	3.4 ± 2.0	2.7 ± 1.8	0.166
Serum markers			
Pentosidine (ng/mL)	4.0 ± 2.1	6.1 ± 3.6	0.030
Soluble RAGE (pg/mL)	599.4 ± 422.1	527.1 ± 249.7	0.374

**LDL-C, low-density lipoprotein cholesterol; **ACEI, angiotensin-converting enzyme inhibitors; **ARB, angiotensin II receptor blockers; #DHP-CCB, dihydropyridine calcium channel blockers.*

gene expression as a marker for osteogenic differentiation potential, the isolated PBMC from DM were divided into 2 groups including DM with preserved osteogenic differentiation potential (DM-pD) and DM with impaired osteogenic differentiation potential (DM-iD). Forty percent (16/40) of the PBMC-isolated from diabetic patients showed expression of osteoblast-specific genes including *ALPL*, *BGLAP*, *COL1A1* and *RUNX2/PPAR*; therefore, the isolated-PBMC in this group were classified as DM-pD. The other 60% (24/40) of PBMC-isolated from DM did not express those osteoblast-specific genes, so the isolated-PBMC in this group were classified as DM-iD. While almost all the isolated PBMC from NDM expressed osteoblast-specific genes (NDM-pD), only 40% of the isolated PBMC from DM expressed osteoblast-specific genes (DM-pD) (90% *vs* 40%; $p<0.0001$). As shown by the *RUNX2/PPAR* ratio, the PBMC-derived from DM-pD expressed *RUNX2*, a master transcription factor for osteogenic differentiation, and *PPARγ*, a transcription factor driving differentiation against osteoblasts, at a similar extent to that of NDM-pD but at 3.8 times higher than that of DM-iD (**Figure 1**). Moreover, the PBMC-isolated from DM-pD showed the expression of *ALPL*, *COL1A1* and *BGLAP* to be comparable to those of NDM-pD but at 7.3, 5.9, and 4.3 times higher than those of DM-iD (**Figure 1**). Factors determining osteoblast differentiation were analyzed in both NDM and DM groups. The multivariate analysis demonstrated that being diabetic is the only factor determining differentiation towards osteoblasts. Being diabetic increased the risk of osteogenic differentiation impairment 13.5 times (OR 13.5; 95% CI 3.21-77.91; $p<0.001$).

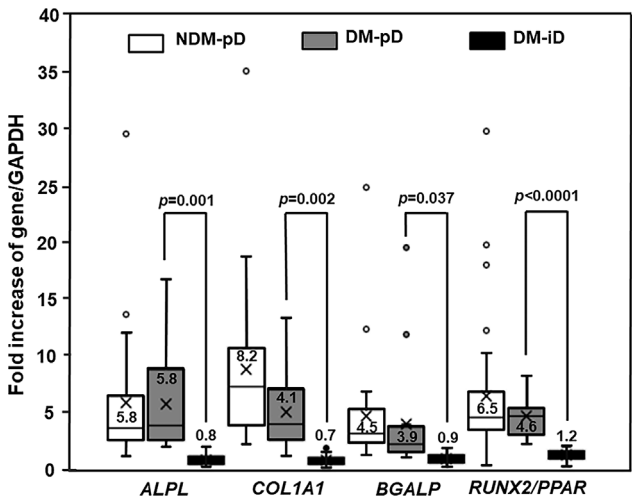

FIGURE 1 | Osteogenic differentiation marker expression. Box and whisker plots to show comparison of osteoblast-specific gene expression in participants without diabetes showing preserved osteogenic differentiation potential (NDM-pD), patients with diabetes showing preserved osteogenic differentiation potential (DM-pD) and patients with diabetes showing impaired osteogenic differentiation potential (DM-iD)(mean ± SD). DM-pD had higher levels of expression of ALPL, COL1A1, BGLAP and RUNX2/PPARγ ratio (RUNX2/PPAR) than those in DM-iD by 7.3, 5.9, 4.3 and 3.8 times, respectively. DM-pD had significantly higher levels of expression of all osteoblast-specific genes than those in DM-iD but had comparable levels of expression of all osteoblast-specific genes to those in NMD-pD.

Forty percent of the PBMC-isolated from diabetic patients demonstrated a similar level of osteoblast-specific gene expression compared to those from non-diabetic individuals, indicating the preservation of osteogenic differentiation potential only in some individuals with type 2 diabetes. We next determined the factors influencing the preservation of osteogenic differentiation potential in the PBMC-derived from diabetic patients. Ten percent of PBMC-isolated from non-diabetic controls (3/30) which did not express osteoblast-specific genes, was excluded from the following analysis. When comparing DM-pD and NDM-pD, patients in the DM-pD group had significantly higher FPG (137.7 ± 30.2 mg/dL *vs* 96.1 ± 9.4 mg/dL, $p<0.0001$), HbA1c (7.5 ± 1.1% *vs* 6.0 ± 0.4%, $p<0.0001$) and serum pentosidine (7.3 ± 4.7 ng/mL *vs* 3.7 ± 1.8 ng/mL, $p=0.008$) than those in the NDM-pD group (**Table 3**). In addition, individuals with DM-pD were younger (54.4 ± 3.2 years *vs* 59.7 ± 7.9 years, $p=0.004$) than those in NDM-pD group (**Table 3**). When comparing within diabetic groups, FPG (137.7 ± 30.2 mg/dL *vs* 139.2 ± 23.49, $p=0.859$) and HbA1c (7.5 ± 1.1% *vs* 7.5 ± 0.86%, $p=0.963$) were comparable in both DM-pD and DM-iD groups. Serum pentosidine level was slightly higher in DM-pD in comparison to those in DM-iD group (7.3 ± 4.7 ng/mL *vs* 5.2 ± 2.53 ng/mL, $p=0.120$); however, the difference did not reach statistical significance (**Table 3**). Because FPG, HbA1c and serum pentosidine level were comparable between DM-pD and DM-iD, those factors should not influence the maintenance of osteogenic differentiation ability in cases of diabetes. There were also no differences in other parameters between DM-pD and DM-iD, including BMI, SBP, DBP, duration of being diabetic, the dosage of metformin, the usage rate of anti-hypertensive agents and statins, LDL-C and eGFR (**Table 3**). In contrast, age showed significant differences between DM-pD and DM-iD. Individuals in DM-iD were older than those in DM-pD group (60.5 ± 7.4 years *vs* 54.4 ± 3.2 years, $p=0.001$) but were at the same age as those in NDM-pD (60.5 ± 7.4 years *vs* 59.7 ± 7.9 years, $p=0.701$) (**Table 3**). The multivariate analysis demonstrated that age correlated with the potential for osteogenic differentiation in the PBMC-isolated from patients with diabetes, indicating that age is an independent risk factor for determining the differentiation potential toward osteoblasts of the PBMC-isolated from individuals with T2DM. Therefore, younger age was a protective factor for the preservation of osteoblast differentiation potential in T2DM.

AGER Overexpression Was Associated With Enhanced Cellular Apoptotic Signals and Impaired Osteogenic Differentiation, and Was Influenced by Age

Our previous study demonstrated higher *AGER* expression in patients with long-standing type 2 diabetes compared to that in non-diabetic controls, as well as the association of that RAGE overexpression with cellular apoptotic signal enhancement and osteogenic differentiation impairment. In this study, we analyzed PBMC isolated from 40 diabetic participants with metformin-monotherapy and 27 non-diabetic participants showing

TABLE 3 | Factors determining osteogenic differentiation in type 2 diabetes.

Parameters	NDM-pD (n=27)	DM-pD (n=16)	*p*-value*	DM-iD (n=24)	*p*-value#
Age (years)	59.7 ± 7.9	54.4 ± 3.2	0.004	60.5 ± 7.4	0.001
BMI (kg/m²)	25.2 ± 3.2	25.7 ± 4.6	0.705	25.8 ± 4.1	0.953
FPG (mg/dL)	96.1 ± 9.4	137.7 ± 30.2	<0.0001	139.2 ± 23.4	0.859
HbA1c (%)	6.0 ± 0.4	7.5 ± 1.1	<0.0001	7.5 ± 0.8	0.963
LDL-C (mg/dL)	107.9 ± 28.9	96.1 ± 32.9	0.249	103.4 ± 48.1	0.601
DM duration (years)	–	5.1 ± 3.3	–	5.8 ± 4.6	0.615
Metformin dosage (mg/day)	–	1709.4 ± 655.3	–	1614.6 ± 619.3	0.646
Other drugs (% use)					
•ACEI or ARB**	46.2	75.0	0.109	62.5	0.503
•DHP-CCB##	50.0	50.0	1.000	62.5	0.522
•Thiazide-like diuretics	15.4	18.8	1.000	20.8	1.000
•Statins	70.3	81.3	0.494	78.2	1.000
Microvascular complications (%)	–	50.0		45.8	0.796
Macrovascular complications (%)	–	6.3		12.5	0.519
eGFR (ml/min)	86.3 ± 14.9	89.9 ± 12.6	0.442	82.6 ± 19.1	0.156
Pentosidine (ng/mL)	3.7 ± 1.8	7.3 ± 4.7	0.008	5.2 ± 2.5	0.120
sRAGE (pg/mL)	597.1 ± 422.4	519.1 ± 281.6	0.516	532.4 ± 232.2	0.871

**comparison between NDM-pD and DM-pD; #comparison between DM-pD and DM-iD.*
***ACEI, angiotensin-converting enzyme inhibitors; **ARB, angiotensin II receptor blockers.*
##DHP-CCB, dihydropyridine calcium channel blockers.

osteogenic differentiation (NDM-pD) to explore whether there was: 1) cellular RAGE overexpression in early-stage diabetes, 2) an association between RAGE overexpression with cellular apoptotic signal enhancement and osteogenic differentiation impairment, and 3) factors influencing cellular RAGE overexpression.

Since pentosidine has been documented in other studies as being an *AGER* enhancer, and age was confirmed earlier as an independent risk factor for the determination of osteogenic differentiation potential, the expression of *AGER* in both DM-iD and DM-pD was compared with the level of *AGER* expression in age- and pentosidine-matched NDM-pD individuals. This comparison aimed to explore if there was only a higher level of *AGER* expression in DM-iD, which would in turn suggest a link between cellular RAGE overexpression and defects in osteogenic differentiation. Using NDM-pD as a reference group, *AGER* expression in DM-iD was 6.6 times higher than that in the reference while the *AGER* expression in DM-pD was comparable to that in the reference (**Figure 2**). The *AGER* expression in DM-iD was significantly higher than that in DM-pD (6.6-fold *vs* 0.7-fold, $p<0.0001$), suggesting cellular RAGE overexpression in DM-iD as well as a connection between that RAGE overexpression and osteogenic differentiation defects in the PBMC. Consistent with higher *AGER* expression, the *BAX/BCL2* expression ratio in DM-iD was 5.0 times higher than that in the reference while the *BAX/BCL2* expression ratio in DM-pD was comparable to that in the reference (**Figure 2**). The *BAX/BCL2* expression ratio in DM-iD was also significantly higher than in DM-pD (5.0-fold *vs* 0.6-fold, $p=0.003$), suggesting higher cellular apoptotic rate only in cases of diabetes with impaired osteogenic differentiation ability. Furthermore, *AGER* expression showed a strongly positive correlation with the *BAX/BCL2* expression ratio (r=0.735, $p<0.001$), but showed a negative correlation with multiple osteoblast-specific gene expression including *ALPL* (r= -0.757, $p<0.001$), *BGLAP* (r= -0.670, $p<0.001$), *COL1A1* (r= -0.478, $p=0.003$) and *RUNX2/PPARγ* ratio (r= -0.770, $p<0.001$) (**Table 4**). These association analyses suggest a direct relationship between cellular RAGE overexpression and cellular apoptotic signals, as well as an inverse relationship between cellular RAGE overexpression and osteogenic differentiation ability in the PBMC derived from diabetic

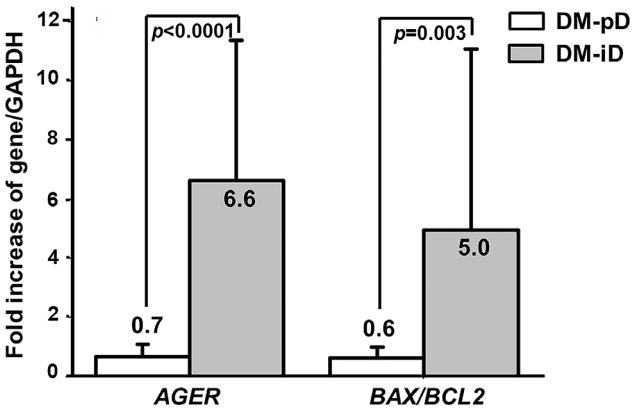

FIGURE 2 | The expression of AGER, BAX and BCL2 genes. Comparison of the expression of the AGER, and BAX/BCL2 ratio between PBMC-isolated from subjects with diabetes with preserved osteogenic differentiation potential (DM-pD) and PBMC-isolated from diabetics with impaired osteogenic differentiation potential (DM-iD) by using age- and pentosidine-matched PBMC-isolated from non-diabetics with preserved osteogenic differentiation (NDM-pD) as a reference group. DM-iD showed higher expression of AGER and BAX/BCL2 ratio than the reference by 6.6 and 5.0 times, respectively, while DM-pD showed similar expression of AGER and BAX/BCL2 ratio to the reference. The expression of AGER and BAX/BCL2 ratio in DM-iD was significantly higher than that in DM-pD.

TABLE 4 | Factors associated with *AGER* expression.

Parameter	*r*	*p*-value
Demographic parameters		
Age (years)	0.470	0.003
BMI (kg/m²)	0.042	0.807
DM duration (years)	0.052	0.769
Serum markers		
FPG (mg/dL)	-0.002	0.988
HbA1c (%)	-0.111	0.512
Pentosidine (ng/mL)	-0.039	0.819
sRAGE (pg/mL)	0.082	0.629
Gene expression		
BAX/BCL2 ratio	0.735	<0.001
ALPL	-0.757	<0.0001
BGALP	-0.670	<0.0001
COL1A1	-0.478	0.003
RUNX2/PPARγ ratio	-0.770	<0.0001

patients. Interestingly, *AGER* expression showed a positive correlation with age (r=0.470, p=0.003) (**Table 4**), suggesting that age influences cellular RAGE overexpression.

DISCUSSION

This study demonstrated the preservation of osteogenic differentiation in 40% of PBMC-derived from type 2 diabetic patients who have had diabetes for an average of 5 years and are being treated with metformin monotherapy. Higher *AGER* expression was demonstrated only in PBMC-isolated from diabetics with poor osteogenic differentiation. This study not only demonstrated the existence of cellular RAGE overexpression in early stages of type 2 diabetes but also strengthened the link between that cellular RAGE overexpression and osteogenic differentiation retardation. This study also provided evidence to suggest that cellular RAGE overexpression increased with age. In addition, age and *AGER* expression were shown to be independent risk factors determining osteogenic differentiation potential of the PBMC-derived from T2DM.

In animal models with T2DM, a dramatic decrease in osteoblast/osteoid surface and bone mineral apposition rate has been demonstrated which indicates osteoblast differentiation and function impairment (46). Consistent with findings from animal studies, a reduction in osteoblast/osteoid surface, osteoid volume and thickness, which indicates a low bone formation state, has also been shown in humans with T2DM (10, 11, 47). Our previously study also demonstrated an impairment in osteogenic differentiation of the PBMC-isolated from long-standing type 2 diabetic patients (41). In agreement with previous studies, the present study illustrated impaired osteogenic differentiation in cases of type 2 diabetes. In the multivariate analysis, being diabetic significantly increased the risk of osteogenic differentiation impairment by 13.5 times (OR 13.5; 95% CI 3.21-77.91; p<0.001). In this study, 40% of cells from diabetic patients expressed osteoblast differentiation markers to a similar extent of those in non-diabetic individuals, suggesting a preserved potential of osteogenic differentiation only in some of the population among the whole diabetic group. Even though being diabetic increases the risk of osteogenic differentiation defects, diabetes at the different stages may have different degrees of that defect. Our previous study, which included long-standing type 2 diabetic subjects with an average of 10.7 ± 7.7 years of diagnosis, demonstrated that only 7.3% of PBMC-isolated from these diabetic patients expressed osteoblast-specific genes while 86.7% in non-diabetic controls expressed those genes (7.3% *vs* 86.7%, p<0.0001) (41). However, the present study was carried out with cells from patients at an earlier stage of diabetes with an average of 5.5 ± 4.1 years of diagnosis and showed that 40% of PBMC-isolated from diabetic subjects expressed osteoblast-specific genes while 90% in non-diabetic controls expressed those genes (40% *vs* 90%, p<0.0001). The present study showed a much higher number of PBMC with preserved osteogenic differentiation potential than those in the previous study which was done at a later stage of diabetes. However, it remains to be elucidated whether newly diagnosed type 2 diabetes still results in an impaired osteogenic differentiation.

Our previous study demonstrated cellular RAGE overexpression in type 2 diabetes which may lead to higher cellular apoptosis and poorer differentiation toward osteoblasts in T2DM. Because most PBMC-isolated from diabetic patients lose their ability to differentiate into osteoblasts, no firm conclusion can be made regarding the influence of cellular RAGE overexpression shown in type 2 diabetes on cellular apoptosis and the poorer differentiation found in type 2 diabetes. In this study, we focused on the earlier stage of diabetes and we demonstrated that only 60% (24/40) of the PBMC-isolated from diabetic patients lose their osteogenic differentiation potential (DM-iD). Therefore, we had the opportunity to explore whether there was only cellular RAGE overexpression in PBMC-isolated from diabetic patients showing impaired osteogenic differentiation. As pentosidine is an *AGER* enhancer and age is an independent risk factor for determining osteogenic differentiation as described above, *AGER* expression in an age- and pentosidine-matched NDM-pD group was used as a reference to compare the level of *AGER* expression between DM-iD and DM-pD for determining whether higher cellular *AGER* expression occurred only in the DM-iD group. Interestingly, higher *AGER* expression was demonstrated in DM-iD group but not in DM-pD, suggesting the existence of RAGE overexpression only in PBMC with poor osteogenic differentiation ability that isolated from diabetic patients. To further explore the association between cellular apoptosis and osteogenic differentiation, *BAX* and *BCL2* expression in DM-iD and DM-pD were compared by using *BAX/BCL2* expression in an age- and pentosidine-matched NDM-pD group as a reference. As seen with *AGER* expression, the ratio of *BAX/BCL2* expression was higher only in the DM-iD group, suggesting a link between cellular apoptotic signal enhancement and osteogenic differentiation impairment. Consistent with our previous study (41), the expression of *AGER* and *BAX/BCL2* ratio showed a strong correlation with each other (r=0.735, p<0.001). Therefore, the present study not only confirmed the existence of RAGE overexpression in PBMC with poor osteogenic differentiation potential but also strengthened the link between the cellular RAGE overexpression with osteogenic differentiation impairment and cellular apoptotic signal enhancement in the PBMC-isolated from T2DM patients.

Since the hyperglycemic state in diabetes accelerates the accumulation of AGEs in various tissues including those in the skeleton, accumulation of AGEs is one of the factors proposed as being responsible for the impairment in bone quality associated with diabetes and may be a useful predictor of fracture in diabetic individuals. Several studies have shown that the skeletal accumulation of AGEs alters bone mechanical properties, leading to fragility fractures (22–24). In addition, studies in primary culture osteoblasts and mesenchymal stem cells demonstrated that AGEs attenuated osteoblast differentiation and enhanced osteoblast apoptosis (25–29). In humans, serum pentosidine showed a positive correlation with fracture risk in T2DM (32–34). In contrast, esRAGE, an AGE neutralizer, showed a negative correlation with fracture risk in T2DM (34, 35). In this study, serum pentosidine was significantly higher in the group with diabetes than that in the age-matched non-diabetic group, implying accelerated accumulation of AGEs in diabetes mellitus. However, the levels of serum pentosidine in the group of diabetics with preserved osteogenic differentiation was comparable to the group of diabetics with impaired osteogenic differentiation. Moreover, a higher cellular *AGER* expression was illustrated only in the cells from the group of diabetics with impaired osteogenic differentiation, and that higher *AGER* expression was shown to be associated with the differentiation potential toward osteoblasts. Therefore, it is conceivable that serum pentosidine level has poor potential for the prediction of osteogenic differentiation in diabetes. Nevertheless, due to a small sample size and the wide standard deviation of serum pentosidine concentration found, the results of our study cannot exclude its potential for predicting osteoblast differentiation ability.

As 40% of PBMC-isolated from the diabetic group were shown to maintain their osteogenic differentiation potential, there was a potential for the exploration of the factors determining the preservation of osteogenic differentiation ability in our present study. These factors will be valuable in future exploration for guidance of fracture prevention in type 2 diabetes. Using the results of the multivariate analysis, this study demonstrated that age was a factor showing a correlation with the osteogenic differentiation potential of the PBMC-isolated from individuals with diabetes, indicating that age is an independent risk factor for determining the differentiation potential towards osteoblasts of the PBMC in diabetics. There is a higher probability for the preservation of the osteogenic differentiation potential in the younger diabetic individuals. In addition to age, *AGER* expression was also a risk factor for determining osteogenic differentiation, suggesting the contribution of higher cellular RAGE overexpression to the potential of differentiation of the PBMC towards osteoblasts. Interestingly, this study also demonstrated a positive correlation between age and *AGER* expression. Since age was an independent risk factor for osteogenic differentiation, as well as age showing a positive correlation with *AGER* expression, age itself is conceivably a contributor to cellular RAGE overexpression which in turn negatively affects osteogenic differentiation. Son and colleagues (48) demonstrated that accumulation of tissue AGEs and AGE-RAGE binding intensity increased with age and were different in organs in a non-diabetic mice model. In the liver and kidney, AGEs progressively accumulated with age, and AGE-RAGE binding intensity also increased with age, leading to an increase in its downstream signaling cascade. To the contrary, the accumulation of AGEs and AGE-RAGE binding intensity did not increase with age in skeletal muscles. Therefore, it remains a need for further elucidation as to whether RAGE activation in the skeleton conforms to an age-dependent pattern, leading to the probability of higher RAGE activation with increasing age. If AGEs-RAGE activation in the skeleton is an age-dependent pattern, being diabetic would drive accelerated accumulation of AGEs and even perpetuate RAGE activation as individuals inevitable grow older, resulting in the accelerated impairment of bone quality and increased fragility fracture in type 2 diabetes. From the evidence shown in this study, being diabetic increased the risk of osteogenic differentiation impairment and younger age is the single protective factor identified for preservation of osteogenic differentiation in T2DM, it is pertinent to state that prevention of becoming diabetic may be the most effective way to preserve the potential for osteogenic differentiation of the PBMC.

Several different types of medication prescribed for participants in this study were shown to influence bone metabolism. Metformin was the only anti-hyperglycemia agent given to all diabetic individuals in this study and it was not taken by non-diabetic controls. Metformin has been shown to promote the differentiation of osteoblasts from mesenchymal stem cells through the activation of the AMPK pathway (49, 50). Zhou Z and colleague (51) also demonstrated that metformin suppresses AGE-dependent RAGE activation in bone marrow derived macrophages. Even though all diabetic participants in this study may get benefit from metformin therapy, this medication did not overcome the detrimental effects of diabetes on osteogenic differentiation in 60% of cases. Metformin was used at the same dosage in both DM-pD and DM-iD, suggesting that the quantity of metformin did not influence the preservation of osteogenic differentiation ability found in this study. ACEI and ARB have been previously shown to have beneficial effects on bone metabolism and fractures (52–54). Liu YY and colleagues (52) showed that captopril, a type of ACEI, promoted osteoblast differentiation of primary cultured osteoblast cells as well as enhanced bone formation and bone strength in ovariectomized rats. In human, Kao YT and colleagues (53) showed that hypertensive individuals treated with ACEI or ARB had a decreased risk of osteoporotic fracture compared to those treated with other medications. Even though the difference did not reach statistical significance, participants in diabetic group used ACEI or ARB at a higher rate than those in non-diabetic group in this study (67.5% *vs* 44.8%, p=0.084). Therefore, it is reasonable to state that ACEI and ARB do not contribute to a lower rate of osteogenic differentiation in the diabetic group. In patients with diabetes, ACEI and ARB were used in the DM-pD group at a higher rate than those in DM-iD (75% *vs* 62.5%, p=0.503); however, the difference was nowhere near statistical significance. Therefore, it is reasonable to state that ACEI or ARB usage is not a contributory factor in the maintenance of osteogenic

differentiation shown in DM-pD. Statins have been previously shown to have beneficial effects on bone metabolism and osteoporosis (55–58). Statins have been demonstrated to promote osteoblast differentiation and bone formation by stimulating the Akt/PI3 kinase and the β-catenin/Wnt signaling pathway, as well as to inhibit osteoblast apoptosis *via* activation of the TGFβ/Smad3 pathway (55). Zhang M and colleagues (56) demonstrated that simvastatin promoted differentiation of rat mesenchymal stem cells toward osteoblasts through the up-regulation of β-catenin (56). In humans, Lin TK and colleagues (57) carried out a nation-wide population cohort study to illustrate that statin use was associated with the decreased risk of osteoporosis in both females and males. In this study, participants in the diabetic group used statins at a higher rate than those in non-diabetic controls (79.5% *vs* 66.7%, p=0.275); however, the difference did not reach statistical significance. Therefore, from these findings the higher usage rate of statins in the diabetic group should not contribute to a lower rate of osteogenic differentiation in diabetic group.

This study provides evidence to support that cellular RAGE overexpression leads to osteogenic differentiation impairment in early stages type 2 diabetes, and that cellular RAGE overexpression is influenced by age. However, this evidence should be carefully interpreted due to several limitations. First, this study only demonstrated signal activation by mRNA level not protein expression due to the limited number of isolated cells from the relatively small 35-40 mL sample of peripheral blood collected from recruited patients. This raises the possibility the chance that transcription is activated but not translated into proteins. Therefore, it is probable that *AGER* overexpression will not lead to higher RAGE activation. The further studies involving RAGE knock-down would clarify whether cellular RAGE overexpression directly entail an impaired osteoblast differentiation. Second, this study presented data to show the pattern of association between parameters, so the causes and effects of those parameters cannot be definitely concluded. Finally, this study was a cross-sectional study which had several unexpected confounding factors by the nature of this type of study, for examples, *AGER* polymorphisms. Even though all baseline characters of the enrolled participants were generally comparable, those unexpected confounding factors might influence the results of the study. Multiple single nucleotide polymorphisms (SNPs) of *AGER* gene have been reported for association with diabetes and chronic diabetic complications (58–60). Cheng H and colleagues (58) showed that rs1800624 and rs2070600 SNPs associated with an increased risk of type 2 diabetes in South Asians and Caucasian, respectively. The rs1800624 SNP was documented for increasing *AGER* expression *in vitro* by enhancing the binding affinity of the transcription factor site while the rs207600 SNP was documented for enhancing the affinity of RAGE for its ligands (59). Since *AGER* polymorphism was not determined in this study, the contribution of *AGER* polymorphism to RAGE overexpression in PBMC was still possible. However, the evidence showing detrimental effects of *AGER* polymorphism on bone metabolism remains to be elucidated in cases of diabetes. To date, Raska Jr I and colleagues (60) showed that both rs1800624 and rs2070600 did not associate with sRAGE level, bone mineral density and fractures in postmenopausal women with T2DM.

DATA AVAILABILITY STATEMENT

The original contributions presented in the study are included in the article/supplementary material. Further inquiries can be directed to the corresponding author.

ETHICS STATEMENT

The studies involving human participants were reviewed and approved by the Research Ethics Committee of the Faculty of Medicine, Chiang Mai University. The patients/participants provided their written informed consent to participate in this study.

AUTHOR CONTRIBUTIONS

MP was involved in conceptualization, funding acquisition, methodology, formal analysis, original draft writing, review and editing of the manuscript. PP was involved in the methodology, original draft writing, review and editing of the manuscript. PK was involved in original draft writing, as well as review and editing of the manuscript. All authors contributed to the article and approved the submitted version.

FUNDING

This work is supported by Merck. The funder had no roles in the study design, data collection and analysis, preparation of the manuscript or decision to publish.

REFERENCES

1. Furth AJ. Glycated Proteins in Diabetes. *Br J BioMed Sci* (1997) 54(3):192–200.
2. Singh R, Barden A, Mori T, Beilin L. Advanced Glycation End-Products: A Review. *Diabetologia* (2001) 44(2):129–46. doi: 10.1007/s001250051591
3. Saito M, Fujii K, Mori Y, Marumo K. Role of Collagen Enzymatic and Glycation Induced Cross-Links as a Determinant of Bone Quality in Spontaneously Diabetic WBN/Kob Rats. *Osteoporos Int* (2006) 17(10):1514–23. doi: 10.1007/s00198-006-0155-5
4. Tomasek JJ, Meyers SW, Basinger JB, Green DT, Shew RL. Diabetic and Age-Related Enhancement of Collagen-Linked Fluorescence in Cortical Bones of Rats. *Life Sci* (1994) 55(11):855–61. doi: 10.1016/0024-3205(94)90041-8
5. Odetti P, Rossi S, Monacelli F, Poggi A, Cirnigliaro M, Federici M, et al. Advanced Glycation End Products and Bone Loss During Aging. *Ann NY Acad Sci* (2005) 1043:710–17. doi: 10.1196/annals.1333.082
6. Hein G, Weiss C, Lehmann G, Niwa T, Stein G, Franke S. Advanced Glycation End Product Modification of Bone Proteins and Bone Remodelling:

Hypothesis and Preliminary Immunohistochemical Findings. *Ann Rhem Dis* (2006) 65(1):101–4. doi: 10.1136/ard.2004.034348
7. Garay-Sevilla ME, Regalado JC, Malacara JM, Nava LE, Wróbel-Zasada K, Castro-Rivas A, et al. Advanced Glycosylation End Products in Skin, Serum, Saliva and Urine and Its Association With Complications of Patients With Type 2 Diabetes Mellitus. *J Endocrinol Invest* (2005) 28(3):223–30. doi: 10.1007/BF03345377
8. Kilhovd BK, Juutilainen A, Lehto S, Rönnemaa T, Torjesen PA, Hassen KF, et al. Increased Serum Levels of Advanced Glycation End Products Predict Total, Cardiovascular and Coronary Mortality in Women With Type 2 Diabetes: A Population-Based 18 Year Follow-Up Study. *Diabetogia* (2007) 50(7):1409–17. doi: 10.1007/s00125-007-0687-z
9. Yamanaka M, Matsumura T, Ohno R, Fujiwara Y, Shinagawa M, Sugawa H, et al. Non-Invasive Measurement of Skin Fluorescence to Evaluate Diabetic Complications. *J Clin Biochem Nutr* (2016) 58(2):135–40. doi: 10.3164/jcbn.15-132
10. Shu A, Yin MT, Stein E, Cremers S, Dworakowski E, Ives R, et al. Bone Structure and Turnover in Type 2 Diabetes Mellitus. *Osteoporos Int* (2012) 23 (2):635–41. doi: 10.1007/s00198-011-1595-0
11. Reyes-García R, Rozas-Moreno P, López-Gallardo G, García-Martín A, Varsavsky M, Avilés-Perez MD, et al. Serum Levels of Bone Resorption Markers Are Decreased in Patients With Type 2 Diabetes. *Acta Diabetol* (2013) 50(1):47–52. doi: 10.1007/s00592-011-0347-0
12. Paccou J, Ward KA, Jameson KA, Dennison EM, Cooper C, Edwards MH. Bone Microarchitecture in Men and Women With Diabetes: The Importance of Cortical Porosity. *Calcif Tissue Int* (2016) 98(5):465–73. doi: 10.1007/s00223-015-0100-8
13. Bonds DE, Larson JC, Schwartz AV, Strotmeyer ES, Robbins J, Rodriquez BL, et al. Risk of Fracture in Women With Type 2 Diabetes: The Women's Health Initiative Observational Study. *J Clin Endocrinol Metab* (2006) 91(9):3404–10. doi: 10.1210/jc.2006-0614
14. Janghorbani M, Van Dam RM, Willett WC, Hu FB. Systematic Review of Type 1 and Type 2 Diabetes Mellitus and Risk of Fracture. *Am J Epidemiol* (2007) 166(5):495–505. doi: 10.1093/aje/kwm106
15. Vestergaard P. Discrepancies in Bone Mineral Density and Fracture Risk in Patients With Type 1 and Type 2 Diabetes–A Meta-Analysis. *Osteoporos Int* (2007) 18(4):427–44. doi: 10.1007/s00198-006-0253-4
16. Yamamoto M, Yamaguchi T, Yamauchi M, Kaji H, Sugimoto T. Bone Mineral Density Is Not Sensitive Enough to Assess the Risk of Vertebral Fractures in Type 2 Diabetic Women. *Calcif Tissue Int* (2007) 80(6):353–58. doi: 10.1007/s00223-007-9003-7
17. Melton LJ3rd, Leibson CL, Achenbach SJ, Therneau TM, Khosla S. Fracture Risk in Type 2 Diabetes: Update of a Population-Based Study. *J Bone Miner Res* (2008) 23(8):1334–42. doi: 10.1359/jbmr.080323
18. Ma L, Oei L, Jiang L, Estrada K, Chen H, Wang Z, et al. Association Between Bone Mineral Density and Type 2 Diabetes Mellitus: A Meta-Analysis of Observational Studies. *Eur J Epidemiol* (2012) 27(5):319–32. doi: 10.1007/s10654-012-9674-x
19. Oei L, Zillikens MC, Dehghan A, Buitendijk GH, Castano-Betancourt MC, Estrada K, et al. High Bone Mineral Density and Fracture Risk in Type 2 Diabetes as Skeletal Complications of Inadequate Glucose Control: The Rotterdam Study. *Diabetes Care* (2013) 36(6):1619–28. doi: 10.2337/dc12-1188
20. Schneider AL, Williams EK, Brancati FL, Blecker S, Coresh J, Selvin E. Diabetes and Risk of Fracture-Related Hospitalization: The Atherosclerosis Risk in Communities Study. *Diabetes Care* (2013) 36(5):1153–8. doi: 10.2337/dc12-1168
21. Li CI, Liu CS, Lin WY, Meng NH, Chen CC, Yang SY, et al. Glycated Hemoglobin Level and Risk of Hip Fracture in Older People With Type 2 Diabetes: A Competing Risk Analysis of Taiwan Diabetes Cohort Study. *J Bone Mineral Res* (2015) 30(7):1338–46. doi: 10.1002/jbmr.2462
22. Tang SY, Zeenath U, Vashishth D. Effects of Non-Enzymatic Glycation on Cancellous Bone Fragility. *Bone* (2007) 40(4):1144–51. doi: 10.1016/j.bone.2006.12.056
23. Poundarik AA, Wu PC, Evis Z, Sroga GE, Ural A, Rubin M, et al. A Direct Role of Collagen Glycation in Bone Fracture. *J Mech Behav BioMed Mater* (2015) 52:120–30. doi: 10.1016/j.jmbbm.2015.08.012
24. Epstein S, Defeudis G, Manfrini S, Napoli N, Pozzilli P. Scientific Committee of the First International Symposium on Diabetes and Bone. Diabetes and Disordered Bone Metabolism (Diabetic Osteodystrophy): Time for Recognition. *Osteoporos Int* (2016) 27(6):1931–51. doi: 10.1007/s00198-015-3454-x
25. Alikhani M, Alikhani Z, Boyd C, MacLellan CM, Raptis M, Liu R, et al. Advanced Glycation End Products Stimulate Osteoblast Apoptosis *via* the MAP Kinase and Cytosolic Apoptotic Pathways. *Bone* (2007) 40(2):345–53. doi: 10.1016/j.bone.2006.09.011
26. Franke S, Siggelkow H, Wolf G, Hein G. Advanced Glycation Endproducts Influence the mRNA Expression of RAGE, RANKL and Various Osteoblastic Genes in Human Osteoblasts. *Arch Physiol Biochem* (2007) 113(3):154–61. doi: 10.1080/13813450701602523
27. Sanguineti R, Storace D, Monacelli F, Federici A, Odetti P. Pentosidine Effects on Human Osteoblasts *In Vitro*. *Ann NY Acad Sci* (2008) 1126:166–72. doi: 10.1196/annals.1433.044
28. Okazaki K, Yamaguchi T, Tanaka K, Notsu M, Ogawa N, Yano S, et al. Advanced Glycation End Products (AGEs), But Not High Glucose, Inhibit the Osteoblastic Differentiation of Mouse Stromal ST2 Cells Through the Suppression of Osterix Expression, and Inhibit Cell Growth and Increasing Cell Apoptosis. *Calcif Tissue Int* (2012) 91(4):286–96. doi: 10.1007/s00223-012-9641-2
29. Notsu M, Yamaguchi T, Okazaki K, Tanaka K, Ogawa N, Kanazawa I, et al. Glycation End Product 3 (AGE3) Suppresses the Mineralization of Mouse Stromal ST2 Cells and Human Mesenchymal Stem Cells by Increasing TGF-β Expression and Secretion. *Endocrinology* (2014) 155(7):2402–10. doi: 10.1210/en.2013-1818
30. Miranda C, Giner M, Montoya MJ, Vázquez MA, Miranda MJ, Pérez-Cano R. Influence of High Glucose and Advanced Glycation End-Products (Ages) Levels in Human Osteoblast-Like Cells Gene Expression. *BMC Musculoskelet Disord* (2016) 17:377. doi: 10.1186/s12891-016-1228-z
31. Furst JR, Bandeira LC, Fan WW, Agarwal S, Nishiyama KK, McMahon DJ, et al. Advanced Glycation End Products and Bone Material Strength in Type 2 Diabetes. *J Clin Endocrinol Metab* (2016) 101(6):2502–10. doi: 10.1210/jc.2016-1437
32. Yamamoto M, Yamaguchi T, Yamauchi M, Yano S, Sugimoto T. Serum Pentosidine Levels Are Positively Associated With the Presence of Vertebral Fractures in Postmenopausal Women With Type 2 Diabetes. *J Clin Endocrinol Metab* (2008) 93(3):1013–19. doi: 10.1210/jc.2007-1270
33. Schwartz AV, Garnero P, Hillier TA, Sellmeyer DE, Strotmeyer ES, Feingold KR, et al. Health, Aging, and Body Composition Study. Pentosidine and Increased Fracture Risk in Older Adults With Type 2 Diabetes. *J Clin Endocrinol Metab* (2009) 94(7):2380–6. doi: 10.1210/jc.2008-2498
34. Tamaki J, Kouda K, Fujita Y, Iki M, Yura A, Miura M, et al. Ratio of Endogenous Secretory Receptor for Advanced Glycation End Products to Pentosidine Predicts Fractures in Men. *J Clin Endocrinol Metab* (2018) 103 (1):85–94. doi: 10.1210/jc.2017-00929
35. Yamamoto M, Yamaguchi T, Yamauchi M, Sugimoto T. Low Serum Level of the Endogenous Secretory Receptor for Advanced Glycation End Products (esRAGE) Is a Risk Factor for Prevalent Vertebral Fractures Independent of Bone Mineral Density in Patients With Type 2 Diabetes. *Diabetes Care* (2009) 32(12):2263–8. doi: 10.2337/dc09-0901
36. Xie J, Méndez JD, Méndez-Valenzuela V, Aguilar-Hernández MM. Cellular Signaling of the Receptor for Advanced Glycation End Products (RAGE). *Cell Signal* (2013) 25(11):2185–97. doi: 10.1016/j.cellsig.2013.06.013
37. Suryavanshi SV, Kulkarni YA. NF-Kβ: A Potential Target in the Management of Vascular Complications of Diabetes. *Front Pharmacol* (2017) 8:798. doi: 10.3389/fphar.2017.00798
38. Yao D, Brownlee M. Hyperglycemia-Induced Reactive Oxygen Species Increase Expression of the Receptor for Advanced Glycation End Products (RAGE) and RAGE Ligands. *Diabetes* (2010) 59(1):249–55. doi: 10.2337/db09-0801
39. Mercer N, Ahmed H, Etcheverry SB, Vasta GR, Cortizo AM. Regulation of Advanced Glycation End Product (AGE) Receptors and Apoptosis by AGEs in Osteoblast-Like Cells. *Mol Cell Biochem* (2007) 306(1-2):87–94. doi: 10.1007/s11010-007-9557-8
40. Liu J, Mao J, Jiang Y, Xia L, Mao L, Wu Y, et al. AGEs Induced Apoptosis in Rat Osteoblast Cells by Activating the Caspase-3 Signaling Pathway Under a High-Glucose Environment *In Vitro*. *Appl Biochem Biotechnol* (2016) 178 (5):1015–27. doi: 10.1007/s12010-015-1925-3

41. Phimphilai M, Pothachareon P, Kongtawelert P, Chattipakorn N. Impaired Osteogenic Differentiation and Enhanced Cellular Receptor of Advanced Glycation End Products Sensitivity in Patients With Type 2 Diabetes. *J Bone Miner Metab* (2017) 35(6):631–41. doi: 10.1007/s00774-016-0800-9
42. Cesselli D, Beltrami AP, Rigo S, Bergamin N, D'Aurizio F, Verardo R, et al. Multipotent Progenitor Cells Are Present in Human Peripheral Blood. *Circ Res* (2009) 104(10):1225–34. doi: 10.1161/CIRCRESAHA.109.195859
43. Chong PP, Selvaratnam L, Abbas AA, Kamarul T. Human Peripheral Blood Derived Mesenchymal Stem Cells Demonstrate Similar Characteristics and Chondrogenic Differentiation Potential to Bone Marrow Derived Mesenchymal Stem Cells. *J Orthop Res* (2012) 30(4):634–42. doi: 10.1002/jor.21556
44. Yang HS, Kim GH, La WG, Bhang SH, Lee TJ, Lee JH, et al. Enhancement of Human Peripheral Blood Mononuclear Cell Transplantation-Mediated Bone Formation. *Cell Transplant* (2011) 20(9):1445–52. doi: 10.3727/096368910X557272
45. *Centre for Metabolic Bone Diseases, University of Sheffield, UK[Internet]: The Fracture Risk Assessment Tool (FRAX®)*. Available at: https://www.sheffield.ac.uk/FRAX/tool.aspx?country=57.
46. Verhaeghe J, van Herck E, Visser WJ, Suiker AM, Thomasset M, Einhorn TA, et al. Bone and Mineral Metabolism in BB Rats With Long-Term Diabetes. *Decreased Bone turnover osteoporosis Diabetes* (1990) 39(4):477–82. doi: 10.2337/diab.39.4.477
47. Leite Duarte ME, da Silva RD. Histomorphometric Analysis of the Bone Tissue in Patients With Non-Insulin-Dependent Diabetes (DMNID). *Rev Hosp Clin Fac Med Sao Paulo* (1996) 51(1):7–11.
48. Son M, Chung WJ, Oh S, Ahn H, Choi CH, Hong S, et al. Age Dependent Accumulation Patterns of Advanced Glycation End Product Receptor (RAGE) and Binding Intensities Between RAGE and Its Ligands Differ in the Liver, Kidney, and Skeletal Muscle. *Immun Ageing* (2017) 14:12. doi: 10.1186/s12979-017-0095-2
49. Molinuevo MS, Schurman L, McCarthy AD, Cortizo AM, Tolosa MJ, Gangoiti MV, et al. Effect of Metformin on Bone Marrow Progenitor Cell Differentiation: *In Vivo* and *In Vitro* Studies. *J Bone Miner Res* (2010) 25(2):211–21. doi: 10.1359/jbmr.090732
50. Shaik AR, Singh P, Shaik C, Kohli S, Vohora D, Ferrari SL. Metformin: Is It the Well Wisher of Bone Beyond Glycemic Control in Diabetes Mellitus? *Calcified Tissue Int* (2021) 108:693–707. doi: 10.1007/s00223-021-00805-8
51. Zhou Z, Tang Y, Jin X, Chen C, Lu Y, Liu L, et al. Metformin Inhibits Advanced Glycation End Products-Induced Inflammatory Response in Murine Macrophages Partly Through AMPK Activation and RAGE/NF κ B Pathway Suppression. *J Diabetes Res* (2016) 2016:4847812. doi: 10.1155/2016/4847812
52. Liu YY, Yao WM, Wu T, Xu BL, Chen F, Cui L. Captopril Improves Osteopenia in Ovariectomized Rats and Promotes Bone Formation in Osteoblasts. *J Bone Miner Metab* (2011) 29(2):149–58. doi: 10.1007/s00774-010-0209-9
53. Kao YT, Huang CY, Fang YA, Liu JC. The Association Between Renin Angiotensin Aldosterone System Blockers and Future Osteoporotic Fractures in a Hypertensive Population – A Population-Based Cohort Study in Taiwan. *Int J Cardiol* (2020) 305:147–53. doi: 10.1016/j.ijcard.2019.12.069
54. Mo C, Ke J, Zhao D, Zhang B. Role of the Renin-Angiotensin-Aldosterone System in Bone Metabolism. *J Bone Miner Metab* (2020) 38(6):772–9. doi: 10.1007/s00774-020-01132-y
55. Chamani S, Liberale L, Mobasheri L, Montecucco F, Al-Rasadi K, Jamialahmadi T, et al. The Role of Statins in the Differentiation and Function of Bone Cells. *Eur J Clin Invest* (2021) 51:e13534. doi: 10.1111/eci.13534
56. Zhang M, Bian YQ, Tao HM, Yang XF, Mu WD. Simvastatin Induces Osteogenic Differentiation of MSCs via Wnt/β-Catenin Pathway to Promote Fracture Healing. *Eur Rev Med Pharmacol Sci* (2018) 22(9):2896–905. doi: 10.26355/eurrev_201805_14992
57. Lin TK, Chou P, Lin CH, Hung YJ, Jong GP. Long-Term Effect of Statins on the Risk of New-Onset Osteoporosis: A Nationwide Population-Based Cohort Study. *PloS One* (2018) 13(5):e0196713. doi: 10.1371/journal.pone.0196713
58. Cheng H, Zhu W, Zhu M, Sun Y, Sun X, Jia D, et al. Susceptibility of Six Polymorphisms in the Receptor for Advanced Glycation End Products to Type 2 Diabetes: A Systematic Review and Meta-Analysis. *Endocr J* (2021). doi: 10.1507/endocrj.EJ21-0130
59. Serveaux-Dancer M, Jabaudon M, Creveaux I, Belville C, Blondonnet R, Gross C, et al. Pathological Implications of Receptor for Advanced Glycation End-Product (AGER) Gene Polymorphism. *Dis Markers* (2019). doi: 10.1155/2019/2067353
60. Raška I Jr, Rašková M, Zikán V, Škrha J. Prevalence and Risk Factors of Osteoporosis in Postmenopausal Women With Type 2 Diabetes Mellitus. *Cent Eur J Public Health* (2017) 25(1):3–10. doi: 10.21101/cejph.a4717

Conflict of Interest: The authors declare that the research was conducted in the absence of any commercial or financial relationships that could be construed as a potential conflict of interest.

Publisher's Note: All claims expressed in this article are solely those of the authors and do not necessarily represent those of their affiliated organizations, or those of the publisher, the editors and the reviewers. Any product that may be evaluated in this article, or claim that may be made by its manufacturer, is not guaranteed or endorsed by the publisher.

frontiers in Endocrinology

ORIGINAL RESEARCH
published: 24 September 2021
doi: 10.3389/fendo.2021.736863

Peiminine Suppresses RANKL-Induced Osteoclastogenesis by Inhibiting the NFATc1, ERK, and NF-κB Signaling Pathways

Mengbo Zhu[1,2†], Wenbin Xu[2†], Jiuzhou Jiang[2†], Yining Wang[3†], Yanjing Guo[1,4], Ruijia Yang[1,4], Yaqiong Chang[1], Bin Zhao[1], Zhenyu Wang[1], Jianfeng Zhang[2], Te Wang[3], Liqin Shangguan[2*] and Shaowei Wang[1,4*]*

[1] Department of Orthopedic, Second Hospital of Shanxi Medical University, Taiyuan, China, [2] Department of Orthopedic Surgery, Sir Run Run Shaw Hospital, Medical College of Zhejiang University, Hangzhou, China, [3] Department of Orthopaedics, The Second Affiliated Hospital and Yuying Children's Hospital of Wenzhou Medical University, Wenzhou, China, [4] Department of Biochemistry, Basic Medical College, Shanxi Medical University, Taiyuan, China

OPEN ACCESS

Edited by:
Chandi C. Mandal,
Central University of Rajasthan, India

Reviewed by:
Florence Figeac,
Odense University Hospital, Denmark
Ciro Menale,
University of Naples Federico II, Italy

***Correspondence:**
Shaowei Wang
dreamkobe@163.com
Liqin Shangguan
lqshangguan@zju.edu.cn
Te Wang
289726269@qq.com

[†]These authors have contributed equally to this work

Specialty section:
This article was submitted to Bone Research, a section of the journal Frontiers in Endocrinology

Received: 06 July 2021
Accepted: 02 September 2021
Published: 24 September 2021

Citation:
Zhu M, Xu W, Jiang J, Wang Y, Guo Y, Yang R, Chang Y, Zhao B, Wang Z, Zhang J, Wang T, Shangguan L and Wang S (2021) Peiminine Suppresses RANKL-Induced Osteoclastogenesis by Inhibiting the NFATc1, ERK, and NF-κB Signaling Pathways. Front. Endocrinol. 12:736863. doi: 10.3389/fendo.2021.736863

Osteoclasts (OCs) play an important role in osteoporosis, a disease that is mainly characterized by bone loss. In our research, we aimed to identify novel approach for regulating osteoclastogenesis and thereby treating osteoporosis. Previous studies have set a precedent for screening traditional Chinese herbal extracts for effective inhibitors. Peiminine is an alkaloid extracted from the bulb of *Fritillaria thunbergii Miq* that reportedly has anticancer and anti-inflammatory effects. Thus, the potential inhibitory effect of peiminine on OC differentiation was investigated *via* a series of experiments. According to the results, peiminine downregulated the levels of specific genes and proteins *in vitro* and consequently suppressed OC differentiation and function. Based on these findings, we further investigated the underlying molecular mechanisms and identified the NF-κB and ERK1/2 signaling pathways as potential targets of peiminine. *In vivo*, peiminine alleviated bone loss in an ovariectomized mouse model.

Keywords: peiminine, osteoclast, NFATc1, NF-κB, osteoporosis

INTRODUCTION

Osteoporosis, common in elderly individuals, especially women, is characterized mainly by microarchitectural degeneration of the trabeculae and intrinsic bone tissues as well as pathological bone remodeling (1). Due to these pathological changes, which are often described as bone loss, patients suffering from osteoporosis are at an enhanced risk for osteoporosis-related fractures (2). A critical cause of bone loss is the imbalance between bone formation and osteoclast (OC)-related bone resorption (3). Estrogen replacement therapy (ERT) is considered to be effective for menopausal osteoporosis but increases the risk of endometrial cancer, breast cancer, and asthma (4, 5), and bisphosphonates are the mainstays for the in-clinical treatment of osteoporosis. However, bisphosphonates exhibit nephrotoxicity, hepatic toxicity, and alimentary canal toxicity (6). Thus, we expect to explore safer strategies for regulating the differentiation of OCs to treat osteoporosis. Natural compounds with a broad spectrum of biological activity and limited side-effects have

become the main targets of our research. There have been many studies on the treatment of osteoporosis using natural compounds (7–9) that have provided us with a reliable theoretical and technological basis for our exploration into the field.

Peiminine is an alkaloid extracted from the bulb of *Fritillaria thunbergii Miq*, a traditional Chinese medicinal herb (for the chemical structure of peiminine, see **Figure 1A**) (10). A study performed in 2018 reported that peiminine exerted a protective effect on lipopolysaccharide-induced mastitis by repressing signaling pathways such as protein kinase B (Akt), nuclear factor-κB (NF-κB), and mitogen-activated protein kinases (MAPKs) (11), and peiminine was shown to similarly protect dopaminergic neurons from neuroinflammation by inhibiting the extracellular-regulated protein kinase (ERK1/2) and NF-κB pathways in another study (12). The process of osteoclastogenesis shares these pathways.

OCs are multinuclear giant cells derived from bone marrow monocytes (BMMs) (13), and the receptor activator of nuclear factor-κB ligand (RANKL)-receptor activator of nuclear factor-κB (RANK)-osteoprotegerin (RANK-RANKL-OPG) signaling pathway is the most influential mechanism known to regulate the process of OC differentiation (3, 13–15). Groping towards

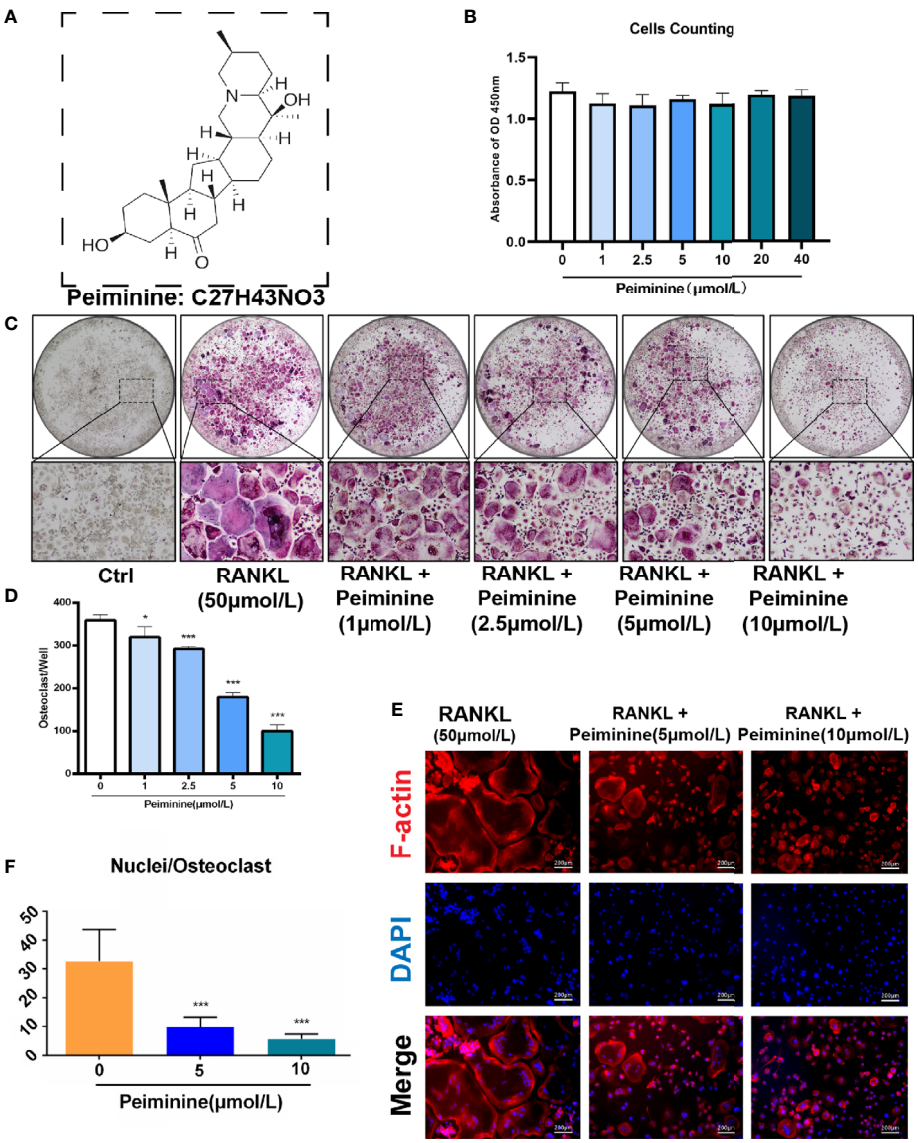

FIGURE 1 | Peiminine dose-dependently inhibits osteoclastogenesis induced by RANKL and is not cytotoxic *in vitro*. **(A)** The molecular structure of peiminine. **(B)** Evaluation of the cytotoxicity of peiminine by the CCK-8 assay. n= 5, **(C)** TRAP staining of OCs treated with peiminine at every concentration. **(D)** Quantitative analysis of the TRAP-positive cells with more than 3 nuclei in each well of a 96-well plate. n= 5, *P < 0.05, ***P < 0.001. **(E)** Fluorescence staining images of OCs treated without or with peiminine at different concentrations (5 μmol/L and 10 μmol/L). The scale bar is 200 μm. **(F)** Analysis of the average number of OC nuclei (dots with blue fluorescence indicated by DAPI staining). n= 5, ***P < 0.001.

this way, NF-κB and ERK pathways are all crucial downstream signaling pathways of RANKL-RANK axis (16–18). Hence, blocking these pathways is probably a promising direction of osteoporosis treatment.

We herein hypothesized that peiminine exerts similar inhibitory effects on osteoclastogenesis. Besides, many previous studies have reported that peiminine has certain anticancer effects (19, 20) and is also effective against acute and chronic inflammatory injury (21–24). In the context of orthopedic diseases, peiminine is known to protect articular cartilage from destructive cytokines (25), but its inhibitory effect on OCs and its effect on bone loss have not yet been reported. Thus, this study aimed to provide a novel and comprehensive solution for combating degenerative and aging-related bone diseases.

In our study, we found for the first time that peiminine suppressed osteoclastogenesis by inhibiting the NF-κB signaling pathway. The expression of OC-related genes and proteins was measured to evaluate the influence of peiminine on OC differentiation and function. Our results indicated the alleviating promise of peiminine for osteolytic bone diseases, and its effect on bone loss alleviation was confirmed by animal experiments *in vivo*. The results obtained from a mouse model of osteoporosis induced by estrogen deficiency indicated the potential of peiminine as an alleviating option for osteoporosis.

METHODS AND MATERIALS

Cell Culture

The indispensable basic cell culture materials were produced by Thermo Fisher Scientific (Carlsbad, CA, USA), including alpha-modified minimal essential medium (α-MEM), penicillin/streptomycin (P/S), and fetal bovine serum (FBS). We extracted BMMs from the tibias and femur marrow of C57BL/6 mice at 6 weeks of age in accordance with the *National Institutes of Health (NIH) Guide for the Care and Use of Laboratory Animals* and the guidelines for *The Laboratory Animal Center of Sir Run Run Shaw Affiliated Hospital of Zhejiang University School of Medicine* (Hangzhou, Zhejiang).

Under sterile conditions, 6-week-old mice were sacrificed, and their tibias and femurs were immediately harvested. The two ends of the bones (osteoepiphysis) were clipped to expose the bone marrow, which was harvested from the diaphysis *via* a 1 ml syringe and placed into medium. After triturating with a pipette, M-CSF was added to the bone marrow cell suspension for BMM sorting. The suspended cells were discarded after 48 h of culture in the presence of M-CSF, and the adherent cells were deemed the BMMs. The medium was comprised of α-MEM, 1% (v/v) P/S, 10% (v/v) FBS, and 50 ng/ml M-CSF.

Evaluation of Peiminine Efficacy and Toxicity

BMMs were seeded in plates (96-well plate) at a concentration of 8×10^3 cells per well and cultured in α-MEM (Thermo Fisher Scientific, CA, USA) supplemented with 50 ng/ml M-CSF (R&D Systems, MN, USA) overnight according to the method published by Jin and Chen in 2019 (7, 26). After adherence, the BMMs were stimulated with GST-rRANKL (50 ng/ml) (R&D Systems, MN, USA), and peiminine (Feiyubio, Jiangsu, China, CAS no. 18059-10-4) was added to the cultured cells at varying concentrations (1, 2.5, 5, and 10 μmol/L). The medium was changed every 2 days, and GST-rRANKL and the drug were refreshed every 2 days until the sixth day, when OCs formed. The differentiated OCs were stained with tartrate-resistant acid phosphatase (TRAP) (Sigma-Aldrich Corp., St. Louis, MO, USA) solution after fixation with 2.5% glutaraldehyde (DAMAO chemical reagent factory, Tianjin, China) for 15 min, and the number of cells in each well was then counted under a bright-field optical microscope (Olympus, Tokyo, Japan). Cells with three or more nuclei were considered OCs, and the number of TRAP-positive multinucleated cells was used to indicate the differentiation of OCs.

Additionally, the response of the cells to increasing concentrations of peiminine (1, 2.5, 5, and 10 μmol/L) was assessed. BMMs were treated with varying concentrations of peiminine for 5 days, after which 20 μl of WST-8 solution (Cell Counting Kit-8; Dojindo Laboratories, Kumamoto, Japan) was added to the wells for another 4 h. The absorbance at 450 nm was measured by the enzyme-linked immunosorbent assay (Thermo Fisher Scientific, Waltham, MA, USA).

Fluorescence Staining

BMMs were seeded in 96-well plates (8×10^3 cells per well) and cultured in α-MEM containing M-CSF (50 ng/ml) for 24 h; after adherence, the medium was replaced in each well. The control group BMMs were cultured in α-MEM containing M-CSF (50 ng/ml) and GST-rRANKL (50 ng/ml) for 6 days, while the BMMs in the two experimental groups were cultured in α-MEM containing M-CSF (50 ng/ml), GST-rRANKL (50 ng/ml), and peiminine (5 and 10 μmol/L separately) for 6 days (medium refreshed every 2 days). On the seventh day after cell seeding, the cells were fixed with 4% paraformaldehyde, and the membrane permeability was increased with 0.5% Triton X-100 (Sigma-Aldrich Corp., St. Louis, MO, USA).

F-actin filaments were stained with rhodamine phalloidin (Thermo Fisher Scientific, Waltham, MA, USA) after blocking with 5% bovine serum albumin. According to the manufacturer's instructions, the vial contents were dissolved in 150 μl of anhydrous DMSO to yield a 400× stock solution at a concentration of 2,000 assays/ml, which was equivalent to approximately 66 μM. During the experiment, 0.5 μl of the 400× stock solution was diluted in 200 μl of PBS, and approximately 100 μl was added to each well. After 45 min of staining, the cells were washed with PBS and stained with DAPI, and the results were observed with a fluorescence microscope (CKX53; Olympus, Tokyo, Japan). The numbers of multinucleated cells and nuclei in each multinucleated cell were counted under a fluorescence microscope, and the average number of nuclei in each well was then calculated.

Bone Resorption Assay *In Vitro*

First, sterile bone slices were placed on the well bottoms of 96-well plates, after which BMMs were seeded onto the bone slices (1×10^4 cells per well) and cultured in α-MEM containing M-CSF

(50 ng/ml) for 24 h; after adherence, the medium in each well was replaced. The negative control group cells were cultured in α-MEM containing M-CSF (50 ng/ml), while those in the positive control group were cultured in α-MEM supplemented with M-CSF (50 ng/ml) and GST-rRANKL (50 ng/ml), and those in the two experimental groups were cultured in α-MEM supplemented with M-CSF (50 ng/ml), GST-rRANKL (50 ng/ml), and peiminine (5 and 10 μmol/L). The cells in all groups were cultured for 14 days, and the medium was changed every 2 days. On the 15th day after cell seeding, the cell cultures were removed, and the bone slices from the different groups were obtained.

To prepare scanning electron microscopy (SEM) samples, adherent cells were removed from the bone slices by washing with 75% alcohol and trypsin to ensure that the bone slices were completely decellularized. Then, these decellularized bone slices were fully dried and covered with conductive carbon powder with a vacuum spray plating device (JEOL Ltd., Japan) prior to SEM. The resorption pits on the dried bone slices were observed by SEM (TM-1000; Hitachi, Tokyo, Japan). ImageJ software was used to measure the gross resorption pit areas as follows: adjust the scanning picture to 8-bit and set an appropriate gray value threshold; select dark recessed areas as the resorption area and deselect all scratch-like recessed areas (scratches were engendered during the process of slice cutting); and calculate the gross resorption pit areas in each well.

Real-Time Quantitative Polymerase Chain Reaction

BMMs were seeded in 6-well plates (15×10^4 cells per well) and cultured in α-MEM containing M-CSF (50 ng/ml) for 24 h; after adherence, the medium in each well was changed. Cells in the negative control group were cultured in α-MEM containing M-CSF (50 ng/ml), while those in the positive control group were cultured in α-MEM containing M-CSF (50 ng/ml) and GST-rRANKL (50 ng/ml), and those in the two experimental groups were cultured in α-MEM containing M-CSF (50 ng/ml), GST-rRANKL (50 ng/ml), and peiminine (5 and 10 μmol/L). Cells in all the groups were cultured for 6 days, and the medium was changed every 2 days. On the seventh day after cell seeding, total RNA was extracted from the cells with TRIzol reagent and the Ultrapure RNA Kit (DNase I) (CW Biotech, Beijing, China).

The RNA concentration in each sample was detected by measuring the absorbance at 260 nm with a spectrophotometer (Thermo Fisher Scientific, Waltham, MA, USA). Evo M-MLV RT Premix for qPCR (Accurate Biotechnology, Hunan, China) was used to reverse transcribe the total RNA (500 ng) into single-stranded cDNA.

According to the manufacturer's protocol, the expression of the target genes was determined with a SYBR polymerase chain reaction Master Mix Kit (Yeasen Co., Shanghai, China) on the ABI QuantStudio 6 Real-Time PCR System (Thermo Fisher Scientific, Waltham, MA, USA). The relative expression levels of the target genes were analyzed by the 2−ΔΔCq method, and the expression level of the mouse glyceraldehyde-3-phosphate dehydrogenase (GAPDH) gene was used as the normalization parameter in our analysis. The primer sequences are listed in **Table 1**.

Western Blot Analysis

To evaluate the expression of proteins related to the NFATc1 signaling pathway and bone resorption, BMMs were seeded in six-well plates (1.5×10^5 cells per well) overnight and allowed to adhere. The cells were cultured with or without peiminine (10 μmol/L) in medium containing M-CSF (50 ng/ml) and GST-rRANKL (50 ng/ml), and total proteins were then harvested separately from each well on days 0, 1, 3, and 5. Radioimmunoprecipitation assay (RIPA) lysis buffer (consisting of phosphatase inhibitors, 500 g/ml DNase I, and 100 g/ml PMSF) was used to extract the total protein.

To assess the expression of signaling pathway-related proteins at early time points, BMMs were seeded at a density of 5×10^5 cells per well in six-well plates and incubated in GST-rRANKL-free medium overnight. The cells were starved for more than 6 h and then pretreated with peiminine for 2 h. GST-rRANKL (50 ng/ml) was then added to each well, and total protein was harvested in RIPA buffer at the following time points: 0, 10, 20, 30, and 60 min.

The proteins were separated by sodium dodecyl sulfate-polyacrylamide gel electrophoresis (10%), transferred onto nitrocellulose membranes, and blocked with 5% BSA for 2 h. The membranes were incubated with the following primary antibodies: anti-c-Fos (1:1,000, Cat. #2250), anti-NF-κB (anti-p65) (1:1,000, Cat. #8242), anti-phospho-NF-κB (anti-pp65) (1:1,000, Cat. #3033), anti-NFATc1 (1:1,000, Cat. #sc-7294), anti-integrin β3 (1:1,000, Cat. #sc-365679), anti-cathepsin K (CTSK) (1:1,000, Cat. #sc-48353), anti-ATP6v0s2 (1:1,000, Cat. #sc-69108), anti-p-IκB-α (1:1,000, Cat. #sc-8404), and anti-β-actin (1:5,000, Cat. #sc-47778), anti-phospho-ERK1/2 (1:1,000, Cat. #AF1015), anti-ERK1/2 (1:1,000, Cat. #AF0155), anti-

TABLE 1 | Primer sequences used in qRT-PCR.

GENE	FROWARD (5'-3')	REVERSE (5'-3')	Tm (℃)
CTSK	CCA GTG GGA GCT ATG GAA GA	AAG TGG TTC ATG GCC AGT TC	60
DC-STAMP	TTC ATC CAG CAT TTG GGA GT	ACA GAA GAG AGC AGG GCA AC	60
Acp5	CAG CAG CCA AGG AGG ACT AC	ACA TAG CCC ACA CCG TTC TC	59
V-ATPase-d2	GTG AGA CCT TGG AAG TCC TGA A	GAG AAA TGT GCT CAG GGG CT	60
Nfatc1	CAA CGC CCT GAC CAC CGA TAG	GGC TGC CTT CCG TCT CAT AGT	60
c-Fos	TTT CAA CGC CGA CTA CGA GG	GCG CAA AAG TCC TGT GTG TT	60
TNFRSF11	GAA GAT GCT TTG GTG GGT GT	TCA GTC GGG ATC AGT GTG AG	60
GAPDH	ACC CAG AAG ACT GTG GAT GG	CAC ATT GGG GGT AGG AAC AC	60

phospho-P38 (1:1,000, Cat. #AF4001), anti-P38 (1:1,000, Cat. #AF6456).

Primary antibodies specific for c-Fos, phospho-NF-κB (pp65), and NF-κB (p65) were acquired from Cell Signaling Technology (Beverly, MA, USA). Primary antibodies specific for NFATc1, integrin β3, CTSK, V-ATPase-d2 (ATP6v0d2), phosphorylated iκB (p-IκB)-α, and β-actin were obtained from Santa Cruz Biotechnology (San Jose, CA, USA). Primary antibodies specific for ERK1/2, phospho-ERK1/2, phospho-P38, and P38 were acquired from Affinity Biosciences (Jiangsu, China).

The membranes were incubated with primary antibodies at 4°C for more than 12 h and then with secondary antibodies conjugated to horseradish peroxidase at room temperature for more than 2 h. Immunoreactive bands were visualized with the Touch Imaging System made by Bio-Rad (ChemiDoc™, Bio-Rad, CA, USA).

The relative protein content was calculated with ImageJ software as follows: adjust the protein band images to 8-bit and obtain clean protein bands using the *Subtract Background* function; use the *Measurement* function to calculate the gray value of each band; divide the gray values of the control proteins by the gray values of the corresponding target proteins to determine the relative protein amounts.

Ovariectomy Mouse Model

Female 10-week-old C57BL/6 mice (n=30), acquired from the Animal Experimental Center of Sir Run Run Shaw Hospital (Zhejiang, China), were randomly separated into three groups: the sham group (control group) (n=10), the OVX group (n=10), and the intervention group (n=10). Mice from the OVX and intervention groups were ovariectomized according to the method published by Zhou in 2016 (27). As a control, mice in the sham group underwent a sham operation; mice in the intervention group were treated with peiminine (10 mg/kg), while those in the OVX and sham groups were injected with PBS.

All mice were housed in ventilated and sterilized cages and subjected to surgery after adaptive feeding for 1 week. Each of these specific pathogen-free cages held five mice. Seven days after the surgery, mice in the OVX and sham groups were administered PBS, while those in the intervention group were intraperitoneally injected with peiminine (10 mg/kg) every 2 days for 6 weeks. All the mice survived and were healthy in the interim. At the seventh week after surgery, all the mice were sacrificed, and their femurs were harvested for histological and micro-CT (μCT) analysis.

μCT Scanning of Mouse Femurs

We measured the following parameters of mouse femur samples: the bone volume/tissue volume ratio (BV/TV), trabecular number (Tb. N), trabecular separation (Tb. Sp), and trabecular thickness (Tb. Th). Samples were scanned with a BRUKER skyscan1176 μCT instrument (Bruker Daltonic Inc. USA) after fixation with 4% paraformaldehyde for 1 day (24 h). The μCT setup was as follows: 50 kV scanning voltage, 500 μA scanning current, 9 μm spatial resolution, and 1,600 × 2,672-pixel image matrix. Then, a 1-mm-high area 0.5 mm beneath the growth plate was designated for qualitative and quantitative analysis. N-Recon software was used for three-dimensional image rebuilding, and CT-AN software was used for quantitative analysis.

Histological Staining

Left femur samples from all mice were fixed in 4% paraformaldehyde for 2 days (48 h) and then decalcified by 14% EDTA at 37°C for 14 days (9). Sagittal paraffin sections at thickness of 5 μm were obtained from the decalcified bone tissues. Representative images of TRAP staining and hematoxylin and eosin (H&E) staining were collected, and the claret red cells around the resorbed bone were considered TRAP-positive OCs. In addition, we assessed the OCs surface (OC. S) and bone surface (BS) by measuring the TRAP-positive cells' perimeters and bone perimeters separately.

Statistical Analysis

In the *Results* section, all quantitative data are presented as the mean ± standard deviation. Statistical analyses were conducted using one-way analysis of variance (ANOVA) followed by Tukey's *post hoc* test with GraphPad Prism 8. All data are presented as the means ± SDs; *P < 0.05, **P < 0.01, ***P < 0.001 compared to the control.

RESULTS

Peiminine Is Not Toxic in BMMs and Suppresses OC Formation and Fusion Induced by RANKL

Before assessing the inhibitory effect of peiminine on osteoclastogenesis, we investigated its cytotoxicity. The CCK-8 assays confirmed that the reduction in the number of OCs was not due to BMM cytotoxicity, as the number of live cells did not differ after treatment with varying concentrations of peiminine as determined by absorbance detection (**Figure 1B**). The number of cells in each group did not change significantly in the presence of various concentrations of peiminine, indicating that peiminine had no toxic effect on living BMMs (1 μmol/L group: p= 0.0665; 1 μmol/L: p= 0.0503; 5 μmol/L: p= 0.0909; 10 μmol/L: p=0.0682; 20 μmol/L: p=0.3824; 40 μmol/L: p=0.3174).

To evaluate the inhibitory effect of peiminine on the generation of OCs, TRAP staining was used to assess the cellular responses to increasing peiminine concentrations (1, 2.5, 5, and 10 μmol/L). As shown in **Figures 1C, D**, the number of TRAP-positive OCs in each well was dose-dependently decreased, and significantly fewer multinuclear TRAP-positive cells were observed in the cells treated with 10 μmol/L peiminine than in untreated cells (p= 2.04798E-09). Similarly, the numbers of cells treated with 1, 2.5, and 5 mol/L peiminine were obviously decreased (1 μmol/L: p= 0.0129; 2.5 μmol/L: p= 6.93569E-06; 5 μmol/L: p= 1.27028E-08).

Additionally, to determine whether peiminine disrupts the cellular fusion of OCs, fluorescence staining was performed to assess their fusion and the quantity of nuclei in every multinucleated cell. **Figures 1E, F** show that cell fusion was

reduced in the presence of 5 and 10 μmol/L peiminine, which is consistent with the TRAP staining results. Specifically, the number of nuclei per OC was markedly decreased (5 μmol/L: p= 0.0004652; 10 μmol/L: p= 9.86236E-05).

The Inhibitory Effect of Peiminine Is Time-Dependent

In addition, BMMs were treated with peiminine on days 1–3, 3–5, 5–6, and 1–6 to assess its inhibitory effect at various stages of OC differentiation. In **Figure 2A**, the pink boxes represent the time points of the dosing. Compared with the control group, peiminine had a notable inhibitory effect in all treatment groups. The number of OCs in the 1–6day group was dramatically lower than that in the control group (p=0.00000060), and those in the remaining groups were lower than that in the control group (1–3day group: p= 0.00000175; 3–5day group: p= 0.0000189; 5–6day group: p= 0.00636).

Moreover, direct comparisons of the treatment groups revealed that the effect of peiminine was limited on days 5–6, as the number of OCs in the 5–6day group was higher than that in the other treatment groups (1–3day group: p= 0.019; 3–5day group: p= 0.049; 1–6day group: p= 0.001). Additionally, peiminine exerted an optimal inhibitory effect on the 1–6day group, as the OC number was lower than that in the other groups (1–3 group: p= 0.002; 3–5 group: p= 0.005; 5–6 group: p= 0.001) (**Figures 2B, C**).

Peiminine Suppresses the Resorptive Activity of OCs

To further demonstrate the ability of peiminine to disrupt OC resorption, BMMs were seeded on bone slices and treated with or without varying concentrations of peiminine (5 and 10 μmol/L) together with M-CSF (50 ng/ml) and GST-rRANKL (50 ng/ml). Then, the freeze-dried bone slices were observed by SEM, and the resorption area was measured with ImageJ.

Compared to the control, the non-treatment group, induced by GST-rRANKL, was expected to have the maximum number of OCs and to exhibit the most obvious effect on resorption. Owing to the inhibitory effect of peiminine on OC function, the bone slices in the intervention group were expected to have a smaller

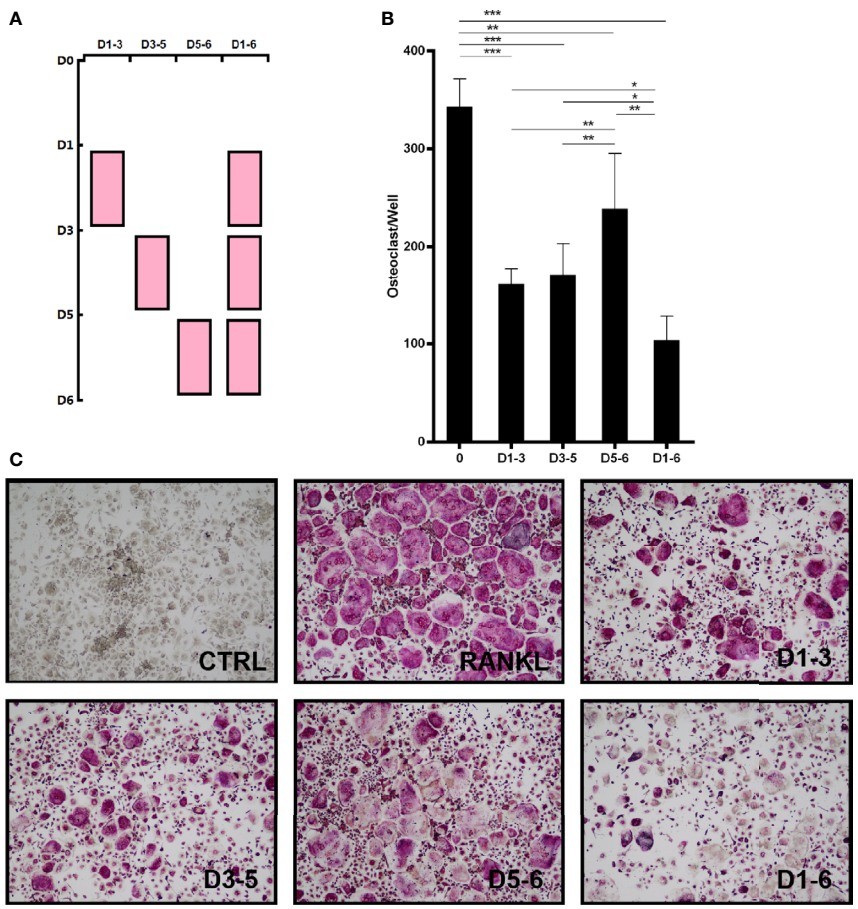

FIGURE 2 | Peiminine has a suppressive effect on OC formation at different time points. **(A)** BMMs were treated with peiminine on days 1–3, 3–5, 5–6, and 1–6. **(B)** Quantitative analysis of the OC numbers in groups with different administration times (TRAP-positive cells were counted as OCs). n= 5, *P < 0.05, **P < 0.01, ***P < 0.001. **(C)** Representative images of the TRAP-positive cells in the different administration time groups.

resorption area. According to the SEM results and analysis of the data shown in **Figures 3A, B**, the peiminine-free group had the largest resorption pit area, and the resorption area decreased as the drug concentration increased (5 μmol/L: p= 0.0071; 10 μmol/L: p= 0.0005). The results obtained from bone slices were consistent with our hypothesis.

Peiminine Downregulates Formation- and Function-Related Genes

The expression levels of genes critical for RANKL-induced OC differentiation and function, including NFATc1, c-Fos, Acp5 (TRAP), ATP6V0D2, DC-STAMP, and TNF, were analyzed by qRT-PCR to further investigate the mechanism underlying the inhibitory effect of peiminine. Compared with those in the control group, the expression levels of OC-related genes in the RANKL-treated group were substantially elevated. The expression levels of genes related to OC function, such as CTSK (5 μmol/L: p= 0.0082; 10 μmol/L: p= 0.0040) and Acp5 (5 μmol/L: p= 0.0120; 10 μmol/L: p= 0.0005) (**Figures 4A, B**), and fusion-related genes, such as ATP6v0d2 (5 μmol/L: p= 0.0263; 10 μmol/L: p= 0.0039) and DC-STAMP (5 μmol/L: p= 0.0246; 10 μmol/L: p= 0.0041) (**Figures 4C, D**), were detected in cells treated with peiminine at concentrations of 5 and 10 μmol/L.

Similarly, after peiminine intervention, genes related to OC formation (NFATc1 and c-Fos) were downregulated (NFATc1: 5 μmol/L: p= 0.2051; 10 μmol/L: p= 0.451; c-Fos: 5 μmol/L: p= 0.0158; 10 μmol/L: p= 0.0061) (**Figures 4E, F**). In addition, the expression of the TNFRSF11 gene, which encodes the RANK protein, was inhibited by peiminine (5 μmol/L: p= 0.1065; 10 μmol/L: p= 0.0119) (**Figure 4G**). These results confirm that peiminine indeed inhibited the RANKL-induced differentiation and function of OCs.

Peiminine Suppresses the Expression of Critical Proteins of RANKL-Induced OCs

The Western blot results were consistent with the qRT-PCR results, demonstrating that peiminine effectively inhibited the expression of essential genes and proteins related to OC differentiation and thereby reduced the expression of downstream genes and proteins associated with OC function.

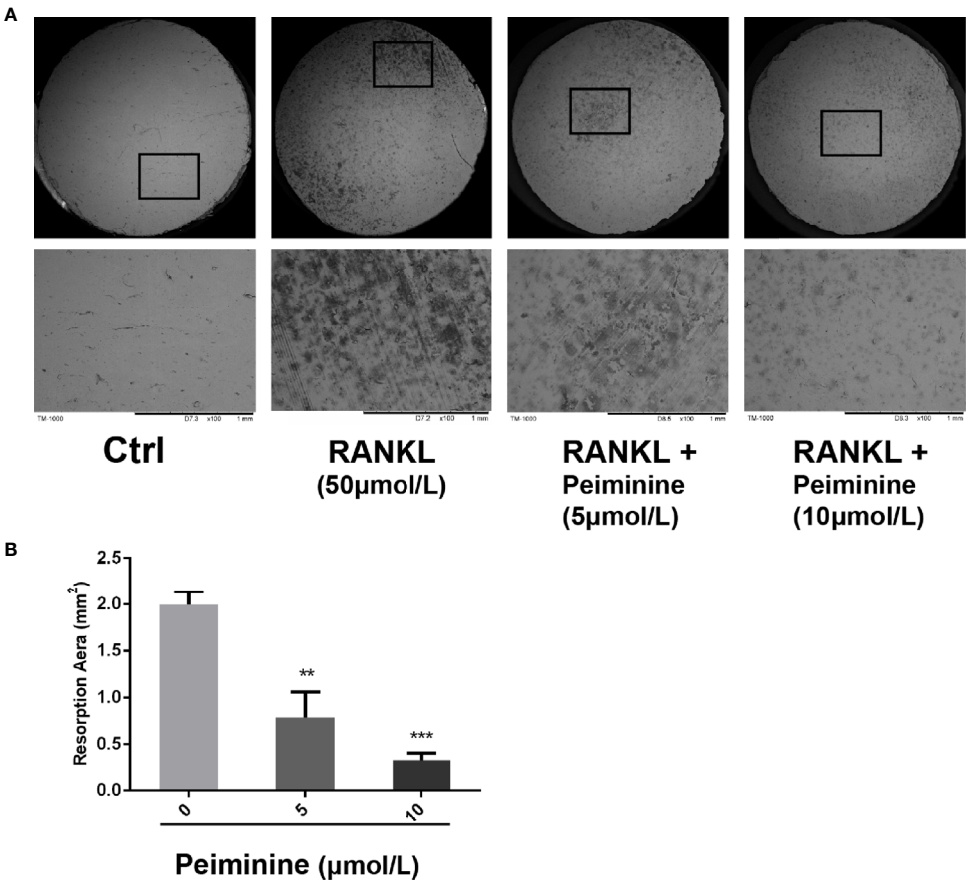

FIGURE 3 | OC resorption is inhibited by peiminine. **(A)** Representative images of the bone slice resorption areas in the different groups. BMMs in the first group (control) were neither induced by RANKL nor treated with peiminine; BMMs in the second group were induced by RANKL but not treated with peiminine; and BMMs in the third and fourth groups were induced by RANKL and treated with peiminine at concentrations of 5 μmol/L and 10 μmol/L, respectively. **(B)** The bone slice resorption areas in all groups were quantitatively analyzed. n= 3, **P < 0.01, ***P < 0.001.

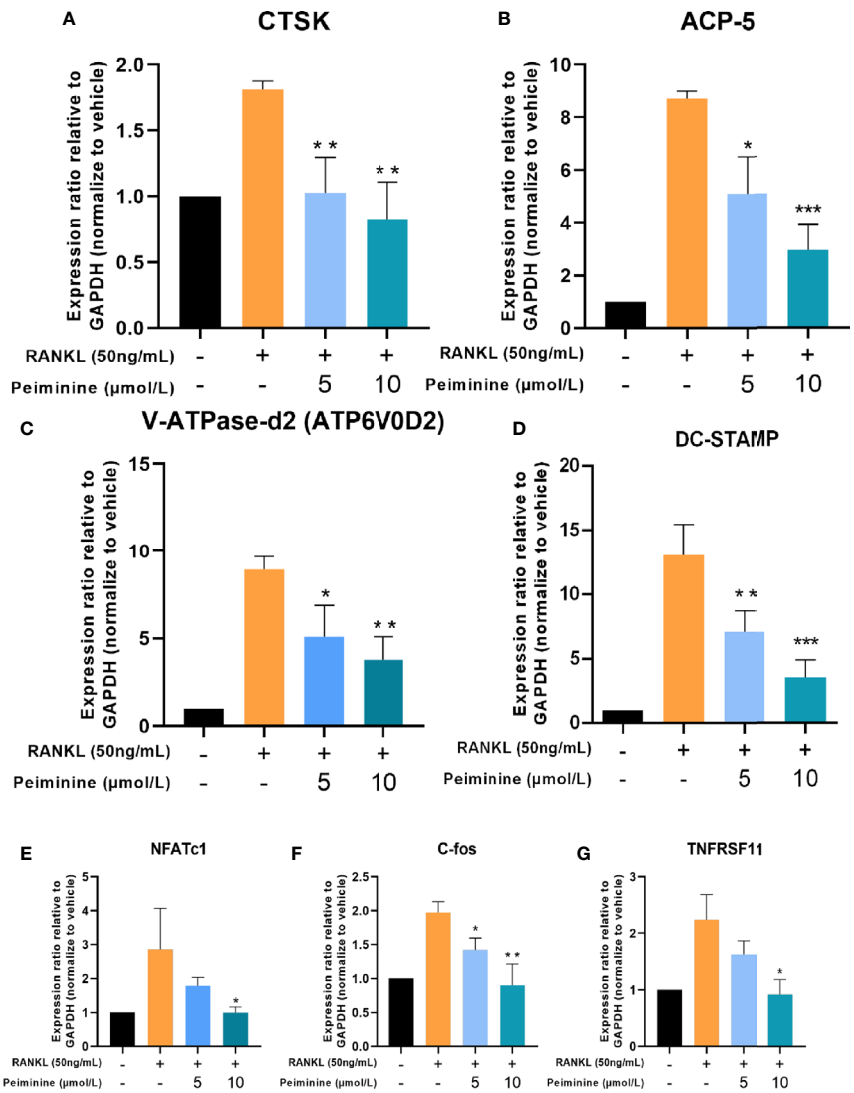

FIGURE 4 | Osteoclastogenesis-related genes are downregulated by peiminine. **(A)** CTSK, **(B)** ACP-5, **(C)** V-ATPase-d2 (ATP6V0D2), **(D)** DC-STAMP, **(E)** NFATc1, **(F)** c-Fos, and **(G)** TNFRSF11. GAPDH was selected as the control gene. n= 3, *P < 0.05, **P < 0.01, ***P < 0.001.

The expression levels of a series of critical factors in the control and experimental groups were measured by Western blot, and the results are shown in **Figure 5A**.

As mentioned previously, integrin β3, CTSK, and ATP6v0d2 are critical for OC function, and their protein expression levels were reduced in cells treated with peiminine (integrin β3: 0-day: p= 0.9161; 1-day: p= 0.6606; 3-day: p= 0.0373; 5-day: p= 0.0306; CTSK: 0-day: p= 0.8770; 1-day: p= 0.9627; 3-day: p= 0.0167; 5-day: p= 0.0028; ATP6v0d2: 0-day: p= 0.9432; 1-day: p= 0.8401; 3-day: p= 0.0440; 5-day: p= 0.0055) (**Figures 5B–D**).

NFATc1 and c-Fos, regulatory factors upstream of the abovementioned proteins, were also remarkably downregulated by peiminine in the 3- and 5-day groups (NFATc1: 0-day: p= 0.6205; 1-day: p= 0.9749; 3-day: p= 0.0031; 5-day: p= 0.0117; c-Fos: 0-day: p= 0.1781; 1-day: p= 0.7359; 3-day: p= 0.0296; 5-day: p= 0.0152) (**Figures 5E, F**).

The NF-κB and ERK1/2 Signaling Pathways Are the Potential Targets of Peiminine

A key molecular event of early RANKL-induced osteoclastogenesis is the activation of NF-κB (28, 29), and activated NF-κB is an integral upstream regulator of NFATc1 (30). As shown in **Figure 6B**, the levels of NF-κB were notably downregulated by peiminine in the presence of RANKL for 10 min (p= 0.0097), 20 min (p= 0.0043), 30 min (p= 0.0195), and 60 min (p= 0.0324). As shown in **Figure 6C**, the level of Phosphorylated NF-κB (p-NF-κB) was also decreased by peiminine (p= 0.0083).

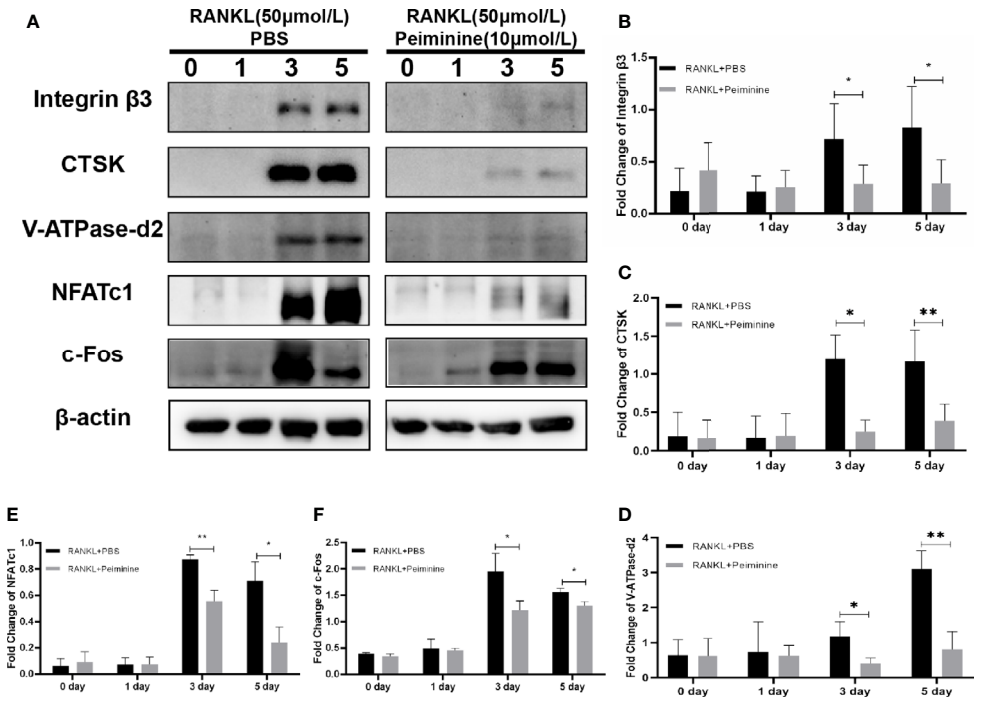

FIGURE 5 | c-Fos, NFATc1 and downstream proteins are suppressed by peiminine. **(A)** Western blots analysis of the integrin β3, CTSK, V-ATPase-d2, NFATc1, and c-Fos expression induced by treatment with RANKL (50 ng/mL) for 0, 1, 3, and 5 days in the presence or absence of peiminine (10 μmol/L). Quantitative analysis of the differential expression levels of **(B)** integrin β3 (n= 5), **(C)** CTSK (n= 3), **(D)** V-ATPase-d2 (n= 3), **(E)** NFATc1 (n= 3), and **(F)** c-Fos (n= 3). The β-actin was selected as the control protein. *P < 0.05, **P < 0.01.

As an important upstream regulator, iκB can prevent the entry of NF-κB into the nucleus; however, during the process of OC differentiation, iκB is phosphorylated by the combination of RANK and RANKL (31). **Figure 6D** shows that peiminine obviously reduced the expression of p-iκB at 20 min (p= 0.0388), 30 min (p= 1.42687E-05), and 60 min (p= 0.0031) and consequently diminished the levels of p-NF-κB and NF-κB. These findings suggested that peiminine inhibited the NF-κB pathway and thus suppressed OC differentiation and function.

Moreover, MAPK signaling pathways are important regulators of downstream activation (16, 32). We found that the levels of p-ERK1/2 were decreased in cells treated with peiminine for 20 min (p= 0.0166), 30 min (p= 0.0154), and 60 min (p= 0.0208). However, peiminine had no significant effect on the p-P38 level (**Figures 6E, F**).

Peiminine Plays a Role of Alleviation Against Bone Loss *In Vivo*

Animal experiments were performed to evaluate the bio-effect of peiminine *in vivo*. μCT and histomorphometric analyses showed that peiminine obviously alleviated the resorption of bone caused by OCs (**Figure 7A**). The BV/TV was obviously higher in the peiminine-treated group than in the OVX group (p= 1.03253E-05) (**Figure 7B**). Similarly, the Tb. N and Tb. Th were higher in the peiminine-treated group than in the OVX group (Tb.N: p= 6.72736E-05; Tb.Th: p= 2.21584E-05) (**Figures 7C, D**), while the Tb. Sp in the intervention group was lower than that in OVX group (p= 1.55671E-07) (**Figure 7E**).

The histomorphometric analysis results further supported the findings presented above. H&E staining indicated the distribution of OCs and trabecular bone *in vivo*, and the result was consistent with that obtained by μCT analysis. Then, OCs at corresponding positions were stained, revealing that sections from peiminine-treated OVX mice had significantly fewer TRAP-positive cells than those from untreated OVX mice (**Figure 8A**). The OC. S/BS (p= 0.004493691) and OC. N/BS (p= 0.000363396) results also indicated that peiminine inhibited osteoclastogenesis in bone tissue (**Figures 8B, C**).

Additionally, H&E staining of liver and kidney tissues harvested from the mice showed no lesions in any of the groups (**Figure 8D**). The lack of peiminine toxicity *in vivo* corresponded with the results of the CCK-8 assay described in the section *Peiminine Is Not Toxic in BMMs and Suppresses OC Formation and Fusion Induced by RANKL*.

DISCUSSION

In this study, TRAP staining was used as the major determination method to demonstrate many indices of osteoclastogenesis, because

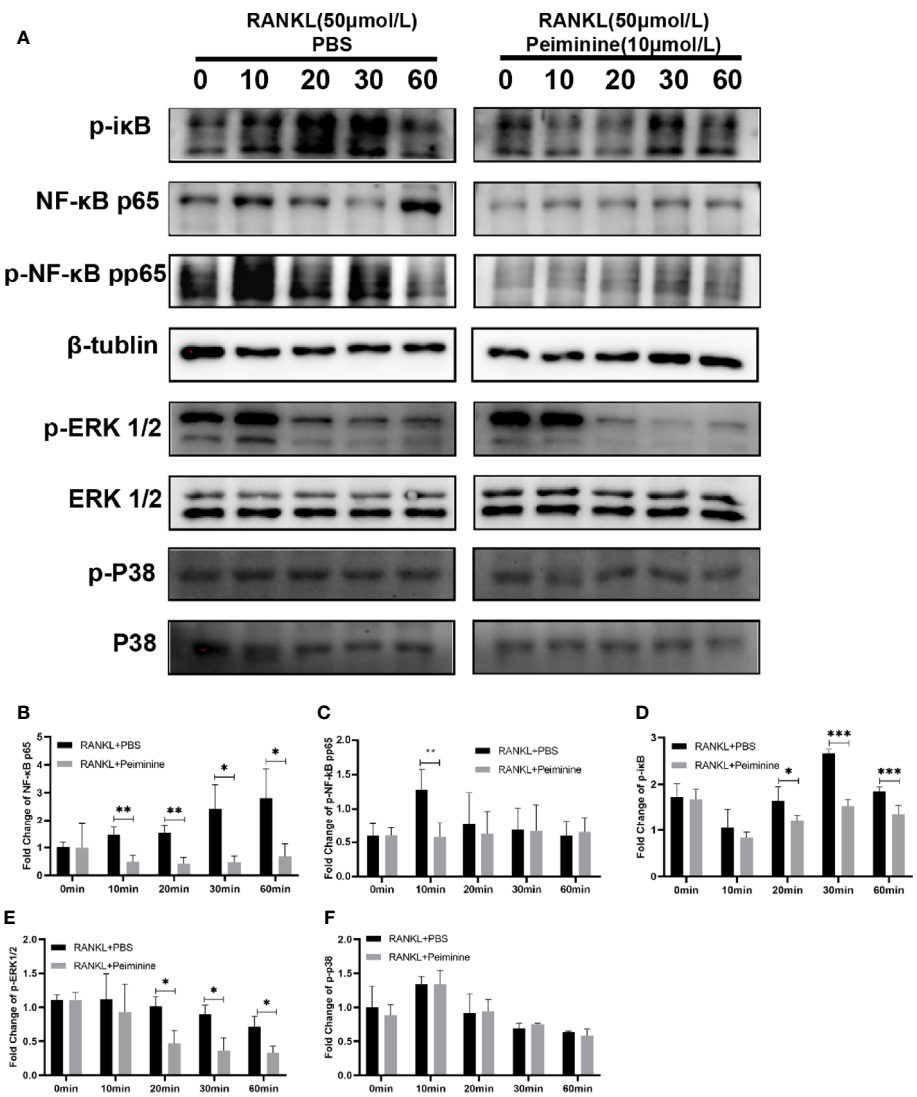

FIGURE 6 | Peiminine interferes with the NF-κB and ERK1/2 pathways. **(A)** Western blot analysis of NF-κB, p-iκB, p-NF-κB, p-ERK1/2, and p-P38 in cells treated with RANKL (50 ng/mL) for different amounts of time (0, 10, 20, 30, and 60 min) in the presence or absence of peiminine (10 μmol/L). Quantitative analysis of the differential expression levels of **(B)** NF-κB (n= 3), **(C)** p-NF-κB (n= 4), **(D)** p-iκB (n= 4), **(E)** p-ERK1/2 (n= 3), **(F)** p-P38 (n= 3). β-tublin was selected as the control protein for the normalization of p-iκB, NF-κB, p-NF-κB, and the ERK1/2 for p-ERK1/2, the P38 for p-P38. *P < 0.05, **P < 0.01, ***P < 0.001.

TRAP is associated with oxidative stress and a crucial indicator of OCs (33). According to our results, under the premise of peiminine's biosafety, we verified peiminine's inhibitory effect in different concentrations and stages. Furthermore, the fluorescence staining and bone slice resorption results strengthen the TRAP staining results and together show that peiminine suppressed both OC fusion and function.

The following experiments were carried out to confirm the conclusions above at the molecular level. The role of NFATc1 is critical throughout osteoclastogenesis (34), and according to previous research, c-Fos is the indispensable bridge between RANK and NFATc1 (17, 35, 36). As shown in **Figures 4** and **5**, the levels of the gene TNFRSF11, which encodes for RANK, and the genes NFATc1 and c-Fos were in decline within the groups treated with peiminine. Results above suggest that peiminine might affect the whole RANK-NFATc1 pathway. Therefore, it can be speculated that peiminine decreases the levels of downstream factors, including CTSK, and Integrinβ3, which are crucial for OCs' resorption (37–39); as well as DC-STAMP and ATP6v0d2, which are indispensable in OCs' cellular fusion and maturation (3, 40–43).

The activation of NF-κB is an important event that occurs in the early stage of RANKL-induced OC differentiation and is vital for the activation of NFATc1 (44). NF-κB is mainly present in the cytosol in the form of a dimer consisting of iκB and NF-κB, and iκB can prevent NF-κB from entering the nuclei (17, 45). RANKL can induce the phosphorylation of iκB and lead to the degradation of iκB. NF-κB is activated in the absence of iκB, and

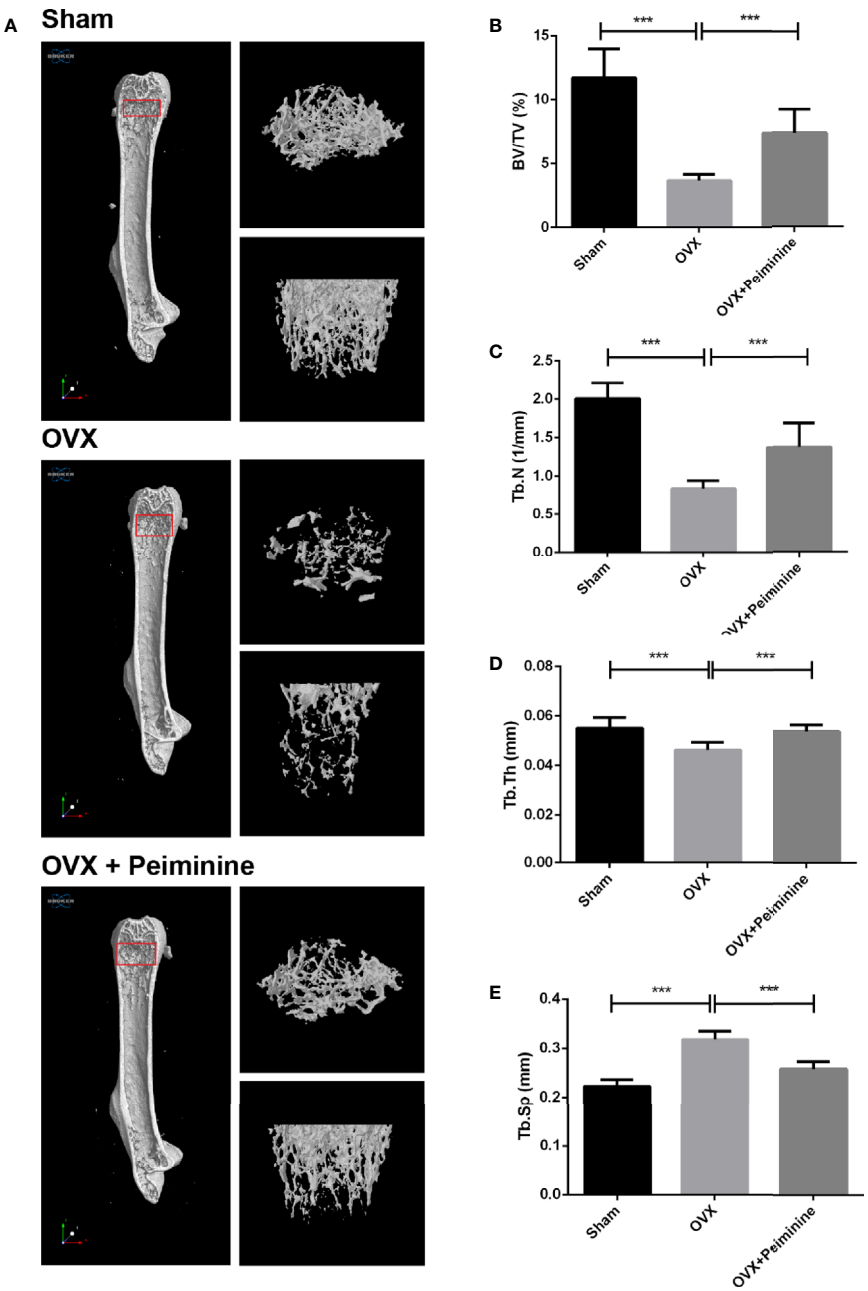

FIGURE 7 | Peiminine ameliorates the systematic bone loss induced by OVX. **(A)** Computer-generated 3D high-resolution micro-CT image of the femur microstructure. Quantitative measurements of **(B)** BV/TV, **(C)** Tb. N, **(D)** Tb. Th, and **(E)** Tb. Sp in the control group (sham), non-treatment group (OVX), and treatment group (OVX+peiminine). n= 10, ***P < 0.001.

p-NF-κB enters the nucleus and is involved in the activation of NFATc1 (32). As shown in **Figures 6A, C, D**, peiminine downregulated the expression of NF-κB and p-NF-κB, suggesting that it has an inhibitory effect on NFATc1. We also found that peiminine significantly decreased the level of p-iκB, suggesting that it suppresses the degradation of iκB by inhibiting iκB phosphorylation. This phenomenon explains why the levels of NF-κB and p-NF-κB were reduced in the presence of peiminine.

MAPK pathways, including ERK, JNK, and P38, are associated with OC formation and function (36, 46), and ERK is indispensable for OC survival (18, 35). We therefore assessed these two signaling pathways, revealing that peiminine downregulated ERK1/2 in the early stage of osteoclastogenesis but did not affect the expression of p-P38. Peiminine inhibited osteoclastogenesis and obviously prevented bone loss in OVX mice, most likely by interfering with the NF-κB, ERK and c-Fos-NFATc1 pathways (**Figure 9**).

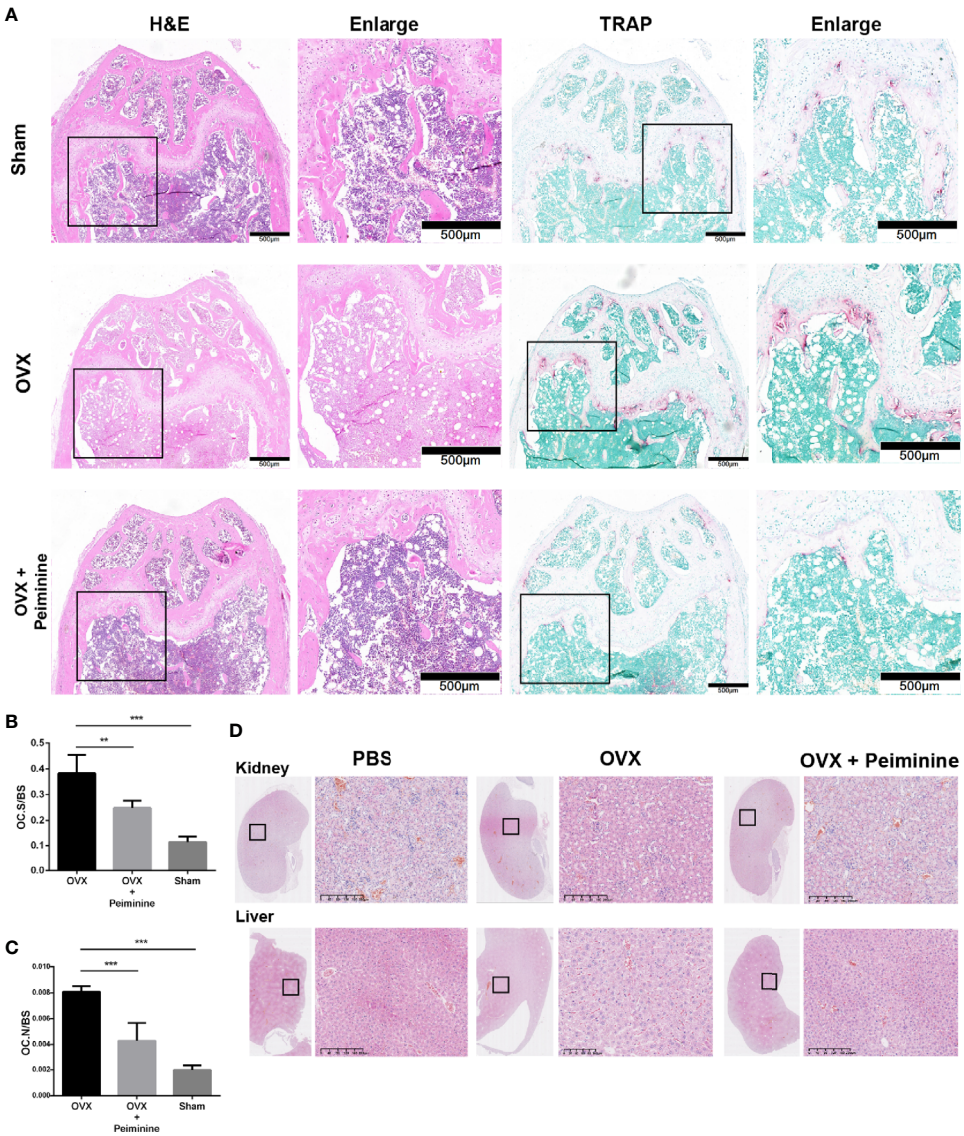

FIGURE 8 | Peiminine had no bio-toxicity and ameliorated the bone loss induced by OVX by inhibiting osteoclastogenesis in vivo. **(A)** Representative H&E and TRAP staining images of decalcified bones from mice in the sham, OVX, and peiminine (10 mg/kg) treatment groups. **(B)** Representative H&E staining images of kidneys and livers of mice from the control and experimental groups. Quantitative measurements of **(B)** OC. S/BS; **(C)** OC. N/BS, in the control group (Sham), non-treatment group (OVX), and treatment group (OVX + peiminine). n= 5, **P < 0.01, ***P < 0.001. **(D)** Representative H&E staining images of kidneys and livers of mouse from control and experimental groups.

Estrogen has the ability to block osteoclastogenesis and increase OC apoptosis, and the withdrawal of estrogen increases the number of OCs and promotes bone resorption (47). Thus, we used OVX mouse as the experimental animal model. Animal experiments further supported the results *in vitro*. Because peiminine can presumably alleviate estrogen deficiency-induced osteoclastogenesis *in vivo*. The μCT and histological analysis results suggested that peiminine effectively decreased the level of osteoporosis in OVX mice, as relatively mild bone loss was observed in these mice treated with peiminine. Besides, the biosafety of peiminine was reconfirmed by animal experiments, as none of the mice injected with peiminine exhibited an abnormal reaction or hypersensitivity, demonstrating its safety.

In this study, we assessed the alleviating effect of peiminine *in vivo* after systemic administration, but there is room for improvement. For example, whether the circumstances of systemic peiminine administration affect bone homeostasis or cause side effects remains unknown. The inclusion of an extra sham-operated group of mice treated with peiminine could help to assess the effect of the drug in the steady state. Additionally, the serum detection of bone turnover markers, such as CTX, OPG, P1NP, and RANKL, after peiminine

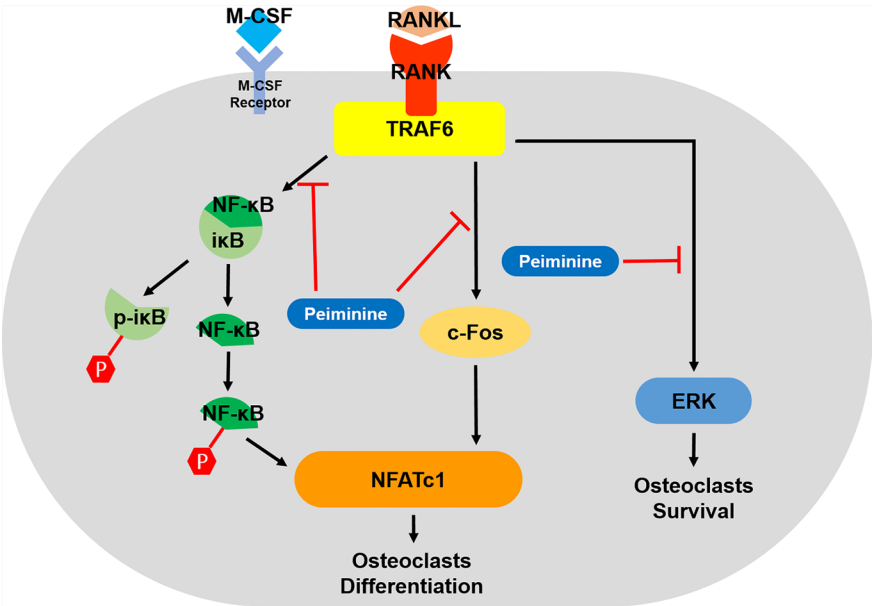

FIGURE 9 | Schematic diagram of how peiminine suppresses RANKL-induced osteoclastogenesis.

treatment would presumably further elucidate its mechanism of action.

In addition, the mode of peiminine needs to be further investigated. In this study, OVX mice were treated before the induction of osteoporosis, which indicated the alleviating effect of peiminine on bone loss, but whether peiminine can ameliorate previous bone loss remains to be determined. In the future, we plan to administer peiminine to osteoporotic mice to study its therapeutic effect upon osteoporosis. It is also important to explore the effects of the drug on mice undergoing long-term treatment, as these experiments can provide more information on the long-term impacts of peiminine on bone quality and potential side effects and thereby aid the development of more scientific therapeutic strategies.

In the future, we hope to study additional dosing strategies. A newly developed smart nanosacrificial layer was shown to precisely target and inhibit osteoclast function. Nanomaterials modified by tetracycline with bone-targeting properties can be used to encapsulate intervening drugs, thereby yielding better targeted drug delivery than that achieved *via* systemic administration (48). This represents a promising research direction for the application of peiminine in the future.

CONCLUSION

This study demonstrates that peiminine, a natural herb-extracted compound, can inhibit the formation and function of OCs *via* multiple targets and is therefore a promising novel therapeutic agent for osteoporosis.

DATA AVAILABILITY STATEMENT

The original contributions presented in the study are included in the article/supplementary material. Further inquiries can be directed to the corresponding authors.

ETHICS STATEMENT

The animal study was reviewed and approved by Laboratory Animal Center of Sir Run Run Shaw Affiliated Hospital of Zhejiang University School of Medicine.

AUTHOR CONTRIBUTIONS

MZ and SW contributed to conception. MZ, LS, and TW designed the study, and MZ wrote the first draft of the manuscript. WX, JZ, and YW organized the database. YG, RY, and YC performed the statistical analysis. BZ, ZW, and JZ wrote sections of the manuscript. All authors contributed to the article and approved the submitted version.

FUNDING

This project was supported by the National Natural Science Foundation of China (Grant Nos. 81572207, 81201435, 82101647), Natural Science Fund of Zhejiang Province (LQ20H060005) Medical Health Science and Technology Project of Zhejiang Provincial Health Commission (2021436226), Health Commission of Shanxi Province (Grant No. 2020075), and the Public Projects of Zhejiang Province (LGF19H060013).

REFERENCES

1. Armas LA, Recker RR. Pathophysiology of Osteoporosis: New Mechanistic Insights. *Endocrinol Metab Clin North Am* (2012) 41(3):475–86. doi: 10.1016/j.ecl.2012.04.006
2. Coughlan T, Dockery F. Osteoporosis and Fracture Risk in Older People. *Clin Med (Lond)* (2014) 14(2):187–91. doi: 10.7861/clinmedicine.14-2-187
3. Chen X, Wang Z, Duan N, Zhu G, Schwarz EM, Xie C. Osteoblast-Osteoclast Interactions. *Connect Tissue Res* (2018) 59(2):99–107. doi: 10.1080/03008207.2017.1290085
4. Judd HL, Meldrum DR, Deftos LJ, Henderson BE. Estrogen Replacement Therapy: Indications and Complications. *Ann Intern Med* (1983) 98(2):195–205. doi: 10.7326/0003-4819-98-2-195
5. Ticconi C, Pietropolli A, Piccione E. Estrogen Replacement Therapy and Asthma. *Pulm Pharmacol Ther* (2013) 26(6):617–23. doi: 10.1016/j.pupt.2013.08.004
6. Maraka S, Kennel KA. Bisphosphonates for the Prevention and Treatment of Osteoporosis. *BMJ* (2015) 351:h3783. doi: 10.1136/bmj.h3783
7. Jin H, Wang Q, Chen K, Xu K, Pan H, Chu F, et al. Astilbin Prevents Bone Loss in Ovariectomized Mice Through the Inhibition of RANKL-Induced Osteoclastogenesis. *J Cell Mol Med* (2019) 23(12):8355–68. doi: 10.1111/jcmm.14713
8. Jin H, Yao L, Chen K, Liu Y, Wang Q, Wang Z, et al. Evodiamine Inhibits RANKL-Induced Osteoclastogenesis and Prevents Ovariectomy-Induced Bone Loss in Mice. *J Cell Mol Med* (2019) 23(1):522–34. doi: 10.1111/jcmm.13955
9. Wang Q, Yao L, Xu K, Jin H, Chen K, Wang Z, et al. Madecassoside Inhibits Estrogen Deficiency-Induced Osteoporosis by Suppressing RANKL-Induced Osteoclastogenesis. *J Cell Mol Med* (2019) 23(1):380–94. doi: 10.1111/jcmm.13942
10. Ruan X, Yang L, Cui WX, Zhang MX, Li ZH, Liu B, et al. Optimization of Supercritical Fluid Extraction of Total Alkaloids, Peimisine, Peimine and Peiminine From the Bulb of Fritillaria Thunbergii Miq, and Evaluation of Antioxidant Activities of the Extracts. *Materials (Basel)* (2016) 9(7):524–41. doi: 10.3390/ma9070524
11. Gong Q, Li Y, Ma H, Guo W, Kan X, Xu D, et al. Peiminine Protects Against Lipopolysaccharide-Induced Mastitis by Inhibiting the AKT/NF-Kappab, ERK1/2 and P38 Signaling Pathways. *Int J Mol Sci* (2018) 19(9):2637–49. doi: 10.3390/ijms19092637
12. Chen G, Liu J, Jiang L, Ran X, He D, Li Y, et al. Peiminine Protects Dopaminergic Neurons From Inflammation-Induced Cell Death by Inhibiting the ERK1/2 and NF-kappaB Signalling Pathways. *Int J Mol Sci* (2018) 19(3):821–33. doi: 10.3390/ijms19030821
13. Miyamoto T. Regulators of Osteoclast Differentiation and Cell-Cell Fusion. *Keio J Med* (2011) 60(4):101–5. doi: 10.2302/kjm.60.101
14. Amin N, Boccardi V, Taghizadeh M, Jafarnejad S. Probiotics and Bone Disorders: The Role of RANKL/RANK/OPG Pathway. *Aging Clin Exp Res* (2020) 32(3):363–71. doi: 10.1007/s40520-019-01223-5
15. Tobeiha M, Moghadasian MH, Amin N, Jafarnejad S. RANKL/RANK/OPG Pathway: A Mechanism Involved in Exercise-Induced Bone Remodeling. *BioMed Res Int* (2020) 2020:6910312. doi: 10.1155/2020/6910312
16. Boyle WJ, Simonet WS, Lacey DL. Osteoclast Differentiation and Activation. *Nature* (2003) 423(6937):337–42. doi: 10.1038/nature01658
17. Hayden MS, Ghosh S. Signaling to NF-Kappab. *Genes Dev* (2004) 18(18):2195–224. doi: 10.1101/gad.1228704
18. Koga Y, Tsurumaki H, Aoki-Saito H, Sato M, Yatomi M, Takehara K, et al. Roles of Cyclic AMP Response Element Binding Activation in the ERK1/2 and P38 MAPK Signalling Pathway in Central Nervous System, Cardiovascular System, Osteoclast Differentiation and Mucin and Cytokine Production. *Int J Mol Sci* (2019) 20(6):1346–68. doi: 10.3390/ijms20061346
19. Chao X, Wang G, Tang Y, Dong C, Li H, Wang B, et al. The Effects and Mechanism of Peiminine-Induced Apoptosis in Human Hepatocellular Carcinoma HepG2 Cells. *PloS One* (2019) 14(1):e0201864. doi: 10.1371/journal.pone.0201864
20. Lyu Q, Tou F, Su H, Wu X, Chen X, Zheng Z. The Natural Product Peiminine Represses Colorectal Carcinoma Tumor Growth by Inducing Autophagic Cell Death. *Biochem Biophys Res Commun* (2015) 462(1):38–45. doi: 10.1016/j.bbrc.2015.04.102
21. Du B, Cao L, Wang K, Miu J, Yao L, Xu Z, et al. Peiminine Attenuates Acute Lung Injury Induced by LPS Through Inhibiting Lipid Rafts Formation. *Inflammation* (2020) 43(3):1110–9. doi: 10.1007/s10753-020-01198-w
22. Guo H, Ji F, Liu B, Chen X, He J, Gong J. Peiminine Ameliorates Bleomycin-Induced Acute Lung Injury in Rats. *Mol Med Rep* (2013) 7(4):1103–10. doi: 10.3892/mmr.2013.1312
23. Ma X, Liu A, Liu W, Wang Z, Chang N, Li S, et al. Analyze and Identify Peiminine Target EGFR Improve Lung Function and Alleviate Pulmonary Fibrosis to Prevent Exacerbation of Chronic Obstructive Pulmonary Disease by Phosphoproteomics Analysis. *Front Pharmacol* (2019) 10:737. doi: 10.3389/fphar.2019.00737
24. Zhao B, Shen C, Zheng Z, Wang X, Zhao W, Chen X, et al. Peiminine Inhibits Glioblastoma *In Vitro* and *In Vivo* Through Cell Cycle Arrest and Autophagic Flux Blocking. *Cell Physiol Biochem* (2018) 51(4):1566–83. doi: 10.1159/000495646
25. Luo Z, Zheng B, Jiang B, Xue X, Xue E, Zhou Y. Peiminine Inhibits the IL-1beta Induced Inflammatory Response in Mouse Articular Chondrocytes and Ameliorates Murine Osteoarthritis. *Food Funct* (2019) 10(4):2198–208. doi: 10.1039/c9fo00307j
26. Chen X, Wang C, Qiu H, Yuan Y, Chen K, Cao Z, et al. Asperpyrone A Attenuates RANKL-Induced Osteoclast Formation Through Inhibiting NFATc1, Ca(2+) Signalling and Oxidative Stress. *J Cell Mol Med* (2019) 23(12):8269–79. doi: 10.1111/jcmm.14700
27. Zhou L, Liu Q, Yang M, Wang T, Yao J, Cheng J, et al. Dihydroartemisinin, an Anti-Malaria Drug, Suppresses Estrogen Deficiency-Induced Osteoporosis, Osteoclast Formation, and RANKL-Induced Signaling Pathways. *J Bone Miner Res* (2016) 31(5):964–74. doi: 10.1002/jbmr.2771
28. Anderson DM, Maraskovsky E, Billingsley WL, Dougall WC, Tometsko ME, Roux ER, et al. A Homologue of the TNF Receptor and Its Ligand Enhance T-Cell Growth and Dendritic-Cell Function. *Nature* (1997) 390(6656):175–9. doi: 10.1038/36593
29. Bourette RP, Rohrschneider LR. Early Events in M-CSF Receptor Signaling. *Growth Factors* (2000) 17(3):155–66. doi: 10.3109/08977190009001065
30. Asagiri M, Sato K, Usami T, Ochi S, Nishina H, Yoshida H, et al. Autoamplification of NFATc1 Expression Determines Its Essential Role in Bone Homeostasis. *J Exp Med* (2005) 202(9):1261–9. doi: 10.1084/jem.20051150
31. Jimi E, Takakura N, Hiura F, Nakamura I, Hirata-Tsuchiya S. The Role of NF-kappaB in Physiological Bone Development and Inflammatory Bone Diseases: Is NF-kappaB Inhibition "Killing Two Birds With One Stone"? *Cells* (2019) 8(12):1636–51. doi: 10.3390/cells8121636
32. Asagiri M, Takayanagi H. The Molecular Understanding of Osteoclast Differentiation. *Bone* (2007) 40(2):251–64. doi: 10.1016/j.bone.2006.09.023
33. Hayman AR. Tartrate-Resistant Acid Phosphatase (TRAP) and the Osteoclast/Immune Cell Dichotomy. *Autoimmunity* (2008) 41(3):218–23. doi: 10.1080/08916930701694667
34. Lacey DL, Timms E, Tan HL, Kelley MJ, Dunstan CR, Burgess T, et al. Osteoprotegerin Ligand Is a Cytokine That Regulates Osteoclast Differentiation and Activation. *Cell* (1998) 93(2):165–76. doi: 10.1016/s0092-8674(00)81569-x
35. Miyazaki T, Katagiri H, Kanegae Y, Takayanagi H, Sawada Y, Yamamoto A, et al. Reciprocal Role of ERK and NF-kappaB Pathways in Survival and Activation of Osteoclasts. *J Cell Biol* (2000) 148(2):333–42. doi: 10.1083/jcb.148.2.333
36. Matsumoto M, Kogawa M, Wada S, Takayanagi H, Tsujimoto M, Katayama S, et al. Essential Role of P38 Mitogen-Activated Protein Kinase in Cathepsin K Gene Expression During Osteoclastogenesis Through Association of NFATc1 and PU.1. *J Biol Chem* (2004) 279(44):45969–79. doi: 10.1074/jbc.M408795200
37. Drake MT, Clarke BL, Oursler MJ, Khosla S. Cathepsin K Inhibitors for Osteoporosis: Biology, Potential Clinical Utility, and Lessons Learned. *Endocr Rev* (2017) 38(4):325–50. doi: 10.1210/er.2015-1114
38. Geoghegan IP, Hoey DA, McNamara LM. Integrins in Osteocyte Biology and Mechanotransduction. *Curr Osteoporos Rep* (2019) 17(4):195–206. doi: 10.1007/s11914-019-00520-2
39. Hynes RO. Integrins: Versatility, Modulation, and Signaling in Cell Adhesion. *Cell* (1992) 69(1):11–25. doi: 10.1016/0092-8674(92)90115-s
40. Chiu YH, Ritchlin CT. DC-STAMP: A Key Regulator in Osteoclast Differentiation. *J Cell Physiol* (2016) 231(11):2402–7. doi: 10.1002/jcp.25389

41. Islam R, Bae HS, Yoon WJ, Woo KM, Baek JH, Kim HH, et al. Pin1 Regulates Osteoclast Fusion Through Suppression of the Master Regulator of Cell Fusion DC-STAMP. *J Cell Physiol* (2014) 229(12):2166–74. doi: 10.1002/jcp.24679
42. Lee SH, Rho J, Jeong D, Sul JY, Kim T, Kim N, et al. V-ATPase V0 Subunit D2-Deficient Mice Exhibit Impaired Osteoclast Fusion and Increased Bone Formation. *Nat Med* (2006) 12(12):1403–9. doi: 10.1038/nm1514
43. Mensah KA, Ritchlin CT, Schwarz EM. RANKL Induces Heterogeneous DC-STAMP(lo) and DC-STAMP(hi) Osteoclast Precursors of Which the DC-STAMP(lo) Precursors Are the Master Fusogens. *J Cell Physiol* (2010) 223 (1):76–83. doi: 10.1002/jcp.22012
44. Takatsuna H, Asagiri M, Kubota T, Oka K, Osada T, Sugiyama C, et al. Inhibition of RANKL-Induced Osteoclastogenesis by (-)-DHMEQ, a Novel NF-kappaB Inhibitor, Through Downregulation of Nfatc1. *J Bone Miner Res* (2005) 20(4):653–62. doi: 10.1359/JBMR.041213
45. Ghosh S, Karin M. Missing Pieces in the NF-kappaB Puzzle. *Cell* (2002) 109 (Suppl):S81–96. doi: 10.1016/s0092-8674(02)00703-1
46. Matsumoto M, Sudo T, Saito T, Osada H, Tsujimoto M. Involvement of P38 Mitogen-Activated Protein Kinase Signaling Pathway in Osteoclastogenesis Mediated by Receptor Activator of NF-Kappa B Ligand (RANKL). *J Biol Chem* (2000) 275(40):31155–61. doi: 10.1074/jbc.M001229200
47. Pacifici R. Estrogen, Cytokines, and Pathogenesis of Postmenopausal Osteoporosis. *J Bone Miner Res* (1996) 11(8):1043–51. doi: 10.1002/jbmr.5650110802
48. Lin X, Wang Q, Gu C, Li M, Chen K, Chen P, et al. Smart Nanosacrificial Layer on the Bone Surface Prevents Osteoporosis Through Acid-Base Neutralization Regulated Biocascade Effects. *J Am Chem Soc* (2020) 142 (41):17543–56. doi: 10.1021/jacs.0c07309

Conflict of Interest: The authors declare that the research was conducted in the absence of any commercial or financial relationships that could be construed as a potential conflict of interest.

Publisher's Note: All claims expressed in this article are solely those of the authors and do not necessarily represent those of their affiliated organizations, or those of the publisher, the editors and the reviewers. Any product that may be evaluated in this article, or claim that may be made by its manufacturer, is not guaranteed or endorsed by the publisher.

frontiers in Endocrinology

ORIGINAL RESEARCH
published: 02 December 2021
doi: 10.3389/fendo.2021.703167

The miR-4739/DLX3 Axis Modulates Bone Marrow-Derived Mesenchymal Stem Cell (BMSC) Osteogenesis Affecting Osteoporosis Progression

Ding Li[1]*, *Qi Yuan*[2], *Liang Xiong*[1], *Aoyu Li*[1] and *Yu Xia*[1]

[1] Department of Orthopedics, The Second Xiangya Hospital, Central South University, Changsha, China,
[2] Department of Hepatopathy, The Hunan Provincial People's Hospital, The First Affiliated Hospital of Hunan Normal University, Changsha, China

OPEN ACCESS

Edited by:
Michaela Tencerova, Academy of Sciences of the Czech Republic (ASCR), Czechia

Reviewed by:
Elizabeth Rendina-Ruedy, Vanderbilt University Medical Center, United States
Florence Figeac, Odense University Hospital, Denmark

***Correspondence:**
Ding Li
liding2209@csu.edu.cn

Specialty section:
This article was submitted to Bone Research, a section of the journal Frontiers in Endocrinology

Received: *30 April 2021*
Accepted: *08 November 2021*
Published: *02 December 2021*

Citation:
Li D, Yuan Q, Xiong L, Li A and Xia Y (2021) The miR-4739/DLX3 Axis Modulates Bone Marrow-Derived Mesenchymal Stem Cell (BMSC) Osteogenesis Affecting Osteoporosis Progression. Front. Endocrinol. 12:703167. doi: 10.3389/fendo.2021.703167

Osteoporosis is a complex multifactorial disorder linked to various risk factors and medical conditions. Bone marrow-derived mesenchymal stem cell (BMSC) dysfunction potentially plays a critical role in osteoporosis pathogenesis. Herein, the study identified that miR-4739 was upregulated in BMSC cultures harvested from osteoporotic subjects. BMSCs were isolated from normal and osteoporotic bone marrow tissues and identified for their osteogenic differentiation potential. In osteoporotic BMSCs, miR-4739 overexpression significantly inhibited cell viability, osteoblast differentiation, mineralized nodule formation, and heterotopic bone formation, whereas miR-4739 inhibition exerted opposite effects. Through direct binding, miR-4739 inhibited distal-less homeobox 3 (DLX3) expression. In osteoporotic BMSCs, DLX3 knockdown also inhibited BMSC viability and osteogenic differentiation. Moreover, DLX3 knockdown partially attenuated the effects of miR-4739 inhibition upon BMSCs. Altogether, the miR-4739/DLX3 axis modulates the capacity of BMSCs to differentiate into osteoblasts, which potentially plays a role in osteoporosis pathogenesis. The *in vivo* and clinical functions of the miR-4739/DLX3 axis require further investigation.

Keywords: Osteoporosis, bone marrow-derived mesenchymal stem cell (BMSC), osteogenic differentiation, miR-4739, DLX3

INTRODUCTION

Osteoporosis is a complex multifactorial disorder that is related to various risk factors and medical conditions. Three common types of osteoporosis are senile osteoporosis, sex steroid deficiency osteoporosis, and secondary osteoporosis (1–5). Moreover, in postmenopausal women with osteoporosis, the aging of osteocytes and their microenvironment, low levels of estrogen, and increased reactive oxygen species (ROS) production provoke a decline in bone formation and an increase in bone resorption (2, 6). Reportedly, bone regeneration through BMSCs infusion could

trigger osteogenesis, thereby providing a potential therapeutic strategy for primary osteoporosis (7). The identification of the alterations occurring in the bone marrow population dynamics, namely the dysfunction of BMSCs, is essential for designing optimized strategies to restore bone formation.

MicroRNAs (miRNAs) are small, single-stranded non-coding RNAs having an average of 22 nucleotides in length. miRNAs exert their biological functions through the downregulation of gene expression *via* translational repression or degradation of mRNA targets (8, 9). As per recent reports, multiple miRNAs could potentially play a part in osteogenesis (10–12). Several studies indicated the potential roles of miRNAs in osteoporosis pathogenesis, affecting BMSC osteogenic differentiation (13–16). For instance, Li et al. (13) indicated that miR-188 is an important regulator of the age-associated switch between osteoblast and adipocyte differentiation of BMSCs, representing an underlying therapeutic target for age-associated bone loss. Hu et al. (15) reported that miR-26b modulated osteoactivin-induced osteoblast differentiation of BMSCs *via* the GSK3β/β-catenin signaling. Over the past decades, RNA-sequencing and miRNA-microarray have been performed to identify differentially expressed miRNAs in the BMSCs in control or osteoporotic subjects or at different stages of osteogenic differentiation. For instance, Wang and colleagues analyzed RNA-seq and miRNA-microarray data for differentially expressed between the ovariectomized (OVX) mice and controls, and 22 miRNAs were identified (17). Considering that miRNAs exert regulatory roles in target gene expression, identifying more miRNA/mRNA axes modulating BMSC osteogenic differentiation could potentially provide potential agents for osteoporosis treatment.

In this study, online microarray chip data from Gene Expression Omnibus (GEO) were analyzed to select miRNAs differentially expressed in osteoporotic subjects, and miR-4739 was subsequently selected. BMSCs were isolated from normal and osteoporotic bone marrow tissues, respectively, and identified. BMSCs were induced towards osteogenic differentiation, and the differentiation was verified. miR-4739 overexpression or inhibition was achieved in BMSCs, and the effects of miR-4739 upon osteogenesis were then examined. Downstream targets of miR-4739 were analyzed, and DLX3 was selected. Predicted miR-4739 binding to DLX3 and miR-4739 regulation of DLX3 were investigated. The co-effects of the miR-4739/DLX3 axis upon BMSC osteogenesis were determined.

MATERIALS AND METHODS

Tissue Sample Collection

Osteoporotic bone marrow tissues were harvested from patients (n=5, 62.80 ± 6.61 years, female/male is 4/1) who were diagnosed with osteoporosis and who underwent hip surgery. The normal bone marrow tissues were donated by the patients who underwent lower limbs traumatic fracture (n=5, 53.20 ± 4.32 years, female/male is 3/2). No differences were observed in age, BMI, serum vitamin D status, serum calcium, and parathyroid hormone status between the controls and osteoporosis patients. All tissue samples were collected under sterile conditions and transferred to a tube containing heparin anticoagulant immediately after resection. Informed consent was signed by each enrolled patient, and the sampling was approved by the Ethics Committee of the Second Xiangya Hospital of Central South University [approval No. 2018(Yan001)].

Isolating BMSCs From Bone Marrow Tissues

BMSCs were isolated from osteoporotic or normal bone marrow tissues following the aforementioned methods (18, 19). Collected BMSCs were maintained in Dulbecco modified Eagle's medium (DMEM; Invitrogen, Carlsbad, CA, USA) supplemented with 10% heat-inactivated FBS and 1% penicillin, at 37°C in 5% CO_2. The medium was replaced with fresh medium every 2 days. Passage 2-5 BMSCs were used in all experiments. Flow cytometry was performed to identify isolated osteoporotic and normal BMSCs by detecting CD34, CD45, CD73, CD90, and CD105.

Flow Cytometry

When the density of the BMSCs reached 80%, BMSCs were trypsinized, centrifuged, and the supernatant was discarded. Cells were resuspended and adjusted to the density of 3-6 × 10^3 cells/μl. CD73, CD90, CD105, CD45, and CD34 antibodies (obtained from Abcam, Cambridge, MA, USA) were used for a 30-min incubation at room temperature for cell labeling, using untreated BMSCs and isotype-control (FITC- or PE-labeled Mouse IgG1 obtained from Abcam) as controls.

Bioinformatics Analysis

To identify miRNAs or genes potentially regulating the osteogenic differentiation during osteoporosis, the Gene Expression Omnibus (GEO) datasets, including GSE74209 (Specific miRNAs profiles in Fresh femoral neck trabecular bone from 12 postmenopausal women who had undergone hip replacement due to either osteoporotic fracture or osteoarthritis without osteoporosis) (20), GSE93883 (Specific miRNAs profiles in the plasma from non-osteoporotic patients and osteoporotic patients with and without vertebral fractures), and GSE80614 (different genes expression profile in human BMSC and differentiation osteoblast) (21) were downloaded using the R language GEOquery package. The differential expression miRNAs or genes were analyzed by the Limma package. For the selection of miR-4739 targeted genes, miRDIP (22) (https://ophid.utoronto.ca/mirDIP/) was used to predict the miR-4739 targeted genes.

Real-Time Reverse Transcription-Polymerase Chain Reaction (qRT-PCR) Analysis

The TRIzol reagent (Invitrogen, Carlsbad, CA, USA) was used for extracting total RNA from target cells. A PrimeScript RT kit (Takara Bio, Shiga, Japan) was used for total RNA reverse

transcription. An ABI Prism 7500 Sequence Detection System (Applied Biosystems, Foster City, CA, USA) was used to run the reaction using the SYBR Green Quantitative Kit (Toyobo, Osaka, Japan). The level of U6 (for miRNA) or GAPDH (for mRNA) was used as an internal reference. The relative expression levels of each factor were calculated using the $2^{\Delta\Delta-ct}$ method. The primers are listed in **Table S1**.

Protein Isolation and Immunoblotting

The RIPA buffer containing protease inhibitors (Beyotime, Shanghai, China) was used to extract protein samples from target cells. The BCA quantitative method (Beyotime) was used to quantify the protein sample concentration. SDS-PAGE (10%; Invitrogen) was used to separate collected protein samples, which were then transferred to PVDF membranes (Millipore, Burlington, MA, USA). BSA (5%) was used to incubate the membranes for 2 h to prevent non-specific bindings. The following antibodies were used to incubate the membranes at 4°C overnight: ALP (ab67228, Abcam), OCN (ab93876, Abcam), RUNX2 (ab76956, Abcam), Osterix (ab209484, Abcam), DLX3 (ab178428, Abcam). Proper secondary antibodies (Cowin Biotech Co, Beijing, China) were used to incubate the membranes at room temperature for 2 h after the primary antibody incubation. Enhanced Chemiluminescence (ECL) Fluorescence Detection Kit (BB-3501; Amersham Pharmacia, Piscataway, NJ, USA) was used to visualize the blot signal on a Bio-Rad image analysis system (Bio-Rad, Hercules, CA, USA). The relative protein content is expressed by the gray value of the corresponding protein band/GAPDH protein band.

Alkaline Phosphatase (ALP) Staining

BMSCs were cultured in an osteogenic induction culture medium (complete culture medium contains 5 mM β-glycerophosphate, 50 μM ascorbate, and 100 nM dexamethasone) for 14 days and were stained with the ALP staining solution (Nanjing Jiancheng, Nanjing, China) on day 0, 7, and 14 of osteogenic induction. The staining results were observed under a microscope (Olympus, Tokyo, Japan), and representative images were photographed.

Alizarin Red Staining

BMSCs were cultured in an osteogenic induction culture medium for 21 days, and alizarin red staining was performed on days 0 and 21 of osteogenic induction as previously described (23). In general, the differentiated BMSCs were washed twice with PBS, fixed in isopropanol (60%) for 1 min at room temperature, washed twice with ddH_2O, and dyed with 1% Alizarin Red (Sigma-Aldrich, St. Louis, USA, MO) for 10 min at room temperature. A microscope (Olympus) was used to observe the staining and representative images were photographed.

Cell Transfection

miR-4739 overexpression or inhibition was achieved by transfecting agomir-4739 or antagomir-4739 (GenePharma, Shanghai, China). DLX3 knockdown was achieved by transfecting the shRNA vector containing short hairpin RNA against DLX3 (sh-DLX3, GenePharma). The transfection was performed using Lipofectamine 3000 (Life Technologies, Carlsbad, CA, USA) as per the aforementioned methods (24); 48 h after transfection, cells were harvested for subsequent experiments.

Cell Counting Kit 8 (CCK-8) Assay for Cell Viability

Cells, either treated or transfected, were seeded into 96-well plates at a density of 2×10^3 cells per well and incubated with 10 μl CCK-8 solution (Dojindo Co. Tokyo, Japan) at 37°C for 3 h. A microplate reader was then used to determine the optical density (OD) value at the wavelength of 450 nm at the end of the incubation with CCK-8 solution.

Dual-Luciferase Reporter Assay

Wild- and mutant-type DLX3 3'UTR luciferase reporter vectors were constructed based on psiCheck-2 (Promega, Madison, WI, USA) and named wt-/mut-DLX3; mut-DLX3 contains a 5-bp mutation in the predicted miR-4739 binding site. Reporter vectors were co-transfected in 293T cells with agomir-4739/antagomir-4739, and the luciferase activity was subsequently determined.

Heterotopic Bone Formation Assay *In Vivo*

BMSCs were transfected with miR-4739 antagomir mimics and mimics-NC for 24 h. Hydroxyapatite (HA) powder (40 mg, Sigma, USA) was diluted with 200 μl of the standard growth medium and mixed with BMSCs (5×10^6 cells) and incubated at 37°C for 2 h in 5% CO_2. Next, the BMSCs-HA mixtures were injected subcutaneously on the dorsal side of 6 weeks old BALB/C nude mice. Six weeks later, the mice were sacrificed, and the implants were collected. All the animal experiments were approved by the Animal Care and Use Ethics Committee of Central South University [approval No. 2018(Yan001)].

Histological Analysis

The heterotopic bone tissues were fixed in 10% buffered formalin for 48 h, decalcified using an EDTA-Decalcifying-fluid (Boster, Wuhan, China). The decalcified bone tissues were then embedded in paraffin. Histological analyses were performed on specimen cross-sections 5-μm thick stained with hematoxylin-eosin (HE) and Masson staining using the HE stain kit (Boster) and Masson's trichrome stain kit (Solarbio, Beijing, China). The sections were observed through an optical microscope (Olympus). The semiquantitative image analysis was performed by ImageJ (NIH, USA).

Statistics Analyses

Statistical analyses were carried out using GraphPad software. Data were reported as mean ± SD based on at least three replicates. *P* values are shown in the figures or figure legends. *P* values were calculated with unpaired Student's *t*-test for two groups or analysis of variation (ANOVA) with Tukey's *post-hoc*

for experiments with more than two groups. *P* values less than 0.05 were considered statistically significant.

RESULTS

miR-4739 Expression Is Upregulated in Osteoporotic BMSCs

To identify miRNAs that potentially regulate the osteogenic differentiation of osteoporotic BMSCs, differentially expressed miRNAs were analyzed using online microarray chip data from Gene Expression Omnibus (GEO) (**Figure 1A**). According to GSE74209 containing miRNAs differentially expressed in postmenopausal women experiencing hip arthroplasty due to either osteoporotic fracture or osteoarthritis without osteoporosis (**Figure 1C**, **Figure S1A** and **Table S2**) and GSE93883 containing miRNAs differentially expressed in non-osteoporotic patients and patients with osteoporosis in the presence or absence of vertebral fractures (**Figure 1D**, **Figure S1B** and **Table S2**), 3 upregulated miRNAs (miR-4739, miR-3202, and miR320c) were overlapped in two datasets (**Figures 1A, C, D**). In osteoporotic BMSCs, miR-4739 expression was mostly upregulated when compared with normal BMSCs (**Figure 1B**). Thus, miR-4739 was selected for subsequent experiments.

Isolation and Osteogenic Differentiation of BMSCs

To investigate the effect of miR-4739 on osteoporotic BMSC osteogenesis, the study isolated normal and osteoporotic BMSCs from normal and osteoporotic bone marrow tissues, respectively (**Figure 2A**). The identification of BMSCs was conducted using Flow cytometry detecting CD34, CD45, CD73, CD90, and CD105; as illustrated in **Figure 2B**, BMSCs were CD34-negative, CD45-negative, CD73-positive, CD90-positive, and CD105-positive. Normal and osteoporotic BMSCs were induced towards osteogenic differentiation for 21 days and examined for differentiation. On days 0, 7, and 14, the protein levels of ALP, OCN, Runx2, and Osterix were examined. As depicted in **Figure 2C**, the levels of all the four markers increased time-dependently; on day 14, the levels of the four markers in normal BMSCs exceeded those in osteoporotic BMSCs, suggesting the impaired osteogenic differentiation potential of osteoporotic BMSCs. Consistently, ALP staining confirmed the osteoblast differentiation in both types of BMSCs on days 7 and 14, and

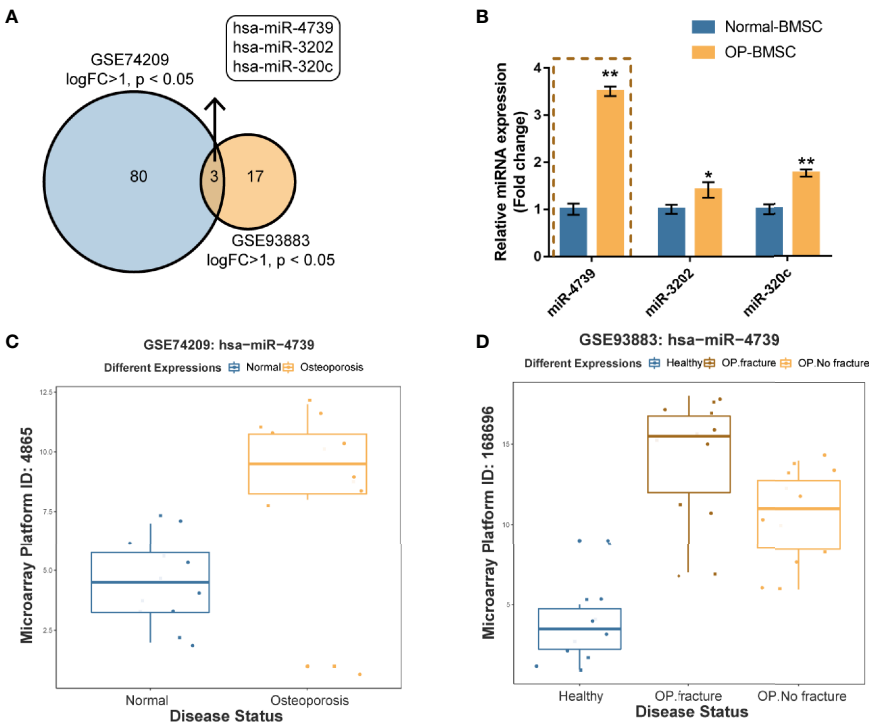

FIGURE 1 | miR-4739 expression is deregulated in osteoporotic bone marrow-derived mesenchymal stem cells (BMSCs) **(A)** miRNAs differentially expressed in postmenopausal women undergoing hip replacement due to either osteoporotic fracture or osteoarthritis in the absence of osteoporosis (GSE74209) or plasma from non-osteoporotic and osteoporotic patients with and without vertebral fractures (GSE93883) were compared (logFC >1, p < 0.05) and 3 miRNAs (miR-4739, miR-3202, and miR320c) were overlapped in two datasets. **(B)** The expression of miR-4739, miR-3202, and miR-320c in normal and osteoporotic BMSCs was determined by RT-PCR. (n=3) **(C, D)** The expression of miR-4739 is based on GSE74209 and GSE93883. *p < 0.05, **p < 0.01.

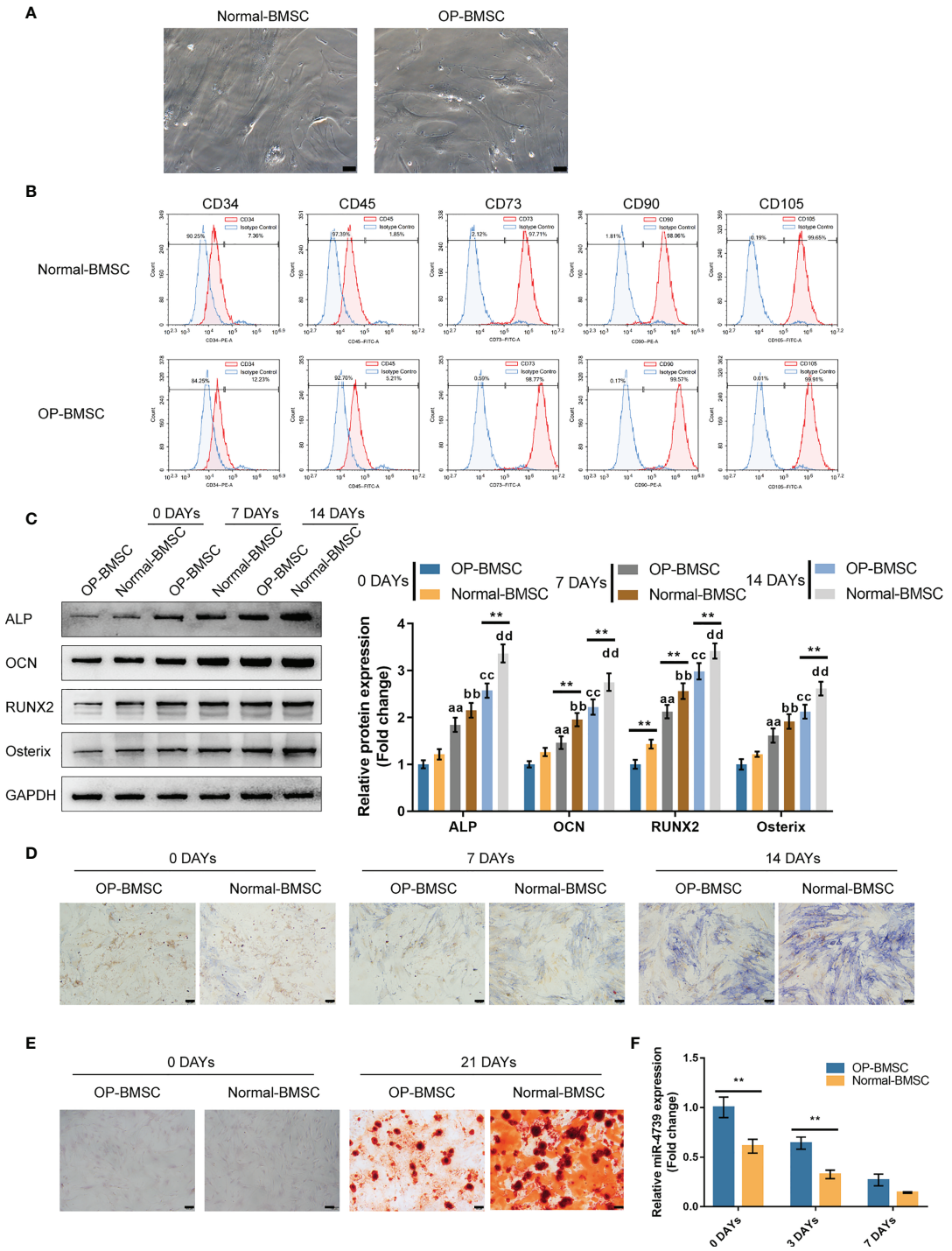

FIGURE 2 | Isolation and osteogenic differentiation of BMSCs **(A)** Normal and osteoporotic BMSCs were isolated from normal and osteoporotic bone marrow tissues, respectively (the scale bar is 50 μm). **(B)** Flow cytometry was performed to identify isolated BMSCs detecting CD34, CD45, CD73, CD90, and CD105. **(C)** Normal and osteoporotic BMSCs were induced towards osteogenic differentiation for 21 days, and the protein levels of ALP, OCN, Runx2, and Osterix were examined using Immunoblotting on days 0, 7, and 14 of osteogenic induction **(C)**; ALP staining was performed on day 0, 7, and 14 of osteogenic induction **(D)**; the formation of mineralized nodules were examined using Alizarin red staining on days 0 and 21 of osteogenic induction **(E)**; the expression of miR-4739 was examined using qRT-PCR on day 0, 3, and 7 of osteogenic induction in normal BMSCs and osteoporotic BMSCs **(F)**. n=3, **p < 0.01 compared to OP-BMSC. aa p<0.01 compared between 0 days OP-BMSC and 3 days OP-BMSC; bb p < 0.01 compared between 0 days normal-BMSC and 3 days normal-BMSC; cc p<0.01 compared between 0 days OP-BMSC and 14 days OP-BMSC; dd p < 0.01 compared between 0 days normal-BMSC and 14 days normal-BMSC.

Alizarin red staining confirmed the formation of mineralized nodules in both types of BMSCs on day 21; the osteoblast differentiation and mineralized nodule formation ability in osteoporotic BMSCs were impaired (**Figures 2D, E**). Meanwhile, miR-4739 expressions showed to be downregulated in the process of osteogenic differentiation time-dependently (**Figure 2F**).

Effects of miR-4739 Overexpression and Inhibition on Osteoporotic and Normal BMSC Osteogenic Differentiation

Considering the downregulation of miR-4739 during BMSC osteogenesis, the specific effect of miR-4739 on BMSC osteogenesis was further validated. The study achieved miR-4739 overexpression or inhibition in osteoporotic BMSCs through the transfection of agomir-4739 or antagomir-4739; qRT-PCR was performed to confirm miR-4739 expression (**Figure 3A**). In osteoporotic BMSCs, miR-4739 overexpression inhibited BMSC cell viability, whereas miR-4739 inhibition exerted opposite effects (**Figure 3B**). Osteoporotic BMSCs were subsequently transfected with agomir-4739 or antagomir-4739, induced towards osteogenic differentiation for 21 days, and examined for the effects of miR-4739 on BMSC osteogenesis. ALP staining showed that, on day 14 of osteogenic induction, miR-4739 overexpression inhibited, whereas miR-4739 inhibition promoted osteoblast differentiation (**Figure 3C**). Alizarin red staining revealed that, on day 21 of osteogenic

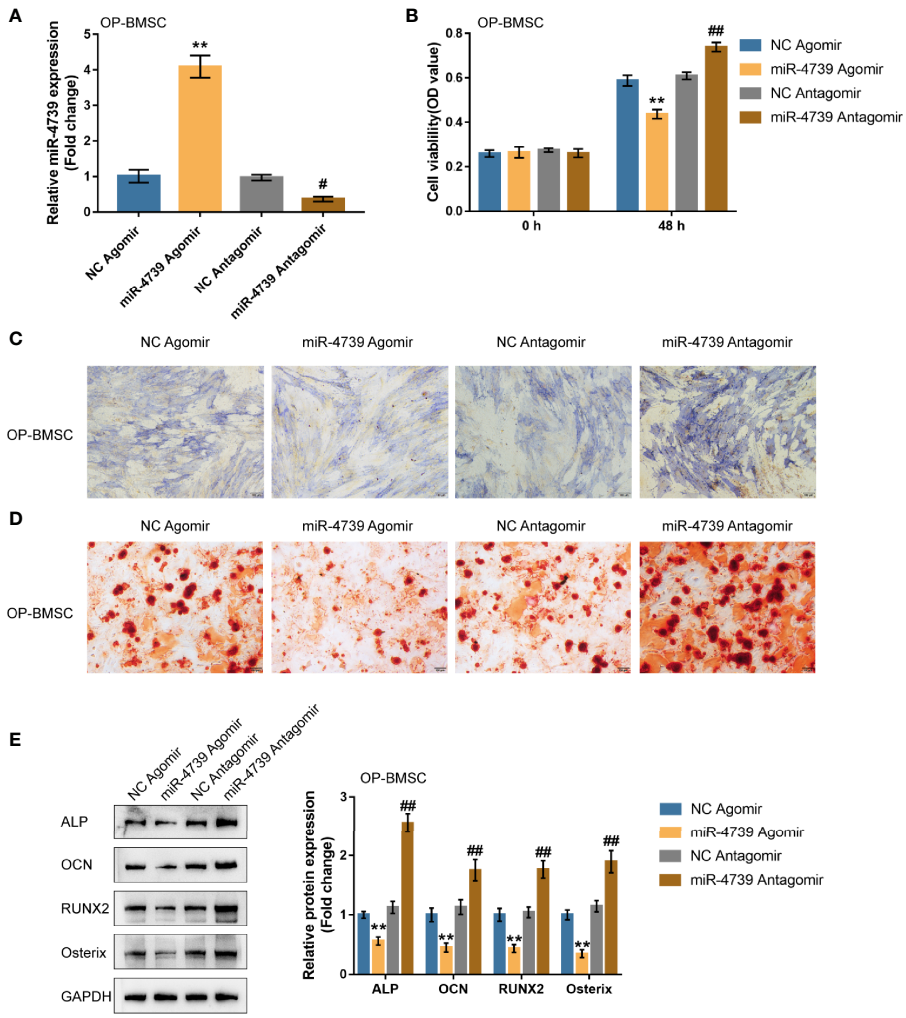

FIGURE 3 | Effects of miR-4739 overexpression and inhibition on osteoporotic BMSC osteogenic differentiation **(A)** miR-4739 overexpression or inhibition was achieved in osteoporotic BMSCs by transfecting agomir-4739 or antagomir-4739; miR-4739 expression was confirmed using qRT-PCR. n=3. **(B)** Osteoporotic BMSCs were transfected with agomir-4739 or antagomir-4739 and examined for cell viability by CCK-8 assay (n=3). Then, osteoporotic BMSCs were transfected with agomir-4739 or antagomir-4739, induced towards osteogenic differentiation for 21 days, and examined using ALP staining on day 14 of osteogenic induction **(C)**; examined for the formation of mineralized nodules using Alizarin red staining on day 21 of osteogenic induction **(D)**; examined for the protein levels of ALP, OCN, Runx2, and Osterix using Immunoblotting on day 14 of osteogenic induction **(E)** (n=3). $^{**}P < 0.01$, compared to NC agomir; $^{\#}P < 0.05$, $^{\#\#}P < 0.01$, compared to NC antagomir.

induction, miR-4739 overexpression inhibited, whereas miR-4739 inhibition promoted the formation of mineralized nodules (**Figure 3D**). Meanwhile, the levels of osteogenic differentiation markers were monitored. On day 14 of osteogenic induction, miR-4739 overexpression decreased, whereas miR-4739 inhibition increased the protein levels of ALP, OCN, Runx2, and Osterix (**Figure 3E**). Moreover, in normal BMSCs, miR-4739 overexpression also inhibited BMSC cell viability, osteogenic ability, and the expression of ALP, OCN, RUNX2, and Osterix proteins, while miR-4739 inhibition exerted opposite effects (**Figure S2**). These data indicate that miR-4739 overexpression impairs the osteogenic differentiation potential of both normal and osteoporotic BMSCs.

The effects of miR-4739 on bone formation *in vivo* were subsequently determined. MiR-4739 agomir or antagomir-transfected osteoporotic BMSCs were mixed with the osteoconductive carrier HA and injected subcutaneously in nude mice (**Figure 4A**). Six weeks later, the implants were harvested and measured. The results show that miR-4739 agomir transfected osteoporotic BMSCs formed smaller bone masses than NC agomir transfected osteoporotic BMSCs, while miR-4739 antagomir transfected BMSCs formed larger bone masses than NC

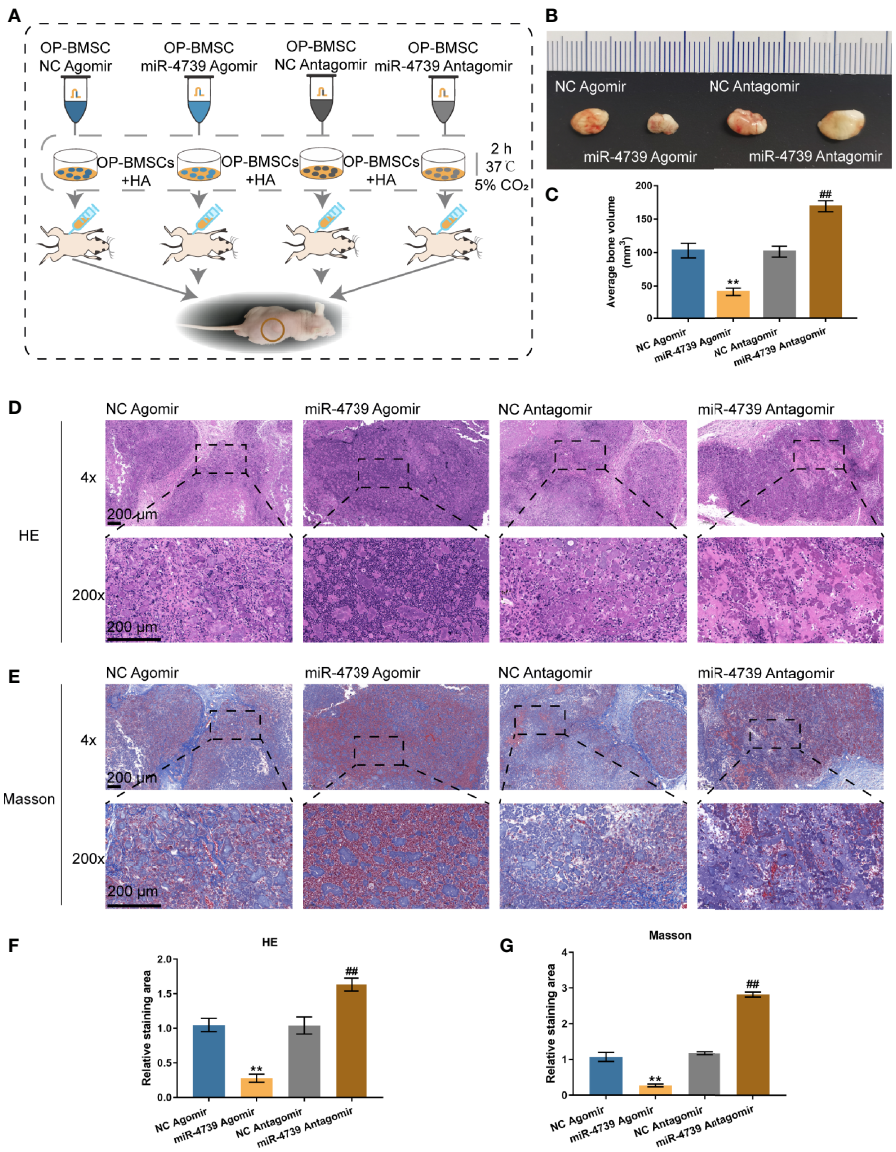

FIGURE 4 | miR-4739 modulated heterotopic bone formation from osteoporotic BMSCs *in vivo*. **(A)** The protocol of heterotopic bone formation. **(B, C)** Gross view and volume of heterotopic bone from miR-4739 agomir or antagomir transfected osteoporotic BMSCs. **(D, E)** Histological analysis of heterotopic bone formation with HE and Masson staining (the scale bar is 200 μm). The relative staining area of HE and Masson was shown in **(F, G)**. n=4. $^{**}P < 0.01$, compared to NC agomir; $^{\#\#}P < 0.01$, compared to NC antagomir.

antagomir transfected BMSCs (**Figures 4B, C**). The heterotropic bone sections were treated with HE or Masson staining. The results revealed that bone areas were significantly decreased in the miR-4739 agomir group and increased in the miR-4739 antagomir, compared to the NC group (**Figures 4D–G**). This result was consistent with the *in vitro* result that miR-4739 inhibited BMSC growth and osteogenic differentiation.

miR-4739 Targets DLX3 and Inhibits DLX3

miRNAs exert their biological functions by targeting the 3'UTR of downstream mRNA (25). Firstly, genes that are potentially targeted by miR-4739 were identified using the online tool miRDIP (https://ophid.utoronto.ca/mirDIP/) to predict the targeted genes. The top 20 highest integrated score genes were selected. The differentially expressed genes in BMSCs on days 0 and 3 of osteogenic differentiation were subsequently selected according to GSE80614 (logFC>0.3, p<0.05). These two datasets intersected in LASP1 (LIM and SH3 Protein 1) and DLX3 (**Figures 5A, B** and **Table S2**). Among them, only DLX3 has been reported to be associated with osteogenesis (26). The expression of DLX3 and LASP1 was subsequently determined in normal BMSCs and osteoporotic BMSCs. As illustrated in

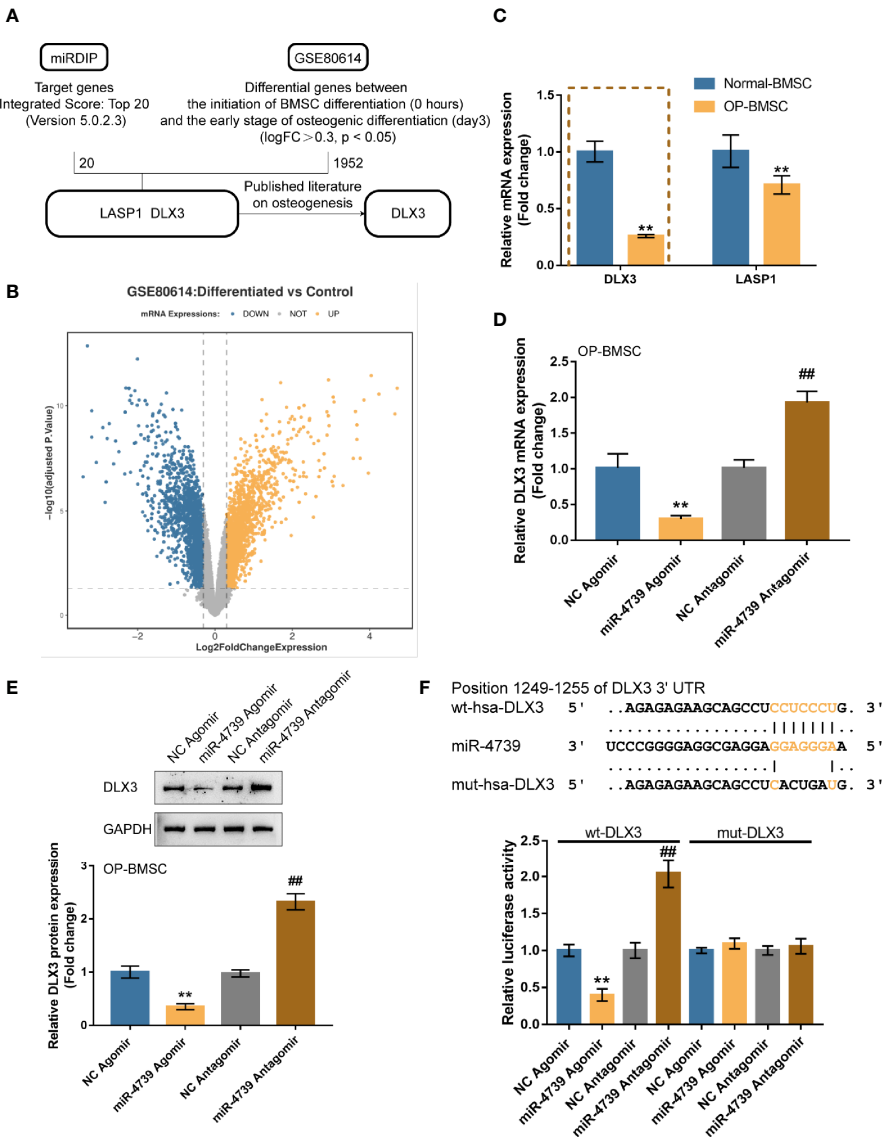

FIGURE 5 | miR-4739 targets DLX3 and inhibits DLX3 **(A, B)** miRDIP was used to predict miR-4739 targets (top 20 highest integrated score genes); differentially expressed genes in BMSCs on day 0 and 3 of osteogenic differentiation were analyzed according to GSE80614 (logFC >0.3, *P* <0.05). These two datasets intersected in LASP1and DLX3. **(C)** The expression of DLX3 and LASP1 in normal or osteoporotic BMSCs. n=3. **(D)** Osteoporotic BMSCs were transfected with agomir-4739 or antagomir-4739 and examined for DLX3 expression using qRT-PCR. n=3. **(E)** DLX3 protein levels using Immunoblotting. n=3. **(F)** Wild- and mutant-type DLX3 luciferase reporter vectors were generated and co-transfected in 293T cells with agomir-4739 or antagomir-4739; the luciferase activity was determined. n=3. $^{**}P < 0.01$, compared to NC agomir; $^{\#\#}P < 0.01$, compared to NC antagomir.

Figure 5C showed, both DLX3 and LASP1 were downregulated in osteoporotic BMSCs. The reduced fold change of DLX3 is larger than LASP1; consequently, DLX3 was chosen for further investigation (**Figure 5C**). In osteoporotic BMSCs, miR-4739 overexpression downregulated DLX3 mRNA expression and decreased DLX3 protein levels, whereas miR-4739 inhibition exerted opposite effects of DLX3 (**Figures 5D, E**). A dual-luciferase reporter assay was subsequently conducted to confirm the predicted binding between miR-4739 and DLX3 3'UTR. Wild- and mutant-type DLX3 3'UTR luciferase reporter vectors were generated and were co-transfected in 293T cells with agomir-4739/antagomir-4739. The luciferase activity was subsequently examined. When co-transfected with wt-DLX3, miR-4739 overexpression inhibited, whereas miR-4739 inhibition enhanced the luciferase activity; when co-transfected with mut-DLX3, miR-4739 caused no changes in the luciferase activity (**Figure 5F**). These data indicate that miR-4739 targets DLX3 and inhibits DLX3 expression.

Co-Effects of the miR-4739/DLX3 Axis on Osteoporotic BMSC Osteogenic Differentiation

After confirming miR-4739 binding to DLX3, the co-effects of miR-4739 and DLX3 upon the osteogenic differentiation capacity of BMSCs were evaluated. DLX3 knockdown was achieved in osteoporotic BMSCs through the transfection of short hairpin RNA against DLX3 (sh1/2-DLX3); DLX3 knockdown was confirmed by qRT-PCR (**Figure 6A**). Osteoporotic BMSCs were then co-transfected with sh-DLX3 and antagomir-4739 and examined for DLX3 protein levels. **Figure 6B** illustrated that miR-4739 inhibition increased, whereas DLX3 knockdown decreased DLX3 protein levels. The inhibitory effects of miR-4739 upon DLX3 protein levels were partially attenuated by DLX3 knockdown. Meanwhile, miR-4739 inhibition promoted, whereas DLX3 knockdown inhibited cell viability; DLX3 knockdown significantly attenuated the inhibitory effects of miR-4739 upon cell viability (**Figure 6C**).

Then, osteoporotic BMSCs were co-transfected with sh-DLX3 and antagomir-4739, induced towards osteogenic differentiation for 21 days, and examined for osteogenic differentiation. ALP staining revealed that, on day 14 of osteogenic induction, miR-4739 inhibition promoted, whereas DLX3 knockdown inhibited the osteoblast differentiation; the effects of miR-4739 inhibition were partially attenuated by DLX3 knockdown (**Figure 6D**). Alizarin red staining showed that, on day 21 of osteogenic induction, miR-4739 inhibition promoted, whereas DLX3 knockdown inhibited the formation of mineralized nodules; the effects of miR-4739 inhibition were partially attenuated by DLX3 knockdown (**Figure 6E**). Consistently, on day 14 of osteogenic induction, miR-4739 inhibition increased, whereas DLX3 knockdown decreased ALP, OCN, Runx2, and osterix protein contents. The effects of miR-4739 inhibition were partially attenuated by DLX3 knockdown (**Figure 6F**). These data indicate that miR-4739 influences BMSC osteogenesis through targeting DLX3.

DISCUSSION

Herein, the study identified that miR-4739 was upregulated in BMSC cultures established from osteoporotic subjects. BMSCs were isolated from normal and osteoporotic bone marrow tissues and identified for their osteogenic differentiation potential. In osteoporotic BMSCs, miR-4739 overexpression significantly inhibited cell viability, osteoblast differentiation, mineralized nodule formation and heterotopic bone formation, whereas miR-4739 inhibition exerted opposite effects. Through direct binding, miR-4739 inhibited DLX3 expression. In osteoporotic BMSCs, DLX3 knockdown also inhibited BMSC viability and osteogenic differentiation. DLX3 knockdown partially attenuated the effects of miR-4739 inhibition upon BMSCs.

Studies have revealed that the imbalance of BMSCs is an essential mechanism in the pathogenesis of osteoporosis (27, 28). The osteoblast-mediated bone formation is crucial for maintaining bone homeostasis (29, 30). In osteoporosis patients, BMSCs differentiate into more adipocytes than osteoblasts, resulting in continuous bone loss and accumulation of bone marrow fat (31, 32). Compared with normal BMSCs, osteoporotic BMSCs showed impaired osteoblast differentiation and mineralized nodule formation abilities, consistent with previous studies. Nevertheless, the mechanism underlying this shift of lineage commitment of BMSCs requires further investigation.

miRNAs were found to contribute extensively to regulating gene expression during life activities. Some miRNAs can promote osteogenic differentiation of BMSCs, while others exert opposite functions (33–35). miR-31 regulates osteogenic differentiation by targeting Runx2 and Satb2 formation regulatory loops (36). miR-204 affects the precursor by regulating Runx2 expression (37). miR-205 regulates BMSC osteogenic differentiation by influencing SATB2/Runx2 and ERK/MAPK pathways (38). Herein, it was identified that miR-4739 was upregulated within osteoporotic tissue samples and BMSCs. Conversely, miR-4739 expression was downregulated in BMSCs during osteogenic differentiation. As previously reported, miR-4739 could regulate the capacity of human BMSCs to differentiate into osteoblasts. Elsafadi et al. (39) demonstrated that hsa-miR-4739-transfected BMSCs exhibited impaired osteoblast differentiation. This was demonstrated by a significant reduction in the mineralized matrix formation, mineralized nodule quantification, and decreased expression of osteoblastic markers. Similarly, in this study, miR-4739 overexpression in normal and osteoporotic BMSCs inhibited mineralized matrix formation, suppressed the formation of mineralized nodules, and decreased the levels of osteoblastic markers, such as ALP, OCN, Runx2, and Osterix. Thus, our findings further confirm the inhibitory effects of miR-4739 upon the capacity of BMSCs to differentiate into osteoblasts.

miRNAs exert their functions through downregulating gene expression *via* translational repression or degradation of mRNA targets (8, 9). Elsafadi et al. (39) reported that miR-4739 modulates the capacity of immortalized human BMSCs to differentiate into osteoblasts and adipocytes *via* targeting LRP3. miR-4739 targeted regulation of Notch2 expression also regulated osteogenic differentiation (40). The multiple-to-

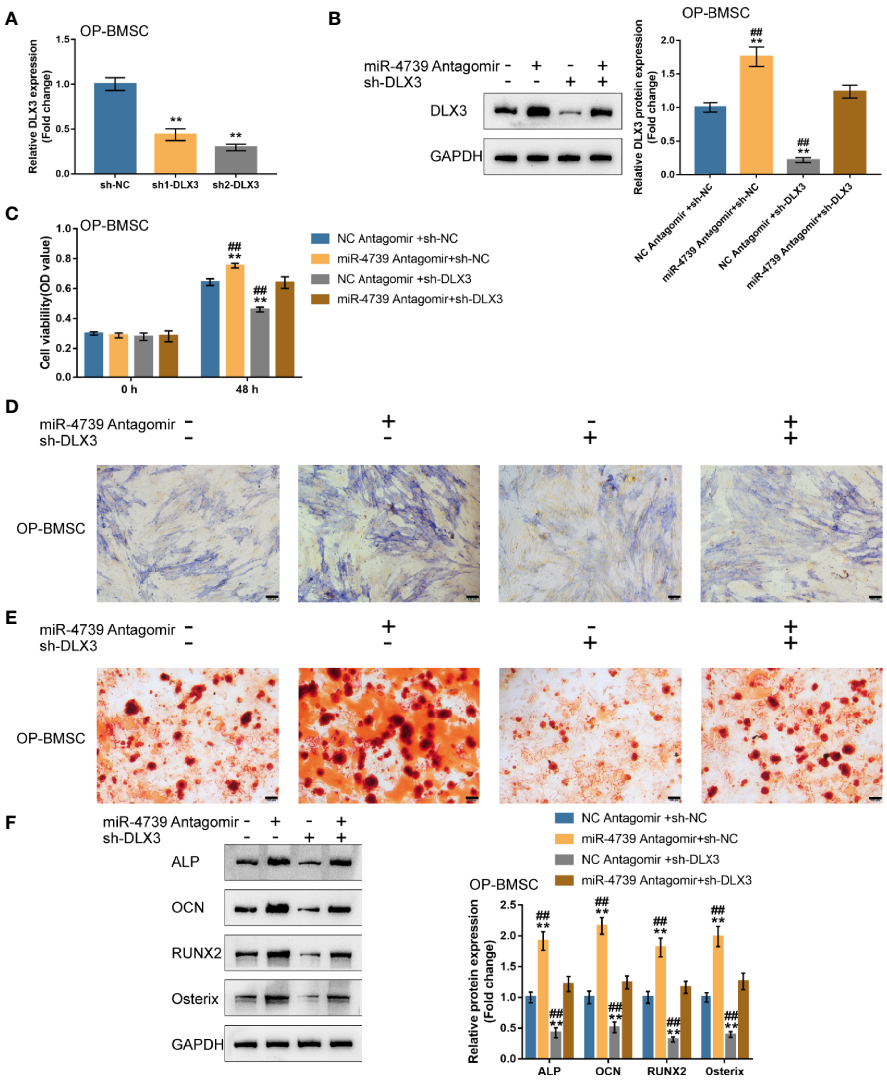

FIGURE 6 | Co-effects of the miR-4739/DLX3 axis on osteoporotic BMSC osteogenic differentiation **(A)** DLX3 knockdown was achieved in osteoporotic BMSCs by transfecting short hairpin RNA against DLX3 (sh1/2-DLX3); DLX3 knockdown was confirmed by qRT-PCR. n=3. Then, osteoporotic BMSCs were co-transfected with sh-DLX3 and antagomir-4739 and examined for the protein levels of DLX3 by Immunoblotting **(B)** and cell viability by CCK-8 assay **(C)** (n=3). Then, normal BMSCs were co-transfected with sh-DLX3 and antagomir-4739, induced towards osteogenic differentiation for 21 days, and examined using ALP staining on day 14 of osteogenic induction **(D)**; the formation of mineralized nodules using Alizarin red staining on day 21 of osteogenic induction **(E)**; the protein levels of ALP, OCN, Runx2, and Osterix using Immunoblotting on day 14 of osteogenic induction **(F)**. n=3. $^{**}P < 0.01$, $^{\#\#}P < 0.01$.

multiple relations between miRNAs and mRNAs lead to the even more complex miRNA regulatory mechanisms (41). Herein, DLX3 was identified as a novel direct downstream target of miR-4739. DLX3, a homeodomain transcription factor, belongs to the DLX family that comprises 6 different members, DLX1-DLX6 (42, 43). DLX3 exerts a substantial effect on embryogenesis and organ development, such as epidermis and ectodermal appendages (44, 45). DLX3 promoted osteogenic differentiation of BMSCs and the induced pluripotent stem cell-derived mesenchymal stem cells (46, 47). DLX3 overexpression promoted the differentiation of BMSCs into osteoblasts through the Wnt/beta-catenin signaling-mediated histone methylation of DKK4 (26). Besides, DLX3 could inhibit adipogenic differentiation of dental pulp stem cells (48). Increased adipogenic differentiation or reduced osteogenic differentiation of BMSCs might lead to osteoporosis (49). Altogether, DLX3 may play a key role in osteoporosis. Herein, DLX3 knockdown in osteoporotic BMSCs leads to impaired mineralized matrix formation, mineralized nodule formation, and decreased levels of osteogenic markers, suggesting that DLX3 knockdown hindered BMSC osteogenic differentiation. More importantly, DLX3 knockdown partially reversed the inhibitory effects of miR-4739 upon BMSCs, suggesting that miR-4739 plays its role through DLX3 during the osteogenic

differentiation. However, the function of miR-4739/DLX3 axis in adipogenic differentiation remains to be further studied.

Altogether, the miR-4739/DLX3 axis modulates the capacity of BMSCs to differentiate into osteoblasts, which are potentially involved in osteoporosis pathogenesis. The *in vivo* and clinical functions of the miR-4739/DLX3 axis require further investigation.

DATA AVAILABILITY STATEMENT

The original contributions presented in the study are included in the article/**Supplementary Material**. Further inquiries can be directed to the corresponding author.

ETHICS STATEMENT

The studies involving human participants were reviewed and approved by Ethics Committee of the Second Xiangya Hospital of Central South University. The patients/participants provided their written informed consent to participate in this study. The animal study was reviewed and approved by Animal Care and Use Ethics Committee of Central South University.

AUTHOR CONTRIBUTIONS

DL: Writing- Reviewing and Editing, Project administration. QY: Writing- Reviewing and Editing. LX: Conceptualization, Methodology. AL: Data curation, Visualization, Investigation. YX: Software, Validation. All authors contributed to the article and approved the submitted version.

ACKNOWLEDGMENTS

This study was supported by Changsha Municipal Natural Science Foundation (kq2014240).

SUPPLEMENTARY MATERIAL

The Supplementary Material for this article can be found online at: https://www.frontiersin.org/articles/10.3389/fendo.2021.703167/full#supplementary-material

Supplementary Figure 1 | Differentially expressed miRNAs in non-osteoporotic or osteoporotic tissues based on the GSE datasets. **(A)** In GSE74209, 83 upregulated miRNAs and 60 downregulated miRNAs in postmenopausal women bone tissues from osteoporotic fracture induced hip replacement compared to bone tissues from osteoarthritis without osteoporosis induced hip replacement based on (|logFC| >1, $p < 0.05$). The top 20 differentially expressed miRNAs were shown in the heatmap. **(B)** In GSE93883, 20 upregulated miRNAs and 117 downregulated miRNAs in plasma from osteoporotic patients with and without vertebral fractures compared to non-osteoporotic patients(|logFC| >1, $p < 0.05$). The top 20 differentially expressed miRNAs were shown in the heatmap.

Supplementary Figure 2 | Effects of miR-4739 overexpression and inhibition on normal BMSC osteogenic differentiation **(A)** miR-4739 overexpression or inhibition was achieved in normal BMSCs by transfecting agomir-4739 or antagomir-4739; miR-4739 expression was confirmed using qRT-PCR. n=3. **(B)** Normal BMSCs were transfected with agomir-4739 or antagomir-4739 and examined for cell viability by CCK-8 assay. n=3. Then, normal BMSCs were transfected with agomir-4739 or antagomir-4739, induced towards osteogenic differentiation for 21 days, and examined using ALP staining on day 14 of osteogenic induction **(C)**; examined for the formation of mineralized nodules using Alizarin red staining on day 21 of osteogenic induction **(D)**; examined for the protein levels of ALP, OCN, Runx2, and Osterix using Immunoblotting on day 14 of osteogenic induction **(E)**. n=3. $^{**}P < 0.01$, compared to NC agomir; $^{\#}P < 0.05$, $^{\#\#}P < 0.01$. compared to NC antagomir.

REFERENCES

1. Manolagas SC, Parfitt AM. For Whom the Bell Tolls: Distress Signals From Long-Lived Osteocytes and the Pathogenesis of Metabolic Bone Diseases. *Bone* (2013) 54(2):272–8. doi: 10.1016/j.bone.2012.09.017
2. Armas LA, Recker RR. Pathophysiology of Osteoporosis: New Mechanistic Insights. *Endocrinol Metab Clin North Am* (2012) 41(3):475–86. doi: 10.1016/j.ecl.2012.04.006
3. Khosla S, Melton LJ3rd, Riggs BL. The Unitary Model for Estrogen Deficiency and the Pathogenesis of Osteoporosis: Is a Revision Needed? *J Bone Miner Res* (2011) 26(3):441–51. doi: 10.1002/jbmr.262
4. Pietschmann P, Rauner M, Sipos W, Kerschan-Schindl K. Osteoporosis: An Age-Related and Gender-Specific Disease–a Mini-Review. *Gerontology* (2009) 55(1):3–12. doi: 10.1159/000166209
5. Duque G, Troen BR. Understanding the Mechanisms of Senile Osteoporosis: New Facts for a Major Geriatric Syndrome. *J Am Geriatr Soc* (2008) 56 (5):935–41. doi: 10.1111/j.1532-5415.2008.01764.x
6. Schuiling KD, Robinia K, Nye R. Osteoporosis Update. *J Midwifery Womens Health* (2011) 56(6):615–27. doi: 10.1111/j.1542-2011.2011.00135.x
7. Perez JR, Kouroupis D, Li DJ, Best TM, Kaplan L, Correa D. Tissue Engineering and Cell-Based Therapies for Fractures and Bone Defects. *Front Bioeng Biotechnol* (2018) 6:105. doi: 10.3389/fbioe.2018.00105
8. Kim VN, Han J, Siomi MC. Biogenesis of Small RNAs in Animals. *Nat Rev Mol Cell Biol* (2009) 10(2):126–39. doi: 10.1038/nrm2632
9. Bartel DP. MicroRNAs: Genomics, Biogenesis, Mechanism, and Function. *Cell* (2004) 116(2):281–97. doi: 10.1016/S0092-8674(04)00045-5
10. Cetin Z, Saygili EI, Gorgisen G, Sokullu E. Preclinical Experimental Applications of miRNA Loaded BMSC Extracellular Vesicles. *Stem Cell Rev Rep* (2021) 17:471–501. doi: 10.1007/s12015-020-10082-x
11. Wang J, Liu S, Li J, Zhao S, Yi Z. Roles for miRNAs in Osteogenic Differentiation of Bone Marrow Mesenchymal Stem Cells. *Stem Cell Res Ther* (2019) 10(1):197. doi: 10.1186/s13287-019-1309-7
12. Li B. MicroRNA Regulation in Osteogenic and Adipogenic Differentiation of Bone Mesenchymal Stem Cells and its Application in Bone Regeneration. *Curr Stem Cell Res Ther* (2018) 13(1):26–30. doi: 10.2174/1574888X12666170605112727
13. Li CJ, Cheng P, Liang MK, Chen YS, Lu Q, Wang JY, et al. MicroRNA-188 Regulates Age-Related Switch Between Osteoblast and Adipocyte Differentiation. *J Clin Invest* (2015) 125(4):1509–22. doi: 10.1172/JCI77716
14. Lu GD, Cheng P, Liu T, Wang Z. BMSC-Derived Exosomal miR-29a Promotes Angiogenesis and Osteogenesis. *Front Cell Dev Biol* (2020) 8:608521. doi: 10.3389/fcell.2020.608521
15. Hu H, Zhao C, Zhang P, Liu Y, Jiang Y, Wu E, et al. miR-26b Modulates OA Induced BMSC Osteogenesis Through Regulating GSK3beta/beta-Catenin Pathway. *Exp Mol Pathol* (2019) 107:158–64. doi: 10.1016/j.yexmp.2019.02.003
16. Lin Z, He H, Wang M, Liang J. MicroRNA-130a Controls Bone Marrow Mesenchymal Stem Cell Differentiation Towards the Osteoblastic and Adipogenic Fate. *Cell Prolif* (2019) 52(6):e12688. doi: 10.1111/cpr.12688
17. Wang H, Zhou K, Xiao F, Huang Z, Xu J, Chen G, et al. Identification of circRNA-Associated ceRNA Network in BMSCs of OVX Models for Postmenopausal Osteoporosis. *Sci Rep* (2020) 10(1):10896. doi: 10.1038/s41598-020-67750-8
18. Chen HT, Lee MJ, Chen CH, Chuang SC, Chang LF, Ho ML, et al. Proliferation and Differentiation Potential of Human Adipose-Derived Mesenchymal Stem Cells Isolated From Elderly Patients With Osteoporotic Fractures. *J Cell Mol Med* (2012) 16(3):582–93. doi: 10.1111/j.1582-4934.2011.01335.x

19. Yang X, Yang J, Lei P, Wen T. LncRNA MALAT1 Shuttled by Bone Marrow-Derived Mesenchymal Stem Cells-Secreted Exosomes Alleviates Osteoporosis Through Mediating microRNA-34c/SATB2 Axis. *Aging (Albany NY)* (2019) 11(20):8777–91. doi: 10.18632/aging.102264
20. De-Ugarte L, Yoskovitz G, Balcells S, Güerri-Fernández R, Martinez-Diaz S, Mellibovsky L, et al. MiRNA Profiling of Whole Trabecular Bone: Identification of Osteoporosis-Related Changes in MiRNAs in Human Hip Bones. *BMC Med Genomics* (2015) 8:75. doi: 10.1186/s12920-015-0149-2
21. van de Peppel J, Strini T, Tilburg J, Westerhoff H, van Wijnen AJ, van Leeuwen J. Identification of Three Early Phases of Cell-Fate Determination During Osteogenic and Adipogenic Differentiation by Transcription Factor Dynamics. *Stem Cell Rep* (2017) 8(4):947–60. doi: 10.1016/j.stemcr.2017.02.018
22. Tokar T, Pastrello C, Rossos AEM, Abovsky M, Hauschild AC, Tsay M, et al. mirDIP 4.1-Integrative Database of Human microRNA Target Predictions. *Nucleic Acids Res* (2018) 46(D1):D360–d370. doi: 10.1093/nar/gkx1144
23. Jing H, Liao L, An Y, Su X, Liu S, Shuai Y, et al. Suppression of EZH2 Prevents the Shift of Osteoporotic MSC Fate to Adipocyte and Enhances Bone Formation During Osteoporosis. *Mol Ther* (2016) 24(2):217–29. doi: 10.1038/mt.2015.152
24. Zhang X, Sai B, Wang F, Wang L, Wang Y, Zheng L, et al. Hypoxic BMSC-Derived Exosomal miRNAs Promote Metastasis of Lung Cancer Cells *via* STAT3-Induced EMT. *Mol Cancer* (2019) 18(1):40. doi: 10.1186/s12943-019-0959-5
25. Thomson DW, Bracken CP, Goodall GJ. Experimental Strategies for microRNA Target Identification. *Nucleic Acids Res* (2011) 39(16):6845–53. doi: 10.1093/nar/gkr330
26. Sun S, Yu M, Fan Z, Yeh IT, Feng H, Liu H, et al. DLX3 Regulates Osteogenic Differentiation of Bone Marrow Mesenchymal Stem Cells *via* Wnt/β-Catenin Pathway Mediated Histone Methylation of DKK4. *Biochem Biophys Res Commun* (2019) 516(1):171–6. doi: 10.1016/j.bbrc.2019.06.029
27. Qin Y, Wang L, Gao Z, Chen G, Zhang C. Bone Marrow Stromal/Stem Cell-Derived Extracellular Vesicles Regulate Osteoblast Activity and Differentiation *In Vitro* and Promote Bone Regeneration *In Vivo*. *Sci Rep* (2016) 6:21961. doi: 10.1038/srep21961
28. Martin-Merino E, Huerta-Alvarez C, Prieto-Alhambra D, Alvarez-Gutierrez A, Montero-Corominas D. Secular Trends of Use of Anti-Osteoporotic Treatments in Spain: A Population-Based Cohort Study Including Over 1.5million People and More Than 12years of Follow-Up. *Bone* (2017) 105:292–8. doi: 10.1016/j.bone.2017.08.031
29. Wang L, Niu N, Li L, Shao R, Ouyang H, Zou W. H3K36 Trimethylation Mediated by SETD2 Regulates the Fate of Bone Marrow Mesenchymal Stem Cells. *PloS Biol* (2018) 16(11):e2006522. doi: 10.1371/journal.pbio.2006522
30. van Tok MN, van Duivenvoorde LM, Kramer I, Ingold P, Pfister S, Roth L, et al. Interleukin-17a Inhibition Diminishes Inflammation and New Bone Formation in Experimental Spondyloarthritis. *Arthritis Rheumatol* (2019) 71(4):612–25. doi: 10.1002/art.40770
31. Mastrogiacomo M, Papadimitropoulos A, Cedola A, Peyrin F, Giannoni P, Pearce SG, et al. Engineering of Bone Using Bone Marrow Stromal Cells and a Silicon-Stabilized Tricalcium Phosphate Bioceramic: Evidence for a Coupling Between Bone Formation and Scaffold Resorption. *Biomaterials* (2007) 28(7):1376–84. doi: 10.1016/j.biomaterials.2006.10.001
32. Chen S, Jia L, Zhang S, Zheng Y, Zhou Y. DEPTOR Regulates Osteogenic Differentiation *via* Inhibiting MEG3-Mediated Activation of BMP4 Signaling and Is Involved in Osteoporosis. *Stem Cell Res Ther* (2018) 9(1):185. doi: 10.1186/s13287-018-0935-9
33. Weilner S, Skalicky S, Salzer B, Keider V, Wagner M, Hildner F, et al. Differentially Circulating miRNAs After Recent Osteoporotic Fractures can Influence Osteogenic Differentiation. *Bone* (2015) 79:43–51. doi: 10.1016/j.bone.2015.05.027
34. Baud'huin M, Lamoureux F, Jacques C, Rodriguez Calleja L, Quillard T, Charrier C, et al. Inhibition of BET Proteins and Epigenetic Signaling as a Potential Treatment for Osteoporosis. *Bone* (2017) 94:10–21. doi: 10.1016/j.bone.2016.09.020
35. Lv C, Hao Y, Han Y, Zhang W, Cong L, Shi Y, et al. Role and Mechanism of microRNA-21 in H2O2-Induced Apoptosis in Bone Marrow Mesenchymal Stem Cells. *J Clin Neurosci* (2016) 27:154–60. doi: 10.1016/j.jocn.2015.07.029
36. Deng Y, Wu S, Zhou H, Bi X, Wang Y, Hu Y, et al. Effects of a miR-31, Runx2, and Satb2 Regulatory Loop on the Osteogenic Differentiation of Bone Mesenchymal Stem Cells. *Stem Cells Dev* (2013) 22(16):2278–86. doi: 10.1089/scd.2012.0686
37. Huang J, Zhao L, Xing L, Chen D. MicroRNA-204 Regulates Runx2 Protein Expression and Mesenchymal Progenitor Cell Differentiation. *Stem Cells* (2010) 28(2):357–64. doi: 10.1002/stem.288
38. Hu N, Feng C, Jiang Y, Miao Q, Liu H. Regulative Effect of Mir-205 on Osteogenic Differentiation of Bone Mesenchymal Stem Cells (BMSCs): Possible Role of SATB2/Runx2 and ERK/MAPK Pathway. *Int J Mol Sci* (2015) 16(5):10491–506. doi: 10.3390/ijms160510491
39. Elsafadi M, Manikandan M, Alajez NM, Hamam R, Dawud RA, Aldahmash A, et al. MicroRNA-4739 Regulates Osteogenic and Adipocytic Differentiation of Immortalized Human Bone Marrow Stromal Cells *via* Targeting LRP3. *Stem Cell Res* (2017) 20:94–104. doi: 10.1016/j.scr.2017.03.001
40. Guo Z, Xie M, Zou Y, Liang Q, Liu F, Su J, et al. Circular RNA Hsa_circ_0006766 Targets microRNA miR-4739 to Regulate Osteogenic Differentiation of Human Bone Marrow Mesenchymal Stem Cells. *Bioengineered* (2021) 12(1):5679–87. doi: 10.1080/21655979.2021.1967712
41. Liu B, Li J, Cairns MJ. Identifying miRNAs, Targets and Functions. *Briefings Bioinf* (2012) 15(1):1–19. doi: 10.1093/bib/bbs075
42. Zhao N, Zeng L, Liu Y, Han D, Liu H, Xu J, et al. DLX3 Promotes Bone Marrow Mesenchymal Stem Cell Proliferation Through H19/miR-675 Axis. *Clin Sci (Lond)* (2017) 131(22):2721–35. doi: 10.1042/CS20171231
43. Duverger O, Ohara T, Bible PW, Zah A, Morasso MI. DLX3-Dependent Regulation of Ion Transporters and Carbonic Anhydrases Is Crucial for Enamel Mineralization. *J Bone Miner Res* (2017) 32(3):641–53. doi: 10.1002/jbmr.3022
44. Qadir AS, Lee J, Lee YS, Woo KM, Ryoo HM, Baek JH. Distal-Less Homeobox 3, a Negative Regulator of Myogenesis, Is Downregulated by microRNA-133. *J Cell Biochem* (2018) 120:2226–35. doi: 10.1002/jcb.27533
45. Duverger O, Chen SX, Lee D, Li T, Chock PB, Morasso MI. SUMOylation of DLX3 by SUMO1 Promotes its Transcriptional Activity. *J Cell Biochem* (2011) 112(2):445–52. doi: 10.1002/jcb.22891
46. Zhao N, Han D, Liu H, Li Y, Wong SW, Cao Z, et al. Senescence: Novel Insight Into DLX3 Mutations Leading to Enhanced Bone Formation in Tricho-Dento-Osseous Syndrome. *Sci Rep* (2016) 6:38680. doi: 10.1038/srep38680
47. Li J, Lin Q, Lin Y, Lai R, Zhang W. Effects of DLX3 on the Osteogenic Differentiation of Induced Pluripotent Stem Cell–Derived Mesenchymal Stem Cells. *Mol Med Rep* (2021) 23(4):1–1. doi: 10.3892/mmr.2021.11871
48. Lee H-L, Nam H, Lee G, Baek J-H. Dlx3 and Dlx5 Inhibit Adipogenic Differentiation of Human Dental Pulp Stem Cells. *Int J Oral Biol* (2012) 37(1):31–6.
49. Chen G, Zhuo Y, Tao B, Liu Q, Shang W, Li Y, et al. Moderate SMFs Attenuate Bone Loss in Mice by Promoting Directional Osteogenic Differentiation of BMSCs. *Stem Cell Res Ther* (2020) 11(1):487. doi: 10.1186/s13287-020-02004-y

Conflict of Interest: The authors declare that the research was conducted in the absence of any commercial or financial relationships that could be construed as a potential conflict of interest.

frontiers in Endocrinology

ORIGINAL RESEARCH
published: 15 December 2021
doi: 10.3389/fendo.2021.763646

Liraglutide Inhibits Osteoclastogenesis and Improves Bone Loss by Downregulating Trem2 in Female Type 1 Diabetic Mice: Findings From Transcriptomics

Jie Yu[1], Yan-Chuan Shi[2,3†], Fan Ping[1], Wei Li[1], Hua-Bing Zhang[1], Shu-Li He[1], Yuan Zhao[1], Ling-Ling Xu[1] and Yu-Xiu Li[1*]*

[1] Key Laboratory of Endocrinology of National Health Commission, Department of Endocrinology, Peking Union Medical College Hospital, Chinese Academy of Medical Sciences & Peking Union Medical College, Beijing, China, [2] Group of Neuroendocrinology, Diabetes and Metabolism Division, Garvan Institute of Medical Research, St Vincent's Hospital, Sydney, NSW, Australia, [3] Faculty of Medicine, UNSW, Sydney, NSW, Australia

Background: The mechanisms of bone fragility in type 1 diabetes (T1D) are not fully understood. Whether glucagon-like peptide-1 receptor (GLP-1R) agonists could improve bone quality in T1D context also remains elusive.

Aims: We aimed to explore the possible mechanisms of bone loss in T1D and clarify whether liraglutide has effects on bone quality of T1D mice using transcriptomics.

Methods: Female streptozotocin-induced diabetic C57BL/6J mice were randomly divided into four groups and received the following treatments daily for 8 weeks: saline as controls, insulin, liraglutide, and liraglutide combined with insulin. These groups were also compared with non-STZ-treated normal glucose tolerance (NGT) group. Trunk blood and bone tissues were collected for analysis. Three tibia from each of the NGT, saline-treated, and liraglutide-treated groups were randomly selected for transcriptomics.

Results: Compared with NGT mice, saline-treated T1D mice manifested markedly hyperglycemia and weight loss, and micro-CT revealed significantly lower bone mineral density (BMD) and deficient microarchitectures in tibias. Eight weeks of treatment with liraglutide alone or combined with insulin rescued the decreased BMD and partly corrected the compromised trabecular microarchitectures. Transcriptomics analysis showed there were 789 differentially expressed genes mainly mapped to osteoclastogenesis and inflammation pathways. The RT-qPCR verified that the gene expression of *Trem2*, *Nfatc1*, *Trap*, and *Ctsk* were significantly increased in the tibia of T1D compared with those in the NGT group. Liraglutide treatment alone or combined with insulin could effectively suppress osteoclastogenesis by downregulating the gene expression of *Trem2*, *Nfatc1*, *Ctsk*, and *Trap*.

OPEN ACCESS

Edited by:
Antonino Catalano, University of Messina, Italy

Reviewed by:
Divya Singh, Central Drug Research Institute (CSIR), India
Hong Xing Zheng, Shaanxi University of Technology, China
Zheer Al-Mashhadi, Aarhus University Hospital, Denmark

***Correspondence:**
Ling-Ling Xu
llxuwsh@163.com
Yu-Xiu Li
liyuxiu@medmail.com.cn

†ORCID:
Yan-Chuan Shi
orcid.org/0000-0002-8368-6735

Specialty section:
This article was submitted to Bone Research, a section of the journal Frontiers in Endocrinology

Received: *26 August 2021*
Accepted: *08 November 2021*
Published: *15 December 2021*

Citation:
Yu J, Shi Y-C, Ping F, Li W, Zhang H-B, He S-L, Zhao Y, Xu L-L and Li Y-X (2021) Liraglutide Inhibits Osteoclastogenesis and Improves Bone Loss by Downregulating Trem2 in Female Type 1 Diabetic Mice: Findings From Transcriptomics. Front. Endocrinol. 12:763646. doi: 10.3389/fendo.2021.763646

Conclusions: Taken together, increased osteoclastogenesis with upregulated expression of *Trem2* played an important role in bone loss of T1D mice. Liraglutide provided protective effects on bone loss in T1D mice by suppressing osteoclastogenesis.

Keywords: type 1 diabetes, bone loss, bone density, bone microarchitecture, osteoclastogenesis, Triggering receptor expressed on myeloid cells 2, liraglutide, transcriptomics

INTRODUCTION

Type 1 diabetes (T1D) is characterized by autoimmune destruction of pancreatic islet β cells leading to severe hyperglycemia (1). Glucose metabolism disturbance can gradually lead to diabetes-related chronic complications. These complications include diabetic nephropathy, diabetic retinopathy, and diabetic neuropathy. In addition, skeletal fragility has also been associated with type 1 diabetes, which exhibited as deficits in bone mineral density (BMD) and bone microarchitectures compared with controls, leading to increased fracture risks (2, 3).

The increased bone fragility in type 1 diabetes has been attributed to complex and multifactorial pathophysiological mechanisms which are only partially understood. Hyperglycemia, hypoinsulinemia, accumulation of advanced glycation end products, and increased marrow adiposity lead to a decrease in bone formation, bone mineralization, and poor osteoblast activity, but the effects on osteoclasts are less studied and inconsistent (4).

Transcriptomics, one of the omics technologies, focuses on the RNA transcripts that are produced by the genome under specific circumstances or in a specific cell. Transcriptomics is a powerful tool to investigate the molecular mechanisms behind complex and multifactorial systemic diseases in an unbiased and comprehensive manner (5). Thus far, there is no study showing the transcriptomic analysis of T1D-associated osteopenia or osteoporosis.

Furthermore, certain antidiabetic medications might also affect fracture risk independent of their glucose-lowering effects. Glucagon-like peptide-1 receptor (GLP-1R) agonists as adjunctive therapies have been tested in T1D patients (6), and some individuals who are overweight or have detectable levels of C-peptide might benefit from those medications (6). GLP-1R agonists also exert protective effects on bone tissue *in vitro* and *in vivo* (7–9). Some clinical studies have found neutral effects of liragutide on bone, but there was also a few meta-analysis of 16–59 randomized controlled trials with 11,206–49,602 patients with T2DM which showed that compared with placebo and other antidiabetic drugs, liraglutide was associated with a significant reduction in the risk of bone fractures (10–13). However, clinical and experimental research data in the context of T1D are scarce. Till now, only one experimental research by Mansur et al. found that liraglutide treatment for 21 days in streptozotocin (STZ)-induced T1D mice significantly increased indicators such as bone maximum force and hardness but failed to improve trabecular and cortical microarchitectures (14). We hypothesized that GLP-1R agonists might provide beneficial effects on T1D-associated osteopenia or osteoporosis.

Thus, in this study, we intended to explore underlying molecular mechanisms of bone fragility in T1D mouse models using transcriptomics. Then, liraglutide was administrated alone or in combination with insulin to T1D mice to explore their effects on bone quality and possible mechanisms.

RESEARCH DESIGN AND METHODS

Animals and Experimental Design

Ten- to 11-week-old female C57BL/6J mice were purchased from Beijing Huafukang Co., Ltd. (Beijing, China) and allowed to acclimate to the environment for 1 week. Then, mice were treated either with STZ to induce diabetes (150 mg/kg body weight once) or with vehicle (100 mM citrate, pH 4.2–4.5), by intraperitoneal (i.p.) injection (15).

Two weeks later, the vehicle-injected mice with normal glucose tolerance (NGT) (n = 8) were assigned to group 1 (referred as to NGT). At the same time, STZ-injected confirmed diabetic mice (random blood glucose ≥250 mg/dl) (16) were randomly assigned to four treatment groups for 8 weeks (n = 8 per group): group 2 treated with saline (referred to as T1D); group 3 (referred to as INS) treated with insulin by subcutaneous injection (insulin dose 10 units/kg body weight/day, as detemir insulin, Levemir®, Novo Nordisk, Denmark), which referred to the insulin dose used in the previous study (17); group 4 (referred to as Lira), treated with liraglutide by subcutaneous injection (liraglutide dose: 0.6 mg/kg/day, Novo Nordisk, Denmark); and group 5 (referred to as Lira+INS), treated with insulin (10 units/kg/day) and liraglutide (0.6 mg/kg/day). The doses of liraglutide used in previous studies ranged from 0.2 to 1 mg/kg, so we chose a relatively large dose of 0.6 mg/kg (16, 18, 19).

All mice were maintained in a 12-h light–dark cycle at 22°C and provided *ad libitum* access to water and food for 8 weeks. Body weight and pedal dorsal vein blood glucose *via* Accu-Chek compact glucometer (Roche) were measured weekly. Upon the completion of the experiments, mice were killed by isoflurane overdose followed by decapitation, and trunk blood and bone tissues were collected. All animal procedures were approved by the Institutional Animal Care and Use Committee (IACUC) at the Institute of Laboratory Animals Science, CAMS and PUMC and conducted according to the Laboratory Animal Management Regulations in China and adhered to the Guide for the Care and Use of Laboratory Animals published by the National Institutes of Health (NIH Publication No. 85-23, revised 2011). All animal studies complied with the ARRIVE guidelines.

Assessment of Skeletal Microarchitecture

After euthanasia, the left tibia was harvested and stored at −80°C until analysis. For bone microarchitecture analyses, the mid-shaft and proximal metaphysis regions along the axis of the bone were scanned by Inveon MM micro-CT manufactured by Siemens (Berlin, Germany) at a voltage of 70 kV and a current of 400 μA, with an entire scan length of 1 cm in a spatial resolution of 35 μm used for animal experimental studies and reconstructed using the Inveon analysis workstation. Tibia trabecular bone analyses were performed from 0.5 mm distal to the growth plate, extending 1 mm toward the diaphysis and excluding the cortical bone. Cortical measurements were performed in a 1-mm length centered midway down the length of the bone. Trabecular volumetric bone mineral density (Tb.vBMD), bone volume fraction (BV/TV), trabecular thickness (Tb.Th), trabecular separation (Tb.Sp), trabecular number (Tb.N), cortical volumetric bone mineral density (Ct.vBMD), and cortical bone thickness (Ct.Th) were computed according to the instruction of the manufacturer.

Bone Histomorphometry

After mice were sacrificed, left femurs were harvested, cleaned, fixed in 4% paraformaldehyde solution at 4°C for 10–24 h, and decalcified in 10% ethylenediamine tetraacetic acid disodium (EDTA-2Na, pH 7.2) for 5–7 days. The decalcified femurs were dehydrated, embedded in paraffin, sectioned at 5 μm, stained with H&E, and observed for histopathological changes using standard light microscopy. The 1-mm region of trabecular bone starting from 0.5 mm below the distal femoral growth plate was selected as the region of interest. Measurements of tissue area (T.Ar, mm^2), trabecular bone area (Tb.Ar, mm^2), and trabecular perimeter (Tb.Pm, mm) and visible adipocytes which were greater than 30 μm were obtained directly from the software Image Pro Plus 6.0 (Media Cybernetics, Rockville, MD, USA) (20, 21). Then, bone volume fraction (BV/TV, %), trabecular thickness (Tb.Th, mm), trabecular separation (Tb.Sp, mm), trabecular number (Tb.N, 1/mm), and marrow adipose number ($1/mm^2$) were obtained using standard formulas shown in **Supplementary Table 1** (22).

Biochemical Measurements

The serum levels of procollagen type 1 N-terminal propeptide (P1NP) and C-terminal telopeptides of type 1 collagen (CTX) and C-peptide were measured using commercially available enzyme-linked immunosorbent assay (ELISA) kits (Cloud-Clone Corp., Ltd., Wuhan, China) according to the instructions of the manufacturer.

Transcriptomics Sequencing and Bioinformatics Analysis

Immediately after euthanasia, bone samples were cleaned of all muscle and connective tissues, snap frozen in liquid nitrogen, and stored at −80°C until RNA extraction. Three tibia tissues were selected from each of the following groups: NGT, T1D, and Lira groups for high-throughput RNA sequencing. In total, nine tibia tissues were used for the analysis. In brief, total RNA was extracted using TRIzol reagent (Invitrogen Co., USA) according to the protocol of the manufacturer. The RNA was then checked for purity and stability by gel electrophoresis, and the concentration was determined using the Agilent 2100 Bioanalyzer (Agilent Technologies, Inc.). The qualified total RNA was digested with DNase I, enriched using oligo(dT) magnetic beads, and then fragmented. Fragmented mRNA was added to random primers for cDNA synthesis and PCR reaction to obtain a single-stranded DNA library. The qualified library was formed into DNA nanospheres (DNB) by rolling circle replication and finally sequenced on the computer.

Clean reads were obtained and aligned to the reference genome of mice. Based on the alignment results, the expression level of each gene was calculated, and the samples were analyzed further in terms of difference, enrichment, and cluster analysis.

Differentially expressed genes (DEGs) were defined as having a fold change >2 and Q-value <0.05 using one-way analysis of variance (ANOVA). DEGs had to appear in all three mice in the group to be considered. The Gene Ontology (GO) platform (http://www.geneontology.org/) was used to perform functional enrichment analysis of the DEGs (23). The Kyoto Encyclopedia of Genes and Genomes (KEGG; http://www.genome.jp/kegg/pathway.html) was used to determine significant pathways associated with the DEGs (24). Pathways with Q-value thresholds of <0.05 were considered potential target pathways.

Verification of Identified Genes Using Quantitative Reverse Transcription Polymerase Chain Reaction

Total RNA was extracted using TRIzol reagent and reverse-transcribed to cDNA using oligo(dT). Quantitative reverse transcription polymerase chain reaction (RT-qPCR) for target genes was performed by using a SYBR Green kit (Biotium, USA). PCR was carried out on an ABI 7700 system (Roche LightCycler® 480II, Switzerland) using the following reaction conditions: 5 min at 95°C, followed by 45 cycles of 10 s at 95°C and 30 s at 60°C. All gene expression levels were normalized to β-actin expression. The primers are listed in **Table 1**.

Statistical Analysis

Continuous variables were expressed as mean ± standard deviations (SDs); one-way ANOVA was used for comparison between groups, and the least significant difference (LSD) method was used for multiple comparisons. Two-tailed tests were used for all statistics, and p <0.05 was defined as statistically significant differences. Statistical analysis of all data was performed in SPSS 25.0 software (SPSS Inc., Chicago, IL, USA). All figures were performed in GraphPad Prism 8.0 software (GraphPad, La Jolla, USA).

RESULTS

Effects of Liraglutide on Body Weight and Glucose Control in T1D Mice

As expected, saline-treated T1D mice manifested markedly hyperglycemia and weight loss when compared with NGT

TABLE 1 | Primers used in our experiments.

Primer name	Sequence (5′ to 3′)	Number of bases	Product length (bp)
β-Actin	F: GAGATTACTGCTCTGGCTCCTA	22	150
	R: GGACTCATCGTACTCCTGCTTG	22	
Trem2	F: ACTTATGACGCCTTGAAGCACTGG	24	236
	R: CCTCGGAGACTCTGACACTGGTAG	24	
Ctsk	F: CAGTGTTGGTGGTGGGCTATGG	22	174
	R: TGGCTGGCTGGAATCACATCTTG	23	
c-Fos	F: GCTGCACTACTTACACGTCTTCCT	24	169
	R: GCTGCCTTGCCTTCTCTGACTG	22	
Trap	F: ACGGCTACTTGCGGTTTCACTATG	24	172
	R: AAGCAGGACTCTCGTGGTGTTCA	23	
Nfatc1	F: GGTGAGGCTGGTCTTCCGAGTT	22	139
	R: GCTGTCTGTGCTCTGCTTCTCC	22	
Opg	F: CGGAGAGTGAGGCAGGCTATT	21	135
	R: GCTGTGAGGAGAGGAAGGAAGG	22	
Rankl	F: CATCGGGTTCCCATAAAG	18	141
	R: GAAAGCAAATGTTGGCGTA	19	
Tnfa	F: TAACTTAGAAAGGGGATTATGGCT	24	264
	R: TGGAAAGGTCTGAAGGTAGGAA	22	

controls, confirming the successful establishment of the disease model (**Figure 1** and **Supplementary Tables 2**, **3**). However, in comparison with saline-treated T1D mice, once-daily insulin detemir treatment failed to control blood sugar well or recover weight loss but reduced deaths due to hyperglycemia (**Figure 1** and **Supplementary Tables 2**, **3**). Furthermore, liraglutide monotherapy significantly improved glucose control especially in the second half of the experiment compared with the saline-treated T1D group and insulin treatment group but did not restore weight loss, probably because liraglutide partly restored β-cell function but also had weight loss effect (**Figure 1** and **Supplementary Tables 2**, **3**). However, the combined treatment with liraglutide and insulin did not improve glycemic control and even caused further weight loss compared with saline-treated T1D mice (**Figure 1** and **Supplementary Tables 2**, **3**).

Effects of Liraglutide on Bone Mineral Density and Microarchitectures

In the tibia, saline-treated T1D mice showed reduction in cortical volumetric bone mineral density (Ct.vBMD) and cortical thickness (Ct.Th) compared with NGT controls, while the difference in cortical thickness did not reach statistical significance (**Figures 2, 3** and **Supplementary Table 4**). In addition, deficits in trabecular bone of the tibia were also apparent; especially, reductions in trabecular number (Tb.N) and trabecular volumetric bone mineral density (Tb.vBMD), along with an increase in trabecular separation, were significant in T1D mice in relation to NGT controls (**Figures 2**, **3** and **Supplementary Table 4**).

Compared with the T1D group, treatment with insulin alone rectified the decreased Ct.vBMD, but seemed to further

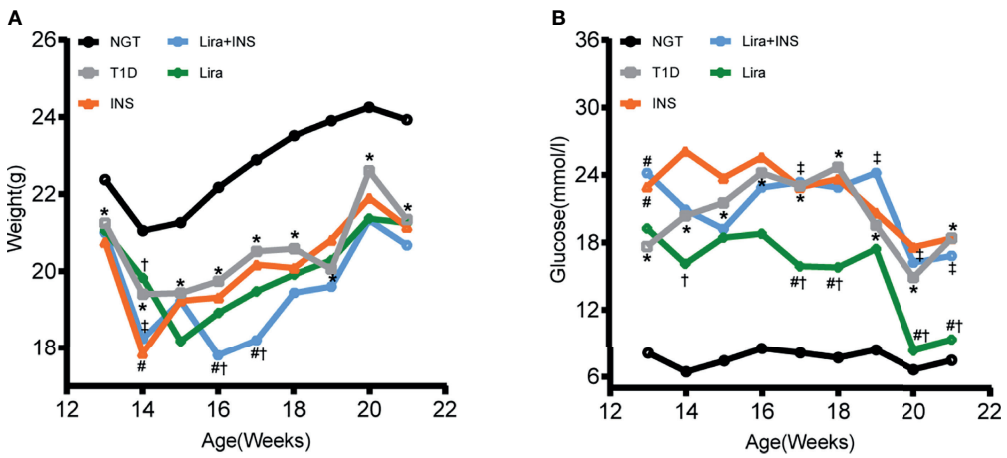

FIGURE 1 | Changes of body weight and blood glucose during treatments. **(A)** Weekly body weight (g); **(B)** weekly blood glucose levels at fed states (mmol/l). NGT: normal glucose tolerance group; T1D, saline-treated type 1 diabetes group; INS, insulin treatment group; Lira, liraglutide treatment group; INS+Lira, insulin + liraglutide treatment group; ANOVA was used for comparison between groups, and p <0.05 was defined as statistically significant. *compared with NGT; #compared with T1D; †compared with INS; ‡compared with Lira. All data are expressed as mean ± SDs.

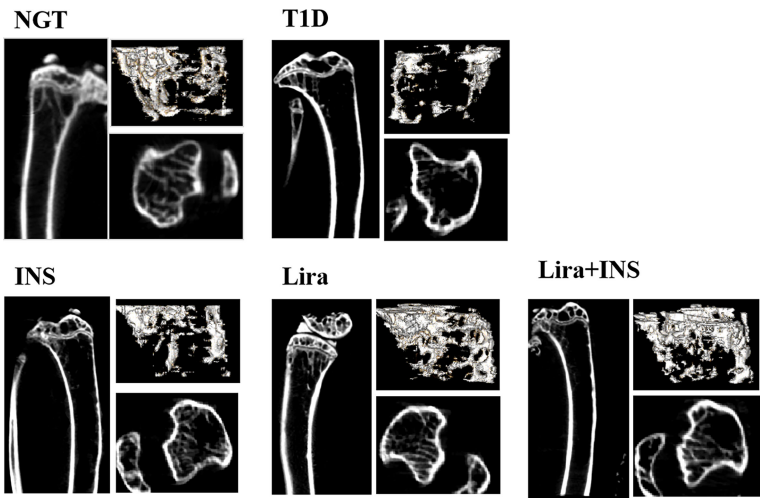

FIGURE 2 | Typical 2D and 3D images of micro-CT. NGT, normal glucose tolerance group; T1D, type 1 diabetes group; INS, insulin treatment group; Lira, liraglutide treatment group; INS+Lira, insulin + liraglutide treatment group.

deteriorate the trabecular microarchitectures, especially significantly increased Tb.Sp of the tibia (**Figures 2**, **3** and **Supplementary Table 4**). However, when treated with liraglutide alone or combined with insulin, significant recovery of the tibia Tb.vBMD and Ct.vBMD, along with partially recovery of tibia trabecular microarchitectures, was evident in mice receiving monotherapy or combined therapy (**Figures 2**, **3** and **Supplementary Table 4**).

Effects of Liraglutide on Bone Histomorphometry

As shown in typical pictures of femur histomorphometry, saline-treated T1D mice showed thinner and broken trabeculae, increased trabecular spacing, and more adipocytes in bone marrow. Liragutide treatment alone or combined with insulin partly improved those defects (**Figure 4**). However, quantitative analysis did not demonstrate significance between group differences for BV/TV, Tb.Th, Tb.N, Tb.Sp, and marrow adipose number (**Figure 5** and **Supplementary Table 5**).

Effects of Liraglutide on Bone Turnover and C-Peptide

Bone turnover markers in serum were then detected. P1NP is a marker of bone formation, and CTX is a marker of bone resorption. P1NP and CTX both showed non-significant trends toward an increased level in T1D mice compared with NGT mice (**Figure 6**, **Supplementary Table 6**). Insulin treatment slightly increased P1NP and decreased CTX, liraglutide treatment alone decreased CTX more than PINP, while liraglutide combined with insulin treatment decreased PINP and increased CTX, but all these comparisons did not reach significance (**Figures 6B, C** and **Supplementary Table 6**). The CTX in the liraglutide +insulin treatment group seemed increased; however, the sample in this group was relatively small and might be greatly affected by extreme values.

Serum C-peptide was detected using the serum obtained at the end of the experiment. There was no significant difference among each group (**Figure 6A**). These results were inconsistent with the blood glucose, and we found that C-peptide levels in the insulin treatment groups were higher than those in the other groups. Therefore, we speculated that there might be cross-reactions with insulin during the C-peptide detection.

Transcriptome Analysis of DEGs Between the NGT, T1D, and Liraglutide Treatment Groups

To further explore the mechanisms of diabetic-associated bone loss, we selected three tibia specimens from each of the NGT, T1D, and liraglutide treatment groups for transcriptome sequencing and bioinformatics analysis.

Transcripts of DEGs were characterized using RNA-sequencing (RNA-seq) analyses of tibia tissues from the NGT, T1D, and liraglutide treatment groups. A fold change >2 and *Q*-value <0.05 were used to screen the DEGs. The results revealed obvious differences between the NGT group and the T1D group and between the T1D group and the liraglutide treatment group, which are presented in histogram and volcano map (**Figures 7A, C, D**). Compared with the NGT group, 1,464 genes were significantly changed in the tibia tissues in T1D mice consisting of 1,262 upregulated and 202 downregulated genes. On the other hand, compared with the untreated T1D group, 1,692 genes were significantly changed in the tibia tissues in liraglutide treatment mice consisting of 593 upregulated and 1,099 downregulated genes. A total of 789 DEGs were shared by these two comparisons (**Figure 7B**).

Then, GO and KEGG databases were used to annotate and classify those 789 shared DEGs. The enrichment analysis indicated that those DEGs were mainly distributed in the signals such as osteoclast differentiation (osteoclastogenesis) signaling pathway, tumor necrosis factor (TNFa) signaling

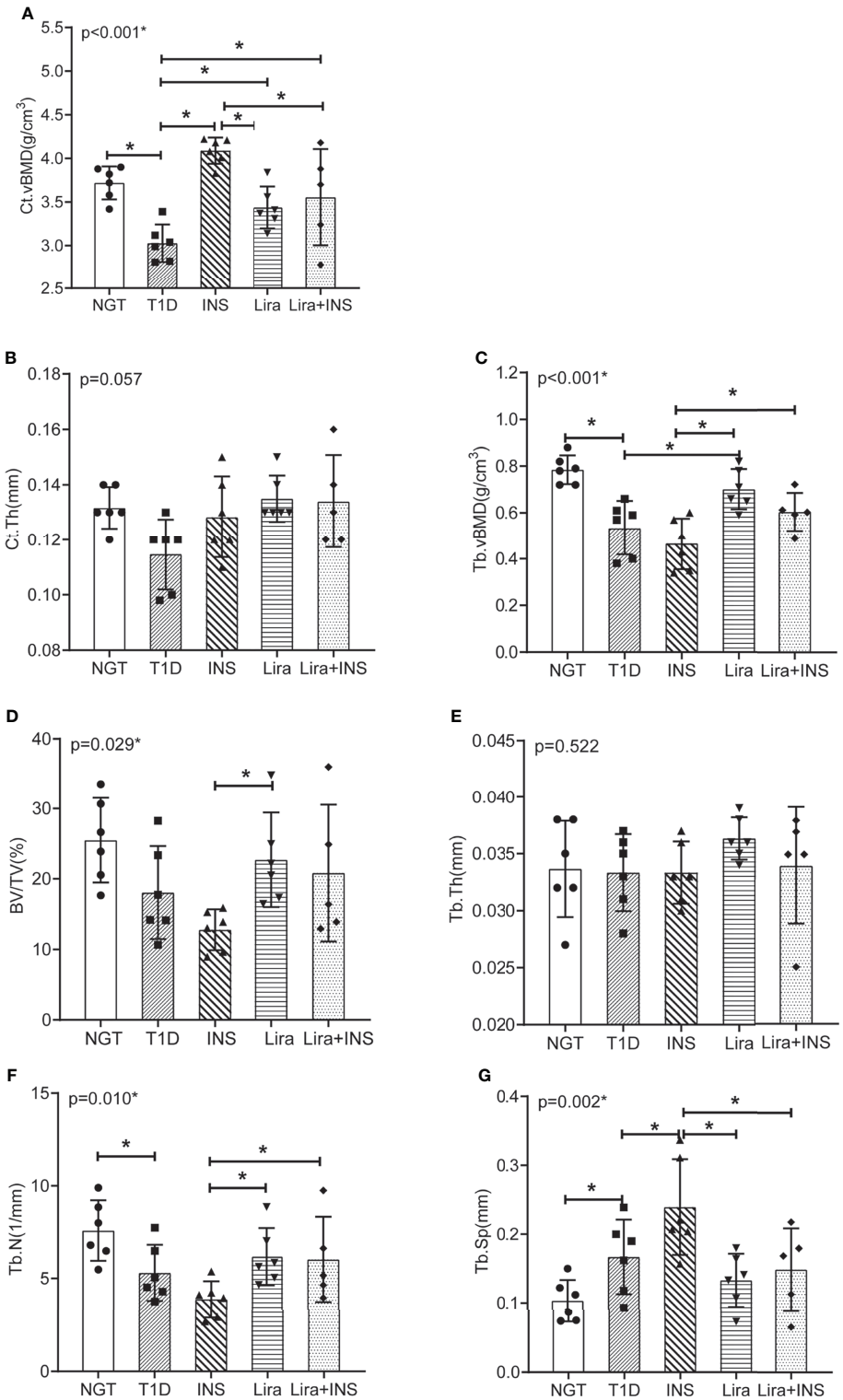

FIGURE 3 | Bone mineral density and microarchitectures of tibia measured by micro-CT. **(A)** Cortical volumetric bone mineral density (Ct.vBMD); **(B)** cortical bone thickness (Ct.Th); **(C)** trabecular volumetric bone mineral density (Tb.vBMD); **(D)** bone volume fraction (BV/TV); **(E)** trabecular thickness (Tb.Th); **(F)** trabecular number (Tb.N); **(G)** trabecular separation (Tb.Sp). NGT, normal glucose tolerance group; T1D, type 1 diabetes group; INS, insulin treatment group; Lira, liraglutide treatment group; INS+Lira, insulin + liraglutide treatment group. ANOVA was used for comparison between groups, and $p < 0.05$ was defined as statistically significant. *was used to indicate statistical difference. All data are expressed as mean ± SDs.

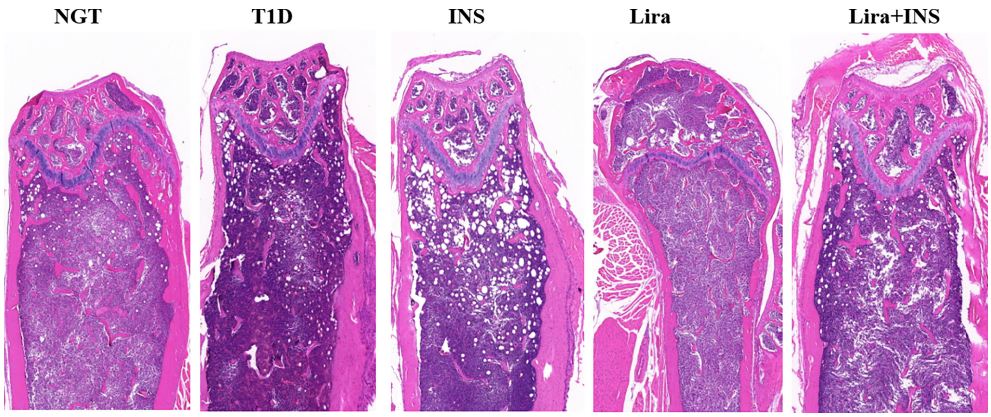

FIGURE 4 | Typical H&E images of bone histomorphometry. NGT, normal glucose tolerance group; T1D, type 1 diabetes group; INS, insulin treatment group; Lira, liraglutide treatment group; INS+Lira, insulin + liraglutide treatment group.

pathway, and nuclear factor-κB (NF-κB) signaling pathway (according to the KEGG database), and the functional enrichment was mainly concentrated in processes, such as chemokine activity and cytokine activity (according to the GO-MF database) (**Figures 7E, F** and **Tables 2**, **3**). Thus, the increased osteoclastogenesis and enhanced inflammation were the characteristic biological changes in tibia bone remodeling in diabetic bone, and liraglutide treatment might inhibit osteoclastogenesis and inflammation. Significantly enriched DEGs in the osteoclastogenesis pathway are manifested in **Table 4**, and the fold change of Triggering receptor expressed on myeloid cells 2 (*Trem2*) gene expression ranked among the top (**Table 4**).

RT-qPCR Verification of Differentially Expressed Genes Identified by RNA-Seq

To validate transcriptomics analysis results, we analyzed the mRNA expression levels of representative genes using RT-qPCR. The selected genes were mainly in the signaling pathways of osteoclastogenesis and TNFa inflammation, including osteoprotegerin (*Opg*), nuclear factor receptor activator κB ligand (*Rankl*), *Tnfa*, *Trem2*, *c-Fos*, tartrate-resistant acid phosphatase (*Trap*), cathepsin K (*Ctsk*), and nuclear factor-activated T cell 1 (*Nfatc1*) (**Table 4**).

The mRNA expression of genes expressed in the late phase of osteoclastogenesis including *Nfatc1*, *Trap*, and *Ctsk* were significantly increased in T1D mice compared with NGT except c-Fos, indicating enhanced osteoclast activity in diabetic bone (**Figures 8D–G**). The ratio of Rankl/Opg mRNA, a key regulator of osteoclastogenesis, only showed non-significant trends toward an increased level in T1D mice compared with NGT mice. However, the mRNA level of *Trem2*, a key co-stimulatory molecular of osteoclastogenesis, was significantly increased in T1D mice compared with that in NGT mice (**Figures 8A, C**). Tnfa mRNA, an inflammation marker, also increased in T1D mice compared with that in NGT mice, but did not reach significance (**Figure 8B**).

Compared with untreated T1D mice, treatment with insulin alone, liraglutide alone, or liraglutide combined with insulin all significantly decreased *Trem2*, *Nfatc1*, *Trap*, and *Ctsk* expression, indicating their role in inhibiting osteoclastogenesis (**Figure 8**).

DISCUSSION

In this study, our main findings were as follows: 1) compared with the NGT group, T1D mice showed decreased BMD and compromised microarchitectures. Insulin treatment alone only rectified the decreased Ct.vBMD but seemed to further deteriorate the trabecular microarchitectures. However, liraglutide treatment alone or combined with insulin significantly recovered the tibia Tb.vBMD and Ct.vBMD and partially recovered the tibia trabecular microarchitectures. 2) Transcriptome analysis showed enhanced osteoclastogenesis and increased inflammation in tibia bone remodeling in diabetic bone. Further RT-qPCR verified that osteoclastogenesis was prominently increased in T1D mice, including upregulated expression of *Trem2, Nfatc1, Trap* and *Ctsk*, which could be inhibited by liraglutide treatment alone or combined with insulin.

In terms of bone turnover markers, we found no significant intergroup differences overall. Compared with bone histomorphology or local gene expression, serum turnover markers may be less sensitive. In our study and other studies, serum CTX or P1NP in T1D patients was within the normal range or similar to the control groups, while micro-CT found significant compromised microarchitectures (3, 25). Previous studies have found low bone turnover especially reduced bone formation in the T1D context (26); however, the bone resorption can be enhanced, inhibited, or unaltered, which might be attributed to the timing of onset of T1D, the duration of diabetes, and the disease-associated inflammatory environment (27). In our study, STZ-induced T1D mice showed significantly elevated blood glucose for an enough duration (at least 8 weeks), resulting in decreased BMD and

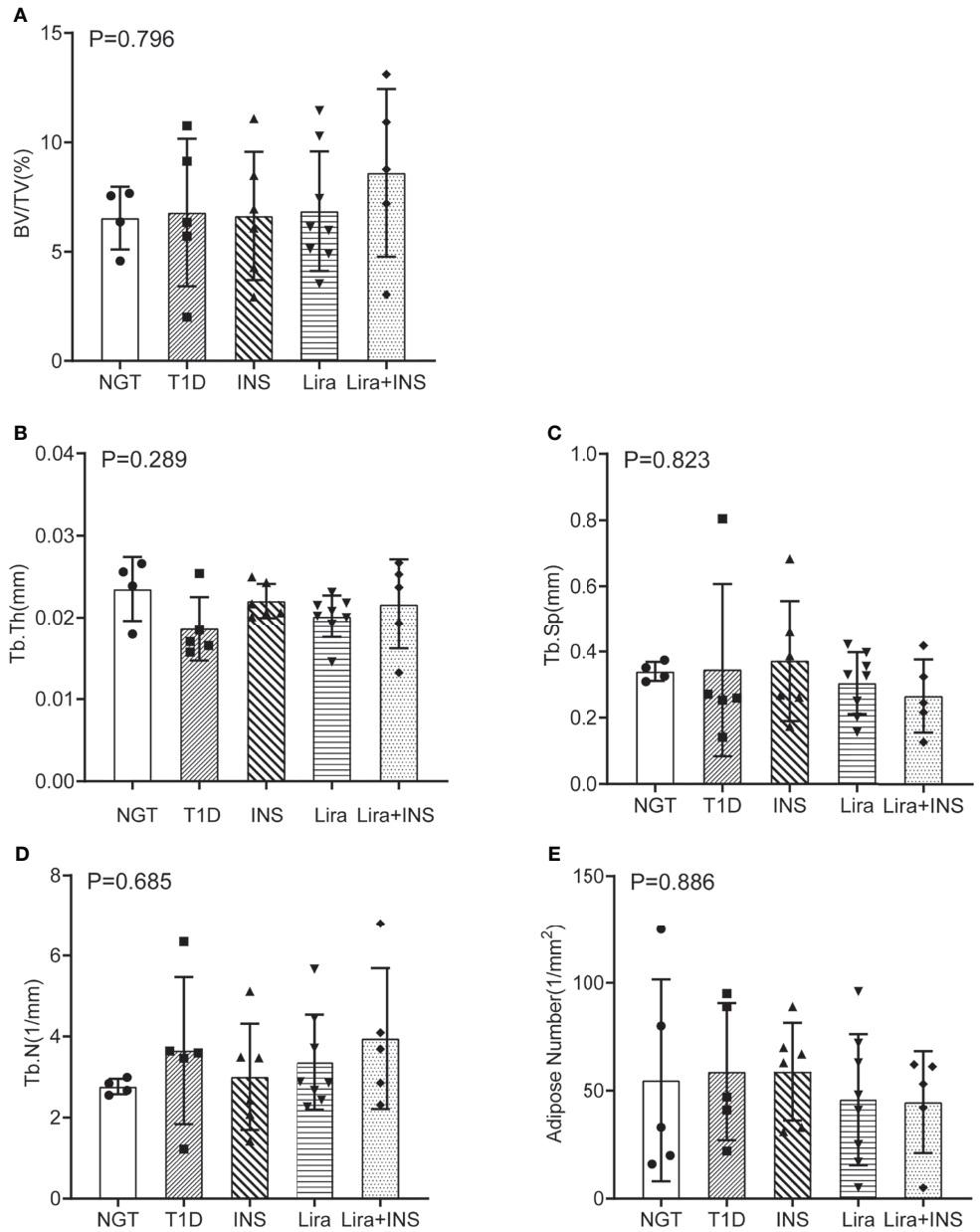

FIGURE 5 | Bone histomorphometry of the femur. **(A)** Bone volume fraction (BV/TV); **(B)** trabecular thickness (Tb.Th); **(C)** trabecular separation (Tb.Sp); **(D)** trabecular number (Tb.N); **(E)** adipose number in marrow. NGT, normal glucose tolerance group; T1D, type 1 diabetes group; INS, insulin treatment group; Lira, liraglutide treatment group; INS+Lira, insulin + liraglutide treatment group. ANOVA was used for comparison between groups, and $p < 0.05$ was defined as statistically significant. All data are expressed as mean ± SDs.

compromised microarchitectures, which was consistent with previous clinical and animal studies (3, 14, 25, 28), indicating our successful establishment of the disease model. Thus, the STZ-induced T1D model could be a convenient and reliable model for studying T1D-related bone loss.

Furthermore, bone fragility of T1D is attributed to complex and multifactorial pathophysiological mechanisms, but much remained unknown. In order to have a more comprehensive and unbiased understanding of pathophysiologic mechanisms behind the bone fragility in T1D, we conducted transcriptomics and bioinformatics analyses, which have not been carried out in this setting till now. The transcriptomics in our study showed that there were a total of 789 DEGs including upregulated or downregulated genes, which were mainly mapped to osteoclastogenesis and inflammation pathways. A previous study using microarray analysis in a fracture healing mouse model revealed an upregulation of gene sets related to inflammation and elevated osteoclast numbers in the type 1 diabetic group (29),

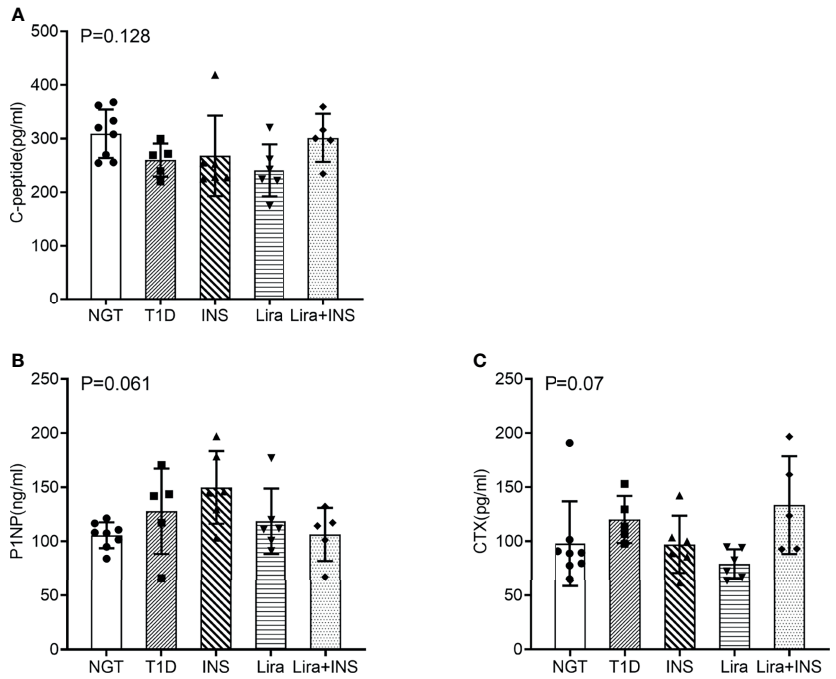

FIGURE 6 | Serum bone turnover markers and C-peptide. **(A)** C-peptide; **(B)** procollagen type 1 N-terminal propeptide (P1NP); **(C)** C-terminal cross-linking telopeptide of type 1 collagen (CTX). NGT, normal glucose tolerance group; T1D, type 1 diabetes group; INS, insulin treatment group; Lira, liraglutide treatment group; INS+Lira, insulin + liraglutide treatment group; ANOVA was used for comparison between groups, and $p < 0.05$ was defined as statistically significant. All data are expressed as mean ± SDs.

which was consistent with our results. On the other hand, in the distraction osteogenesis model, microarray analysis also found that T1D negatively affected the expression of transcription factors regulating osteoblast differentiation (30). Transcriptomic findings were only reported in a guided bone regeneration model under T1D circumstance and a differential expression of genes associated with the ossification process was evident at 15 days of healing between the healthy controls and diabetic animals (31). Different animal models and experimental conditions might lead to those inconsistent results.

RT-qPCR verified some key findings obtained from the transcriptome analysis. Previously, studies about T1D effects on osteoclasts most focused on gene expression of *Rankl/Opg* ratio, *Trap*, or *Cstk*. TRAP and CSTK, which are both important enzymes expressing in the late phase of osteoclastogenesis, have been found to increase in T1D, supporting our results (32). However, studies about RANKL/OPG ratio in T1D, the key regulator of osteoclastogenesis, have not been consistent, suggesting that RANKL/RANK-induced osteoclast activation might not be the primary mechanism that drives bone resorption throughout the course of T1D (27). In our study, RANKL/OPG ratio was not different between the T1D group and NGT mice, indicating that there might be alternative mechanisms in regulating osteoclastogenesis. Indeed, we have identified two significant DEGs in osteoclastogenesis pathways which have not been reported previously: *Nfatc1* and *Trem2*. *NFATc1* is the important transcription factor of osteoclastogenesis, while *Trem2* is upstream of *NFATc1* and is the key co-stimulatory molecule of osteoclastogenesis. *In vivo* studies have shown that mutations in *Trem2* have been associated with Nasu–Hakola disease that is characterized by cystic bone lesions, osteoporotic features, and loss of white matter in the brain (33). *In vitro* evidence suggests that the dysfunction of *Trem2* leads to significantly impaired osteoclastogenesis (34). In the present study, the *Trem2* gene ranked among the top of DEGs in the osteoclastogenesis pathway, suggesting its important role in regulating osteoclastogenesis in bone in the T1D context.

In this study, we also explored whether hypoglycemic therapy improved bone loss in T1D mice. Insulin is the primary therapy for T1D and two previous studies found that systemic insulin therapy could rescue inhibited osteogenesis and correct distorted bone microstructures (30, 35). In our study, insulin treatment alone was found to inhibit the gene expression of osteoclastogenesis and rectified the decreased Ct.vBMD, but paradoxically seemed to further deteriorate trabecular microarchitectures. The exact mechanisms that cause the discrepancy are not clear. In the two previous studies, insulin implants were used to achieve optimal glucose control, but in our study, once-daily insulin detemir treatment failed to control glucose well and caused large glucose fluctuations. Irwin et al. found that bone loss in T1D was caused by hyperglycemia more than the lack of insulin signaling in bone (36), which might explain our negative results of insulin treatment.

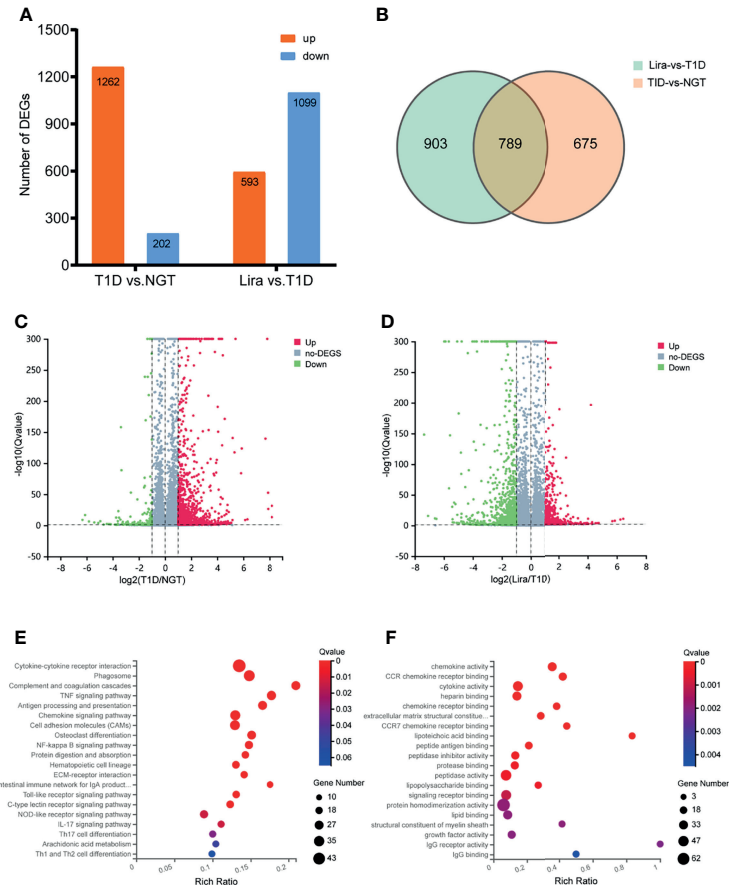

FIGURE 7 | Transcriptomic analysis of DEGs between NGT, T1D, and liraglutide treatment groups. **(A)** Number of DEGs in histogram; **(B)** Venn diagram of pairwise comparison; **(C)** volcano map of DEGs between the NGT and T1D groups; **(D)** volcano map of DEGs between the T1D and liraglutide groups. **(E)** Bubble plots using the KEGG database; **(F)** bubble plots using the GO-MF database. NGT, normal glucose tolerance group; T1D, type 1 diabetes group; Lira, liraglutide treatment group.

TABLE 2 | Significantly enriched pathways of DEGs using the KEGG database.

ID	Description	Gene number	Rich ratio	*Q*-value
4060	Cytokine–cytokine receptor interaction	43	0.135	<0.001
4145	Phagosome	33	0.148	<0.001
4610	Complement and coagulation cascades	22	0.210	<0.001
4668	TNF signaling pathway	25	0.177	<0.001
4612	Antigen processing and presentation	22	0.165	<0.001
4062	Chemokine signaling pathway	28	0.130	<0.001
4514	Cell adhesion molecules (CAMs)	27	0.129	<0.001
4380	Osteoclast differentiation	21	0.151	<0.001
4064	NF-kappa B signaling pathway	18	0.148	<0.001
4974	Protein digestion and absorption	14	0.143	0.001
4640	Hematopoietic cell lineage	15	0.130	0.001
4512	ECM–receptor interaction	13	0.141	0.001
4672	Intestinal immune network for IgA production	10	0.175	0.001
4620	Toll-like receptor signaling pathway	14	0.131	0.001
4625	C-type lectin receptor signaling pathway	15	0.123	0.001
4621	NOD-like receptor signaling pathway	18	0.089	0.013
4657	IL-17 signaling pathway	12	0.111	0.013
4659	Th17 cell differentiation	12	0.100	0.031
590	Arachidonic acid metabolism	10	0.104	0.048
4658	Th1 and Th2 cell differentiation	10	0.099	0.065

TABLE 3 | Significantly enriched processes of DEGs using the GO-MF database.

GO_F term ID	Description	Gene number	Rich ratio	*Q*-value
GO:0008009	Chemokine activity	24	0.358	<0.001
GO:0048020	CCR chemokine receptor binding	16	0.421	<0.001
GO:0005125	Cytokine activity	34	0.145	<0.001
GO:0008201	Heparin binding	25	0.140	<0.001
GO:0042379	Chemokine receptor binding	10	0.385	<0.001
GO:0030020	Extracellular matrix structural constituent conferring tensile strength	11	0.282	<0.001
GO:0031732	CCR7 chemokine receptor binding	8	0.444	<0.001
GO:0070891	Lipoteichoic acid binding	5	0.833	<0.001
GO:0042605	Peptide antigen binding	12	0.211	<0.001
GO:0030414	Peptidase inhibitor activity	17	0.130	<0.001
GO:0002020	Protease binding	17	0.127	<0.001
GO:0008233	Peptidase activity	41	0.074	<0.001
GO:0001530	Lipopolysaccharide binding	8	0.267	<0.001
GO:0005102	Signaling receptor binding	36	0.075	0.001
GO:0042803	Protein homodimerization activity	62	0.060	0.002
GO:0008289	Lipid binding	26	0.084	0.002
GO:0019911	Structural constituent of myelin sheath	5	0.417	0.002
GO:0008083	Growth factor activity	17	0.108	0.002
GO:0019770	IgG receptor activity	3	1.000	0.002
GO:0019864	IgG binding	4	0.500	0.004

GLP-1R agonists have demonstrated some benefits as adjunct therapies in T1D patients (6). The only experimental research by Mansur et al. found that liraglutide treatment for 21 days in STZ-induced T1D mice significantly increased bone maximum force and hardness but failed to improve trabecular and cortical microarchitectures (14). In our study, we found that liraglutide treatment alone or in combination with insulin for 8 weeks not only rectified the decreased trabecular and cortical BMD, but also partly rectified the trabecular microarchitectures, which might be due to the longer treatment duration than the study of Mansur and colleagues. Moreover, mechanical forces are associated with proper skeletal homeostasis (37). Bone loss occurs in humans after immobilization and in animals subjected to tail suspension, in which case sclerostin is increased to mainly inhibit bone formation (37). Studies also found that weight loss is generally associated with decreased bone mass in humans and rodents accompanied by increased bone resorption and decreased bone formation (38, 39). In our study, the mice in the liraglutide treatment groups suffered greater weight loss than the T1D mice which might cause negative effect on bone, which might partly explain the only partial improvement of bone microarchitectures. Metformin was also found to have an effect on bone metabolism, which was also mainly associated with neutral outcomes or decreased fracture risk in comparison to treatment with other glucose-lowering drugs (10). Metformin was found to decrease ALP, CTX-1, TRACP 5b, PINP, and

TABLE 4 | Significantly enriched DEGs in the osteoclastogenesis pathway.

Gene ID	Gene symbol	log2 (T1D/NGT)	*Q*-value (T1D/NGT)
15978	"Ifng"	4.545	0.00
246256	"Fcgr4"	3.904	<0.001
83433	"Trem2"	3.722	<0.001
14129	"Fcgr1"	3.397	<0.001
435653	"Fcrlb"	2.932	0.001
320832	"Sirpb1a"	2.906	<0.001
100038947	"LOC100038947"	2.714	<0.001
18729	"Pira6"	2.336	<0.001
13038	"Ctsk"	2.335	<0.001
14130	"Fcgr2b"	2.176	<0.001
11433	"Acp5"	2.163	<0.001
14131	"Fcgr3"	2.160	<0.001
21934	"Tnfrsf11a"	2.059	<0.001
12703	"Socs1"	2.001	<0.001
232790	"Oscar"	1.947	<0.001
18722	"Pira1"	1.825	<0.001
12978	"Csf1r"	1.825	<0.001
20846	"Stat1"	1.820	<0.001
12702	"Socs3"	1.705	<0.001
14200	"Fhl2"	1.419	<0.001
21943	"Tnfsf11"	1.281	0.002

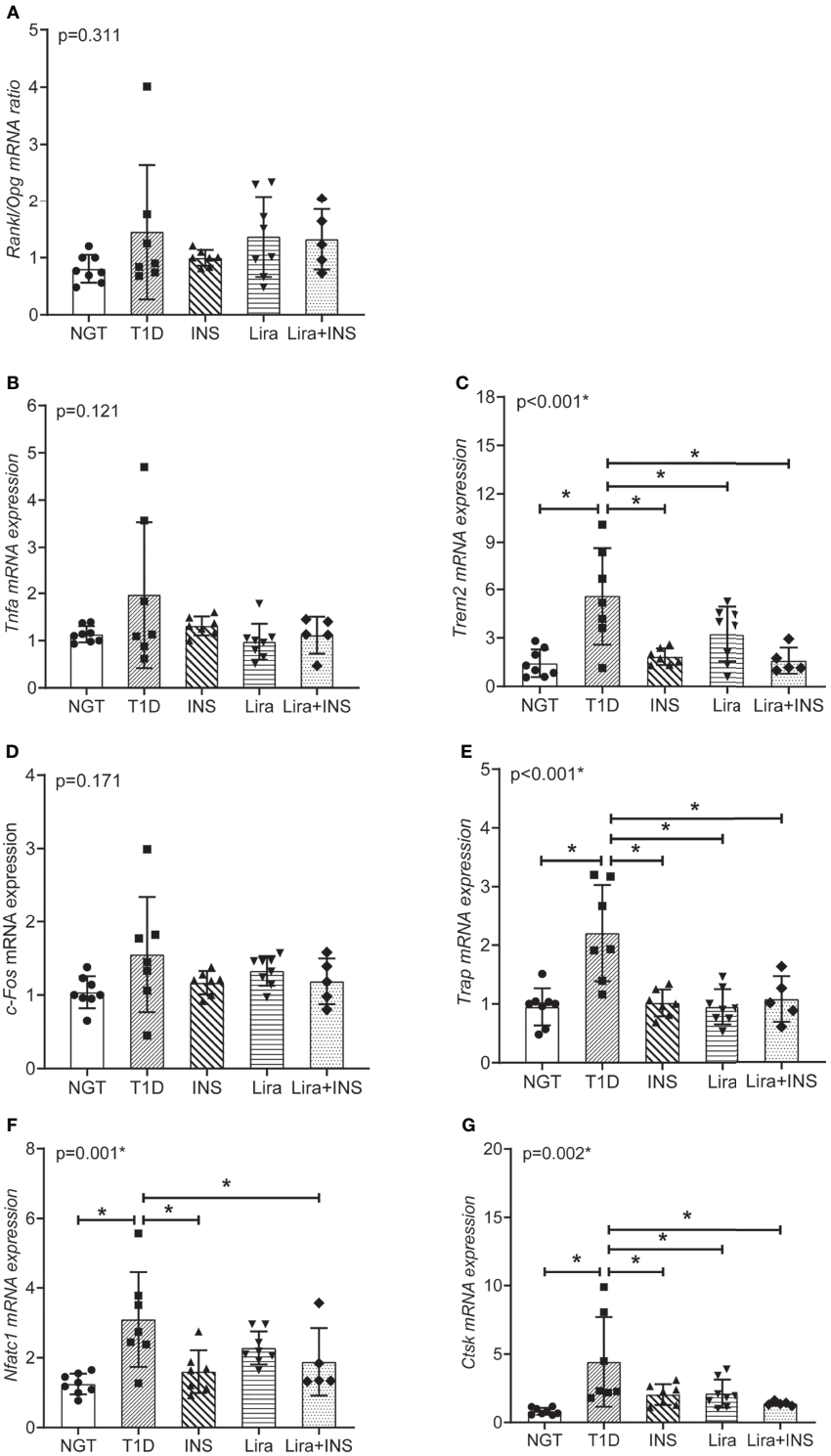

FIGURE 8 | Relative mRNA expression in the signaling pathways of osteoclastogenesis and TNFa inflammation in tibia tissues. **(A)** The ratio of *Rankl*/*Opg* mRNA expression; **(B)** *Tnfa* mRNA expression; **(C)** *Trem2* mRNA expression; **(D)** *c-Fos* mRNA expression; **(E)** *Trap* mRNA expression; **(F)** *Nfatc1* mRNA expression; **(G)** *Ctsk* mRNA expression. NGT, normal glucose tolerance group; T1D, type 1 diabetes group; Lira, liraglutide treatment group; INS+Lira, insulin + liraglutide treatment group. ANOVA was used for comparison between groups, and $p < 0.05$ was defined as statistically significant. * was used to indicate statistical difference. All data are expressed as mean ± SDs.

RANKL, but increase OPG, RUNX2, and OPG/RANKL ratio in diabetic rat, indicating a bone protection role (40), but it was not exactly the same as liraglutide.

As for the mechanisms, previous studies found that Glp1-r KO mouse manifested an increased number of osteoclasts and eroded surfaces (7) and GLP-1RAs could decrease osteoclastic surfaces (41, 42), indicating a control of bone resorption. However, the downstream molecular mechanisms underlying this effect have not ever been identified. Yamada et al. once proposed an indirect effect through a reduction in calcitonin gene expression in GLP-1r-deficient animals. In our study, liraglutide treatment alone or in combination with insulin could not only effectively suppress osteoclastogenesis by downregulating the expression of Trem2 and NFATc1, but also downregulated the expression of CTSK and TRAP to inhibit the resorptive activity, confirming its effect on bone resorption. Liraglutide was also found to inhibit osteoclastogenesis *in vitro*, which supported our results (43). However, due to the scarcity of research in this area, more evidence may be required to further clarify its role in osteoclastogenesis.

Our research has some limitations: although dynamic bone formation rate and bone resorption surface were not calculated, detailed micro-CT analysis and serum bone turnover indicators could also reflect the bone turnover process well; in addition, due to the small amount of serum in mice, serum TREM2 protein was not measured.

CONCLUSION

In our study, T1D mice were confirmed to show decreased BMD and compromised microarchitectures. Transcriptomics was innovatively used to clarify pathophysiologic mechanisms, and we found that strengthened osteoclastogenesis regulated by increased expression of *Trem2* and downstream genes played an important role in type 1 diabetic bone phenotype. Moreover, liraglutide generated a bone-protective effect in T1D mice by suppressing osteoclastogenesis to inhibit bone resorption.

DATA AVAILABILITY STATEMENT

The data presented in the study are deposited in the Gene Expression Omnibus (GEO) repository, accession number GSE189112.

ETHICS STATEMENT

The animal study was reviewed and approved by the Institutional Animal Care and Use Committee (IACUC) at the Institute of Laboratory Animal Sciences, CAMS and PUMC.

AUTHOR CONTRIBUTIONS

JY: animal experiment, data acquisition, and drafting of the manuscript; FP, HZ, WL, SH, and YZ: data acquisition and analysis and interpretation of the data. YS, LX, and YL: study concept and design, critical revision of the manuscript for important intellectual content, and study supervision. All authors contributed to the article and approved the submitted version.

FUNDING

This study was supported by grants from the National Key Research and Development Program of China (Grant No.2016YFC1305000), China Diabetes Young Scientific Research Project (Grant No.2018-N-01), Non-profit Central Research Institute Fund of Chinese Academy of Medical Sciences (Grant No.2019XK320031), National Natural Science Foundation of China (Grant No.82100947), and the Science and Technology Base and Talent Project of the Guangxi Zhuang Autonomous Region, China (AD19259001).

ACKNOWLEDGMENTS

The authors would like to thank the National Key Research and Development Program of China (Grant No.2016YFC1305000), China Diabetes Young Scientific Research Project (Grant No.2018-N-01), Non-profit Central Research Institute Fund of Chinese Academy of Medical Sciences (Grant No.2019XK320031), National Natural Science Foundation of China (Grant No.82100947), and all of the participants in this study.

SUPPLEMENTARY MATERIAL

The Supplementary Material for this article can be found online at: https://www.frontiersin.org/articles/10.3389/fendo.2021.763646/full#supplementary-material

REFERENCES

1. Saberzadeh-Ardestani B, Karamzadeh R, Basiri M, Hajizadeh-Saffar E, Farhadi A, Shapiro AMJ, et al. Type 1 Diabetes Mellitus: Cellular and Molecular Pathophysiology at A Glance. *Cell J (Yakhteh)* (2018) 20(3):294–301. doi: 10.22074/cellj.2018.5513
2. Thong EP, Herath M, Weber DR, Ranasinha S, Ebeling PR, Milat F, et al. Fracture Risk in Young and Middle-Aged Adults With Type 1 Diabetes Mellitus: A Systematic Review and Meta-Analysis. *Clin Endocrinol* (2018) 89 (3):314–23. doi: 10.1111/cen.13761
3. Xu L, Yu J, Wang O, Hou Y, Li W, Zhang H, et al. Comparison of Differences in Bone Microarchitecture in Adult- Versus Juvenile-Onset Type 1 Diabetes Asian Males Versus Non-Diabetes Males: An Observational Cross-Sectional Pilot Study. *Endocrine* (2021) 71(1):87–95. doi: 10.1007/s12020-020-02480-5
4. Napoli N, Chandran M, Pierroz DD, Abrahamsen B, Schwartz AV, Ferrari SL. Mechanisms of Diabetes Mellitus-Induced Bone Fragility. *Nat Rev Endocrinol* (2017) 13(4):208–19. doi: 10.1038/nrendo.2016.153
5. Calciolari E, Donos N. Proteomic and Transcriptomic Approaches for Studying Bone Regeneration in Health and Systemically Compromised Conditions. *Proteomics – Clin Appl* (2020) 14(3):1900084. doi: 10.1002/prca.201900084

6. Nally LM, Sherr JL, Van Name MA, Patel AD, Tamborlane WV. Pharmacologic Treatment Options for Type 1 Diabetes: What's New? *Expert Rev Clin Phar* (2019) 12(5):471–9. doi: 10.1080/17512433.2019.1597705
7. Mabilleau G, Pereira M, Chenu C. Novel Skeletal Effects of Glucagon-Like Peptide-1 (GLP-1) Receptor Agonists. *J Endocrinol* (2018) 236(1):R29–42. doi: 10.1530/JOE-17-0278
8. Herold KC, Reynolds J, Dziura J, Baidal D, Gaglia J, Gitelman SE, et al. Exenatide Extended Release in Patients With Type 1 Diabetes With and Without Residual Insulin Production. *Diabetes Obes Metab* (2020) 22(11):2045–54. doi: 10.1111/dom.14121
9. Snaith JR, Holmes-Walker DJ, Greenfield JR. Reducing Type 1 Diabetes Mortality: Role for Adjunctive Therapies? *Trends Endocrinol Metab* (2020) 31(2):150–64. doi: 10.1016/j.tem.2019.11.007
10. Al-Mashhadi Z, Viggers R, Fuglsang-Nielsen R, de Vries F, van den Bergh JP, Harsløf T, et al. Glucose-Lowering Drugs and Fracture Risk-A Systematic Review. *Curr Osteoporos Rep* (2020) 18(6):737–58. doi: 10.1007/s11914-020-00638-8
11. Cheng L, Hu Y, Li YY, Cao X, Bai N, Lu TT, et al. Glucagon-Like Peptide-1 Receptor Agonists and Risk of Bone Fracture in Patients With Type 2 Diabetes: A Meta-Analysis of Randomized Controlled Trials. *Diabetes Metab Res Rev* (2019) 35(7):e3168. doi: 10.1002/dmrr.3168
12. Zhang YS, Weng WY, Xie BC, Meng Y, Hao YH, Liang YM, et al. Glucagon-Like Peptide-1 Receptor Agonists and Fracture Risk: A Network Meta-Analysis Of Randomized Clinical Trials. *Osteoporos Int* (2018) 29(12):2639–44. doi: 10.1007/s00198-018-4649-8
13. Su B, Sheng H, Zhang M, Bu L, Yang P, Li L, et al. Risk of Bone Fractures Associated With Glucagon-Like Peptide-1 Receptor Agonists' Treatment: A Meta-Analysis of Randomized Controlled Trials. *Endocrine* (2015) 48(1):107–15. doi: 10.1007/s12020-014-0361-4
14. Mansur SA, Mieczkowska A, Bouvard B, Flatt PR, Chappard D, Irwin N, et al. Stable Incretin Mimetics Counter Rapid Deterioration of Bone Quality in Type 1 Diabetes Mellitus. *J Cell Physiol* (2015) 230(12):3009–18. doi: 10.1002/jcp.25033
15. King AJ. The Use of Animal Models in Diabetes Research. *Br J Pharmacol* (2012) 166(3):877–94. doi: 10.1111/j.1476-5381.2012.01911.x
16. Rydén AK, Perdue NR, Pagni PP, Gibson CB, Ratliff SS, Kirk RK, et al. Anti-IL-21 Monoclonal Antibody Combined With Liraglutide Effectively Reverses Established Hyperglycemia in Mouse Models of Type 1 Diabetes. *J Autoimmun* (2017) 84:65–74. doi: 10.1016/j.jaut.2017.07.006
17. Hatanaka T, Ogawa D, Tachibana H, Eguchi J, Inoue T, Yamada H, et al. Inhibition of SGLT2 Alleviates Diabetic Nephropathy by Suppressing High Glucose-Induced Oxidative Stress in Type 1 Diabetic Mice. *Pharmacol Res Perspect* (2016) 4(4):e239. doi: 10.1002/prp2.239
18. Zhang Q, Xiao X, Zheng J, Li M, Yu M, Ping F, et al. Liraglutide Protects Cardiac Function in Diabetic Rats Through the Pparα Pathway. *Bioscience Rep* (2018) 38(2):1–13. doi: 10.1042/BSR20180059
19. Wen B, Zhao L, Zhao H, Wang X. Liraglutide Exerts a Bone-Protective Effect in Ovariectomized Rats With Streptozotocin-Induced Diabetes by Inhibiting Osteoclastogenesis. *Exp Ther Med* (2018) 15(6):5077–83. doi: 10.3892/etm.2018.6043
20. Qi S. Synergistic Effects of Genistein and Zinc on Bone Metabolism and the Femoral Metaphyseal Histomorphology in the Ovariectomized Rats. *Biol Trace Elem Res* (2018) 183(2):288–95. doi: 10.1007/s12011-017-1134-8
21. Botolin S, McCabe LR. Inhibition of Pparγ Prevents Type I Diabetic Bone Marrow Adiposity But Not Bone Loss. *J Cell Physiol* (2006) 209(3):967–76. doi: 10.1002/jcp.20804
22. Dempster DW, Compston JE, Drezner MK, Glorieux FH, Kanis JA, Malluche H, et al. Standardized Nomenclature, Symbols, and Units for Bone Histomorphometry: A 2012 Update of the Report of the ASBMR Histomorphometry Nomenclature Committee. *J Bone Miner Res* (2013) 28(1):2–17. doi: 10.1002/jbmr.1805
23. Mi H, Muruganujan A, Ebert D, Huang X, Thomas PD. PANTHER Version 14: More Genomes, a New PANTHER GO-Slim and Improvements in Enrichment Analysis Tools. *Nucleic Acids Res* (2019) 47(D1):D419–26. doi: 10.1093/nar/gky1038
24. Huang DW, Sherman BT, Lempicki RA. Systematic and Integrative Analysis of Large Gene Lists Using DAVID Bioinformatics Resources. *Nat Protoc* (2009) 4(1):44–57. doi: 10.1038/nprot.2008.211
25. Mitchell DM, Caksa S, Joseph T, Bouxsein ML, Misra M. Elevated HbA1c Is Associated With Altered Cortical and Trabecular Microarchitecture in Girls With Type 1 Diabetes. *J Clin Endocrinol Metab* (2020) 105(4):e1648–56. doi: 10.1210/clinem/dgz221
26. Hygum K, Starup-Linde J, Harsløf T, Vestergaard P, Langdahl BL. Mechanisms In Endocrinology: Diabetes Mellitus, a State of Low Bone Turnover - A Systematic Review and Meta-Analysis. *Eur J Endocrinol* (2017) 176(3):R137–57. doi: 10.1530/EJE-16-0652
27. Kalaitzoglou E, Popescu I, Bunn RC, Fowlkes JL, Thrailkill KM. Effects of Type 1 Diabetes on Osteoblasts, Osteocytes, and Osteoclasts. *Curr Osteoporos Rep* (2016) 14(6):310–9. doi: 10.1007/s11914-016-0329-9
28. Coe LM, Zhang J, McCabe LR. Both Spontaneous Ins2(+/-) and Streptozotocin-Induced Type I Diabetes Cause Bone Loss in Young Mice. *J Cell Physiol* (2013) 228(4):689–95. doi: 10.1002/jcp.24177
29. Alblowi J, Kayal RA, Siqueira M, McKenzie E, Krothapalli N, McLean J, et al. High Levels of Tumor Necrosis Factor-Alpha Contribute to Accelerated Loss of Cartilage in Diabetic Fracture Healing. *Am J Pathol* (2009) 175(4):1574–85. doi: 10.2353/ajpath.2009.090148
30. Fowlkes JL, Bunn RC, Liu L, Wahl EC, Coleman HN, Cockrell GE, et al. Runt-Related Transcription Factor 2 (RUNX2) and RUNX2-Related Osteogenic Genes Are Down-Regulated Throughout Osteogenesis in Type 1 Diabetes Mellitus. *Endocrinology* (2008) 149(4):1697–704. doi: 10.1210/en.2007-1408
31. Retzepi M, Calciolari E, Wall I, Lewis MP, Donos N. The Effect of Experimental Diabetes and Glycaemic Control on Guided Bone Regeneration: Histology and Gene Expression Analyses. *Clin Oral Implants Res* (2018) 29(2):139–54. doi: 10.1111/clr.13031
32. Hie M, Shimono M, Fujii K, Tsukamoto I. Increased Cathepsin K and Tartrate-Resistant Acid Phosphatase Expression in Bone of Streptozotocin-Induced Diabetic Rats. *Bone* (2007) 41(6):1050.
33. Verloes A, Maquet P, Sadzot B, Vivario M, Thiry A, Franck G. Nasu-Hakola Syndrome: Polycystic Lipomembranous Osteodysplasia With Sclerosing Leucoencephalopathy and Presenile Dementia. *J Med Genet* (1997) 34(9):753–7. doi: 10.1136/jmg.34.9.753
34. Paloneva J, Mandelin J, Kiialainen A, Böhling T, Prudlo J, Hakola P, et al. DAP12/TREM2 Deficiency Results in Impaired Osteoclast Differentiation and Osteoporotic Features. *J Exp Med* (2003) 198(4):669–75. doi: 10.1084/jem.20030027
35. Lu H, Kraut D, Gerstenfeld LC, Graves DT. Diabetes Interferes With the Bone Formation by Affecting the Expression of Transcription Factors That Regulate Osteoblast Differentiation. *Endocrinology* (2003) 144(1):346–52. doi: 10.1210/en.2002-220072
36. Irwin R, Lin HV, Motyl KJ, McCabe LR. Normal Bone Density Obtained in the Absence of Insulin Receptor Expression in Bone. *Endocrinology* (2006) 147(12):5760–7. doi: 10.1210/en.2006-0700
37. Uda Y, Azab E, Sun N, Shi C, Pajevic PD. Osteocyte Mechanobiology. *Curr Osteoporos Rep* (2017) 15(4):318–25. doi: 10.1007/s11914-017-0373-0
38. Jensen V, Molck AM, Dalgaard M, McGuigan FE, Akesson KE. Changes in Bone Mass Associated With Obesity and Weight Loss in Humans: Applicability of Animal Models. *Bone* (2021) 145:115781. doi: 10.1016/j.bone.2020.115781
39. Pines A. Weight Loss, Weight Regain and Bone Health. *Climacteric J Int Menopause Soc* (2012) 15(4):317–9. doi: 10.3109/13697137.2012.667975
40. Qi SS, Shao ML, Sun Z, Chen SM, Hu YJ, Wang HT, et al. Lycopene Ameliorates Diabetic Osteoporosis *via* Anti-Inflammatory, Anti-Oxidation, and Increasing Osteoprotegerin/RANKL Expression Ratio. *J Funct Foods* (2021) 83:104539. doi: 10.1016/j.jff.2021.104539
41. Ma X, Meng J, Jia M, Bi L, Zhou Y, Wang Y, et al. Exendin-4, a Glucagon-Like Peptide-1 Receptor Agonist, Prevents Osteopenia by Promoting Bone Formation and Suppressing Bone Resorption in Aged Ovariectomized Rats. *J Bone Miner Res* (2013) 28(7):1641–52. doi: 10.1002/jbmr.1898
42. Pereira M, Jeyabalan J, Jørgensen CS, Hopkinson M, Al-Jazzar A, Roux JP, et al. Chronic Administration of Glucagon-Like Peptide-1 Receptor Agonists Improves Trabecular Bone Mass and Architecture in Ovariectomised Mice. *Bone* (2015) 81:459–67. doi: 10.1016/j.bone.2015.08.006

43. Li Z, Li S, Wang N, Xue P, Li Y. Liraglutide, a Glucagon-Like Peptide-1 Receptor Agonist, Suppresses Osteoclastogenesis Through the Inhibition of NF-κb and MAPK Pathways *via* GLP-1r. *BioMed Pharmacother* (2020) 130:110523. doi: 10.1016/j.biopha.2020.110523

Conflict of Interest: The authors declare that the research was conducted in the absence of any commercial or financial relationships that could be construed as a potential conflict of interest.

Publisher's Note: All claims expressed in this article are solely those of the authors and do not necessarily represent those of their affiliated organizations, or those of the publisher, the editors and the reviewers. Any product that may be evaluated in this article, or claim that may be made by its manufacturer, is not guaranteed or endorsed by the publisher.

frontiers in Endocrinology

ORIGINAL RESEARCH
published: 22 February 2022
doi: 10.3389/fendo.2022.826660

Melatonin Accelerates Osteoporotic Bone Defect Repair by Promoting Osteogenesis–Angiogenesis Coupling

Sheng Zheng[1], *Chunhao Zhou*[2], *Han Yang*[1], *Junhua Li*[1], *Ziyu Feng*[1], *Liqing Liao*[1] *and Yikai Li*[1]*

[1] School of Traditional Chinese Medicine, Southern Medical University, Guangzhou, China, [2] Department of Orthopedics-Spine Surgery, Nanfang Hospital, Southern Medical University, Guangzhou, China

Previous studies have revealed that melatonin could play a role in anti-osteoporosis and promoting osteogenesis. However, the effects of melatonin treatment on osteoporotic bone defect and the mechanism underlying the effects of melatonin on angiogenesis are still unclear. Our study was aimed to investigate the potential effects of melatonin on angiogenesis and osteoporotic bone defect. Bone marrow mesenchymal stem cells (BMSCs) were isolated from the femur and tibia of rats. The BMSC osteogenic ability was assessed using alkaline phosphatase (ALP) staining, alizarin red S staining, qRT-PCR, western blot, and immunofluorescence. BMSC-mediated angiogenic potentials were determined using qRT-PCR, western blot, enzyme-linked immunosorbent assay, immunofluorescence, scratch wound assay, transwell migration assay, and tube formation assay. Ovariectomized (OVX) rats with tibia defect were used to establish an osteoporotic bone defect model and then treated with melatonin. The effects of melatonin treatment on osteoporotic bone defect in OVX rats were analyzed using micro-CT, histology, sequential fluorescent labeling, and biomechanical test. Our study showed that melatonin promoted both osteogenesis and angiogenesis *in vitro*. BMSCs treated with melatonin indicated higher expression levels of osteogenesis-related markers [ALP, osteocalcin (OCN), runt-related transcription factor 2, and osterix] and angiogenesis-related markers [vascular endothelial growth factor (VEGF), angiopoietin-2, and angiopoietin-4] compared to the untreated group. Significantly, melatonin was not able to facilitate human umbilical vein endothelial cell angiogenesis directly, but it possessed the ability to promote BMSC-mediated angiogenesis by upregulating the VEGF levels. In addition, we further found that melatonin treatment increased bone mineralization and formation around the tibia defect in OVX rats compared with the control group. Immunohistochemical staining indicated higher expression levels of osteogenesis-related marker (OCN) and angiogenesis-related markers (VEGF and CD31) in the melatonin-treated OVX rats. Then, it showed that melatonin treatment also increased the bone strength of tibia defect in OVX rats, with increased ultimate load and stiffness, as performed by three-point bending test. In conclusion, our study demonstrated that melatonin could promote BMSC-mediated angiogenesis and promote osteogenesis–angiogenesis coupling. We further found that melatonin could accelerate osteoporotic

OPEN ACCESS

Edited by:
Michaela Tencerova, Academy of Sciences of the Czech Republic (ASCR), Czechia

Reviewed by:
Divya Singh, Central Drug Research Institute (CSIR), India
Mattabhorn Phimphilai, Chiang Mai University, Thailand
Bin Feng Cheng, Xinxiang Medical University, China

***Correspondence:**
Yikai Li
ortho@smu.edu.cn

Specialty section:
This article was submitted to Bone Research, a section of the journal Frontiers in Endocrinology

Received: *01 December 2021*
Accepted: *18 January 2022*
Published: *22 February 2022*

Citation:
Zheng S, Zhou C, Yang H, Li J, Feng Z, Liao L and Li Y (2022) MelatoninAccelerates Osteoporotic Bone Defect Repair by Promoting Osteogenesis–Angiogenesis Coupling. Front. Endocrinol. 13:826660. doi: 10.3389/fendo.2022.826660

bone repair by promoting osteogenesis and angiogenesis in OVX rats. These findings may provide evidence for the potential application of melatonin in osteoporotic bone defect.

Keywords: melatonin, osteoporosis, bone defect repair, osteogenesis–angiogenesis coupling, bone marrow mesenchymal stem cells

INTRODUCTION

Osteoporosis, as the most frequent bone disease, results in reduced bone strength. The main characteristics include lower bone mineral density (BMD) and bone mass, impaired bone quality, and abnormal micro-architecture (1–3). Osteoporosis is a common and age-related bone disease throughout the world, affecting more than 20 million individuals (4), which causes bone fragility and fractures (2). It has a major influence on individuals associated with high morbidity and mortality (5). As a global health concern, osteoporosis can affect both sexes and all races, dramatically increasing the social and economic burden worldwide.

Osteoporosis has been recognized as an increased risk of bone fracture and bone defect healing. Rodent studies showed that osteoporosis could cause a striking reduction in the callus size of bone fracture and bone defect, BMD, and mechanical strength (6). Previous studies showed that the healing time of bone fractures or bone defects was significantly longer in patients with osteoporosis than in healthy people (7–10). Maintaining osteogenesis and angiogenesis is crucial for osteoporotic bone regeneration. Ding et al. found that reduced local blood supply to the tibial metaphysis may be associated with ovariectomy-induced osteoporosis (11). In a rat osteoporotic model, new bone trabeculae is arranged in an irregular and loose fashion, indicating the poor bone quality of newly formed bone (12). For patients with osteoporotic bone defect, osteoclast activity is enhanced and bone resorption proceeds at a faster rate than that of bone formation. In addition, the ability of new bone formation is decreased, and bone defect healing is significantly delayed compared with normal bone defect (13). Thus, the treatment is more difficult than that of normal bone defect. In the face of such a severe health problem, how to find more therapeutic strategies and ideal drugs has become an urgent problem to be solved.

Melatonin, synthesized from serotonin in the pineal gland, is a signal molecule that modulates the biological circadian rhythms in humans (14). Except for the pineal gland, melatonin can also be synthesized locally in the bone marrow. Increasing evidence demonstrates that melatonin may play a critical role in bone metabolism. Melatonin, the synthesis of which decreases with aging, is considered to be involved in age-related bone loss and osteoporosis (15, 16). In bone, two types of membrane-bound melatonin receptors, including MT1 and MT2, have been identified and can be expressed in both osteoblasts and osteoclasts (17). The level of melatonin in the bone marrow was twice that of plasma at night (18), suggesting that it may be related to bone metabolism. Multiple studies have revealed that melatonin could promote osteoblast proliferation and differentiation, inhibit osteoclast activity, maintain the steady-state of bone metabolism, and thus play a role in anti-osteoporosis (19–22). Zhang et al. demonstrated that melatonin could restore the osteoporosis-impaired osteogenic potential of bone marrow mesenchymal stem cells (BMSCs) and alleviate bone loss through the HGF/PTEN/Wnt/beta-catenin axis (23). Dong et al. showed that melatonin treatment could upregulate the expressions of neuropeptide Y and its receptor Y1 and promote mesenchymal stem cell proliferation and migration (24). Thus, it indicates that melatonin may be a potential biomolecule for osteoporosis and its related bone defect.

Moderate osteogenesis and angiogenesis is involved in both bone repair and fracture healing (25). Currently, accumulating evidence has indicated the associations between melatonin and osteogenesis. However, few studies have been conducted to research the relationship between melatonin and angiogenesis. Ramírez-Fernández et al. observed that only the melatonin group showed a significantly increased number of blood vessels compared to the control group in a bone defect rabbit model (26). However, the mechanism underlying the effects of melatonin on angiogenesis was not clarified. Thus, how melatonin affects angiogenesis and what its effects are on osteoporotic bone defect are still unclear. The purpose of this study was to evaluate the potential effects of melatonin on angiogenesis and osteoporotic bone defect, which may provide evidence for the potential application of melatonin in osteoporosis and osteoporotic bone defect.

MATERIALS AND METHODS

Isolation and Culture of Rat BMSCs

BMSC isolation was performed as previously described (27, 28). BMSCs were harvested from the bone marrow of femurs and tibias in 2-week-old Sprague–Dawley (SD) rats. The rats were euthanized and sterilized in 75% ethanol for 15 min. BMSCs were flushed out by an injection of alpha modified Eagle's minimum essential medium (α-MEM; HyClone, USA) using a 5-ml syringe fitted with a 25-gauge needle under sterile conditions. After centrifugation, the BMSCs were cultured in α-MEM, which was supplemented with 10% fetal bovine serum (Gibco, USA) and 1% penicillin/streptomycin (Gibco, USA). The BMSCs between passages 3 and 5 were used in the following experiments. All of the above-mentioned cells were cultured at 37°C in a humidified atmosphere containing 5% CO_2.

Cell Proliferation Assay

BMSC proliferation was detected using Cell Counting kit-8 (CCK-8; Dojindo, Kumamoto, Japan) following the manufacturer's instructions. Specifically, the BMSCs were seeded with a density of 2,000 cells per well in a 96-well plate

and cultured in complete medium containing melatonin with various gradient concentrations (10 nM, 100 nM, 1 μM, and 10 μM) for various durations (1, 3, 5, and 7 days). Melatonin (purity >99%, cat. no. S20287) was purchased from Yuanye Bio-Technology Co., Ltd. (Shanghai, China). The untreated wells served as the control group. Then, each well was subjected to a 10-μl CCK-8 solution, and the cells were incubated at 37°C for 1 h. Then, the optical density was measured at 450 nm using a microplate reader (Thermo, USA).

Osteoblastic Determination and Mineralization Assessment

BMSCs were seeded in a 24-well plate with a density of 2×10^4 cells per well. The medium was replaced with an osteogenic medium (complete α-MEM containing 10 nM dexamethasone, 50 μM ascorbic acid, and 10 mM β-glycerophosphate) after reaching over 80% confluence. For treatment, melatonin with various gradient concentrations (10 nM, 100 nM, and 1 μM) was added into the medium. The untreated wells served as the control group. Then, protein was extracted, and the supernatant liquid was harvested after 7 days of osteogenic induction for western blotting analysis and enzyme-linked immunosorbent assay (ELISA) test of vascular endothelial growth factor (VEGF), respectively. Alkaline phosphatase (ALP) activity was determined at day 7 of differentiation using ALP Staining Kit (cat. no. P0321S, Beyotime Biotechnology, China). The mineralization of the calcium nodule was detected on the 14th day using alizarin red S (ARS) solution (cat. no. G1452, Solarbio Science & Technology, China). The absorbance at 405 nm for ALP and 560 nm for ARS staining was detected using a microplate reader (Thermo, USA).

Quantitative Real-Time PCR

Prior to PCR, total RNA was extracted using RNA Purification Kit (EZBioscience, USA). The RNA was reverse-transcribed by 500 ng of total RNA from each sample using Reverse Transcription Kit (EZBioscience, USA). Next, the cDNA was amplified with SYBR Green qPCR Master Mix (EZBioscience, USA). Data were analyzed, and the relative expression levels were calculated by the $2^{-\Delta\Delta CT}$ method. Housekeeping gene glyceraldehyde-3-phosphate dehydrogenase (GAPDH) was used for normalization. All reactions were carried out with three biological replicates, and each analysis consisted of three technical replicates. The primer sequences were designed by Oligo 7.0 software and are shown in **Table 1**.

Western Blotting

Total protein was extracted by RIPA buffer (Beyotime Biotechnology, China), containing protease and phosphatase inhibitors (Sigma-Aldrich, USA), for 30 min at 4°C. The cell lysates were cleared by centrifugation, and the protein concentration was determined using the bicinchoninic acid quantification kit (Beyotime Biotechnology, China). Furthermore, 30 μg protein was electrophoresed with 10% SDS-PAGE electrophoresis (Beyotime Biotechnology, China) and subsequently transferred to a polyvinylidene difluoride membrane (Millipore, USA). The membranes were blocked with 5% bovine serum albumin (BSA) (Solarbio Science & Technology, China) for 1 h at room temperature and incubated overnight at 4°C with primary antibodies against ALP (1:1,000; DF6225, Affinity Biosciences, Cincinnati, OH, USA), osteocalcin (OCN) (1:1,000; DF12303, Affinity Biosciences, Cincinnati, OH, USA), runt-related transcription factor 2 (RUNX2) (1:2,000; AF5186, Affinity Biosciences, Cincinnati, OH, USA), VEGF (1:1,000; AF5131, Affinity Biosciences, Cincinnati, OH, USA), GAPDH (1:5,000; T0004, Affinity Biosciences, Cincinnati, OH, USA), and β-actin (1:5,000; T0022, Affinity Biosciences, Cincinnati, OH, USA). The membranes were then incubated with secondary antibody (1:5,000; S0001, Affinity Biosciences, Cincinnati, USA). Finally, the membranes were visualized with enhanced chemiluminescence reagent (Beyotime Biotechnology, China). The band intensity was quantified using Image Lab (Bio-Rad, Hercules, CA, USA).

VEGF Analysis by ELISA

Commercial ELISA kit for VEGF (Cusabio, Wuhan, China) was used to determine the concentrations of VEGF in the supernatant liquid from different groups following the manufacturer's protocols.

Immunofluorescence

BMSCs were fixed with 4% PFA and permeabilized with 0.1% Triton X-100 in phosphate-buffered saline (PBS) containing 5% BSA. After blocking with 5% BSA for 1 h, the cells were stained overnight at 4°C with primary antibodies. Subsequently, the cells

TABLE 1 | Real-time PCR primer sequences used in the study.

Gene	Forward primer (5′–3′)	Reverse primer (5′–3′)
ALP	CCGCAGGATGTGAACTACT	GGTACTGACGGAAGAAGGG
OCN	CAGACAAGTCCCACACAGCA	CCAGCAGAGTGAGCAGAGAGA
RUNX2	ACTTCCTGTGCTCGGTGCT	GACGGTTATGGTCAAGGTGAA
OSX	GGAAAAGGAGGCACAAAGAA	CAGGGGAGAGGAGTCCATT
VEGF	CACGACAGAAGGGGAGCAGAAAG	GGCACACAGGACGGCTTGAAG
Ang-2	GAAGAAGGAGATGGTGGAGAT	CGTCTGGTTGAGCAAACTG
Ang-4	GCTCCTCAGGGCACCAAGTTC	CACAGGCGTCAAACCACCAC
GAPDH	ATGGCTACAGCAACAGGGT	TTATGGGGTCTGGGATGG

ALP, alkaline phosphatase; OCN, osteocalcin; RUNX2, runt-related transcription factor 2; OSX, osterix; VEGF, vascular endothelial growth factor; Ang-2, angiopoietin-2; Ang-4, angiopoietin-4; GAPDH, glyceraldehyde-3-phosphate dehydrogenase.

were incubated with a fluorescein isothiocyanate-conjugated secondary antibody (1:1,000; ab6717, Abcam, UK) for 1 h and then stained with 4′,6-diamidino-2-phenylindole. The fluorescence signal was captured using a fluorescence microscope (DMi8, Leica, Germany).

Angiogenesis-Related Assays *in vitro*

To further assess the angiogenic capability of melatonin, the BMSCs were treated with or without 100 nM melatonin, and the conditioned mediums were harvested after 7 days of osteogenic induction, which were used for the following assays. Subsequently, human umbilical vein endothelial cells (HUVECs) (Procell Life Science &Technology Company, Wuhan, China) were cultured and treated under different conditions (1): fresh medium (2), fresh medium with 100 nM melatonin (3), conditioned medium from BMSCs without melatonin, and (4) conditioned medium from BMSCs with 100 nM melatonin. Then, scratch wound assay, transwell migration assay, and tube formation assay were further detected as will be detailed in the following discussion.

For the scratch wound assay, HUVECs were seeded at a density of 2×10^5/well in a 6-well plate. The cells were scratched after confluence under an inverted microscope (Nikon; Tokyo, Japan). Then, the cells were cultured in the aforementioned mediums. The wound images were obtained immediately and at 12 h later. The width of the wounded areas (%) was calculated as $(A_0 - A_n)/A_0 \times 100$, where A_0 and A_n represent the initial wound area and the residual wound area at the metering point, respectively.

For the transwell migration assay, HUVECs were suspended and loaded into the top chamber of a transwell plate (Corning, NY, USA). The medium from the treated BMSCs was then added to the chamber. After 12 h, the unmigrated HUVECs in the upper chambers were removed by wiping the top of the membranes. The migrated cells were fixed in 4% paraformaldehyde, washed with PBS solution, and then stained with 0.5% crystal violet for 10 min. The cells were imaged and counted under the random fields of the microscope (Nikon; Tokyo, Japan).

For the tube formation assay, HUVECs were seeded into a Matrigel-coated 96-well plate at a density of 5×10^3/well, Then, the cells were incubated in the aforementioned medium. After incubation for 8 h, HUVEC tube formation was observed under an inverted microscope (Nikon; Tokyo, Japan). The number of tubes was calculated by Image-Pro Plus software.

Animal Experiments in Ovariectomized Rats

Ethics Statement

All experiments were approved by the Animal Care and Ethics Committee of the Southern Medical University (no. SMUL2021003), and the procedures were conducted in accordance with the policies of the Ethics Committee for Animal Research.

Animal Surgery and Treatment

A total of 84 female specific-pathogen-free SD rats (weight 250 ± 20 g; 12 weeks old; purchased from Zhuhai BesTest Bio-Tech Co., Ltd., Guangdong) were used in this experiment. All the rats were housed at a standard room temperature of 22 ± 2°C and humidity of 55–70% under a 12-h light/dark cycle with free access to food and water. After adaptation, 78 rats were randomly selected for bilateral ovariectomized (OVX) surgery, and 6 rats received sham surgery as previously described (29). After 3 months, 6 OVX and 6 sham surgery rats were selected for micro-computed tomography (micro-CT) and H&E staining to confirm the OVX rat model of osteoporosis. Then, 72 OVX rats were randomly selected and anesthetized for the longitudinal approach, which was performed on the medial surface of the proximal end with exposure of the proximal anteromedial metaphysis of the right tibia. Specifically, a standardized drill hole defect (3-mm diameter and 4-mm depth) was used to create a monocortical defect. After surgery, all the rats were randomly divided into three groups: low-dose melatonin treatment group (LMEL group, n = 24), high-dose melatonin treatment group (HMEL group, n = 24), and control group (CON group, n = 24). The LMEL and HMEL group rats were intraperitoneally injected with 10 and 50 mg/kg/day melatonin daily for 4 weeks, respectively. The CON group was injected with normal saline under the same conditions. The therapeutic dose of melatonin mentioned above was determined based on previous experiments in which melatonin showed protective effects in an OVX rat model (30, 31). The right tibiae in rats were harvested and assigned to micro-CT analysis and histological studies, which were randomly selected from each group (n = 6/group) at 2 weeks after tibia surgery. All the remaining rats were sacrificed, and the right tibiae were harvested at 4 weeks after treatment. Six tibia specimens were randomly selected from each group for micro-CT analysis and histological studies. The remaining tibia specimens were randomly assigned to fluorescent labeling analysis (n = 6 for each) and biomechanical test (n = 6 for each).

Micro-CT

Micro-CT analysis (Model μCT80, Scanco Medical Inc., Brüttisellen, Switzerland) was first used to confirm the success of the osteoporosis model. We selected the first region of interest (ROI) in the trabecular region of the tibia (1,500 μm in length and approximately 300 μm below the proximal epiphyseal plate) and reconstructed it by a computer analysis program. The histomorphometric parameters were considered as BMD, bone volume fraction (BV/TV), and trabecular number (Tb.N).

Bone repair was monitored by micro-CT at 2 and 4 weeks after tibia surgery. The central 2.5-mm-diameter region of the 3-mm-diameter defect was defined by drawing a circular contour as the second ROI to evaluate bone regeneration within the defect, which could avoid containing the native bone margins and help obtain a consistent volume of interest. After 3D reconstruction, BMD, BV/TV, Tb.N, and trabecular separation (Tb.Sp) in the ROI region were analyzed. All digitalized data and 3D images were generated by the built-in software of the micro-CT.

Histology and Immunohistochemical Staining

For histological and immunohistochemical (IHC) analyses, the samples were decalcified in 10% EDTA for 4 weeks after micro-CT imaging. Then, 4-μm-thick sections were then subjected to

H&E staining and Masson's trichrome staining. For IHC staining, 6-μm-thick sections were incubated with primary antibodies against OCN (1:100; DF12303, Affinity Biosciences, Cincinnati, OH, USA), VEGF (1:200; AF5131, Affinity Biosciences, Cincinnati, OH, USA), and CD31(1:200; AF6191, Affinity Biosciences, Cincinnati, OH, USA). The immunoreactivity of the analysis was determined using horseradish peroxidase detection system.

Sequential Fluorescent Labeling

All of the rats were intraperitoneally injected with 10 mg/kg calcein (cat. no. C0875, Sigma) at 10 and 3 days before the end of the experiment (32). At the end of the observation time (4 weeks after the treatment), the tibia samples were obtained for hard-tissue slicing and then imaged through the laser confocal microscopy (LSM 880, Zeiss, Germany). The bone mineral apposition rate (MAR, μm/d) was measured and calculated by automatic image analysis system.

Biomechanical Test

A three-point bending test was performed on the tibia specimens to determine the biomechanical properties by a material testing machine (ELF-3510AT, Bose, Inc., USA) as previously described (33). The bones were positioned horizontally on two supports. As the location of the bone repair area, the center of the metaphysis was positioned downward. The load and the displacement of the loading device were collected during each experiment until fracture. Data was recorded to the material testing instrument from the load–deformation curve. The maximum force at failure values (N) were recorded from the load data, and the stiffness (N/mm) was calculated as the slope of the initial linear uploading portion of the curves.

Statistical Analysis

SPSS software version 25.0 was used for all statistical analyses. Data were analyzed by two-tailed Student's *t*-test or analysis of variance (ANOVA), with repeated measures where applicable. Differences were determined to be statistically significant when *P*-value <0.05, with the data reported as mean ± SEM.

RESULTS

Melatonin Promoted the Osteogenesis of BMSCs *In Vitro*

First, a CCK-8 assay was conducted to observe whether melatonin can affect the proliferation of BMSCs. As shown in **Figure 1A**, melatonin promoted cell proliferation, and its effect was not in a dose-dependent manner. The most effective concentration was 100 nM, followed by 1 μM, 10 nM, and 10 μM. Then, ALP staining and ARS staining were performed to assess the pro-osteogenic effect of melatonin *in vitro*. BMSCs treated with melatonin indicated a higher level of ALP activities compared to the control group (**Figures 1B, C**). The most effective concentration was also 100 nM, followed by 1 μM and 10 nM, which was consistent with the CCK-8 assay. In addition, ARS staining validated the result. After 14 days of osteogenic induction, ARS staining revealed an increase in the stained area and extracellular deposition of calcium in the melatonin treatment groups compared with the control group (**Figures 1D, E**).

To further investigate how melatonin promotes the osteogenesis of BMSCs, we measured the mRNA and protein expressions of osteogenesis-related genes in cultured BMSCs at 3 and 7 days after various gradient concentrations of melatonin treatment. It showed that the mRNA expression levels of osteogenesis-related markers, including ALP, OCN, RUNX2, and osterix were all significantly increased in the melatonin treatment groups compared with the control group (**Figure 1F**). The most effective concentration is 100 nM. Consistently, the protein expression levels of ALP, OCN, and RUNX2 were all significantly increased in the melatonin treatment groups compared with the control group (**Figures 1G, H**). Immunofluorescence staining also indicated higher expression levels of ALP and OCN after melatonin treatment (**Figures 1I, J**). Thus, all these data indicated that melatonin promoted the osteogenesis of BMSCs *in vitro*.

Melatonin Promoted Angiogenesis *In Vitro*

Then, the mRNA expressions of angiogenesis-related genes in cultured BMSCs at 3 days were detected after various concentrations of melatonin treatment. The mRNA expression levels of angiogenesis-related markers, including VEGF, angiopoietin-2, and angiopoietin-2, were all significantly upregulated compared with the control group (**Figure 2A**). After 7 days of melatonin treatment, the protein expression level of VEGF was significantly increased compared with the control group (**Figure 2B**). Consistently, ELISA and immunofluorescence staining for VEGF both showed significantly higher levels of VEGF in the melatonin-treated groups (**Figures 2C, D**), Notably, the most effective concentration for all of these assays is also 100 nM. It suggested that the most effective concentration of melatonin for promoting osteogenesis and angiogenesis was consistent. These findings imply that melatonin can also promote angiogenesis *in vitro*.

Melatonin Promoted Osteogenesis–Angiogenesis Coupling *In Vitro*

To further assess the angiogenic capability of melatonin, BMSCs were treated with or without 100 nM melatonin, and the conditioned mediums were harvested after 7 days of osteogenic induction. The fresh mediums and the conditioned mediums were used for the following assays, respectively. Scratch wound assay and transwell migration assay were used to explore whether melatonin could affect cell migration. We found that no significant difference in cell migration was observed between the melatonin-treated group and the control group when HUVECs were cultured in fresh medium ($P > 0.05$). However, the migration of the melatonin-treated group was incredibly increased compared to the untreated group when HUVECs were cultured in conditioned medium (**Figures 3A–D**). Consistently, there was no significant difference in the ability to induce capillary tube formation between the melatonin-treated group and the untreated group when HUVECs were cultured in fresh medium ($P > 0.05$). The ability of the melatonin-treated group to induce capillary tube formation was

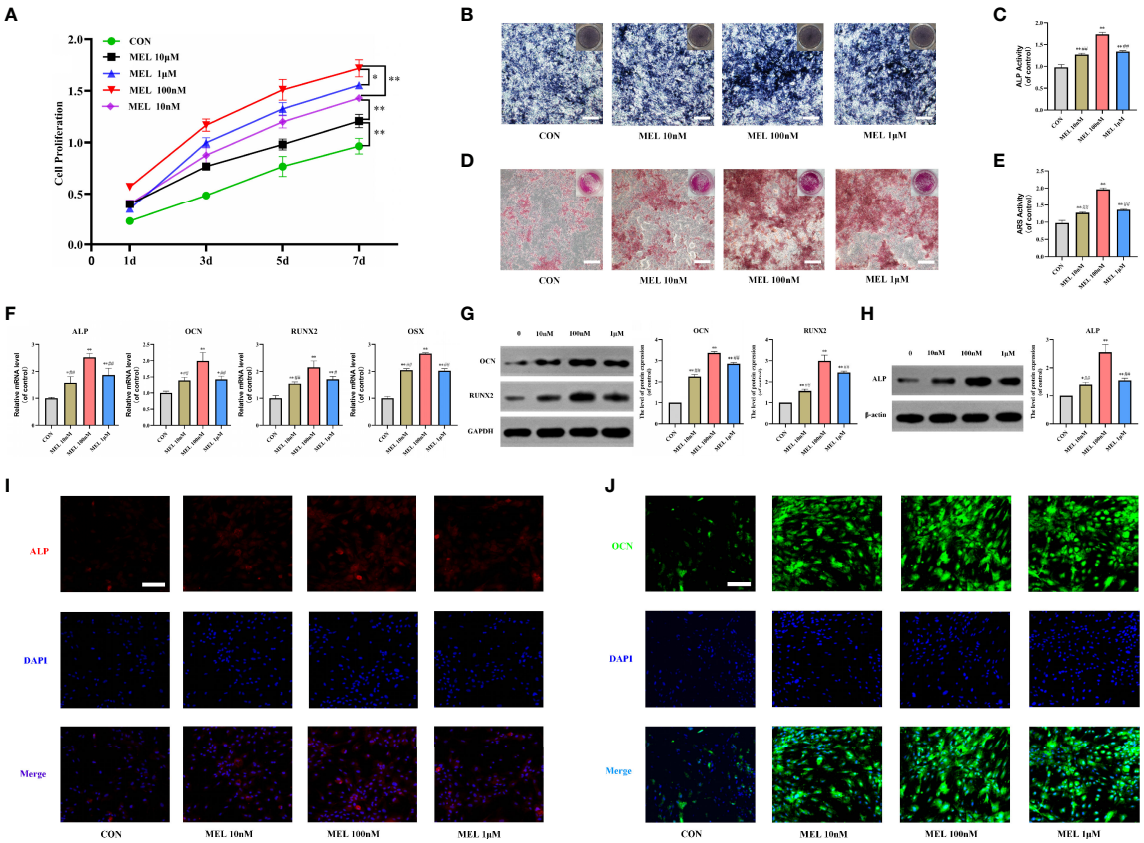

FIGURE 1 | Melatonin promoted the osteogenesis of BMSCs *in vitro*. **(A)** The effect of melatonin on BMSC proliferation measured by CCK-8 assays. **(B, C)** Images and quantification of ALP activity after 7 days of osteogenic induction (scale bars, 200 μm). **(D, E)** Calcium mineralization was assessed *via* ARS staining and quantification (scale bars, 200 μm). **(F)** mRNA expression levels of osteogenesis-related markers in BMSCs following treatment with/without melatonin. **(G, H)** Protein expression levels of osteogenesis-related markers (OCN, RUNX2, and ALP). **(I, J)** Immunofluorescent images of BMSCs stained for ALP and OCN (scale bars, 100 μm). All the experiments were repeated at least 3 times independently. CCK-8, cell counting kit-8; BMSCs, bone marrow mesenchymal stem cells; ARS, alizarin red S; ALP, alkaline phosphatase; OCN, osteocalcin; RUNX2, runt-related transcription factor 2. The data are presented as means ± SEM. $^{*}p < 0.05$, $^{**}p < 0.01$ *vs*. control group, $^{\#}p < 0.05$, $^{\#\#}p < 0.01$ *vs*. 100 nM melatonin group.

significantly enhanced compared to the untreated group when HUVECs were cultured in conditioned medium (**Figures 3E, F**). We also found that the most effective concentration for the above-mentioned assays is 100 nM, which is consistent with our previous results. The results indicated that melatonin treatment was not able to facilitate HUVEC angiogenesis. However, it implied that melatonin possessed the ability to promote BMSC-mediated angiogenesis. This illustrated that the role of melatonin in promoting angiogenesis is coupled with that in promoting osteogenesis. Collectively, it demonstrated that melatonin promoted osteogenesis–angiogenesis coupling *in vitro*.

Confirmation of Osteoporosis Model in OVX Rats

After 3 months of OVX surgery, the efficacy of OVX was confirmed by micro-CT and H&E staining of tibia bones. 2D images and 3D vertically sectioned images of the tibia bone were performed in the Sham group and the OVX group (**Figures 4A, B**). Both 2D and 3D images showed a significant trabecular bone volume, thickness, and density decrease, with a striking trabecular separation increase, compared to the Sham group. To observe this change more clearly, the 2D scanned images were constructed into 3D microstructures for analyses (**Figure 4C**). It showed significantly decreased BMD, BV/TV, and Tb.N in the OVX group compared with the Sham group (**Figure 4D**). Furthermore, H&E staining exhibited that the tibia bone in the OVX group was severely damaged, with increased bone trabecular spacing and broken tibia trabeculae, compared with the Sham group (**Figure 4E**). All of the above-mentioned data demonstrated that the OVX rat model of osteoporosis was successfully established.

Melatonin Enhanced Bone Repairing Ability by Promoting the Osteogenesis of Tibia Defect in OVX Rats

After confirmation of osteoporosis, a tibia defect model was established in rats and then treated with melatonin for 4 weeks. At week 2, the CON group remained primarily empty in the 3D reconstruction images. However, a small amount of mineralized

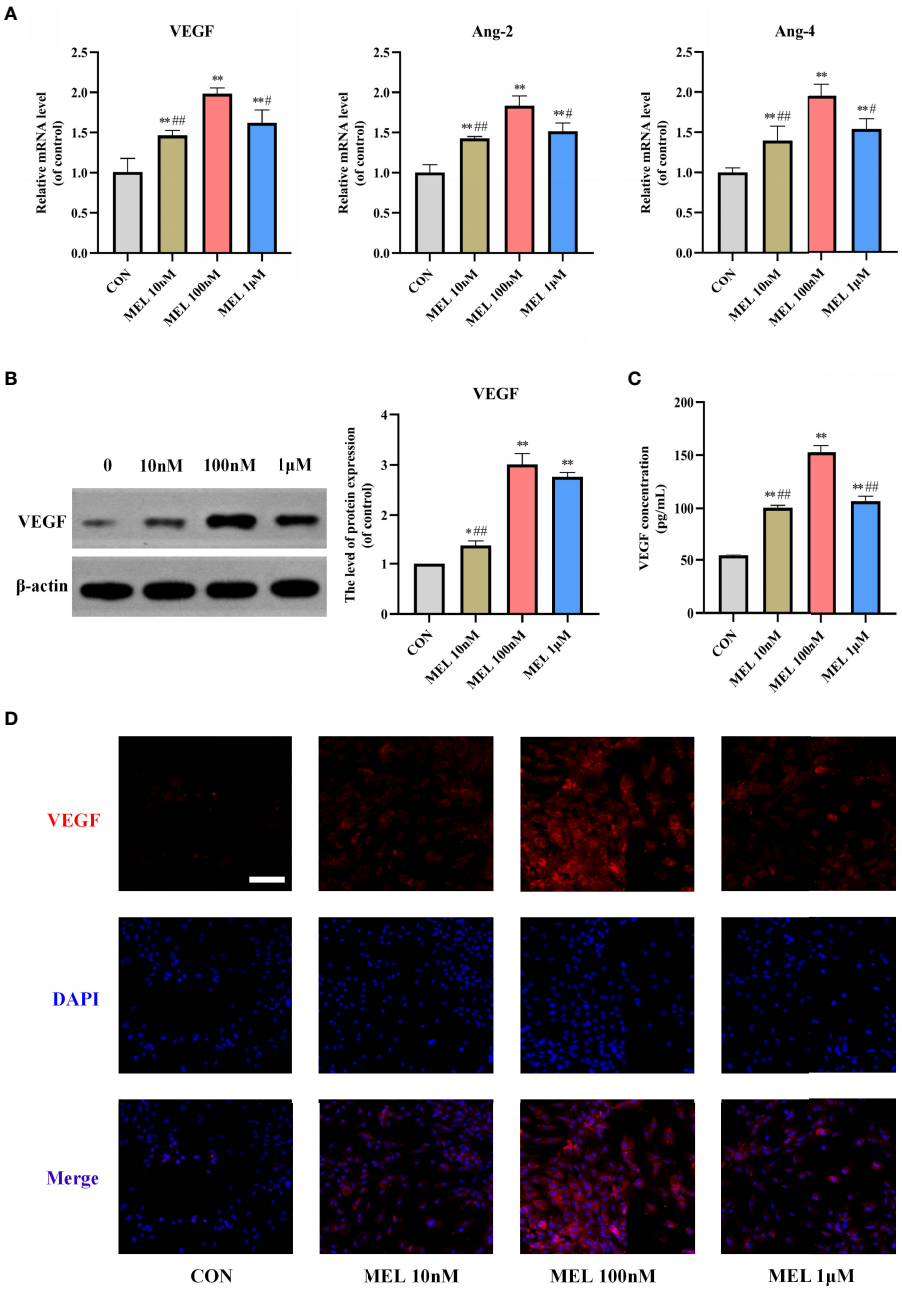

FIGURE 2 | Melatonin promoted angiogenesis *in vitro*. **(A)** mRNA expression levels of osteogenesis-related markers in BMSCs following treatment with/without melatonin. **(B)** Protein expression levels of osteogenesis-related marker VEGF. **(C)** VEGF content secreted in the supernatant liquid assessed by ELISA kits. **(D)** Immunofluorescent images of BMSCs stained for VEGF (scale bars, 100 μm). All the experiments were repeated at least 3 times independently. BMSCs, bone marrow mesenchymal stem cells; VEGF, vascular endothelial growth factor. The data are presented as means ± SEM. $^{*}p < 0.05$, $^{**}p < 0.01$ *vs*. control group, $^{\#}p < 0.05$, $^{\#\#}p < 0.01$ *vs*. 100 nM melatonin group.

tissue was predominantly located at the defect periphery in the LMEL and HMEL groups (**Figure 5A**). At week 4, increased bone volume can be observed in the LMEL and HMEL groups compared with the CON group (**Figure 5B**). Histological representation of bone formation further confirmed the results of micro-CT (**Figures 5C, D**). In addition, BMD, BV/TV, Tb.N, and Tb.Sp in the ROI were further analyzed. The CON group showed the lowest values in BMD, BV/TV, and Tb.N, with the highest value in Tb.Sp among all groups at both time points (**Figure 5E**). It indicated that melatonin treatment promoted the osteogenesis of tibia defect in OVX rats. Meanwhile, Masson's trichrome staining showed that melatonin treatment increased

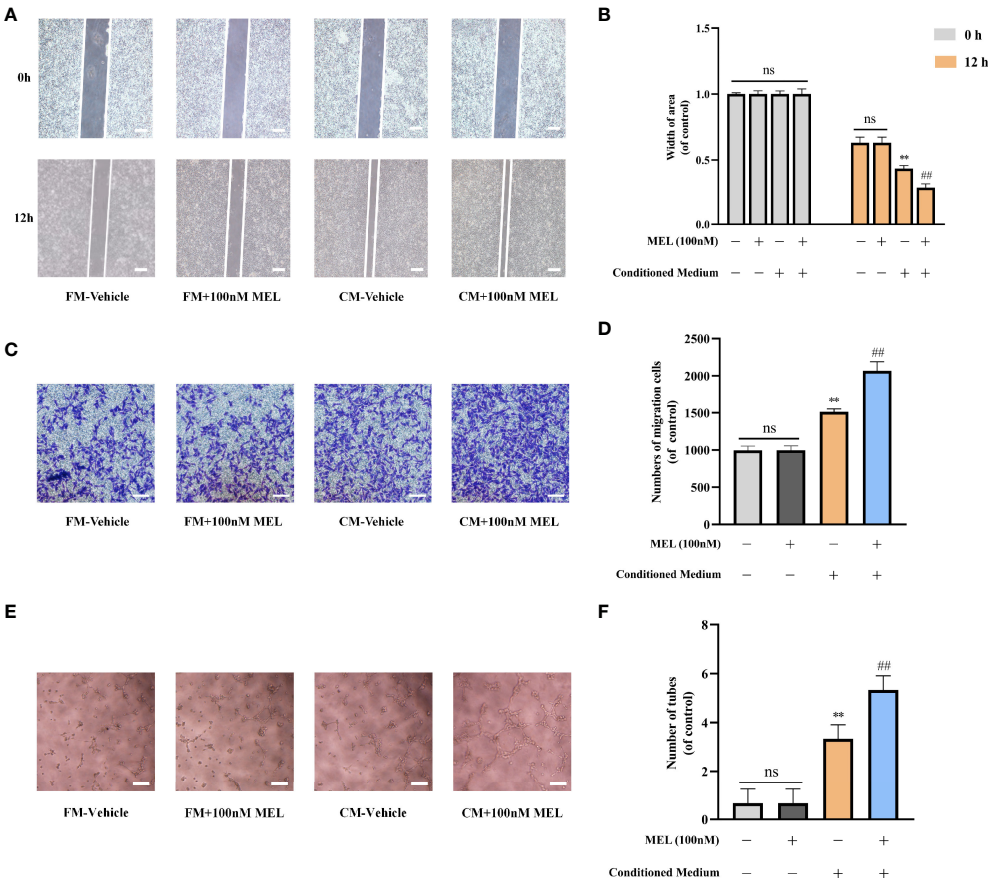

FIGURE 3 | Melatonin promoted osteogenesis-angiogenesis coupling *in vitro*. **(A, B)** Scratch wound assay of HUVECs incubated with the indicated mediums (scale bars, 100 μm). **(C, D)** Transwell migration assay of HUVECs incubated with the indicated mediums (scale bars, 100 μm). **(E, F)** Tube formation assay of HUVECs incubated with the indicated mediums (scale bars, 100 μm). All the experiments were repeated at least 3 times independently. The data are presented as means ± SEM. $^{**}p < 0.01$ *vs*. control group, $^{\#\#}p < 0.01$ *vs*. CM-vehicle group. HUVECs, human umbilical vein endothelial cells; FM, fresh medium; CM, conditioned medium. ns, no significance.

the bone mineralization and formation around the tibia defect compared with the CON group (**Figures 5F, G**). Remarkably, the HMEL group showed a more striking effect than the LMEL group at both time points. This suggested that melatonin therapy may show a dose-dependent manner *in vivo*. In general, these results revealed that melatonin enhanced the bone repairing ability by promoting the osteogenesis of tibia defect in OVX rats.

Melatonin Accelerated Bone Repair by Promoting the Osteogenesis and Angiogenesis of Tibia Defect in OVX Rats

Immunohistochemical staining of osteogenesis-related marker (OCN) and angiogenesis-related markers (VEGF and CD31) was further performed. Compared with the CON group, OCN immunostaining was denser and more widely distributed in sections in the melatonin-treated groups (**Figure 6A**), which was consistent with the results of VEGF and CD31 (**Figures 6B, C**). The HMEL group showed a more striking effect than the LMEL group at both time points. Sequential fluorescent labeling showed that the distance strip in the melatonin-treated groups was wider than that in the CON group (**Figure 6D**). The bone mineral deposition rate was analyzed to investigate the bone formation activity. It showed that MAR was significantly improved in the melatonin-treated groups, and this effect was more significant in the HMEL group than that in the LMEL group (**Figure 6E**). The three-point bending test revealed that the melatonin treatment increased the ultimate load and stiffness compared with the CON group (**Figures 6F, G**). All these data implied that melatonin could accelerate bone repair and increase bone strength by promoting the osteogenesis and angiogenesis of tibia defect in OVX rats.

DISCUSSION

The repair of bone defects requires recapitulation of complex signaling cascades, including a series of spatiotemporal angiogenesis and osteogenesis (34, 35). However, for

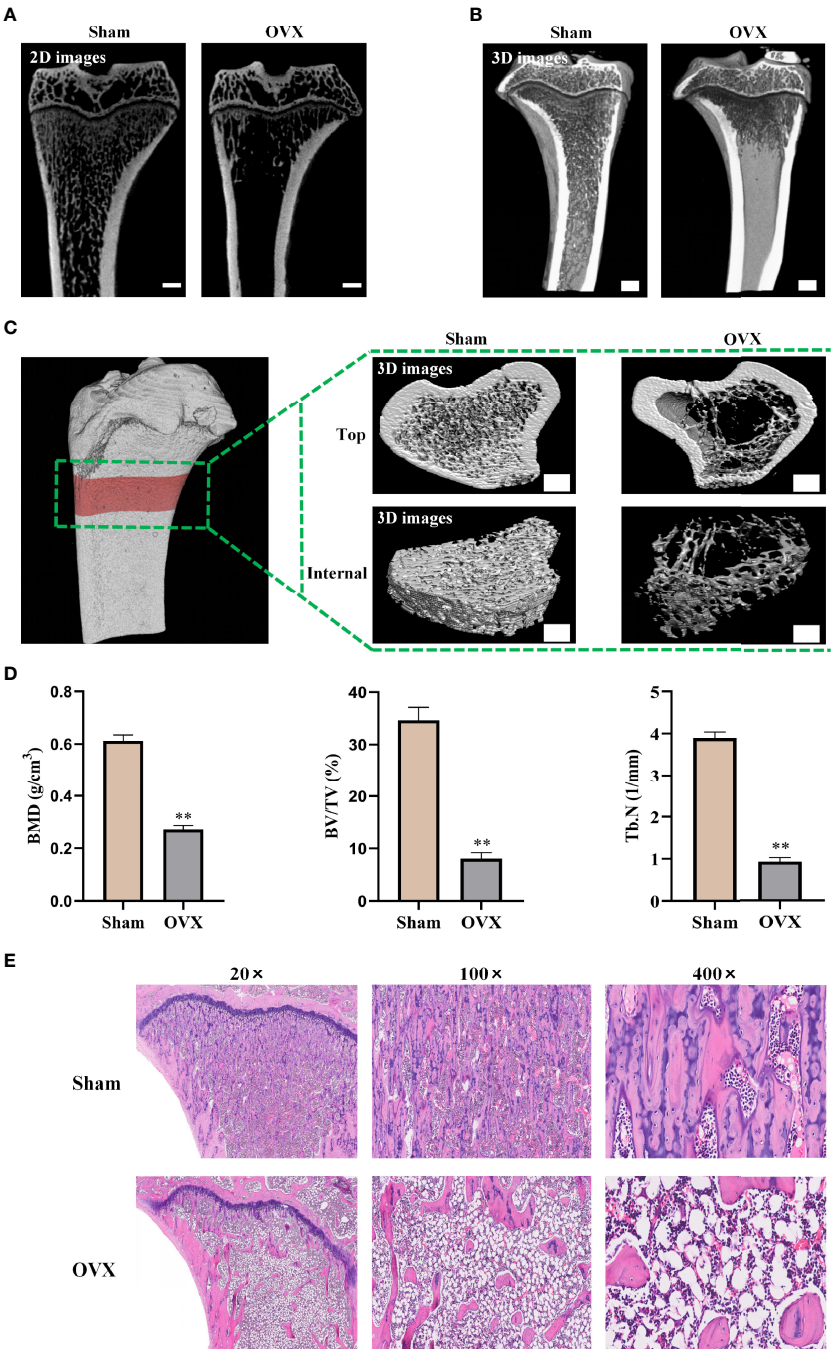

FIGURE 4 | Confirmation of osteoporosis model in ovariectomized rats. **(A)** 2D images of the tibia bone in two groups (scale bars, 1 mm). **(B)** Tibia bone visualized and vertical-sectioned images (scale bars, 1 mm). **(C)** 3D constructed images of the tibia proximal metaphysis (top, trabecular bone with cortical bone; internal, trabecular portion) (scale bars, 1 mm). **(D)** Quantitative presentation of microarchitectural parameters including BMD, BV/TV, and Tb.N. **(E)** H&E staining images of tibia bone. BMD, bone mineral density; BV/TV, trabecular bone volume; Tb.N, trabecular number. The data are presented as means ± SEM. $^{**}p < 0.01$ *vs*. Sham group.

osteoporosis, the bone resorption rate is greater than that of new bone formation, with a decreased ability for new bone formation. The clinical therapy of osteoporotic bone defect is more difficult than that of normal bone defect (36). However, conventional treatment option has limited efficacy and is not satisfactory. Therefore, novel therapeutic drug strategies to tackle osteoporosis and its related complications are warranted, which should be effective, safe, and available. To the best of our knowledge, our study is the first to demonstrate that melatonin could promote osteogenesis–angiogenesis coupling

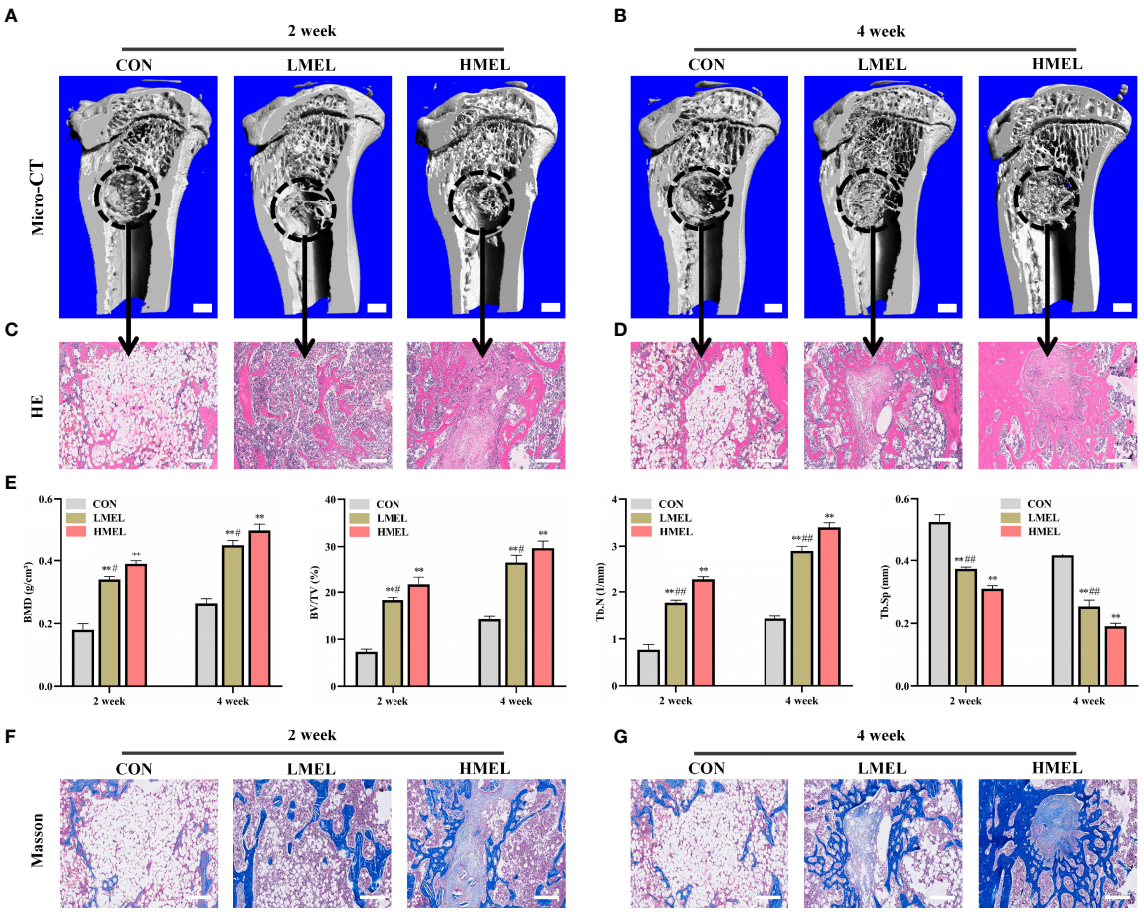

FIGURE 5 | Melatonin enhanced the bone repairing ability by promoting osteogenesis of tibia defect in ovariectomized rats. **(A, B)** 3D images of mineralized bone formation in tibia defect (scale bars, 1 mm). **(C, D)** Histological assessment of the defect area by H&E staining (scale bars, 200 μm). **(E)** Quantitative presentation of microarchitectural parameters, including BMD, BV/TV, Tb.N, and Tb.Sp. **(F, G)** Histological assessment of the defect area by Masson's trichrome staining (scale bars, 200 μm). BMD, bone mineral density, BV/TV, trabecular bone volume, Tb.N, trabecular number; Tb.Sp, trabecular separation; HMEL, high-dose melatonin treatment group. The data are presented as means ± SEM. $^{**}p < 0.01$ *vs*. control group, $^{\#}p < 0.05$, $^{\#\#}p < 0.01$ *vs*. HMEL group.

in vitro. Meanwhile, we further confirmed that melatonin treatment could accelerate bone repair and increase bone strength by promoting the osteogenesis and angiogenesis of tibia defect in OVX rats.

Bone regeneration is inseparable from the supply of nutrients, and angiogenesis in bone is crucial for bone defect repair (37). Vascularization is the premise of bone defect repair (38), which is a key link in the process of fracture healing and bone defect repair (39). The conventional view is that the relationship between osteogenesis and angiogenesis is one way, mainly manifested as angiogenesis providing essential nutrients for bone regeneration and repair and eliminating metabolic wastes (40). However, recent studies have shown that bone regeneration also plays a vital role in the regeneration of blood vessels within the bone (41, 42). Thus, it is critical to focus on the regeneration of blood vessels while investigating bone regeneration.

Increasing studies suggested that melatonin plays beneficial roles in bone metabolism, including bone anabolism as well as anti-bone resorption (43–45). Currently, various studies have been focused on the association between melatonin and osteogenesis. However, few studies are about the effects of melatonin on angiogenesis. In our study, we found that melatonin can promote osteogenesis and angiogenesis simultaneously. An *in vitro* study showed that melatonin promoted osteogenesis at the same optimal concentration as it promoted angiogenesis. The most effective concentration of both was 100 nM. However, it is worth noting that its effect was not in a dose-dependent manner. It indicates that it is important to find the optimal concentration, rather than simply increasing it, for melatonin to maximize its role in osteogenesis and angiogenesis. We further found that melatonin possessed the ability to promote BMSC-mediated angiogenesis and osteogenesis–angiogenesis coupling *in vitro*. When HUVECs were cultured in fresh medium, we found that no significant difference in cell migration and tube formation was observed between the melatonin-treated group and the control group. However, when HUVECs were cultured in conditioned medium, the ability of migration and induction of capillary tube formation

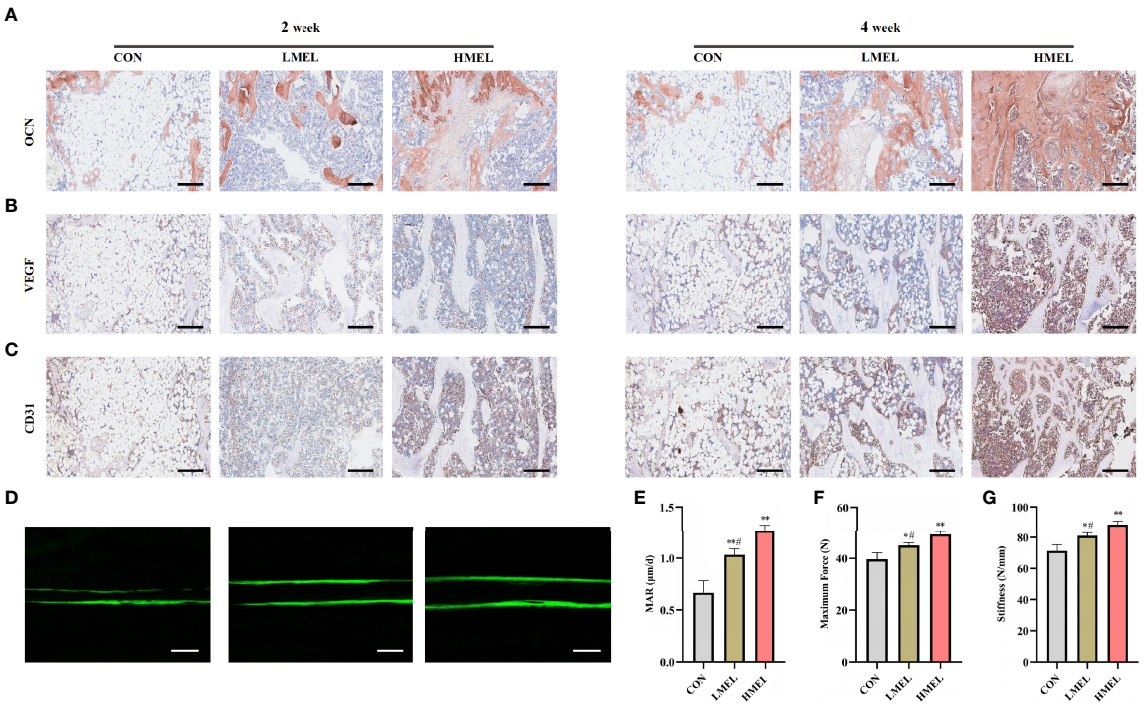

FIGURE 6 | Melatonin accelerated bone repair by promoting the osteogenesis and angiogenesis of tibia defect in ovariectomized rats. **(A)** Images of immunohistochemical staining of osteocalcin in the tibia defect (scale bars, 200 μm). **(B)** Images of immunohistochemical staining of vascular endothelial growth factor in the tibia defect (scale bars, 200 μm). **(C)** Images of immunohistochemical staining of CD31 in the tibia defect (scale bars, 200 μm). **(D)** New bone formation was detected by sequential fluorescent labeling of calcein (scale bars, 10 μm). **(E)** Quantitative analysis of mineral apposition rate. **(F)** Maximum force determined experimentally by three-point bending test. **(G)** Stiffness determined experimentally by three-point bending test. The data are presented as means ± SEM. $^{*}p < 0.05$, $^{**}p < 0.01$ *vs*. control group, $^{\#}p < 0.05$ *vs*. high-dose melatonin treatment group.

of the melatonin-treated group was significantly enhanced compared to the untreated group. The communication between vascular endothelial cells and BMSCs was significantly critical in bone remodeling. The process can be amplified by multiple elements, which participated in the recruitment, differentiation, and proliferation of vascular endothelial cells and BMSCs (46). This association has been illustrated to be due to an osteoblastic and angiogenic factor (VEGF), which was consistent with our findings (47). Combined with the results of the VEGF-related assays in this study, it suggested that melatonin could promote BMSC-mediated angiogenesis by upregulating the VEGF levels.

Previous studies, including animal experiments and clinical findings, have shown that melatonin has a notably anti-osteoporosis effect and high safety profile (48–52). Amstrup et al. demonstrated that melatonin could improve BMD at the femoral neck in postmenopausal women with osteopenia (53). A randomized controlled trial suggested that melatonin treatment is safe in postmenopausal women with osteopenia, and small doses of melatonin can improve sleep quality (54). However, the studies on melatonin mostly focused on the effects of melatonin therapy on osteoporosis. Relative mechanisms are mainly focused on the fact that melatonin can promote osteogenesis in osteoblasts (55–57) and inhibit osteolysis in osteoclasts (58–60). There is little evidence about exploring the relationship between melatonin and angiogenesis. Ramírez-Fernández et al. showed that melatonin could promote angiogenesis in a bone defect rabbit model and may have potential beneficial effects on bone defect repair (26). Hu et al. demonstrated that melatonin could protect cortical bone-derived stem cells against γ-ray radiation and assist in the healing of postradiation bone defects (61). Yildirimturk et al. found that melatonin showed beneficial effects on the healing of bone defects in streptozotocin-induced diabetic rats (62). However, these studies lacked further clarify how melatonin affects angiogenesis and explore its effects on osteoporotic bone defect. Our study is the first to demonstrated that melatonin could promote BMSCs-mediated angiogenesis by upregulating VEGF levels and promote osteogenesis-angiogenesis coupling *in vitro*. In addition, our study is novel in showing that melatonin could accelerate bone repair by promoting osteogenesis and angiogenesis of tibia defect in OVX rats. Therefore, our study is the first to indicate that melatonin treatment was able to accelerate bone repair in rats with osteoporotic bone defect, which was potentially effective to bone regeneration. However, the limitation of our study is that the exact pathway underlying melatonin promoting osteogenesis-angiogenesis coupling has not been clarified, which is our ongoing research.

CONCLUSION

In conclusion, our results demonstrated that melatonin could accelerate osteoporotic bone repair by promoting osteogenesis-angiogenesis coupling. Further investigation is undertaken about the underlying mechanism about how the osteogenesis-angiogenesis coupling process is promoted by melatonin. These findings can advance our thinking about that the application of melatonin may provide new insight and strategy for bone regeneration, and hence it could be a promising therapeutic remedy against osteoporosis and osteoporotic bone defect.

DATA AVAILABILITY STATEMENT

The original contributions presented in the study are included in the article/supplementary material. Further inquiries can be directed to the corresponding author.

ETHICS STATEMENT

The animal study was reviewed and approved by the Animal Care and Ethics Committee of the Southern Medical University.

AUTHOR CONTRIBUTIONS

YL conceived and designed the experiments. SZ, CZ, and HY carried out the experiments. JL, ZF, and LL analyzed the data. All authors were involved in writing the paper and had final approval of the submitted and published versions.

FUNDING

This study was sponsored by the National Natural Science Foundation of China (no. 81674095), the National Administration of Traditional Chinese Medicine TCM Inheritance and Innovation "Hundred-Thousand-Ten Thousand" Talents Project (QiHuang Scholar)–National TCM Leading Personnel Support Program (NATCM Personnel and Education Department, no. F119090038), the Innovation Team and Talents Cultivation Program of National Administration of Traditional Chinese Medicine (no. ZYYCXTD-C-202003), and the Sanming Project of Medicine in Shenzhen (no. SZZYSM202108013). The funders had no role in the study design, data collection, and analysis, or preparation of the manuscript.

REFERENCES

1. Panday K, Gona A, Humphrey MB. Medication-Induced Osteoporosis: Screening and Treatment Strategies. *Ther Adv Musculoskelet Dis* (2014) 6 (5):185–202. doi: 10.1177/1759720X14546350
2. Ghosh M, Majumdar SR. Antihypertensive Medications, Bone Mineral Density, and Fractures: A Review of Old Cardiac Drugs That Provides New Insights Into Osteoporosis. *Endocrine* (2014) 46(3):397–405. doi: 10.1007/s12020-014-0167-4
3. Rosen CJ. The Epidemiology and Pathogenesis of Osteoporosis. (2020). Available at: www.endotext.org.
4. Sözen T, Özışık L, Başaran NÇ. An Overview and Management of Osteoporosis. *Eur J Rheumatol* (2017) 4(1):46–56. doi: 10.5152/eurjrheum.2016.048
5. Keller J, Catala-Lehnen P, Huebner AK, Jeschke A, Heckt T, Lueth A, et al. Calcitonin Controls Bone Formation by Inhibiting the Release of Sphingosine 1-Phosphate From Osteoclasts. *Nat Commun* (2014) 5:5215. doi: 10.1038/ncomms6215
6. Namkung-Matthai H, Appleyard R, Jansen J, Hao LJ, Maastricht S, Swain M, et al. Osteoporosis Influences the Early Period of Fracture Healing in a Rat Osteoporotic Model. *Bone* (2001) 28(1):80–6. doi: 10.1016/s8756-3282(00)00414-2
7. Hegde V, Jo JE, Andreopoulou P, Lane JM. Effect of Osteoporosis Medications on Fracture Healing. *Osteoporos Int* (2016) 27(3):861–71. doi: 10.1007/s00198-015-3331-7
8. McCann RM, Colleary G, Geddis C, Clarke SA, Jordan GR, Dickson GR, et al. Effect of Osteoporosis on Bone Mineral Density and Fracture Repair in a Rat Femoral Fracture Model. *J Orthop Res* (2008) 26(3):384–93. doi: 10.1002/jor.20505
9. Hao YJ, Zhang G, Wang YS, Qin L, Hung WY, Leung K, et al. Changes of Microstructure and Mineralized Tissue in the Middle and Late Phase of Osteoporotic Fracture Healing in Rats. *Bone* (2007) 41(4):631–8. doi: 10.1016/j.bone.2007.06.006
10. Hak DJ. The Biology of Fracture Healing in Osteoporosis and in the Presence of Anti-Osteoporotic Drugs. *Injury* (2018) 49(8):1461–5. doi: 10.1016/j.injury.2018.04.016
11. Ding WG, Wei ZX, Liu JB. Reduced Local Blood Supply to the Tibial Metaphysis Is Associated With Ovariectomy-Induced Osteoporosis in Mice. *Connect Tissue Res* (2011) 52(1):25–9. doi: 10.3109/03008201003783011
12. Wang JW, Li W, Xu SW, Yang DS, Wang Y, Lin M, et al. Osteoporosis Influences the Middle and Late Periods of Fracture Healing in a Rat Osteoporotic Model. *Chin J Traumatol* (2005) 8(2):111–6.
13. Lin K, Xia L, Li H, Jiang X, Pan H, Xu Y, et al. Enhanced Osteoporotic Bone Regeneration by Strontium-Substituted Calcium Silicate Bioactive Ceramics. *Biomaterials* (2013) 34(38):10028–42. doi: 10.1016/j.biomaterials.2013.09.056
14. Stehle JH, Saade A, Rawashdeh O, Ackermann K, Jilg A, Sebestény T, et al. A Survey of Molecular Details in the Human Pineal Gland in the Light of Phylogeny, Structure, Function and Chronobiological Diseases. *J Pineal Res* (2011) 51(1):17–43. doi: 10.1111/j.1600-079X.2011.00856.x
15. Dubocovich ML, Markowska M. Functional MT1 and MT2 Melatonin Receptors in Mammals. *Endocrine* (2005) 27(2):101–10. doi: 10.1385/ENDO:27:2:101
16. Tan DX, Manchester LC, Reiter RJ, Qi WB, Zhang M, Weintraub ST, et al. Identification of Highly Elevated Levels of Melatonin in Bone Marrow: Its Origin and Significance. *Biochim Biophys Acta* (1999) 1472(1-2):206–14. doi: 10.1016/s0304-4165(99)00125-7
17. Slominski RM, Reiter RJ, Schlabritz-Loutsevitch N, Ostrom RS, Slominski AT. Melatonin Membrane Receptors in Peripheral Tissues: Distribution and Functions. *Mol Cell Endocrinol* (2012) 351(2):152–66. doi: 10.1016/j.mce.2012.01.004
18. Amstrup AK, Sikjaer T, Mosekilde L, Rejnmark L. Melatonin and the Skeleton. *Osteoporos Int* (2013) 24(12):2919–27. doi: 10.1007/s00198-013-2404-8
19. de Villiers TJ, Chines AA, Palacios S, Lips P, Sawicki AZ, Levine AB, et al. Safety and Tolerability of Bazedoxifene in Postmenopausal Women With Osteoporosis: Results of a 5-Year, Randomized, Placebo-Controlled Phase 3 Trial. *Osteoporos Int* (2011) 22(2):567–76. doi: 10.1007/s00198-010-1302-6
20. Maria S, Samsonraj RM, Munmun F, Glas J, Silvestros M, Kotlarczyk MP, et al. Biological Effects of Melatonin on Osteoblast/Osteoclast Cocultures, Bone, and Quality of Life: Implications of a Role for MT2 Melatonin Receptors, MEK1/2, and MEK5 in Melatonin-Mediated Osteoblastogenesis. *J Pineal Res* (2018) 64(3):1–12. doi: 10.1111/jpi.12465

21. Park KH, Kang JW, Lee EM, Kim JS, Rhee YH, Kim M, et al. Melatonin Promotes Osteoblastic Differentiation Through the BMP/ERK/Wnt Signaling Pathways. *J Pineal Res* (2011) 51(2):187–94. doi: 10.1111/j.1600-079X.2011.00875.x
22. Zhu G, Ma B, Dong P, Shang J, Gu X, Zi Y. Melatonin Promotes Osteoblastic Differentiation and Regulates PDGF/AKT Signaling Pathway. *Cell Biol Int* (2020) 44(2):402–11. doi: 10.1002/cbin.11240
23. Zhang J, Jia G, Xue P, Li Z. Melatonin Restores Osteoporosis-Impaired Osteogenic Potential of Bone Marrow Mesenchymal Stem Cells and Alleviates Bone Loss Through the HGF/PTEN/Wnt/β-Catenin Axis. *Ther Adv Chronic Dis* (2021) 12:2040622321995685. doi: 10.1177/2040622321995685
24. Dong P, Gu X, Zhu G, Li M, Ma B, Zi Y. Melatonin Induces Osteoblastic Differentiation of Mesenchymal Stem Cells and Promotes Fracture Healing in a Rat Model of Femoral Fracture *via* Neuropeptide Y/Neuropeptide Y Receptor Y1 Signaling. *Pharmacology* (2018) 102(5-6):272–80. doi: 10.1159/000492576
25. Grellier M, Granja PL, Fricain JC, Bidarra SJ, Renard M, Bareille R, et al. The Effect of the Co-Immobilization of Human Osteoprogenitors and Endothelial Cells Within Alginate Microspheres on Mineralization in a Bone Defect. *Biomaterials* (2009) 30(19):3271–8. doi: 10.1016/j.biomaterials.2009.02.033
26. Ramírez-Fernández MP, Calvo-Guirado JL, De-Val JE, Delgado-Ruiz RA, Negri B, Pardo-Zamora G, et al. Melatonin Promotes Angiogenesis During Repair of Bone Defects: A Radiological and Histomorphometric Study in Rabbit Tibiae. *Clin Oral Investig* (2013) 17(1):147–58. doi: 10.1007/s00784-012-0684-6
27. Qin G, Li Y, Wang H, Yang J, Chen Q, Tang H, et al. Lysine-Specific Demethylase 4a Regulates Osteogenic Differentiation *via* Regulating the Binding Ability of H3K9me3 With the Promoters of Runx2, Osterix and Osteocalcin. *J Biomed Nanotechnol* (2020) 16(6):899–909. doi: 10.1166/jbn.2020.2929
28. Zeng Q, Zhou Y, Liang D, He H, Liu X, Zhu R, et al. Exosomes Secreted From Bone Marrow Mesenchymal Stem Cells Attenuate Oxygen-Glucose Deprivation/Reoxygenation-Induced Pyroptosis in PC12 Cells by Promoting AMPK-Dependent Autophagic Flux. *Front Cell Neurosci* (2020) 14:182. doi: 10.3389/fncel.2020.00182
29. Kharode YP, Sharp MC, Bodine PV. Utility of the Ovariectomized Rat as a Model for Human Osteoporosis in Drug Discovery. *Methods Mol Biol* (2008) 455:111–24. doi: 10.1007/978-1-59745-104-8_8
30. Zhou W, Liu Y, Shen J, Yu B, Bai J, Lin J, et al. Melatonin Increases Bone Mass Around the Prostheses of OVX Rats by Ameliorating Mitochondrial Oxidative Stress *via* the SIRT3/SOD2 Signaling Pathway. *Oxid Med Cell Longev* (2019) 2019:4019619. doi: 10.1155/2019/4019619
31. Chen W, Chen X, Chen AC, Shi Q, Pan G, Pei M, et al. Melatonin Restores the Osteoporosis-Impaired Osteogenic Potential of Bone Marrow Mesenchymal Stem Cells by Preserving SIRT1-Mediated Intracellular Antioxidant Properties. *Free Radic Biol Med* (2020) 146:92–106. doi: 10.1016/j.freeradbiomed.2019.10.412
32. Tao ZS, Lu HL, Ma NF, Zhang RT, Li Y, Yang M, et al. Rapamycin Could Increase the Effects of Melatonin Against Age-Dependent Bone Loss. *Z Gerontol Geriatr* (2020) 53(7):671–8. doi: 10.1007/s00391-019-01659-4
33. Osuna L, Soares CJ, Vilela A, Irie MS, Versluis A, Soares P. Influence of Bone Defect Position and Span in 3-Point Bending Tests: Experimental and Finite Element Analysis. *Braz Oral Res* (2020) 35:e001. doi: 10.1590/1807-3107bor-2021.vol35.0001
34. Mousaei GM, Matin MM, Kazemi MH, Naderi-Meshkin H, Moradi A, Rajabioun M, et al. Application of Mesenchymal Stem Cells to Enhance Non-Union Bone Fracture Healing. *J Biomed Mater Res A* (2019) 107(2):301–11. doi: 10.1002/jbm.a.36441
35. Ye D, Chen C, Wang Q, Zhang Q, Li S, Liu H. Short-Wave Enhances Mesenchymal Stem Cell Recruitment in Fracture Healing by Increasing HIF-1 in Callus. *Stem Cell Res Ther* (2020) 11(1):382. doi: 10.1186/s13287-020-01888-0
36. Zhang Y, Cheng N, Miron R, Shi B, Cheng X. Delivery of PDGF-B and BMP-7 by Mesoporous Bioglass/Silk Fibrin Scaffolds for the Repair of Osteoporotic Defects. *Biomaterials* (2012) 33(28):6698–708. doi: 10.1016/j.biomaterials.2012.06.021
37. Jin L, Li P, Wang YC, Feng L, Xu R, Yang DB, et al. Studies of Superb Microvascular Imaging and Contrast-Enhanced Ultrasonography in the Evaluation of Vascularization in Early Bone Regeneration. *J Ultrasound Med* (2019) 38(11):2963–71. doi: 10.1002/jum.15002
38. Linsley CS, Wu BM, Tawil B. Mesenchymal Stem Cell Growth on and Mechanical Properties of Fibrin-Based Biomimetic Bone Scaffolds. *J Biomed Mater Res A* (2016) 104(12):2945–53. doi: 10.1002/jbm.a.35840
39. Kirkeby OJ, Nordsletten L, Skjeldal S, Berg LT. Circulation in Corticocancellous Bone Grafts Measured With Laser Doppler Flowmetry. *Exp Study Rats Scand J Plast Reconstr Surg Handb Surg* (1994) 28(4):249–54. doi: 10.3109/02844319409022007
40. Lafage-Proust MH, Prisby R, Roche B, Vico L. Bone Vascularization and Remodeling. *Joint Bone Spine* (2010) 77(6):521–4. doi: 10.1016/j.jbspin.2010.09.009
41. Kusumbe AP, Ramasamy SK, Adams RH. Coupling of Angiogenesis and Osteogenesis by a Specific Vessel Subtype in Bone. *Nature* (2014) 507 (7492):323–8. doi: 10.1038/nature13145
42. Dhandapani R, Krishnan PD, Zennifer A, Kannan V, Manigandan A, Arul MR, et al. Additive Manufacturing of Biodegradable Porous Orthopaedic Screw. *Bioact Mater* (2020) 5(3):458–67. doi: 10.1016/j.bioactmat.2020.03.009
43. Satomura K, Tobiume S, Tokuyama R, Yamasaki Y, Kudoh K, Maeda E, et al. Melatonin at Pharmacological Doses Enhances Human Osteoblastic Differentiation *In Vitro* and Promotes Mouse Cortical Bone Formation *In Vivo*. *J Pineal Res* (2007) 42(3):231–9. doi: 10.1111/j.1600-079X.2006.00410.x
44. Zhang L, Su P, Xu C, Chen C, Liang A, Du K, et al. Melatonin Inhibits Adipogenesis and Enhances Osteogenesis of Human Mesenchymal Stem Cells by Suppressing Pparγ Expression and Enhancing Runx2 Expression. *J Pineal Res* (2010) 49(4):364–72. doi: 10.1111/j.1600-079X.2010.00803.x
45. Histing T, Anton C, Scheuer C, Garcia P, Holstein JH, Klein M, et al. Melatonin Impairs Fracture Healing by Suppressing RANKL-Mediated Bone Remodeling. *J Surg Res* (2012) 173(1):83–90. doi: 10.1016/j.jss.2010.08.036
46. Clarkin CE, Emery RJ, Pitsillides AA, Wheeler-Jones CP. Evaluation of VEGF-Mediated Signaling in Primary Human Cells Reveals a Paracrine Action for VEGF in Osteoblast-Mediated Crosstalk to Endothelial Cells. *J Cell Physiol* (2008) 214(2):537–44. doi: 10.1002/jcp.21234
47. Leach JK, Kaigler D, Wang Z, Krebsbach PH, Mooney DJ. Coating of VEGF-Releasing Scaffolds With Bioactive Glass for Angiogenesis and Bone Regeneration. *Biomaterials* (2006) 27(17):3249–55. doi: 10.1016/j.biomaterials.2006.01.033
48. Uslu S, Uysal A, Oktem G, Yurtseven M, Tanyalçin T, Başdemir G. Constructive Effect of Exogenous Melatonin Against Osteoporosis After Ovariectomy in Rats. *Anal Quant Cytol Histol* (2007) 29(5):317–25.
49. Zhang WL, Meng HZ, Yang RF, Yang MW, Sun GH, Liu JH, et al. Melatonin Suppresses Autophagy in Type 2 Diabetic Osteoporosis. *Oncotarget* (2016) 7 (32):52179–94. doi: 10.18632/oncotarget.10538
50. Chu ZM, Li HB, Sun SX, Jiang YC, Wang B, Dong YF. Melatonin Promotes Osteoblast Differentiation of Bone Marrow Mesenchymal Stem Cells in Aged Rats. *Eur Rev Med Pharmacol Sci* (2017) 21(19):4446–56.
51. Egermann M, Gerhardt C, Barth A, Maestroni GJ, Schneider E, Alini M. Pinealectomy Affects Bone Mineral Density and Structure–An Experimental Study in Sheep. *BMC Musculoskelet Disord* (2011) 12:271. doi: 10.1186/1471-2474-12-271
52. Wang X, Liang T, Zhu Y, Qiu J, Qiu X, Lian C, et al. Correction to: Melatonin Prevents Bone Destruction in Mice With Retinoic Acid-Induced Osteoporosis. *Mol Med* (2021) 27(1):136. doi: 10.1186/s10020-021-00401-4
53. Amstrup AK, Sikjaer T, Heickendorff L, Mosekilde L, Rejnmark L. Melatonin Improves Bone Mineral Density at the Femoral Neck in Postmenopausal Women With Osteopenia: A Randomized Controlled Trial. *J Pineal Res* (2015) 59(2):221–9. doi: 10.1111/jpi.12252
54. Amstrup AK, Sikjaer T, Mosekilde L, Rejnmark L. The Effect of Melatonin Treatment on Postural Stability, Muscle Strength, and Quality of Life and Sleep in Postmenopausal Women: A Randomized Controlled Trial. *Nutr J* (2015) 14:102. doi: 10.1186/s12937-015-0093-1
55. Rafat A, Mohammadi RA, Alizadeh A, Hashemi-Firouzi N, Golipoor Z. Comparison of The Melatonin Preconditioning Efficacy Between Bone Marrow and Adipose-Derived Mesenchymal Stem Cells. *Cell J* (2019) 20 (4):450–8. doi: 10.22074/cellj.2019.5507
56. Satué M, Ramis JM, Del MAM, Monjo M. A New Role for 5-Methoxytryptophol on Bone Cells Function *In Vitro*. *J Cell Biochem* (2015) 116(4):551–8. doi: 10.1002/jcb.25005

57. Xiong XC, Zhu Y, Ge R, Liu LF, Yuan W. Effect of Melatonin on the Extracellular-Regulated Kinase Signal Pathway Activation and Human Osteoblastic Cell Line hFOB 1.19 Proliferation. *Int J Mol Sci* (2015) 16 (5):10337–53. doi: 10.3390/ijms160510337
58. Ikebuchi Y, Aoki S, Honma M, Hayashi M, Sugamori Y, Khan M, et al. Coupling of Bone Resorption and Formation by RANKL Reverse Signalling. *Nature* (2018) 561(7722):195–200. doi: 10.1038/s41586-018-0482-7
59. Ping Z, Wang Z, Shi J, Wang L, Guo X, Zhou W, et al. Inhibitory Effects of Melatonin on Titanium Particle-Induced Inflammatory Bone Resorption and Osteoclastogenesis *via* Suppression of NF-κb Signaling. *Acta Biomater* (2017) 62:362–71. doi: 10.1016/j.actbio.2017.08.046
60. Kim HJ, Kim HJ, Bae MK, Kim YD. Suppression of Osteoclastogenesis by Melatonin: A Melatonin Receptor-Independent Action. *Int J Mol Sci* (2017) 18 (6):1–13. doi: 10.3390/ijms18061142
61. Hu W, Liang JW, Liao S, Zhao ZD, Wang YX, Mao XF, et al. Melatonin Attenuates Radiation-Induced Cortical Bone-Derived Stem Cells Injury and Enhances Bone Repair in Postradiation Femoral Defect Model. *Mil Med Res* (2021) 8(1):61. doi: 10.1186/s40779-021-00355-y
62. Yildirimturk S, Batu S, Alatli C, Olgac V, Firat D, Sirin Y. The Effects of Supplemental Melatonin Administration on the Healing of Bone Defects in Streptozotocin-Induced Diabetic Rats. *J Appl Oral Sci* (2016) 24(3):239–49. doi: 10.1590/1678-775720150570

Conflict of Interest: The authors declare that the research was conducted in the absence of any commercial or financial relationships that could be construed as a potential conflict of interest.

Publisher's Note: All claims expressed in this article are solely those of the authors and do not necessarily represent those of their affiliated organizations, or those of the publisher, the editors and the reviewers. Any product that may be evaluated in this article, or claim that may be made by its manufacturer, is not guaranteed or endorsed by the publisher.

frontiers | Frontiers in Endocrinology

ORIGINAL RESEARCH
published: 19 May 2022
doi: 10.3389/fendo.2022.846154

Super-Enhancer-Associated Long Non-Coding RNA LINC01485 Promotes Osteogenic Differentiation of Human Bone Marrow Mesenchymal Stem Cells by Regulating MiR-619-5p/RUNX2 Axis

Wenli Gu[1†], Xiao Jiang[1], Wei Wang[1], Prabhakar Mujagond[2], Jingpeng Liu[1], Zhaoyi Mai[1], Hai Tang[1], Simin li[1], Hui Xiao[1‡] and Jianjiang Zhao[3*‡]*

[1] Stomatological Hospital, Southern Medical University, Guangzhou, China, [2] Regional Centre for Biotechnology, Faridabad, India, [3] Shenzhen Stomatological Hospital, Southern Medical University, Shenzhen, China

OPEN ACCESS

Edited by:
Chandi C. Mandal,
Central University of Rajasthan, India

Reviewed by:
Yunli Zhou,
Massachusetts General Hospital and Harvard Medical School, United States
Mark B. Meyer,
University of Wisconsin-Madison, United States

***Correspondence:**
Hui Xiao
zzmmxh@126.com
Jianjiang Zhao
zjj2521@sina.com

[†]Senior author

[‡]These authors have contributed equally to this work

Specialty section:
This article was submitted to Bone Research, a section of the journal Frontiers in Endocrinology

Received: 30 December 2021
Accepted: 05 April 2022
Published: 19 May 2022

Citation:
Gu W, Jiang X, Wang W, Mujagond P, Liu J, Mai Z, Tang H, li S, Xiao H and Zhao J (2022) Super-Enhancer-Associated Long Non-Coding RNA LINC01485 Promotes Osteogenic Differentiation of Human Bone Marrow Mesenchymal Stem Cells by Regulating MiR-619-5p/RUNX2 Axis. Front. Endocrinol. 13:846154. doi: 10.3389/fendo.2022.846154

Objective: To investigate the mechanisms of super-enhancer-associated LINC01485/miR-619-5p/RUNX2 signaling axis involvement in osteogenic differentiation of human bone marrow mesenchymal stem cells (hBMSCs).

Methods: Osteogenic differentiation of hBMSCs was induced *in vitro*. The expression levels of LINC01485 and miR-619-5p during osteogenesis were measured using quantitative real-time polymerase chain reaction (qRT-PCR). Osteogenic differentiation was examined by qRT-PCR, western blot, alkaline phosphatase (ALP) staining, ALP activity measurement, and Alizarin Red S (ARS) staining assays. Thereafter, the effects of LINC01485 and miR-619-5p on osteogenic differentiation of hBMSCs were evaluated by performing loss- and gain-of-function experiments. Subsequently, a fluorescence *in situ* hybridization (FISH) assay was employed to determine the cellular localization of LINC01485. Bioinformatics analysis, RNA antisense purification (RAP) assay, and dual-luciferase reporter assays were conducted to analyze the interactions of LINC01485, miR-619-5p, and RUNX2. Rescue experiments were performed to further delineate the role of the competitive endogenous RNA (ceRNA) signaling axis consisting of LINC01485/miR-619-5p/RUNX2 in osteogenic differentiation of hBMSCs.

Results: The expression of LINC01485 was up-regulated during osteogenic differentiation of hBMSCs. The overexpression of LINC01485 promoted osteogenic differentiation of hBMSCs by up-regulating the expression of osteogenesis-related genes [e.g., runt-related transcription factor 2 (RUNX2), osterix (OSX), collagen type 1 alpha 1 (COL1A1), osteocalcin (OCN), and osteopontin (OPN)], and increasing the activity of ALP. ALP staining and ARS staining were also found to be increased upon overexpression of LINC01485. The opposing results were obtained upon LINC01485 interference in hBMSCs. miR-619-5p was found to inhibit osteogenic differentiation. FISH

assay displayed that LINC01485 was mainly localized in the cytoplasm. RAP assay results showed that LINC01485 bound to miR-619-5p, and dual-luciferase reporter assay verified that LINC01485 bound to miR-619-5p, while miR-619-5p and RUNX2 bound to each other. Rescue experiments illustrated that LINC01485 could promote osteogenesis by increasing RUNX2 expression by sponging miR-619-5p.

Conclusion: LINC01485 could influence RUNX2 expression by acting as a ceRNA of miR-619-5p, thereby promoting osteogenic differentiation of hBMSCs. The LINC01485/miR-619-5p/RUNX2 axis might comprise a novel target in the bone tissue engineering field.

Keywords: LINC01485, miR-619-5p, RUNX2, super-enhancers, bone marrow mesenchymal stem cells, osteogenesis, osteogenic differentiation

INTRODUCTION

Critical-sized bone defects in oral and maxillofacial regions occurring due to tumor resection, trauma, congenital malformation, or alveolar bone resorption after teeth loss remain a significant challenge in oral reconstruction (1). Currently, autologous bone grafts have been considered the gold standard for the repair and reconstruction of maxillofacial bone defects, including critical-sized bone defects (2, 3). However, their clinical application is limited by disadvantages such as additional trauma at the donor site and limited bone availability (1, 4). Because of the limitations of autologous bone transplantation and other currently applied methods, bone tissue engineering that organically combines seed cells, bioactive factors, and biomaterials scaffolds is expected to provide an effective alternative approach for bone repair and reconstruction (5–7). Marrow mesenchymal stem cells (MSCs)-based therapies are considered viable alternatives with promising advantages for restoring the structure and function of damaged bone (5, 8). Bone marrow mesenchymal stem cells (BMSCs) are adult stem cells with high regeneration and multidirectional differentiation potential, which makes them ideal seed cells. Notably, research addressing the potential application of long non-coding RNAs (lncRNAs) in bone tissue engineering constructs for repair of bone defects is scarce. While the use of lncRNAs in combination with scaffolding has been reported in a few recent studies (8, 9), accumulating evidence shows that lncRNAs are involved in the osteogenic differentiation of various types of cells (9–12). Therefore, exploring the regulatory mechanisms related to lncRNAs' roles in osteogenic differentiation could provide a theoretical basis for target discovery in applications within bone tissue engineering.

lncRNAs are a class of little or no protein-coding transcripts longer than 200 nucleotides (9). Improvements in sequencing technologies have led to the identification of thousands of lncRNAs in different cell types, including cells of cartilage and bone (13). Accumulating evidence has shown that lncRNAs are involved in the osteogenic differentiation of various types of cells, and several lncRNAs such as H19 (14, 15), MALAT1 (16, 17), MEG3 (18), and HOTAIR (19) have been found to regulate the osteogenesis of MSCs. lncRNAs are believed to regulate osteoblastic differentiation by mechanisms such as combining with RNA binding protein (RBP), interacting with sense transcripts, binding with EZH2, chromatin modification, binding to transcription factors, and acting as competitive endogenous RNA (ceRNA) (9, 11).

Super-enhancers (SEs) have been attracting attention since their concept was first proposed by Hnisz et al. in 2013 (20). SEs are a large cluster of enriched transcriptional activity enhancers that drive the expression of genes controlling cell identity. Compared with typical enhancers (TEs), SEs enrich a greater number of factors related to enhancer activity, such as Mediator1 (Med1), H3K27ac, H3K4me1, H3K4me2, and chromatin factors such as cohesin, p300, and CBP, RNA polymerase II (RNAPII), and therefore SEs display stronger transcriptional activation ability (21). Moreover, SEs can increase the transcription and production of enhancer-associated ncRNAs (eRNAs, elncRNAs) (21, 22).

SEs have been a particular focus of research in cell development and differentiation, and tumorigenesis. In recent years, accruing data has demonstrated a role of SEs in bone tissue regulation. Studies have reported that SEs are associated with various bone-related diseases, including osteosarcoma, Ewing sarcoma, chordoma, multiple myeloma, cartilage dysplasia, osteoporosis, rheumatoid arthritis, and osteoarthritis (23). These studies have typically identified disease-specific SEs and

Abbreviations: hBMSCs, human bone marrow mesenchymal stem cells; MSCs, marrow stem cells; lncRNAs, long non-coding RNAs; miRNAs, microRNAs; ceRNA, competitive endogenous RNA; RBP, RNA binding protein; SEs, super-enhancers; TEs, typical enhancers; Med1, Mediator1; RNAPII, RNA polymerase II; eRNAs/elncRNAs, enhancer-associated ncRNAs; SNP, single-nucleotide polymorphisms; AS, ankylosing spondylitis; SASEs, ankylosing spondylitis SNP-adjacent SEs; ASMSCs, MSCs from AS patients; SE-lncRNAs, super-enhancer-associated lncRNAs; mESCs, embryonic stem cells; EOC, epithelial ovarian cancer; CPCs, cardiac precursor cells; ChIP-seq, chromatin immunoprecipitation-sequencing; qRT-PCR, quantitative real-time polymerase chain reaction; TSS, transcription start site; FBS, fetal bovine serum; PVDF, polyvinylidene fluoride; ALP, alkaline phosphatase; PFA, paraformaldehyde; ARS, Alizarin Red S; FISH, fluorescence *in situ* hybridization; RAP, RNA antisense purification; DAPI, 4,6-diamidino-2-phenylindole; SD, standard deviation; RUNX2, runt-related transcription factor 2; OSX, Osterix; COL1A1, collagen type 1 alpha 1; OPN, osteopontin; OCN, osteocalcin; CDK, cyclin-dependent kinase; OSE, osteoblasts-specific cis-acting elements.

their target genes using bioinformatics, and then analyzed the functions of the target genes through experimental approaches (23). In conjunction, BRD4 and CDK7 based drugs targeting critical components of SEs have been developed to treat osteosarcoma, Ewing sarcoma, multiple myeloma, osteoarthritis, and other bone-related diseases (24–27). Specifically, Zhang et al. (24) have reported that the specific CDK7 inhibitor THZ2 could suppress the phosphorylation of RNAPII CTD and selectively suppress super-enhancer-related genes, leading to anti-osteosarcoma effects. Considering osteogenic differentiation, Yu et al. (28) have reported that the single-nucleotide polymorphisms (SNP)-unique ankylosing spondylitis (AS) SNP-adjacent SEs (SASEs)-mRNA network participated in the pathological osteogenesis of AS and enhanced the osteogenic differentiation ability of MSCs from AS patients (ASMSCs). Overall, research regarding the role of SEs in bone-related diseases and osteogenic differentiation has mainly focused on SEs-associated mRNAs but few studies have addressed SEs-associated lncRNAs. Thus, the function of SEs-associated lncRNAs (SE-lncRNAs) involved in osteogenic differentiation remains largely unknown.

SE-lncRNAs are typically transcribed from SE genomic regions or their adjacent regions which harbor specific chromatin states of activation senators, H3K4me1, H3K27ac, and related co-factors (such as P300, etc.) or interact with SEs (21, 29). Multiple functional studies have shown that elncRNAs are required for enhancer activity and target promoter transcriptional activity (30–33). In addition, Yan et al. (34) have applied genome-wide analysis and shown that in mouse embryonic stem cells (mESCs), lncRNA genes were preferentially located next to SEs, and consumption of SE-lncRNAs transcripts dysregulated the activity of nearby SEs. Many studies have highlighted the critical roles of SE-lncRNAs in tumorigenesis, cell development, and differentiation (22, 35–39). For example, LINC00162, an SE long non-coding RNA, was shown to bind to THRAP3 to inhibit the expression of PTTG1IP and promote the proliferation of bladder cancer cells (37). A super-enhancer-regulated lncRNA UCA1 in epithelial ovarian cancer (EOC) is shown to enhance the interaction between AMTO and YAP, activating YAP dephosphorylation and nuclear translocation, and promoting binding to TEAD to promote the expression of pro-oncogene signatures (38). CARMEN, an enhancer-associated lncRNA, was shown to cis-regulate the expression of miR-143/145 in adult cardiac precursor cells (CPCs) by producing CARMEN7, thereby regulating the differentiation of adult CPCs into smooth muscle cells (39). These findings highlight the basis for investigating the roles of SE-lncRNAs in the process of osteogenic differentiation.

In our previous studies, the SEs expressed before and after osteogenic differentiation D0 group (before osteogenic induction) and D14 group (day 14 after osteogenic induction) of human bone marrow mesenchymal stem cells (hBMSCs) were identified by chromatin immunoprecipitation sequencing (ChIP-seq) of H3K27ac (40). The associated genes of the specific SEs in the D14 group were analyzed using bioinformatics and quantitative real-time polymerase chain reaction (qRT-PCR), and the SE-lncRNA LINC01485 was found to show significant differences in expression levels before and after osteogenic differentiation. Therefore, the role and regulatory mechanisms of LINC01485 involvement in the differentiation of hBMSCs were considered to merit further research and are addressed in the present investigation.

MATERIALS AND METHODS

Annotation and Prediction of SE-Associated Genes

SEs were assigned to the expressed transcripts, and the transcription start site (TSS) closest to the center of the enhancer was used to identify neighboring genes (20, 24, 41). AnnotatePeaks.pl, a Hypergeometric Optimization of Motif EnRichment (Homer, version 4.11) application for peak annotation, was used to link peaks to the neighboring genes (42, 43).

Culture and Osteogenic Differentiation of hBMSCs

hBMSCs were purchased from Procell Life Science & Technology (CP-H166, Wuhan, China) and Cyagen Biosciences (HUXMA-01001, Guangzhou, China) and cultured in MSC medium (Cyagen, China) supplemented with 10% fetal bovine serum (FBS), 1% penicillin, and streptomycin, 1% glutamine (Cyagen, China) in humidified air of 5% CO_2 at 37°C. The purchased cells were accompanied by quality reports, including flow cytometry identification, which revealed that the hBMSCs were positive for CD29, CD44, CD73, and CD105, and negative for CD34, CD11b, and CD45. The purchased hBMSCs could differentiate into osteoblasts, adipocytes, and chondrocytes under specific inductive conditions. When cells reached 80-90% confluence, subculture was performed at a ratio of 1:2 or 1:3, and the medium was replaced every 2 days. After being cultured to P2-P4, the cells were plated in a 6-well plate at a density of about 1×10^5 cells/well. When cell confluence reached roughly 70%, hBMSCs osteogenic induction medium (Cyagen, China) containing dexamethasone, vitamin C, and β-sodium glycerophosphate was added, and was changed every 3 days.

qRT-PCR

Total RNA was extracted from the cells using TRIzol reagent (Accurate Biotech, Hunan, China). RNA purity and concentration were assessed by NanoDrop 2000 instrument (Thermofisher, US). For the qRT-PCR quantification of mRNAs and lncRNAs, 1000 ng RNA was reverse transcribed into cDNA using the Evo M-MLV RT kit with gDNA Clean for qPCR (Accurate Biotech, China). Reverse transcription of miRNAs was performed using Bulge-Loop SCRIPT Reverse Transcription Kit (RiboBio, Guangzhou, China). qRT-PCR was performed using SYBR Green Premix PCR kit (Accurate Biotech, China) on a CFX Connection Real-Time System (Bio-Rad, California). According to the manufacturer's protocol, the qRT-PCR reaction program for mRNAs and lncRNAs was set as follows: initial activation at 95°C for 30 s, followed by 40 cycles at

95°C for 5 s and 63°C for 30 s, while the cycling conditions for miRNAs were as follows: initial activation at 95°C for 10 min, followed by 40 cycles at 95°C for 2 s, 60°C for 20 s, and 70°C for 10 s. GAPDH was used as an endogenous reference for lncRNAs and mRNAs, while U6 was used to normalize the expression of miRNAs. The $2^{-\Delta\Delta CT}$ method was used to calculate the relative expression level of each gene. All reactions were performed in duplicate to ensure reliability and validity. All primers were obtained from Tsingke (Beijing, China) or RiboBio (Guangzhou, China). The sequences of the primers used are listed in **Supplementary Tables S2**, **S3**.

Western Blot

Total protein was extracted by RIPA lysate (Cwbio, Jiangsu, China) containing protein inhibitors and phosphatase inhibitors (Cwbio, China) and was quantified by bicinchoninic acid (BCA) protein assay kit (Cwbio, China). A total of 20 μg protein from each sample was separated by 10% SDS-PAGE gel at 80V (stacking gel)/120V (resolving gel) for about 2 h and transferred onto polyvinylidene fluoride (PVDF) membranes (Millipore, US) with a diameter of 0.45 um at 250 mA for 150 min. The membrane was blocked with 5% non-fat milk at room temperature for 1 h, washed with TBST (0.1% Tween-20 in Tris-buffered saline (TBS)) and incubated overnight in the primary antibody at 4°C. The primary antibodies were as follows: RUNX2 (1:1000, Cell Signaling Technology, Cat# 12556s), Osterix (1:1000, BOSTER, Cat# A02077-1), COL1A1 (1:1000, BOSTER, Cat# BA0325), OPN (1:1000, Abcam, Cat# ab8448), and GAPDH (1:20000, Proteintech, Cat# 60004–1-Ig). The membrane was washed with TBST three times for 10 min each and then incubated with an HRP-conjugated secondary antibody (Goat Anti-Mouse IgG, 1:5000, Proteintech, Cat # SA00001-1; Goat Anti-Rabbit IgG, 1:5000, Proteintech, Cat# SA00001-2) at room temperature for 1 h followed by washing with TBST three times for 10 min each. Immune complexes were detected using an ECL kit (Merck Millipore, Germany) with a chemiluminescence imaging system (Bio-Rad, US). The density data of each specific protein was normalized to that of GAPDH and analyzed using Image J software (Media Cybernetics, US).

Alkaline Phosphatase (ALP) Staining and ALP Activity Detection

hBMSCs plated in 6-well plates were subjected to osteogenic induction for 7 days, then washed twice with phosphate-buffered saline (PBS), and fixed with 4% paraformaldehyde (PFA) for 15 min. After washing with PBS, the cells were stained with ALP staining solution (Beyotime, Shanghai, China) according to the manufacturer's instructions. After 24 h of staining, the cells were photographed under a microscope (Leica, DMIRB, Germany). In addition, the cells were added with lysates (Beyotime, China), which were collected and used to detect ALP activity using an ALP activity test kit (Beyotime, China). The absorbance at 450 nm was examined.

Alizarin Red S (ARS) Staining and ARS Quantification Assay

hBMSCs were subjected to osteogenic induction for 14 days, washed twice with PBS, and fixed with 4% PFA for 15 min. Next, they were washed with diH_2O and stained with 40 mM ARS (ScienCell, US) at 37°C for 15 min. After dyeing, the cells were washed with diH_2O, and images were obtained under the microscope (Leica, DMIRB, Germany). The stained cells were added with 10% acetic acid and 10% ammonium hydroxide from an Alizarin Red S staining quantification assay kit (ScienCell, US). The absorbance at 405 nm was determined and used to analyze the ARS concentration.

Lentivirus Construction and Cell Transduction

The full-length sequences of LINC01485, LINC01485 short hairpin (sh) RNA targeting LINC01485 (sh-LINC01485), and scrambled control shRNA (sh-NC) were inserted into the GV vector, and the three target plasmid vectors and an empty plasmid vector were transfected into 293T cells with plasmids Helper 1.0 and Helper 2.0, respectively. The cell supernatant was collected to obtain the virus, and the virus was concentrated, purified, and detected. The inserted sequence was confirmed by sequencing analysis. This work was done by GeneChem (GeneChem, Shanghai, China). hBMSCs were plated in a 6-well plate at a density of 6×10^4 cells/well. When the cells became adherent to the wall about 24 h later, and the confluence reached approximately 50%, the cells were infected with lentiviruses at an MOI of 40 for 2-3 days. Then, 3 μg/mL puromycin (Solarbio, Beijing, China) was utilized for screening for 2 days. Finally, the cells were collected to test the overexpression and interference efficiency of LINC01485 and used for further experiments. The sequence of LINC01485 RNAi is listed in **Supplementary Table S4**.

Bioinformatics Analysis of Targeting Relationship Between lncRNA-miRNA and miRNA-mRNA

lncRNA-bound miRNAs and miRNA-targeted mRNAs were predicted using TargetScan and Miranda databases, and the predicted results of the two databases were intersected. First, the target mRNAs of miRNA associated with osteogenesis were selected from the relationship pairs with the highest binding score. Then the RNA antisense purification (RAP) assay was performed to determine the miRNA that was finally interacting with LINC01485.

MiRNA Transfection

hBMSCs were seeded in the 6-well plate at a density of 6×10^4, and the cells reached 70% confluence after about 48 h. According to the manufacturer's instructions, miR-619-5p mimic and miRNA mimic NC (RiboBio, Guangzhou, China) were transfected with Lipofectamine 3000 transfection reagent (Invitrogen, US) at a concentration of 50 nM, and miR-619-5p inhibitor, miRNA inhibitor NC (RiboBio, Guangzhou, China) at a concentration of 100 nM. RNA was extracted 24 h after transfection, the protein was extracted 48 h for detection, and osteogenic induction solution was added for osteogenic induction differentiation. Transfection was performed again

after 3 days. MiR-619-5p mimic and miR-619-5p inhibitor sequence are listed in **Supplementary Table S5**.

FISH Assay

Before and after osteogenic induction, hBMSCs in 6-well plates were fixed with 4% PFA for 15 min upon reaching a cell density of 70-80%. The cells were washed with DEPC water twice for 5 min each time, then added protease K and incubated at 55°C for 5 min for digestion. At room temperature, the cells were fixed again with 1% PFA for 10 min and washed three times with pre-cooled alcohol at -20°C. Pre-hybridization was performed with a 100 μL pre-hybridization solution dropped onto slices at 37°C for 30 min. The prepared LINC01485 probe (Axl-bio, Guangzhou, China) was denatured at 73°C for 8 min. The probe and hybrid solution mixture was added to the sections and hybridized overnight at 42°C. After washing with hybridization solution and PBS, according to the instructions of the FISH test kit (Axl-bio, Guangzhou, China), 4,6-diamidino-2-phenylindole (DAPI) was added for staining, in light avoid conditions for 10 min, followed by washing with PBS 3 times, 5 min each. Then, anti-fluorescence attenuated tablets were used to seal the tablets, and the images were obtained with laser scanning confocal microscopy (Carl Zeiss AG, Germany). LINC01485 FISH probe is listed in **Supplementary Table S6**.

RAP Assay

For this experiment, the RAP kit (Axl-bio, Guangzhou, China) was employed.

RAP uses biotinylated probes that bind to target RNAs and miRNAs, which may subsequently be extracted, reverse transcribed to cDNA, and detected by qRT-PCR. A total of 10^7 hBMSCs were washed in PBS and UV irradiated at 254 nm (0.15 J cm^{-2}) for cross-linkage, 1 mL lysis buffer was used to lyse the cells, and a 0.4-mm syringe was used to homogenize them completely. The lncRNA-RAP system received two separate 25-bp biotinylated antisense probes (0.2 nmol), as well as one 26-bp biotinylated antisense probe (0.2 nmol) targeting the adapter sequence. The probes were denatured at 65°C for 10 min and hybridized at room temperature for 2 h. There were 200μL streptavidin-coated magnetic beads added, washing was employed to remove non-specifically bound RNAs, and Trizol reagent was used to extract miRNAs directly interacting with LINC01485. The miRNAs were reverse transcribed and binding strength was determined using qRT-PCR. The LINC01485 RAP probe sequence is listed in **Supplementary Table S7**.

Luciferase Assay

HEK293T cells were purchased from ATCC cell bank, cultured, and amplified with DMEM (Gibco, US) complete medium containing 10% FBS (Gibco, US). HEK293T cells were plated in 6-well plates at a density of 2×10^6 cells/well. After 16 h, the cell confluence reached about 80%. The possible binding sites of LINC01485 and miR-619-6p were predicted using bioinformatics tools, and the predicted LINC01485 binding sequence and mutated sequence were constructed into psicheck2 reporter plasmid. At the same time, the full-length sequence of LINC01485 was inserted into the pcDNA3.1 plasmid. The plasmids and miR-619-5p mimic or miRNA NC were co-transfected into HEK293T cells with Lipofectmin 3000 transfection reagent (Invitrogen, US). The medium was changed 6 h after transfection, and the culture was continued until 48 h after adding the complete medium. The medium was removed, washed twice with PBS, and 1×PLB lysate (Promega, US) was added for incubation at room temperature for 15 min. A total of 20 μL lysate, 100 μL LARII, and 100 μL stop Glo buffer (Promega, US) were added to a 96-well plate, and luciferase activity was detected using a microplate reader (BioTek, US).

Statistical Analysis

All experiments were carried out three times independently. Data were presented as mean ± standard deviation (SD) based on three replicates. Unpaired two-tailed Student's t-test was used to examine differences between groups. All data were statistically analyzed using GraphPad Prism 8.0 (GraphPad Software, US). Statistical significance was defined as a value of $p<0.05$ (two-sided).

RESULTS

LncRNAs in Specific SE-Associated Genes in the D14 Group

Using HOMER software analysis, the genes closest to the SEs were selected as the SE-associated genes. **Supplementary Table S1** shows lncRNAs in the D14 group specific SE-associated genes. qRT-PCR results showed that the expression levels of 4 lncRNAs were significantly increased after osteogenic differentiation (**Supplementary Figure S1**).

LNC01485 Expression Was Up-Regulated During Osteogenic Differentiation of hBMSCs

At first, the osteogenic differentiation of hBMSCs was confirmed by ALP activity assay and ALP and ARS staining. ALP staining (**Figure 1A**) on Day 7 after induction and ARS staining (**Figure 1B**) on Day 21 after induction showed positive staining results. The ALP activity was significantly enhanced after osteogenic induction on the seventh day (**Figure 1C**). Alizarin Red semi-quantitative analysis showed that the content of Alizarin Red bound to calcium nodules increased significantly 14 days after osteogenesis induction (**Figure 1D**). Western blot and qRT-PCR assays were used to determine the expression levels of runt-related transcription factor (RUNX2), collagen type I alpha 1 chain (COL1A1), osterix (OSX), osteocalcin (OCN), and osteopontin (OPN) during the process of osteogenic induction of hBMSCs. Western blot results showed that protein levels of RUNX2 (**Figures 1E, F**), COL1A1 (**Figures 1E, G**), OSX (**Figures 1E, H**), and OPN (**Figures 1E, I**) were up-regulated after osteogenic induction as compared to uninduced cells. The qRT-PCR results revealed that RUNX2 (**Figure 1J**), OPN (**Figure 1K**), and OCN (**Figure 1L**) increased gradually during

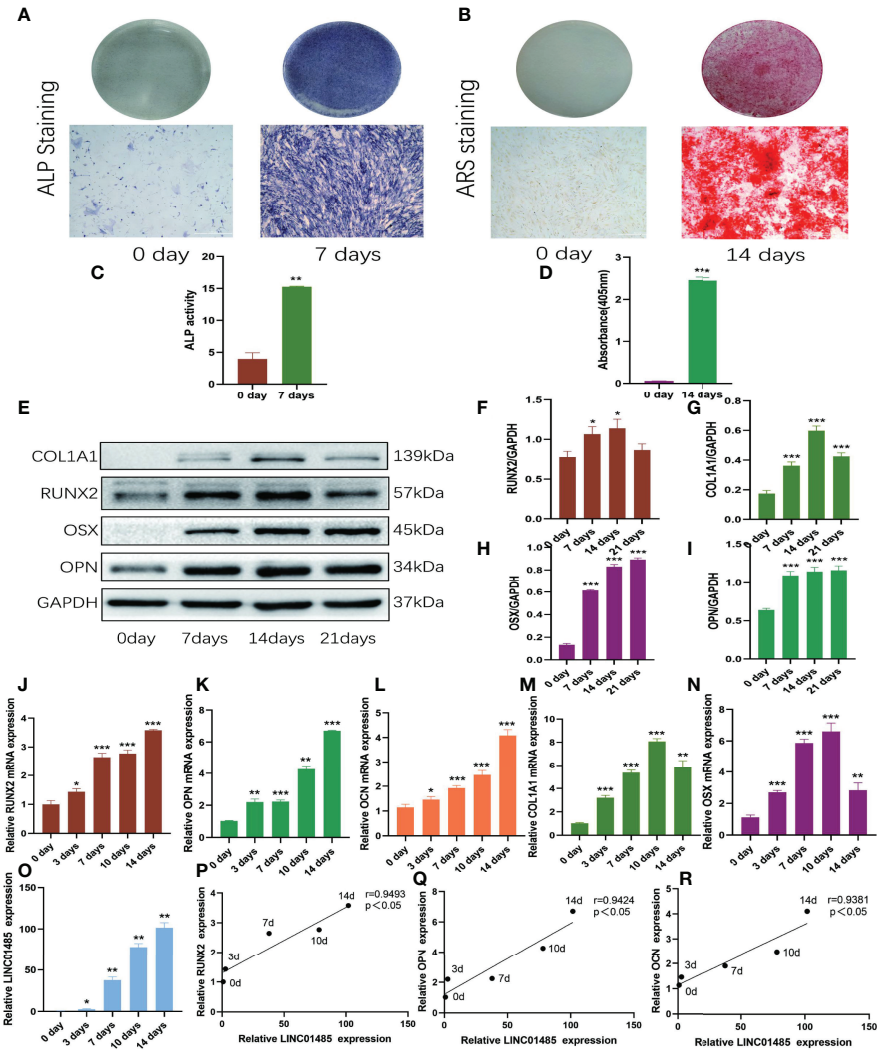

FIGURE 1 | LNC01485 expression was up-regulated during osteogenic differentiation of hBMSCs. **(A, C)** ALP staining **(A)** and ALP activity assay **(C)** of hBMSCs before osteogenic induction and 7 days after induction. **(B, D)** hBMSCs were stained with Alizarin Red S **(B)** before osteogenic induction and at 14 days after induction, and the staining results were analyzed semi-quantitatively **(D)**. **(E-I)** The protein expression levels of RUNX2 **(E, F)**, COL1A1 **(E, G)**, OSX **(E, H)**, and OPN **(E, I)** level on Days 0, 7, 14, and 21 of osteogenic induction were detected by Western blot and quantified analysis by normalized to GAPDH. **(J-O)** The mRNA expression levels of RUNX2 **(J)**, OPN **(K)**, OCN **(L)**, COL1A1 **(M)**, OSX **(N)**, and LINC01485 **(O)** before and after osteogenic differentiation were determined by qRT-PCR. **(P-R)** Expression correlation analysis between LINC01485 and osteogenic genes RUNX2 **(P)**, OPN **(Q)**, and OCN **(R)** during osteogenic differentiation. $^{*}p < 0.05$, $^{**}p < 0.01$, $^{***}p < 0.001$.

14 days of osteogenic induction, and COL1A1 (**Figure 1M**) and OSX (**Figure 1N**) reached their peak on the tenth day. Compared with the uninduced cells, the expression levels of these osteogenic factors were significantly up-regulated ($p<0.05$). These results revealed that the osteogenic induction of hBMSCs *in vitro* was achieved successfully.

The mRNA expression levels of LINC01485 were determined by qRT-PCR during the osteogenic differentiation of hBMSCs. The expression of LINC01485 gradually increased over time during 14 days of osteogenic induction (**Figure 1O**). The expression trend of LINC01485 was consistent with that of osteogenic genes RUNX2, OPN, and OCN; therefore, the correlation between LINC01485 and osteogenic-related genes was analyzed using Spearman's correlation analysis. LINC01485 was evident as significantly positively correlated with RUNX2 (**Figure 1P**), OPN (**Figure 1Q**), and OCN (**Figure 1R**), suggesting that LINC01485 might be involved in osteogenesis regulation.

LINC01485 Regulates Osteogenic Differentiation of hBMSCs

To explore the effects of LINC01485 on osteogenic differentiation of hBMSCs *in vitro*, we infected cells with LINC01485 overexpression and LINC01485 knockdown

lentivirus to maintain continuous expression levels of LINC01485. qRT-PCR was performed to examine the overexpression and interference efficiency of LINC01485. The results verified that the level of LINC01485 expression in the LINC01485-overexpression group was significantly higher than that in the negative control group after transduction (**Figure 2A**). In contrast, LINC01485 was down-regulated after transduction of sh-LINC01485, as compared with the scrambled group (**Figure 2B**). Subsequently, qRT-PCR and western blot assays were used to determine the expression levels of osteogenic specific factors in the infected groups at mRNA and protein levels after 14 days of osteogenic induction. As shown in **Figures 2C–K**, LINC01485 overexpression markedly enhanced the expression of RUNX2 (**Figure 2C**), COL1A1 (**Figure 2D**), OSX (**Figure 2E**), and OCN (**Figure 2F**) at the mRNA level and promoted the expression of RUNX2 (**Figures 2G, H**), COL1A1 (**Figures 2G, I**), OSX (**Figures 2G, J**), and OPN (**Figures 2G, K**) at the protein levels. In contrast, LINC01485 knockdown produced the opposite effects (**Figures 2C–K**). Furthermore, ALP activity detection and ALP staining revealed that the up-regulation of LINC01485 enhanced ALP staining (**Figure 2L**) and the ALP activity

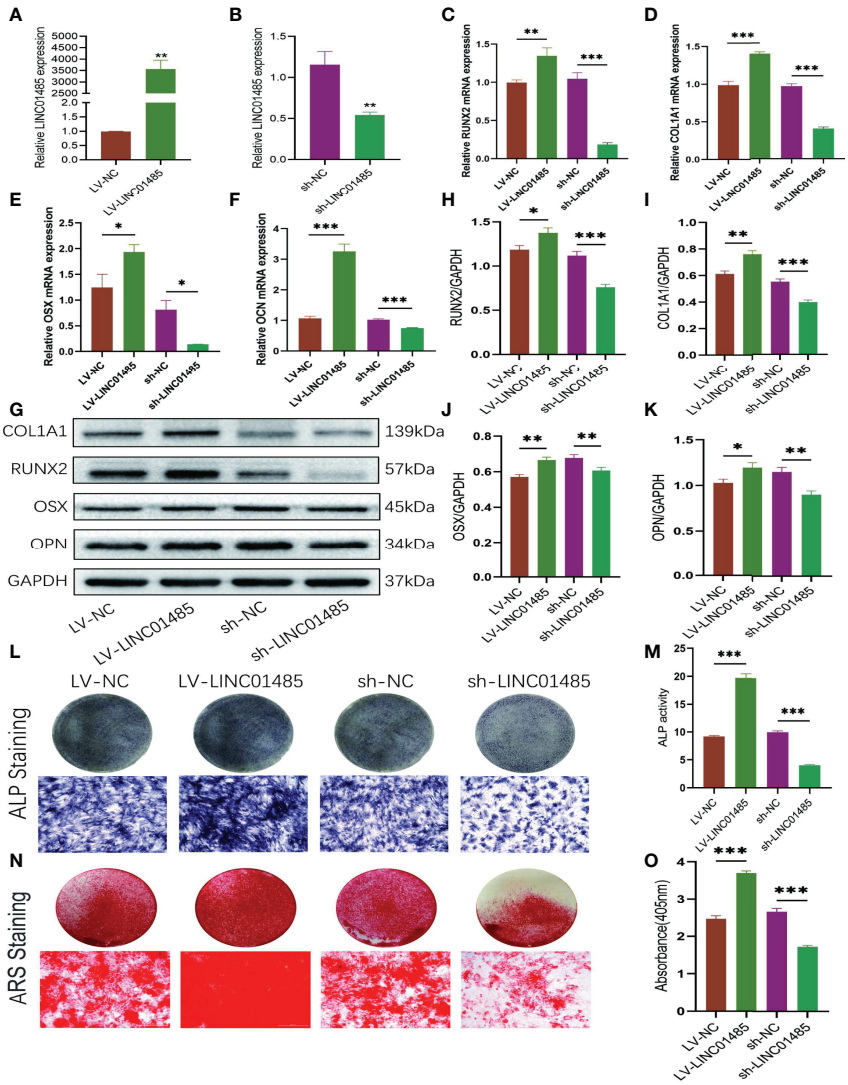

FIGURE 2 | LINC01485 regulates osteogenic differentiation of hBMSCs. **(A, B)** The overexpression **(A)** and interference **(B)** efficiency of LINC01485 was determined by qRT-PCR in hBMSCs after transduction with LV-LINC01485 and sh-LINC01485. **(C–F)** The mRNA levels of RUNX2 **(C)**, COL1A1 **(D)**, OSX **(E)**, and OCN **(F)** after 14 days of osteogenic induction in hBMSC infected with lentivirus by qRT-PCR. **(G, H)** Western blot analysis of the RUNX2 **(G, I)**, COL1A1 **(G, I)**, OSX **(G, J)**, and OPN **(G, K)** protein expression in hBMSCs infected with lentivirus after osteogenic induction 14 days later and the corresponding gray value quantitative analysis. **(L, M)** ALP staining **(L)** and ALP activity **(M)** of hBMSC cells infected with lentivirus after 7 days of osteogenic induction. **(N, O)** Alizarin Red S staining **(N)** and semi-quantitative analysis **(O)** of infected hBMSCs with lentivirus after 14 days osteogenic induction. $^{*}p < 0.05$, $^{**}p < 0.01$, $^{***}p < 0.001$.

(**Figure 2M**), while the down-regulation of LINC01485 reduced ALP staining (**Figure 2L**) and inhibited ALP activity (**Figure 2M**). ARS staining with LINC014845 overexpression led to increase in the mineralized bone matrix as compared to the control group (**Figures 2N, O**), whereas sh-LINC01485 decreased calcium nodules (**Figures 2N, O**). These results manifested that LINC01485 could promote osteogenic differentiation of hBMSCs *in vitro*.

LINC01485 Acts As A Sponge of miR-619-5p in the Osteogenesis of hBMSCs

To investigate the molecular mechanisms of LINC01485 regulation of osteogenic differentiation of hBMSCs, we first evaluated the cellular localization of LINC01485. FISH assay results determined that LINC01485 was mainly expressed in the cytoplasm (**Figure 3A**). This finding is consistent with the results reported by Zhou et al. (44) showing LINC01485 as primarily located in the cytoplasm of gastric cancer cells. In addition, FISH results also suggested greater LINC01485 fluorescence in hBMSCs after osteogenic induction as compared with uninduced cells (**Figure 3A**).

Recent research (12) has shown that lncRNA located in the cytoplasm plays a role in the osteogenic differentiation of MSCs through cross-talk with miRNA. Thus, we used Miranda and TargetScan databases to predict miRNAs that might bind to LINC01485. A Venn diagram depicted the intersection. To further screen target miRNAs, an RAP assay of LINC01485 was conducted to determine the expression levels of several miRNAs that displayed high predicted scores. RAP results showed that among 5 miRNAs with high scores, miR-619-5p was evident in the AP group as compared with the Input group without RAP probe, while the other miRNAs showed negative results in the AP group (**Figure 3B**). The electrophoretic patterns of qRT-PCR products in the RAP experiment also confirmed this result (**Supplementary Figure**

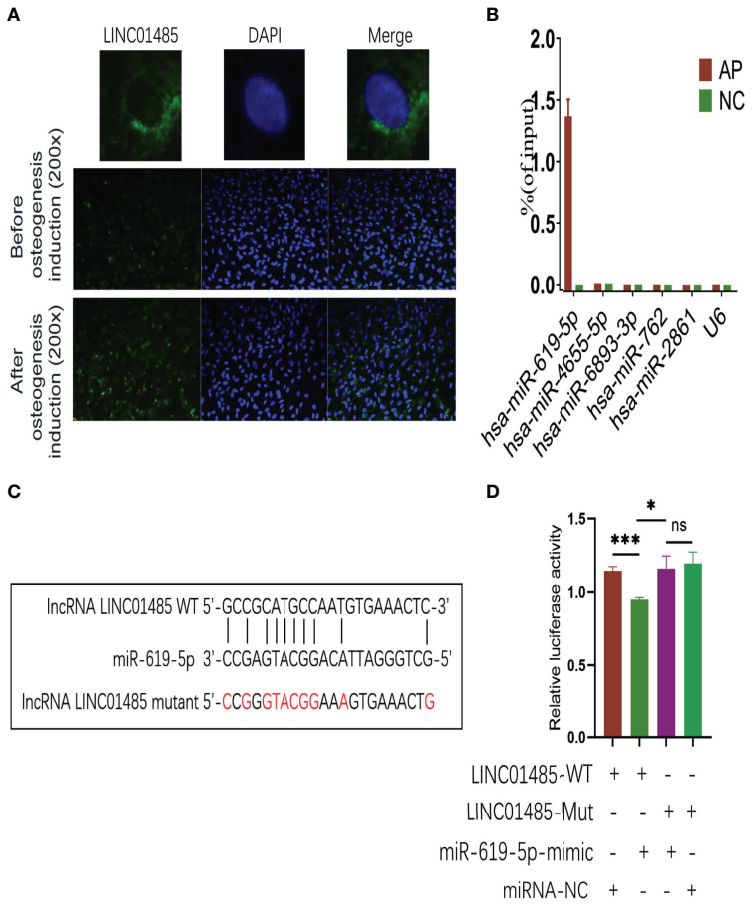

FIGURE 3 | LINC01485 acts as a sponge of miR-619-5p in the osteogenesis of hBMSCs. **(A)** FISH assay for LINC01485 before and after osteogenic induction in hBMSCs. **(B)** Percentage of purified miRNAs identified in the RAP assay relative to the input group detected by qRT-PCR. **(C)** Binding site prediction of LINC01485 and miR-619-5p. **(D)** Luciferase activity of LINC01485-WT and LINC01485-Mut upon transfection of miRNA NC or miR-619-5p mimic into HEK293T cells. ns, no significance. $^{*}p < 0.05$, $^{***}p < 0.001$.

S2). Thus, the RAP results indicated that LINC01485 efficiently pulled down miR-619-5p but did not bind to several other miRNAs.

Furthermore, the binding sites of LINC01485 and miR-619-5p were predicted using bioinformatics (**Figure 3C**). Thereafter, we constructed LINC01485 wild-type (WT) and LINC01485 mutant (MUT) luciferase receptor plasmids based on the putative binding sites. The result of luciferase activity analysis indicated that the luciferase activity of LINC01485-WT reporter vector was significantly inhibited by miR-619-5p mimic, while luciferase activity of LINC01485-MUT type was not affected by miR-619-5p mimic (**Figure 3D**).

MiR-619-5p is Down-Regulated and Inhibits Osteogenesis During Osteogenic Induction of hBMSCs

Since LINC01485 could sponge miR-619-5p to promote osteogenic differentiation, we next studied the expression of miR-619-5p in the osteogenic process and its effect on osteogenic differentiation. qRT-PCR analysis showed that the mRNA level of miR-619-5p decreased gradually during osteogenic differentiation (**Figure 4A**), which was negatively correlated with the expression trend of LINC01485 (**Figure 4B**). Subsequently, miR-619-5p mimic, miRNA mimic negative control (miRNA mimic NC), miR-619-5p inhibitor, and

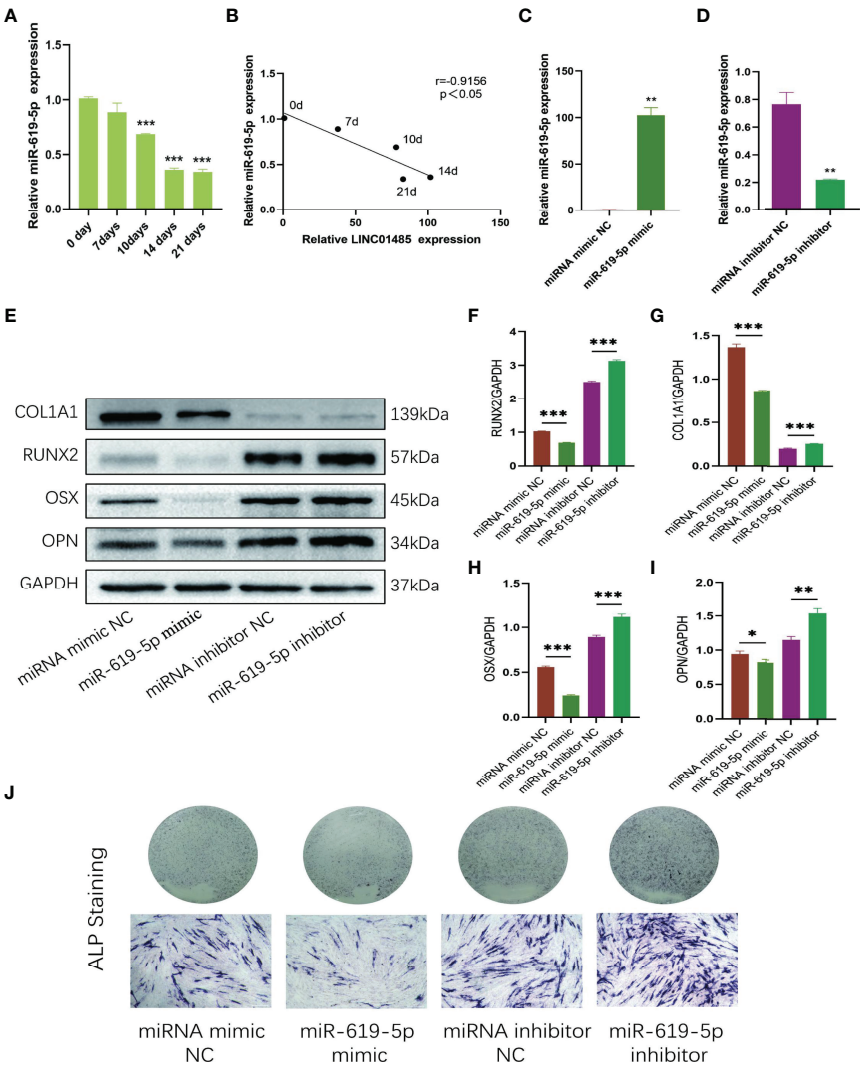

FIGURE 4 | MiR-619-5p is down-regulated and inhibits osteogenesis during osteogenic induction of hBMSCs. **(A)** The relative expression levels of miR-619-5p before and after osteogenic differentiation were determined by qRT-PCR. **(B)** Correlation analysis of LINC01485 and miR-619-5p expression levels during osteogenic differentiation. **(C, D)** The mRNA level of miR-619-5p in hBMSCs transfected with miR-199a-5p mimic **(C)** and miR-199a-5p inhibitor **(D)** by qRT-PCR. **(E–I)** Western blot analysis of the RUNX2 **(E, F)**, COL1A1 **(E, G)**, OSX **(E, H)**, and OPN **(E, I)** protein expression in hBMSCs transfected with miR-619-5p mimic, miRNA mimic NC, miR-619-5p inhibitor, and miRNA inhibitor NC after osteogenic induction and the corresponding gray value quantitative analysis. **(J)** ALP staining analysis of hBMSCs transfected with miR-619-5p mimic, miRNA mimic NC, miR-619-5p inhibitor, and miRNA inhibitor NC after osteogenic induction. *$p < 0.05$, **$p < 0.01$, ***$p < 0.001$.

miRNA inhibitor negative control (miRNA inhibitor NC) were synthesized and transfected into hBMSCs for osteogenic induction, followed by western blot and ALP staining assay. qRT-PCR results showed that the expression level of miR-619-5p in cells transfected with miR-619-5p mimic increased to about 100-fold higher than that in mimic NC (**Figure 4C**). In contrast, the expression level of miR-619-5p in cells transfected with miR-619-5p inhibitor was about 72% lower than that in inhibitor NC (**Figure 4D**). MiR-619-5p mimic significantly reduced the protein levels of RUNX2 (**Figures 4E, F**), COL1A1 (**Figures 4E, G**), OSX (**Figures 4E, H**), and OPN (**Figures 4E, I**), and weakened ALP staining (**Figure 4J**). At the same time, inhibition of miR-619-5p led to an increase in RUNX2 (**Figures 4E, F**), COL1A1 (**Figures 4E, G**), OSX (**Figures 4E, H**), and OPN (**Figures 4E–I**) protein expression and enhanced ALP staining (**Figure 4J**). These results indicated that miR-619-5p overexpression could inhibit osteogenic differentiation, and inhibition of miR-619-5p could promote the osteogenesis of hBMSC. This is contrary to the effect of LINC01485 on osteogenic differentiation and adds to the evidence that LINC01485 promotes osteogenic differentiation through the LINC01485/miR-619-5p axis.

RUNX2 Is A Direct Target of miR-619-5p

We predicted the target genes of miR-619-5p using Miranda and TargetScan databases and found that miR-619-5p could bind to the osteogenic gene RUNX2. The mRNA level of RUNX2 increased gradually during osteogenic differentiation, which was negatively correlated with the expression of miR-619-5p (**Figure 5A**). In addition, Western blot and qRT-PCR analysis showed that protein and mRNA levels of RUNX2 decreased when hBMSCs were transfected with miR-619-5p mimic, while protein and mRNA levels of RUNX2 increased by the treatment with the miR-619-5p inhibitor (**Figures 5B–D**). Moreover, the results of bioinformatic predictions showed that miR-619-5p had a binding site at the 3'UTR of RUNX2, and the binding sequence is shown in **Figure 5E**. The dual-luciferase assay showed that luciferase activity of RUNX2-WT was significantly down-

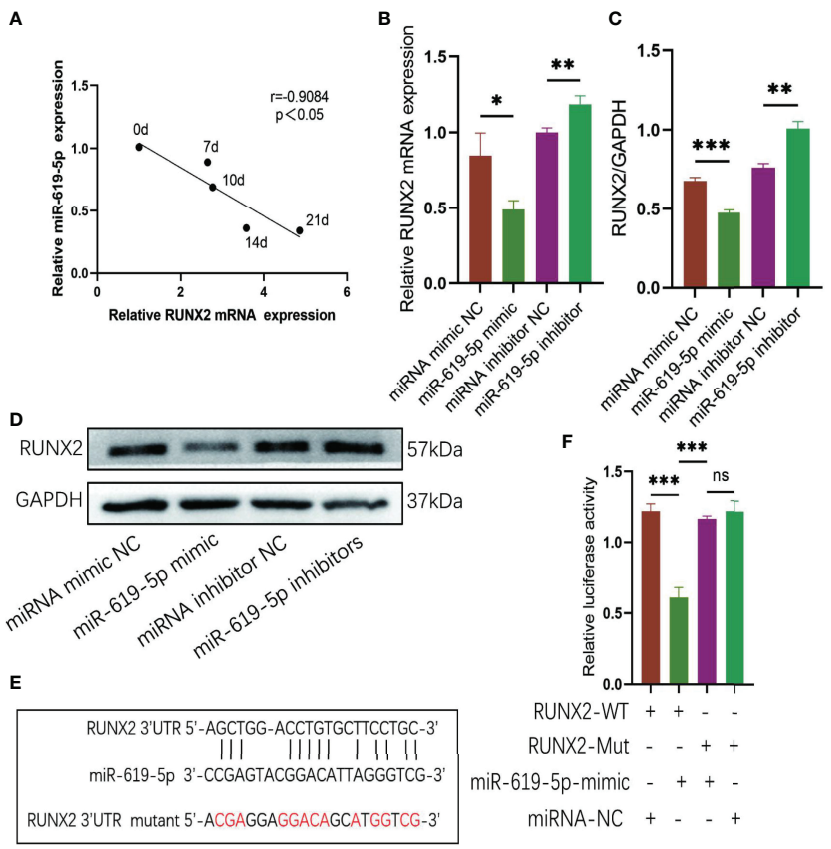

FIGURE 5 | RUNX2 is a direct target of miR-619-5p. **(A)** Correlation analysis of RUNX2 and miR-619-5p expression levels during osteogenic differentiation. **(B)** The mRNA expression of RUNX2 in hBMSCs transfected with miR-619-5p mimic or miR-619-5p inhibitor was determined using qRT-PCR. **(C, D)** The RUNX2 protein level in hBMSCs transfected with miR-619-5p mimic or miR-619-5p inhibitor was determined using Western blotting **(C)** and the gray value quantitative analysis **(D)**. **(E)** The putative binding sites of miR-619-5p in wild type and mutant RUNX2 3′-UTR. **(F)** Luciferase activity of RUNX2-WT and RUNX2-Mut upon transfection of miRNA NC or miR-619-5p mimic into HEK293T cells. ns, no significance. *$p < 0.05$, **$p < 0.01$, ***$p < 0.001$.

regulated by miR-619-5p mimic, but the luciferase activity of RUNX2-MUT was not affected by miR-619-5p (**Figure 5F**). These results confirmed that miR-619-5p targets RUNX2, inhibiting RUNX2 expression by binding to the 3'UTR of RUNX2.

LINC01485 Acts As A ceRNA of miR-619-5p to Regulate RUNX2 and Osteogenic Differentiation

A series of rescue assays was performed to verify whether there is a regulatory relationship among LINC01485, miR-619-5p, and RUNX2. First, we transfected miR-619-5p inhibitor or miRNA inhibitor NC into sh-LINC01485 or sh-NC stable hBMSCs constructed in advance. Western blot results showed that after osteogenic induction of hBMSCs in the LINC01485 interference group, the protein levels of RUNX2 (**Figures 6A, B**), COL1A1 (**Figures 6A, C**), OSX (**Figures 6A, D**), and OPN (**Figures 6A, E**) were decreased, and ALP staining was reduced as compared with the control group (**Figure 6F**). However, miR-619-5p inhibitor treatment compensated for the effect of LINC01485 knockdown on osteogenic differentiation, and the protein levels of RUNX2 (**Figures 6A, B**), COL1A1 (**Figures 6A, C**), OSX (**Figures 6A, D**),

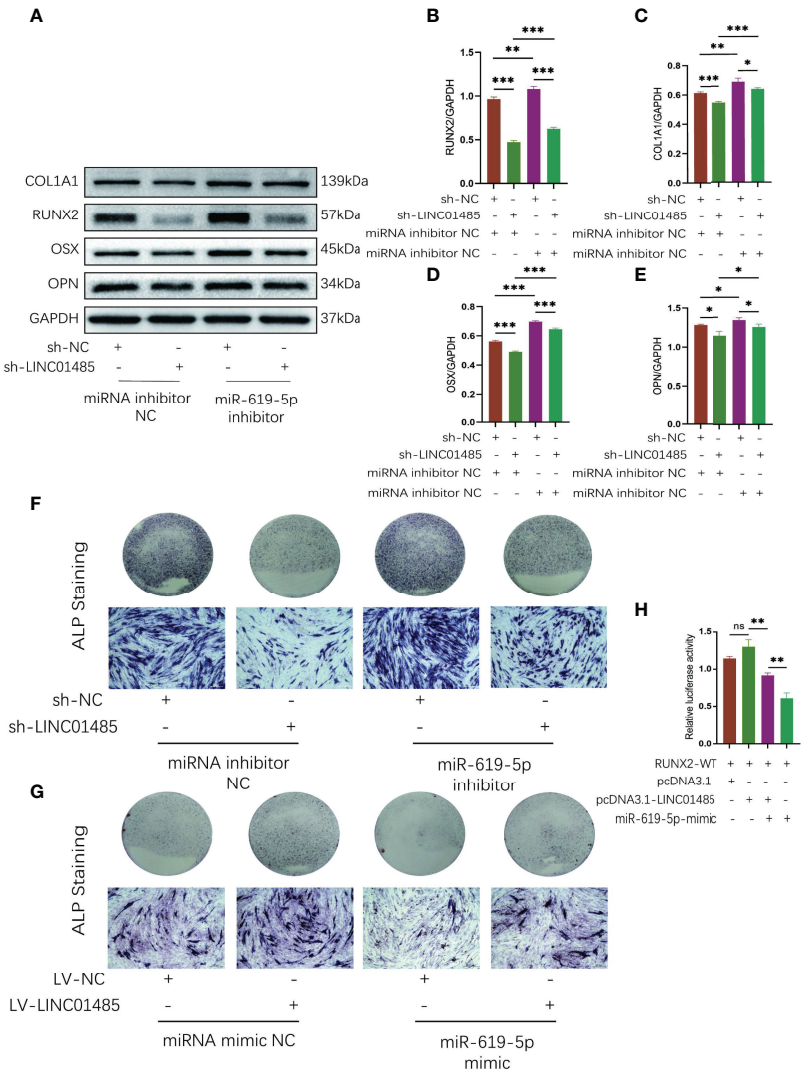

FIGURE 6 | LINC01485 acts as a ceRNA of miR-619-5p to regulate RUNX2 and osteogenic differentiation. **(A–E)** Western blot analysis of the RUNX2 **(A, B)**, COL1A1 **(A, C)**, OSX **(A, D)**, and OPN **(A, E)** protein expression in hBMSCs infected with sh-NC or sh-LINC01485 lentivirus along with miRNA inhibitor NC or miR-619-5p inhibitor after osteogenic induction and the corresponding gray value quantitative analysis. **(F)** ALP staining analysis of hBMSCs infected with sh-NC or sh-LINC01485 lentivirus along with miRNA inhibitor NC or miR-619-5p inhibitor after osteogenic induction. **(G)** ALP staining analysis of hBMSCs infected with LV-NC or LV-LINC01485 lentivirus along with miRNA mimic NC or miR-619-5p mimic after osteogenic induction. **(H)** Luciferase activity of RUNX2-WT upon transfection of pcDNA3.1, pcDNA3.1-LINC01485, or miR-619-5p mimic into HEK293T cells. ns, none significance. *$p < 0.05$, **$p < 0.01$, ***$p < 0.001$.

and OPN (**Figures 6A, E**) were elevated, and ALP staining was more pronounced (**Figure 6F**). Then, miR-619-5p mimic or miRNA mimic NC was transfected into LV-LINC01485 or LV-NC stable hBMSCs for osteogenic differentiation induction. miR-619-5p mimic reduced ALP staining as compared with miRNA mimic NC, but the ALP staining increased after co-transfection of LV-LINC01485 (**Figure 6G**). Luciferase assays indicated that miR-619-5p mimic reduced the luciferase activity of RUNX2-WT, while the co-transfection of LINC01485 overexpressed plasmid with miR-619-5p mimic restoring the luciferase activity of RUNX2-WT (**Figure 6H**). RUNX2-WT luciferase activity was higher in the LINC01485 overexpressed plasmid transfection group than in RUNX2-WT transfected with the empty plasmid but decreased when miR-619-5p mimic was added (**Figure 6H**). Overall, these *in vitro* results suggest that LINC01485, miR-619-5p, and RUNX2 constitute a ceRNA network, and LINC01485 competes with miR-619-5p to regulate RUNX2 expression, thereby regulating the bone formation of hBMSCs.

DISCUSSION

Maxillofacial critical size bone defects caused by several etiological factors pose challenges in successful reconstruction. Therefore, exploring the regulatory mechanisms underlying BMSCs osteogenic differentiation can provide a theoretical basis and target discovery for bone tissue engineering. SEs comprise a genomic region composed of activity enhancer clusters enriched with many factors related to enhancer activity. Compared with TE related genes and genomic regions, SEs are found in all cell lines spanning a highly cell type-specific genomic domain and are associated with master cell-type-specific regulatory genes (45–47). Recent studies have shown that SE-associated genes are involved in multiple bone-related diseases. For instance, *TBXT* has been found to play an essential role in chordoma pathogenesis (48), and was associated with SE, where transcriptional cyclin-dependent kinase(CDK)inhibitors could downregulate the expression of brachyury/TBXT. Similarly, Lin et al. (49) reported that MEIS1, an SE-associated oncogene, promotes the malignant development of Ewing sarcoma by synergistic activation of APCDD1 transcription with EWS-FLI1. These studies indicate that SE-associated mRNAs can play essential roles in bone regulation. In this study, we identified the SE-lncRNA LINC01485 through bioinformatics investigation and found that it was elevated during the osteogenic differentiation of hBMSCs.

SE-lncRNAs are transcribed from or interact with SEs. A higher percentage of SEs are reported to generate eRNAs termed seRNAs compared to TEs (50). LINC01485 is located on chromosome 5q35.2 and has been shown to be an oncogenic gene. In earlier work, LINC01485 has been reported to promote the growth and migration of gastric cancer cells by inhibiting

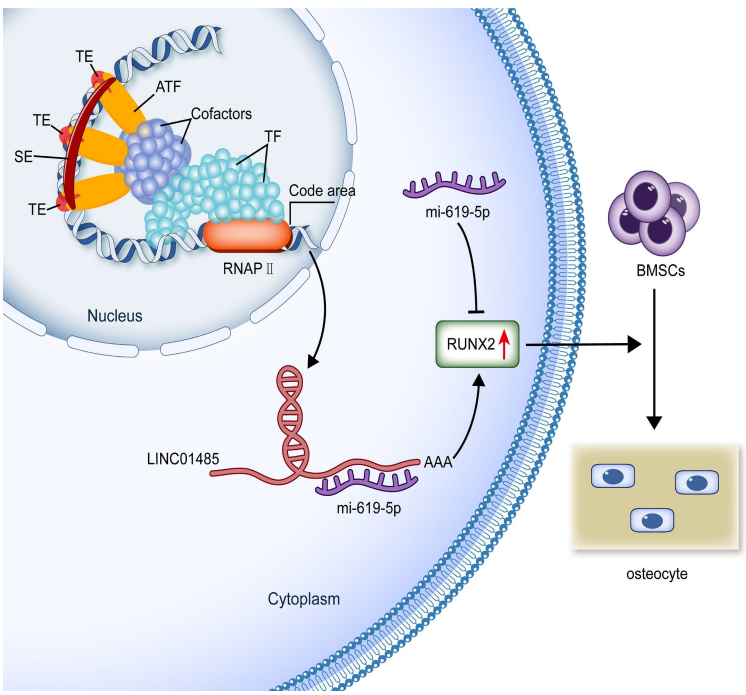

FIGURE 7 | Production and possible functional mechanism of SE-lncRNA LINC01485. SEs are a genomic region composed of activity enhancer clusters enriched with many factors related to enhancer activity. SEs can increase the transcription and production of elncRNAs. SE-lncRNA LINC01485 competitively binds to miR-619-5p in the cytoplasm to promote RUNX2 expression regulating osteogenic differentiation of hBMSCs. (SE, super-enhancer; TE, typical enhancer; ATF, activating transcription factor; TF, transcription factor; RNAPII, RNA polymerase II; BMSCs, bone marrow mesenchymal stem cells.).

EGFR ubiquitination and activating its downstream Akt signal (44). Additionally, LINC01485 was reported among the 6 lncRNAs that emerged as prognostic indicators for colorectal cancer (51). However, no studies have explored the role of LINC01485 in osteogenic differentiation. The present study demonstrated that the overexpression of LINC01485 could promote osteogenic differentiation as indicated by increase in ALP activity and ALP staining, along with enhanced production of calcified nodules and expression of osteoblast differentiation markers, while the knockdown of LINC01485 exerted the opposite effects on osteogenic differentiation. These results indicated that LINC01485 could positively regulate the osteogenic differentiation of hBMSCs.

elncRNAs perform regulatory transcriptional functions by -cis and -trans mechanisms (21). The roles of seRNAs include chromatin loops stabilization, and transcription factor recruitment among others, and thus seRNAs mediate various cellular activities in the cytoplasm (52). To further explore the molecular mechanism of LINC01485 involvement in osteogenic differentiation process, we first identified the subcellular localization of LINC01485 and found that LINC01485 is mainly localized in the cytoplasm, consistent with the results reported by Zhou et al. (44). The cellular localization of lncRNAs is closely related to its mechanism of action. Cytoplasmic lncRNAs can regulate the stability and transcription of mRNA and exert their functions mainly through transcription or translation regulation (53). For instance, in related studies (38, 54) super-enhancer-regulated lncRNA UCA1 has been found to serve as an endogenous competitive RNA binding miR-193a-3p to regulate ERBB4, thereby promoting proliferation and colony formation of lung cancer cells. In yet another finding, Wang et al. (55) reported that UCA1 could repress the host immune system, stimulate the proliferation and migration of gastric cancer cells, and inhibit apoptosis of gastric cancer cells by directly interacting with miR-26a/b, miR-193a, and miR-214 anti-tumor miRNAs to up-regulate PDL1 expression. Here, we predicted the binding of LINC01485 to miR-619-5p using in-silico approaches and verified this relationship by performing RAP and luciferase assays. Cross-talk between lncRNA and miRNA has been found to be involved in a variety of osteogenic signaling pathways, including TGF/BMP-SMAD dependent and non-dependent, and the Wnt/β-catenin pathways (56–58). Specifically, miR-619-5p has been shown to improve pancreatic cancer sensitivity to gemcitabine by targeting Pygo2 and activating the Wnt/β-catenin pathway (59). The Wnt/β-catenin pathway is shown to play a critical role in regulating the osteogenic differentiation of hMSCs (60, 61). Therefore, here we hypothesized that miR-619-5p might be involved in osteodifferentiation of hBMSCs by activating the osteogenesis-related Wnt/β-catenin pathway and subsequently demonstrated that miR-619-5p, as a negative regulator of osteogenic differentiation, could inhibit the protein expression levels of RUNX2, COL1A1, OSX, and OPN, and reduce ALP staining.

Earlier research has revealed the post-transcriptional interaction between lncRNA and miRNA as gene expression regulators in the process of BMSCs osteogenic differentiation (12). We predicted the mRNAs binding to miR-619-5p through bioinformatics. Among these genes, we focused on the osteogenic transcription factor RUNX2, based on the fact that Wnt signaling can promote osteogenesis by directly stimulating RUNX2 gene expression (62). RUNX2 is the primary regulating gene for the osteoblast phenotype (63) and binds to osteoblasts-specific cis-acting elements (OSE)-2 in the promoter region of osteogenic genes (64). RUNX2 has also been well demonstrated to promote the mineralization of bone nodules by up-regulating several osteoblast differentiation marker genes (e.g., ALP, COL1A1, OSX, OCN, and OPN) (65–67). These genes regulated by RUNX2 were found to be up-regulated when hBMSCs overexpressed LINC01485, and vice versa, these genes were downregulated upon interference with LINC01485. These results indirectly indicated that RUNX2 might be a target gene associated with LINC01485 during the osteodifferentiation process of hBMSCs. Previous studies have reported that the osteogenic promoting role of RUNX2 is regulated by other ceRNA signaling axes, including lncRNA NTF3-5/miR-93-3p/RUNX2 (68), LncRNA TUG1/miR-204-5p/RUNX2 (69), lncRNA MALAT1/miR-30/RUNX2 (17), lncRNA MALAT1/miR-124/RUNX2 (70), lncRNA MEG3/miR-140-5p/RUNX2 (71), lncRNA KCNQ1OT1/miR-138/RUNX2 (72), lncRNA MODR/miR-454/RUNX2 (73), and lncRNA DGCR5/miR-30d-5p/RUNX2 (74). Sponging of miRNAs by lncRNAs has been demonstrated as a regulatory mechanism in this context. By sponging miR-93-3p, lnc-NTF3-5 has been found to stimulate osteogenic differentiation of maxillary sinus membrane stem cells (68). LncRNA TUG1 is shown to promote osteogenic differentiation by up-regulating RUNX2 in aortic valve calcification through sponging miR-204-5p (69). Here, a negative relationship between miR-619-5p and LINC01485, a negative correlation between miR-619-5p and RUNX2, and a positive correlation between LINC01485 and RUNX2 were each demonstrated. In addition, the binding of miR-619-5p to RUNX2 was verified by luciferase assay. According to the competing endogenous RNA (ceRNA) hypothesis proposed by Salmena et al. (75), lncRNA can bind competitively to miRNAs and thus further enhance mRNA's stability, transcription, and translation. We designed and conducted rescue experiments to verify the regulatory relationships among LINC01485, miR-619-5p, and RUNX2. Luciferase assays showed that miR-619-5p mimic inhibited the luciferase activity of RUNX2-WT, while the overexpression of LINC01485 promoted luciferase activity. At the cellular level, Western blot and ALP staining indicated that miR-619-5p inhibitor countered the effects of LINC01485 interference on RUNX2 and hBMSCs osteogenic differentiation. MiR-619-5p mimic also reduced the enhanced ALP staining effect of LINC01485 overexpression. These findings are consistent with the ceRNAs hypothesis, confirming the existence of endogenous sponge competition between LINC01485 and miR-619-5p, highlighting the role of the ceRNAs axis LINC01485/miR-619-5p/RUNX2 in regulating bone cell differentiation (**Figure 7**).

The potential limitations of current research must be considered. First, this study did not investigate osteogenesis by performing *in vivo* experiments to verify the reported *in vitro* findings. Animal experiments to confirm whether LNC01485

promotes osteogenesis by competitively binding to miR-619-5p are thus warranted. Second, the regulatory relationships involving SEs and lncRNAs in MSCs osteogenic differentiation remain to be addressed. The interaction between LINC01485 and SEs merits deeper exploration in future research. At the same time, the main findings bear potential implications for future research. The LINC01485/miR-619-5p/RUNX2 signaling axis revealed by the current study suggests a novel target for the genetic and epigenetic modification of hBMSCs. Such an approach could potentially enhance bone formation and thus hold promise in the stem cell-based bone tissue engineering area.

CONCLUSION

In conclusion, this study identified that the SE-lncRNA LINC01485 was up-regulated during the osteogenic differentiation of hBMSCs. The upregulation of LINC015485 was found to promote osteogenic differentiation of hBMSCs by competitively binding miR-619-5p and up-regulating RUNX2 expression. The LINC01485/miR-619-5p/RUNX2 signaling axis emerged as a promising target for translation in the bone tissue engineering arena.

DATA AVAILABILITY STATEMENT

The original contributions presented in the study are included in the article/**Supplementary Material**. Further inquiries can be directed to the corresponding authors.

AUTHOR CONTRIBUTIONS

WG conceptualized the study design, carried out the experiments, performed the statistical analyses, and wrote the manuscript. XJ, WW, JL, ZM, HT, and SL were involved in the statistical analyses. HX and JZ supervised the whole research project. All authors edited and approved the final manuscript.

FUNDING

This study was supported by the National Natural Science Foundation of China (No.81670950).

SUPPLEMENTARY MATERIAL

The Supplementary Material for this article can be found online at: https://www.frontiersin.org/articles/10.3389/fendo.2022.846154/full#supplementary-material

Supplementary Table 1 | lncRNAs in the D14 group of specific SE-associated genes.

Supplementary Table 2 | The forward and reverse sequence of primers for SE-associated lncRNAs in qRT-PCR assay.

Supplementary Table 3 | The forward and reverse sequence of primers for genes examined in qRT-PCR assay.

Supplementary Table 4 | LINC01485 interference sequence.

Supplementary Table 5 | miR-619-5p mimic and miR-619-5p inhibitor sequence.

Supplementary Table 6 | LINC01485 FISH probe sequence (FAM).

Supplementary Table 7 | LINC01485 RAP probe sequence.

Supplementary Figure 1 | The qRT-PCR validation of lncRNAs in the D14 group of specific SE-associated genes before and after osteogenic differentiation of hBMSCs.

Supplementary Figure 2 | Electrophoretic diagram of RAP qRT-PCR products.

REFERENCES

1. Aghali A. Craniofacial Bone Tissue Engineering: Current Approaches and Potential Therapy. *Cells* (2021) 10(11). doi: 10.3390/cells10112993
2. Baldwin P, Li DJ, Auston DA, Mir HS, Yoon RS, Koval KJ. Autograft, Allograft, and Bone Graft Substitutes: Clinical Evidence and Indications for Use in the Setting of Orthopaedic Trauma Surgery. *J Orthop Trauma* (2019) 33(4):203–13. doi: 10.1097/BOT.0000000000001420
3. Xia D, Yang F, Zheng Y, Liu Y, Zhou Y. Research Status of Biodegradable Metals Designed for Oral and Maxillofacial Applications: A Review. *Bioact Mater* (2021) 6(11):4186–208. doi: 10.1016/j.bioactmat.2021.01.011
4. Dave JR, Tomar GB. Dental Tissue-Derived Mesenchymal Stem Cells: Applications in Tissue Engineering. *Crit Rev BioMed Eng* (2018) 46(5):429–68. doi: 10.1615/CritRevBiomedEng.2018027342
5. Aghali A, Arman HE. Photoencapsulated-Mesenchymal Stromal Cells in Biodegradable Thiol-Acrylate Hydrogels Enhance Regeneration of Craniofacial Bone Tissue Defects. *Regener Med* (2020) 15(9):2115–27. doi: 10.2217/rme-2020-0061
6. Khodakaram-Tafti A, Mehrabani D, Shaterzadeh-Yazdi H, Zamiri B, Omidi M. Tissue Engineering in Maxillary Bone Defects. *World J Plast Surg* (2018) 7(1).
7. Diomede F, Gugliandolo A, Cardelli P, Merciaro I, Ettorre V, Traini T, et al. Three-Dimensional Printed PLA Scaffold and Human Gingival Stem Cell-Derived Extracellular Vesicles: A New Tool for Bone Defect Repair. *Stem Cell Res Ther* (2018) 9(1):104. doi: 10.1186/s13287-018-0850-0
8. Emara AA, Shah R. Recent Update on Craniofacial Tissue Engineering. *J Tissue Eng* (2021) 12:20417314211003735. doi: 10.1177/20417314211003735
9. Zhang J, Hao X, Yin M, Xu T, Guo F. Long Non-Coding RNA in Osteogenesis: A New World to be Explored. *Bone Joint Res* (2019) 8(2):73–80. doi: 10.1302/2046-3758.82.BJR-2018-0074.R1
10. Yang Q, Jia L, Li X, Guo R, Huang Y, Zheng Y, et al. Long Noncoding RNAs: New Players in the Osteogenic Differentiation of Bone Marrow- and Adipose-Derived Mesenchymal Stem Cells. *Stem Cell Rev Rep* (2018) 14(3):297–308. doi: 10.1007/s12015-018-9801-5
11. Ju C, Liu R, Zhang Y-W, Zhang Y, Zhou R, Sun J, et al. Mesenchymal Stem Cell-Associated LncRNA in Osteogenic Differentiation. *BioMed Pharmacother* (2019) 115:108912. doi: 10.1016/j.biopha.2019.108912
12. Lanzillotti C, De Mattei M, Mazziotta C, Taraballi F, Rotondo JC, Tognon M, et al. Long Non-Coding RNAs and MicroRNAs Interplay in Osteogenic Differentiation of Mesenchymal Stem Cells. *Front Cell Dev Biol* (2021) 9:646032. doi: 10.3389/fcell.2021.646032

13. Huynh NPT, Anderson BA, Guilak F, McAlinden A. Emerging Roles for Long Noncoding RNAs in Skeletal Biology and Disease. *Connect Tissue Res* (2017) 58(1):116–41. doi: 10.1080/03008207.2016.1194406
14. Zhou Z, Hossain MS, Liu D. Involvement of the Long Noncoding RNA H19 in Osteogenic Differentiation and Bone Regeneration. *Stem Cell Res Ther* (2021) 12(1):74. doi: 10.1186/s13287-021-02149-4
15. Li T, Jiang H, Li Y, Zhao X, Ding H. Estrogen Promotes LncRNA H19 Expression to Regulate Osteogenic Differentiation of Bmscs and Reduce Osteoporosis *via* MiR-532-3p/SIRT1 Axis. *Mol Cell Endocrinol* (2021) 527:111171. doi: 10.1016/j.mce.2021.111171
16. Yang X, Yang J, Lei P, Wen T. LncRNA MALAT1 Shuttled by Bone Marrow-Derived Mesenchymal Stem Cells-Secreted Exosomes Alleviates Osteoporosis Through Mediating MicroRNA-34c/SATB2 Axis. *Aging (Albany NY)* (2019) 11(20):8777–91. doi: 10.18632/aging.102264
17. Yi J, Liu D, Xiao J. LncRNA MALAT1 Sponges MiR-30 to Promote Osteoblast Differentiation of Adipose-Derived Mesenchymal Stem Cells by Promotion of Runx2 Expression. *Cell Tissue Res* (2019) 376(1):113–21. doi: 10.1007/s00441-018-2963-2
18. Wang Q, Li Y, Zhang Y, Ma L, Lin L, Meng J, et al. LncRNA MEG3 Inhibited Osteogenic Differentiation of Bone Marrow Mesenchymal Stem Cells From Postmenopausal Osteoporosis by Targeting MiR-133a-3p. *BioMed Pharmacother* (2017) 89:1178–86. doi: 10.1016/j.biopha.2017.02.090
19. Li R, Zhang W, Yan Z, Liu W, Fan J, Feng Y, et al. Long non-Coding RNA (LncRNA) HOTAIR Regulates BMP9-Induced Osteogenic Differentiation by Targeting the Proliferation of Mesenchymal Stem Cells (MSCs). *Aging (Albany NY)* (2021) 13(3):4199–214. doi: 10.18632/aging.202384
20. Hnisz D, Abraham BJ, Lee TI, Lau A, Saint-André V, Sigova AA, et al. Super-Enhancers in the Control of Cell Identity and Disease. *Cell* (2013) 155(4):934–47. doi: 10.1016/j.cell.2013.09.053
21. Ounzain S, Pedrazzini T. Super-Enhancer Lncs to Cardiovascular Development and Disease. *Biochim Biophys Acta* (2016) 1863(7 Pt B):1953–60. doi: 10.1016/j.bbamcr.2015.11.026
22. Alvarez-Dominguez JR, Knoll M, Gromatzky AA, Lodish HF. The Super-Enhancer-Derived AlncRNA-EC7/Bloodlinc Potentiates Red Blood Cell Development in Trans. *Cell Rep* (2017) 19(12):2503–14. doi: 10.1016/j.celrep.2017.05.082
23. Qu J, Ouyang Z, Wu W, Li G, Wang J, Lu Q, et al. Functions and Clinical Significance of Super-Enhancers in Bone-Related Diseases. *Front Cell Dev Biol* (2020) 8:534. doi: 10.3389/fcell.2020.00534
24. Zhang J, Liu W, Zou C, Zhao Z, Lai Y, Shi Z, et al. Targeting Super-Enhancer-Associated Oncogenes in Osteosarcoma With THZ2, A Covalent CDK7 Inhibitor. *Clin Cancer Res* (2020) 26(11):2681–92. doi: 10.1158/1078-0432.CCR-19-1418
25. Kennedy AL, Vallurupalli M, Chen L, Crompton B, Cowley G, Vazquez F, et al. Functional, Chemical Genomic, and Super-Enhancer Screening Identify Sensitivity to Cyclin D1/CDK4 Pathway Inhibition in Ewing Sarcoma. *Oncotarget* (2015) 6(30):30178–93. doi: 10.18632/oncotarget.4903
26. Lovén J, Hoke HA, Lin CY, Lau A, Orlando DA, Vakoc CR, et al. Selective Inhibition of Tumor Oncogenes by Disruption of Super-Enhancers. *Cell* (2013) 153(2):320–34. doi: 10.1016/j.cell.2013.03.036
27. Jiang Y, Zhu L, Zhang T, Lu H, Wang C, Xue B, et al. BRD4 has Dual Effects on the HMGB1 and NF-κB Signalling Pathways and Is a Potential Therapeutic Target for Osteoarthritis. *Biochim Biophys Acta Mol Basis Dis* (2017) 1863(12):3001–15. doi: 10.1016/j.bbadis.2017.08.009
28. Yu W, Chen K, Ye G, Wang S, Wang P, Li J, et al. SNP-Adjacent Super Enhancer Network Mediates Enhanced Osteogenic Differentiation of Mscs in Ankylosing Spondylitis. *Hum Mol Genet* (2021) 30(3-4):277–93. doi: 10.1093/hmg/ddaa272
29. Chen H, Zheng J, Yan L, Zhou X, Jiang P, Yan F. Super-Enhancer-Associated Long Noncoding RNA RP11-569A11.1 Inhibited Cell Progression and Metastasis by Regulating IFIT2 in Colorectal Cancer. *J Clin Lab Anal* (2021) 35(6):e23780. doi: 10.1002/jcla.23780
30. Hsieh C-L, Fei T, Chen Y, Li T, Gao Y, Wang X, et al. Enhancer RNAs Participate in Androgen Receptor-Driven Looping That Selectively Enhances Gene Activation. *Proc Natl Acad Sci USA* (2014) 111(20):7319–24. doi: 10.1073/pnas.1324151111
31. Iiott NE, Heward JA, Roux B, Tsitsiou E, Fenwick PS, Lenzi L, et al. Long Non-Coding RNAs and Enhancer RNAs Regulate the Lipopolysaccharide-Induced Inflammatory Response in Human Monocytes. *Nat Commun* (2014) 5:3979. doi: 10.1038/ncomms4979
32. Pnueli L, Rudnizky S, Yosefzon Y, Melamed P. RNA Transcribed From a Distal Enhancer is Required for Activating the Chromatin at the Promoter of the Gonadotropin α-Subunit Gene. *Proc Natl Acad Sci USA* (2015) 112 (14):4369–74. doi: 10.1073/pnas.1414841112
33. Schaukowitch K, Joo J-Y, Liu X, Watts JK, Martinez C, Kim T-K. Enhancer RNA Facilitates NELF Release From Immediate Early Genes. *Mol Cell* (2014) 56(1):29–42. doi: 10.1016/j.molcel.2014.08.023
34. Yan P, Lu JY, Niu J, Gao J, Zhang MQ, Yin Y, et al. LncRNA Platr22 Promotes Super-Enhancer Activity and Stem Cell Pluripotency. *J Mol Cell Biol* (2021) 13 (4):295–313. doi: 10.1093/jmcb/mjaa056
35. Jiang Y, Jiang Y-Y, Xie J-J, Mayakonda A, Hazawa M, Chen L, et al. Co-Activation of Super-Enhancer-Driven CCAT1 by TP63 and SOX2 Promotes Squamous Cancer Progression. *Nat Commun* (2018) 9(1):3619. doi: 10.1038/s41467-018-06081-9
36. Xie J-J, Jiang Y-Y, Jiang Y, Li C-Q, Lim M-C, An O, et al. Super-Enhancer-Driven Long Non-Coding RNA LINC01503, Regulated by TP63, Is Over-Expressed and Oncogenic in Squamous Cell Carcinoma. *Gastroenterology* (2018) 154(8). doi: 10.1053/j.gastro.2018.02.018
37. Wang X, Zhang R, Wu S, Shen L, Ke M, Ouyang Y, et al. Super-Enhancer LncRNA LINC00162 Promotes Progression of Bladder Cancer. *iScience* (2020) 23(12):101857. doi: 10.1016/j.isci.2020.101857
38. Lin X, Spindler TJ, de Souza Fonseca MA, Corona RI, Seo J-H, Dezem FS, et al. Super-Enhancer-Associated LncRNA UCA1 Interacts Directly With AMOT to Activate YAP Target Genes in Epithelial Ovarian Cancer. *iScience* (2019) 17:242–55. doi: 10.1016/j.isci.2019.06.025
39. Plaisance I, Perruchoud S, Fernandez-Tenorio M, Gonzales C, Ounzain S, Ruchat P, et al. Cardiomyocyte Lineage Specification in Adult Human Cardiac Precursor Cells *via* Modulation of Enhancer-Associated Long Noncoding RNA Expression. *JACC Basic Transl Sci* (2016) 1(6):472–93. doi: 10.1016/j.jacbts.2016.06.008
40. Huang Z, Jia B, Wang Q, Wang N, Zhao J. The Potential Function of Super Enhancers in Human Bone Marrow Mesenchymal Stem Cells During Osteogenic Differentiation. *BioMed Res Int* (2021) 2021:6614762. doi: 10.1155/2021/6614762
41. Ing-Simmons E, Seitan VC, Faure AJ, Flicek P, Carroll T, Dekker J, et al. Spatial Enhancer Clustering and Regulation of Enhancer-Proximal Genes by Cohesin. *Genome Res* (2015) 25(4):504–13. doi: 10.1101/gr.184986.114
42. Heinz S, Benner C, Spann N, Bertolino E, Lin YC, Laslo P, et al. Simple Combinations of Lineage-Determining Transcription Factors Prime Cis-Regulatory Elements Required for Macrophage and B Cell Identities. *Mol Cell* (2010) 38(4):576–89. doi: 10.1016/j.molcel.2010.05.004
43. Hazan I, Monin J, Bouwman BAM, Crosetto N, Aqeilan RI. Activation of Oncogenic Super-Enhancers is Coupled With DNA Repair by RAD51. *Cell Rep* (2019) 29(3). doi: 10.1016/j.celrep.2019.09.001
44. Zhou J, Wu L, Li W, Xu X, Ju F, Yu S, et al. Long Noncoding RNA LINC01485 Promotes Tumor Growth and Migration *via* Inhibiting EGFR Ubiquitination and Activating EGFR/Akt Signaling in Gastric Cancer. *Onco Targets Ther* (2020) 13:8413–25. doi: 10.2147/OTT.S257151
45. Fang Z, Hecklau K, Gross F, Bachmann I, Venzke M, Karl M, et al. Transcription Factor Co-Occupied Regions in the Murine Genome Constitute T-Helper-Cell Subtype-Specific Enhancers. *Eur J Immunol* (2015) 45(11):3150–7. doi: 10.1002/eji.201545713
46. Hah N, Benner C, Chong L-W, Yu RT, Downes M, Evans RM. Inflammation-Sensitive Super Enhancers Form Domains of Coordinately Regulated Enhancer RNAs. *Proc Natl Acad Sci USA* (2015) 112(3):E297–302. doi: 10.1073/pnas.1424028112
47. Vahedi G, Kanno Y, Furumoto Y, Jiang K, Parker SCJ, Erdos MR, et al. Super-Enhancers Delineate Disease-Associated Regulatory Nodes in T Cells. *Nature* (2015) 520(7548):558–62. doi: 10.1038/nature14154
48. Sharifnia T, Wawer MJ, Chen T, Huang Q-Y, Weir BA, Sizemore A, et al. Small-Molecule Targeting of Brachyury Transcription Factor Addiction in Chordoma. *Nat Med* (2019) 25(2):292–300. doi: 10.1038/s41591-018-0312-3
49. Lin L, Huang M, Shi X, Mayakonda A, Hu K, Jiang Y-Y, et al. Super-Enhancer-Associated MEIS1 Promotes Transcriptional Dysregulation in Ewing Sarcoma in Co-Operation With EWS-FLI1. *Nucleic Acids Res* (2019) 47(3):1255–67. doi: 10.1093/nar/gky1207

50. Zhao Y, Zhou J, He L, Li Y, Yuan J, Sun K, et al. Myod Induced Enhancer RNA Interacts With Hnrnpl to Activate Target Gene Transcription During Myogenic Differentiation. *Nat Commun* (2019) 10(1):5787. doi: 10.1038/s41467-019-13598-0
51. Huang X, Cai W, Yuan W, Peng S. Identification of Key LncRNAs as Prognostic Prediction Models for Colorectal Cancer Based on LASSO. *Int J Clin Exp Pathol* (2020) 13(4):675–84.
52. Xiao S, Huang Q, Ren H, Yang M. The Mechanism and Function of Super Enhancer RNA. *Genesis* (2021) 59(5-6):e23422. doi: 10.1002/dvg.23422
53. Schmitt AM, Chang HY. Long Noncoding RNAs in Cancer Pathways. *Cancer Cell* (2016) 29(4):452–63. doi: 10.1016/j.ccell.2016.03.010
54. Nie W, Ge H-J, Yang X-Q, Sun X, Huang H, Tao X, et al. LncRNA-UCA1 Exerts Oncogenic Functions in Non-Small Cell Lung Cancer by Targeting MiR-193a-3p. *Cancer Lett* (2016) 371(1). doi: 10.1016/j.canlet.2015.11.024
55. Wang C-J, Zhu C-C, Xu J, Wang M, Zhao W-Y, Liu Q, et al. Correction to: The LncRNA UCA1 Promotes Proliferation, Migration, Immune Escape and Inhibits Apoptosis in Gastric Cancer by Sponging Anti-Tumor MiRNAs. *Mol Cancer* (2021) 20(1):120. doi: 10.1186/s12943-021-01387-7
56. Huang Y, Zheng Y, Jia L, Li W. Long Noncoding RNA H19 Promotes Osteoblast Differentiation *via* TGF-β1/Smad3/HDAC Signaling Pathway by Deriving MiR-675. *Stem Cells* (2015) 33(12):3481–92. doi: 10.1002/stem.2225
57. Gong YY, Peng MY, Yin DQ, Yang YF. Long non-Coding RNA H19 Promotes the Osteogenic Differentiation of Rat Ectomesenchymal Stem Cells *via* Wnt/β-Catenin Signaling Pathway. *Eur Rev Med Pharmacol Sci* (2018) 22(24):8805–13.
58. Jiang XR, Guo N, Li XQ, Yang HY, Wang K, Zhang CL, et al. Long non-Coding RNA HULC Promotes Proliferation and Osteogenic Differentiation of Bone Mesenchymal Stem Cells *via* Down-Regulation of MiR-195. *Eur Rev Med Pharmacol Sci* (2018) 22(10):2954–65.
59. Zhou C, Yi C, Yi Y, Qin W, Yan Y, Dong X, et al. LncRNA PVT1 Promotes Gemcitabine Resistance of Pancreatic Cancer *via* Activating Wnt/β-Catenin and Autophagy Pathway Through Modulating the MiR-619-5p/Pygo2 and MiR-619-5p/ATG14 Axes. *Mol Cancer* (2020) 19(1):118. doi: 10.1186/s12943-020-01237-y
60. Yuan Z, Li Q, Luo S, Liu Z, Luo D, Zhang B, et al. PPARγ and Wnt Signaling in Adipogenic and Osteogenic Differentiation of Mesenchymal Stem Cells. *Curr Stem Cell Res Ther* (2016) 11(3):216–25. doi: 10.2174/1574888X10666150519093429
61. Wang Q, Cai J, Cai X-H, Chen L. MiR-346 Regulates Osteogenic Differentiation of Human Bone Marrow-Derived Mesenchymal Stem Cells by Targeting the Wnt/β-Catenin Pathway. *PloS One* (2013) 8(9):e72266. doi: 10.1371/journal.pone.0072266
62. Gaur T, Lengner CJ, Hovhannisyan H, Bhat RA, Bodine PVN, Komm BS, et al. Canonical WNT Signaling Promotes Osteogenesis by Directly Stimulating Runx2 Gene Expression. *J Biol Chem* (2005) 280(39):33132–40. doi: 10.1074/jbc.M500608200
63. An J, Yang H, Zhang Q, Liu C, Zhao J, Zhang L, et al. Natural Products for Treatment of Osteoporosis: The Effects and Mechanisms on Promoting Osteoblast-Mediated Bone Formation. *Life Sci* (2016) 147:46–58. doi: 10.1016/j.lfs.2016.01.024
64. Franceschi RT, Xiao G, Jiang D, Gopalakrishnan R, Yang S, Reith E. Multiple Signaling Pathways Converge on the Cbfa1/Runx2 Transcription Factor to Regulate Osteoblast Differentiation. *Connect Tissue Res* (2003) 44 Suppl 1:109–16. doi: 10.1080/03008200390152188
65. Nishio Y, Dong Y, Paris M, O'Keefe RJ, Schwarz EM, Drissi H. Runx2-Mediated Regulation of the Zinc Finger Osterix/Sp7 Gene. *Gene* (2006) 372:62–70. doi: 10.1016/j.gene.2005.12.022
66. Vimalraj S, Arumugam B, Miranda PJ, Selvamurugan N. Runx2: Structure, Function, and Phosphorylation in Osteoblast Differentiation. *Int J Biol Macromol* (2015) 78:202–8. doi: 10.1016/j.ijbiomac.2015.04.008
67. Hinoi E, Fujimori S, Wang L, Hojo H, Uno K, Yoneda Y. Nrf2 Negatively Regulates Osteoblast Differentiation *via* Interfering With Runx2-Dependent Transcriptional Activation. *J Biol Chem* (2006) 281(26):18015–24. doi: 10.1074/jbc.M600603200
68. Peng W, Zhu S-X, Wang J, Chen L-L, Weng J-Q, Chen S-L. Lnc-NTF3-5 Promotes Osteogenic Differentiation of Maxillary Sinus Membrane Stem Cells *via* Sponging MiR-93-3p. *Clin Implant Dent Relat Res* (2018) 20(2):110–21. doi: 10.1111/cid.12553
69. Yu C, Li L, Xie F, Guo S, Liu F, Dong N, et al. LncRNA TUG1 Sponges MiR-204-5p to Promote Osteoblast Differentiation Through Upregulating Runx2 in Aortic Valve Calcification. *Cardiovasc Res* (2018) 114(1):168–79. doi: 10.1093/cvr/cvx180
70. Zhang Y, Guo H, Ma L, Zhu J, Guo A, He Y. [Study on Adsorption of MicroRNA-124 by Long Chain Non-Coding RNA MALAT1 Regulates Osteogenic Differentiation of Mesenchymal Stem Cells]. *Zhongguo Xiu Fu Chong Jian Wai Ke Za Zhi* (2020) 34(2):240–5.
71. Li Z, Jin C, Chen S, Zheng Y, Huang Y, Jia L, et al. Long non-Coding RNA MEG3 Inhibits Adipogenesis and Promotes Osteogenesis of Human Adipose-Derived Mesenchymal Stem Cells *via* MiR-140-5p. *Mol Cell Biochem* (2017) 433(1-2):51–60. doi: 10.1007/s11010-017-3015-z
72. Yu Y, Chen Y, Zhang X, Lu X, Hong J, Guo X, et al. Knockdown of LncRNA KCNQ1OT1 Suppresses the Adipogenic and Osteogenic Differentiation of Tendon Stem Cell *via* Downregulating MiR-138 Target Genes PPARγ and RUNX2. *Cell Cycle* (2018) 17(19-20):2374–85. doi: 10.1080/15384101.2018.1534510
73. Weng J, Peng W, Zhu S, Chen S. Long Noncoding RNA Sponges MiR-454 to Promote Osteogenic Differentiation in Maxillary Sinus Membrane Stem Cells. *Implant Dent* (2017) 26(2):178–86. doi: 10.1097/ID.0000000000000569
74. Wu Z-H, Huang K-H, Liu K, Wang G-T, Sun Q. DGCR5 Induces Osteogenic Differentiation by Up-Regulating Runx2 Through MiR-30d-5p. *Biochem Biophys Res Commun* (2018) 505(2):426–31. doi: 10.1016/j.bbrc.2018.09.033
75. Salmena L, Poliseno L, Tay Y, Kats L, Pandolfi PP. A ceRNA Hypothesis: The Rosetta Stone of a Hidden RNA Language? *Cell* (2011) 146(3):353–8. doi: 10.1016/j.cell.2011.07.014

Conflict of Interest: The authors declare that the research was conducted in the absence of any commercial or financial relationships that could be construed as a potential conflict of interest.

Publisher's Note: All claims expressed in this article are solely those of the authors and do not necessarily represent those of their affiliated organizations, or those of the publisher, the editors and the reviewers. Any product that may be evaluated in this article, or claim that may be made by its manufacturer, is not guaranteed or endorsed by the publisher.

frontiers | Frontiers in Endocrinology

TYPE Original Research
PUBLISHED 25 August 2022
DOI 10.3389/fendo.2022.924927

OPEN ACCESS

EDITED BY
Michaela Tencerova,
Academy of Sciences of the Czech Republic (ASCR), Czechia

REVIEWED BY
Michelle Griffin,
University College London, United Kingdom
Michaela Bosakova,
Masaryk University, Czechia

*CORRESPONDENCE
Charles K. F. Chan
chazchan@stanford.edu

†These authors have contributed equally to this work and share first authorship

SPECIALTY SECTION
This article was submitted to Bone Research, a section of the journal Frontiers in Endocrinology

RECEIVED 20 April 2022
ACCEPTED 13 July 2022
PUBLISHED 25 August 2022

CITATION
Goodnough LH, Ambrosi TH, Steininger HM, Butler MGK, Hoover MY, Choo H, Van Rysselberghe NL, Bellino MJ, Bishop JA, Gardner MJ and Chan CKF (2022) Cross-species comparisons reveal resistance of human skeletal stem cells to inhibition by non-steroidal anti-inflammatory drugs. *Front. Endocrinol.* 13:924927. doi: 10.3389/fendo.2022.924927

Cross-species comparisons reveal resistance of human skeletal stem cells to inhibition by non-steroidal anti-inflammatory drugs

L. Henry Goodnough[1†], Thomas H. Ambrosi[2,3†], Holly M. Steininger[2†], M. Gohazrua K. Butler[2], Malachia Y. Hoover[2], HyeRan Choo[3], Noelle L. Van Rysselberghe[1], Michael J. Bellino[1], Julius A. Bishop[1], Michael J. Gardner[1] and Charles K. F. Chan[2,3*]

[1]Department of Orthopaedic Surgery, Stanford Hospitals and Clinics, Stanford, CA, United States, [2]Institute for Stem Cell Biology and Regenerative Medicine, Stanford University School of Medicine, Stanford, CA, United States, [3]Division of Plastic and Reconstructive Surgery, Department of Surgery, Stanford University School of Medicine, Stanford, CA, United States

Fracture healing is highly dependent on an early inflammatory response in which prostaglandin production by cyclo-oxygenases (COX) plays a crucial role. Current patient analgesia regimens favor opioids over Non-Steroidal Anti-Inflammatory Drugs (NSAIDs) since the latter have been implicated in delayed fracture healing. While animal studies broadly support a deleterious role of NSAID treatment to bone-regenerative processes, data for human fracture healing remains contradictory. In this study, we prospectively isolated mouse and human skeletal stem cells (SSCs) from fractures and compared the effect of various NSAIDs on their function. We found that osteochondrogenic differentiation of COX2-expressing mouse SSCs was impaired by NSAID treatment. In contrast, human SSCs (hSSC) downregulated COX2 expression during differentiation and showed impaired osteogenic capacity if COX2 was lentivirally overexpressed. Accordingly, short- and long-term treatment of hSSCs with non-selective and selective COX2 inhibitors did not affect colony forming ability, chondrogenic, and osteogenic differentiation potential *in vitro*. When hSSCs were transplanted ectopically into NSG mice treated with Indomethacin, graft mineralization was unaltered compared to vehicle injected mice. Thus, our results might contribute to understanding species-specific differences in NSAID sensitivity during fracture healing and support emerging clinical data which conflicts with other earlier observations that NSAID administration for post-operative analgesia for treatment of bone fractures are unsafe for patients.

KEYWORDS

skeletal stem cells (SSCs), non-steroid antiinflamatory drugs, species specificity, bone regeneration, inflammation, fracture healing

Introduction

Non-steroidal anti-inflammatory drugs (NSAIDs) are commonly used for pain relief after operative treatment of fractures, and there is significant clinical interest as to whether NSAID administration itself has a deleterious effect on fracture healing in humans. NSAIDs inhibit cyclo-oxygenase (COX) enzymes, including COX1 and COX2, that mitigate prostaglandin production and pain. Whether NSAIDs affect osteoblast progenitor differentiation, inhibit fracture healing, and therefore increase the risk of nonunion, remains controversial. Experimental rodent models overwhelmingly have suggested that NSAID administration inhibits new bone formation and fracture healing (1–4). However, the corresponding generalizability of findings in murine models to humans is uncertain. In humans, the role of NSAIDs on fracture healing is inconclusive. In the clinical setting, historical retrospective studies suggested an association between NSAID use and fracture nonunion, but overall there is a lack of high quality, prospective evidence to conclusively demonstrate a relationship between NSAIDs and delayed union or nonunion (5–8). Mixed data from isolated skeletal cell populations tested for differentiation potential when treated with NSAID has contributed to this dilemma (9, 10). One reason explaining this dichotomy is the fact that bone marrow stromal cells are isolated retrospectively by plastic adherence which yield heterogeneous cell populations thereby leading to varying results (11, 12). We recently demonstrated that mouse and human osteochondrogenic cell types arise from a defined skeletal stem cell (SSC), a self-renewing, multi-potential population giving rise to a transient bone-cartilage-stromal-progenitor (BCSP) that can be isolated by fluorescence-activated cell sorting (FACS) from acute fractures based on their differential expression of a combination of specific cell surface markers. These cells show age-related functional impairments and might also be useful for prospectively assaying fracture healing outcome (13–17). Here, we reasoned that if we compared the effect of NSAIDs on freshly purified, functionally defined skeletal lineage cell types in mice and humans, we might be able to delineate species-specific effects on their response regarding bone-forming characteristics.

Materials and methods

Study approval

Studies involving the sourcing of human samples was approved by the Stanford IRB. Animal experiments complied with all relevant ethical regulations and were conducted under approved protocols by Stanford's Administrative Panel on Laboratory Animal Care.

Human tissue

hSSCs, human osteoprogenitors (hOPs), and human chondroprogenitors (hCPs) were collected from acute human fractures, and collected for transcriptomic analysis or expanded in culture medium, and differentiated in the presence or absence of NSAIDs or selective COX2 inhibitors as described before (13). Tissues were collected from acute fractures undergoing direct reduction and fixation. As per our previous observation that hSSCs from different long bone fracture sites are functionally identical, we have included specimens from tibial, humerus, radius and ulna fractures of patients aged 18 to 74 years (16). Any soft callus hematoma, which was impeding fracture reduction and considered medical waste, was collected.

Mouse experiments

All animal experiments complied with all relevant ethical regulations and were conducted under approved protocols by Stanford's Administrative Panel on Laboratory Animal Care. Mice were maintained at the Stanford University Research Animal Facility in accordance with Stanford University guidelines. Animals were given food and water ad libitum and housed in temperature-, moisture-, and light-controlled (12h light/dark cycle) micro-insulators. Fracture experiments were conducted on adult (10-12 weeks) male C57BL6/J mice. Subcutaneous transplants of human SSCs were performed in adult male NSG mice (NOD scid gamma; JAX: 005557).

Skeletal stem cell isolation

hSSC were collected as previously described (16). Briefly, the tissue was initially minced with razor blades, collected in 0.22% collagenase digestion buffer (Sigma-Aldrich, Cat#C6885), and incubated at 37°C for 60 minutes under constant agitation. The supernatant was collected and filtered through a 70 μm nylon mesh and quenched in staining media (2% fetal calf serum, FCS, in phosphate-buffered saline, PBS) for subsequent centrifugation at 200 x g at 4°C and resuspension in staining media. Human skeletal cells were separated from RBCs by ACK lysis and washed with staining media. Cells were stained with fluorochrome-conjugated antibodies against CD45, CD235, CD31, TIE2, CD146, Podoplanin, CD164, CD73 (1:50; eBioscience). Flow cytometry was performed on a FACS Aria II. Gating schemes were established with fluorescence-minus-one (FMO) isotype controls and DAPI was used for viability staining. Human SSCs were isolated by CD45-CD235-CD31-TIE2-CD146-PDPN+CD164+CD73+ and hOPs by CD45-CD235-CD31-TIE2-CD146+PDPN- selection gated from single living cells (DAPI-negative).

Mouse SSCs were isolated from 10-day old femoral fracture calluses. Stabilized mid-diaphyseal femoral bi-cortical fractures were generated after inserting an intramedullary pin. Soft tissue-free femurs were processed as described before (18), antibody stained for CD45, Ter119, Thy1.1, Thy1.2, CD105, CD51, 6c3, Tie2, CD200 (eBiosciences) prior to isolation by flow cytometry. Mouse SSCs were isolated by CD45-Ter119-Thy1-CD105-CD51+6c3-Tie2-CD200+ selection gated from single living cells (Propidium Iodide-negative).

Tissue culture and *in vitro* differentiation

For mouse and human colony forming assays, cells were plated at clonal density (defined number of 100 to 500 cells per well of a 6-well plate depending on experiment) and cultured in MEM alpha medium with 10% FBS and 1% pen strep (mouse) or 10% HPL, 1% pen strep, 0.01% heparin (human) maintained at 37°C incubator with 5% CO_2. After two weeks cells were fixed, stained with 0.5% Crystal Violet and examined under phase microscopy and counted.

Osteogenic differentiation media (ODM) (MEM alpha medium, 10% Fetal Bovine Serum, 1% pen strep, 100 nM dexamethasone, 10 mM sodium β-glycerophosphate, 2.5 mM ascorbic acid) was changed every 3 days for 14 days. Cells were then stained with Alizarin Red to assess osteogenic potential. Alizarin red staining was quantified using spectrophotometry. Chondrogenesis assays were conducted in micromasses. Briefly, cells were resuspended at a cell-density of $1.6x10^7$ cells/ml. A 5 µl droplet of the cell suspension was seeded under high humidity conditions in a 24-well plate for 2 hr. After 2 hr, warmed chondrogenic differentiation media was added to the culture vessel. The growing micromass was fed with fresh chondrogenesis media (DMEMhigh [Thermo Fisher Scientific, Cat# 10569010] with 10% FBS, 100 nM dexamethasone, 1 µM ascorbic acid 2-phosphate, and 10 ng/ml TGFβ1 [Peprotech, Cat# 100-21C]) every other day in a 37°C incubator with 5% CO_2. At day 14 the micromass was fixed and stained with Alcian Blue (Sigma-Aldrich, Cat#A5268).

Non-steroidal anti-inflammatory drugs (NSAIDs)

NSAIDs (Ibuprofen (Sigma; Cat#I4883), Ketorolac tris salt (Sigma; Cat#K1136), Indomethacin (Sigma; Cat#I7378)) and the selective COX2 inhibitor Celecoxib (Sigma; Cat# PZ0008) were purchased, stored at RT, and diluted according to manufacturer's specifications. Concentrations were tested according to previous studies based on pharmacokinetics of plasma levels corresponding to typical and maximum intake. NSAIDs were administered to cells *in vitro* at peak plasma levels corresponding to therapeutic levels reported in pharmacokinetic analyses and as indicated in the figures (19–21).

Lentiviral overexpression

A lentivirus plasmid to overexpress COX2 with a dTomato tag was constructed using Gibson cloning of pHIV-dTomato (Addgene cat# 21374) and PTGS2 (Origene Cat#SC128243). HEK-293T cells were transfected using calcium phosphate transfection with VSV-G (addgene Cat #8454), psPAX2 (addgene Cat #12260), and either ZsGreen (addgene Cat#18121) or PTGS2 dTomato. Lentiviral particles were concentrated using Lenti-X concentrator (Takara, Cat#631232) and then immediately used to transduce hSSCs plated one hour prior at 80% confluency at a dilution of 1:100 with 1:1000 polybrene. Confluent cells were FACS sorted by fluorescence for subsequent expansion and differentiation.

Subcutaneous transplantation of human skeletal stem cells

Freshly sorted patient derived hSSCs were sorted and expanded to confluency. $2x10^6$ cells were mixed with 5 ul of Matrigel and seeded on 20 mg anorganic cancellous bone graft granulat (InterOss®, 0.25-1mm) at 4°C. The solution was transferred to a round-bottom 96-well plate well and allowed to solidify for 5 minutes at room temperature. The gelatinized cell mixture was then transplanted subcutaneously in the dorsum of NSG mice. PBS or Indomethacin was administered at 2 mg/kg for the first 7 days after cell transplant. Grafts were excised and analyzed 4- and 8-weeks later.

Micro-CT analysis of grafts

Grafts were dissected from mice and fixed in 2% PFA overnight. The next day grafts were transferred to tubes containing sterile water and scanned using a Bruker Skyscan 1276 (Bruker Preclinical Imaging) with a source voltage of 85 kV, a source current of 200 µA, a filter setting of AI 1 mm, and pixel size of 12 microns at 2016 x 1344. Reconstructed samples were analyzed using CT Analyser (CTan) v1.17.7.2 and CTvox v3.3.0 software (Bruker). Sections spanning the size of the graft were selected and upper (255) and lower (60) grey threshold were set. The total mineralized volume was measured for each graft assuming equal starting amounts of anorganic cancellous bone graft granulat.

Transcriptomic analysis

Transcriptomic analysis was performed on highly purified, double-sorted mSSCs, mBCSPs, hSSC, hOP, and hCP populations either directly sorted into TRIzol LS (Invitrogen, Cat#10296028) or expanded and differentiated towards the osteogenic lineage for 14 days before collection in TRizol. RNA was isolated with RNeasy Micro Kit (QIAGEN,

Cat#74004) as per manufacturer's instructions. For microarray analysis RNA was twice amplified with an Arcturus RiboAmp PLUS Kit (Applied Biosystems, Cat#KIT0521). Amplified cRNA was streptavidin-labeled, fragmented, and hybridized to Affymetrix arrays HG-U133+ (for human genome; Applied Biosystems, Cat#901569). Arrays were scanned with a Gene Chip Scanner 3000 (Affymetrix) running GCOS 1.1.1 software. Raw microarray data was submitted to Gene Expression Commons (https://gexc.riken.jp/models/2551 and https://gexc.riken.jp/models/2552). On this platform data is normalized by computing against the Common Reference, which is comprised of a large number of array (mouse 11,939 and human 25,229) experiments deposited to the National Institutes of Health Gene Expression Omnibus (NIH GEO) database. GEXC assigns a threshold value to each probeset using the StepMiner algorithm and calculates a percentile value between -100% (inactive) and +100% (active) for each available gene, allowing comparison of human gene expression on a normalized, continuous scale. From there, heatmaps were generated showing fold change in gene expression of Cyclooxygenase mRNAs. For quantitative PCR experiments the following primers were used for timecourse experiments with hSSCs: *COX-1* (PTGS1; NM_000962.4), F-GATGAGCAGCTTTTCCAGACGAC, R-AACTGGACACCG AACAGCAGCT; *COX-2* (PTGS2; NM_000963), F- CGGTGA AACTCTGGCTAGACAG, R-GCAAACCGTAGATGCTCAG GGA.

Histochemistry

Cryo-sections were stained using Movat's Pentachrome or hematoxylin and eosin (H&E). Adjacent sections were used for immunofluorescence (IF) with primary antibodies mouse anti-human Human Nuclear Antigen (HNA; Abcam, Cat#ab191181) and rabbit anti-human Osteocalcin (OC; Abcam, Cat#ab93876) at 1:200 dilutions. The secondary antibodies goat anti-mouse AF-488 (Abcam, Cat#ab150117) and donkey anti-rabbit AF-647 (Abcam, Cat# ab150075) were added at 1:500 dilutions and sections counterstained with DAPI. Fluorescence microscopy (Leica TCS Sp8) was used to capture images.

Immunocytochemistry

For immunocytochemistry, fixated cells in well plates were permeabilized with 0.1% Triton X-100 solution and blocked with 3% BSA in PBS. After incubation with primary antibody for Cox-2 [ThermoFisher, Cat#12375-1-AP]) overnight at 4°C, secondary antibody was applied for 30 min at room temperature. For nuclear staining specimen were treated with DAPI (BioLegend, Cat# 422801). Fluorescence Quantification of Cox-2 expression in cultured hSSCs was measured by Corrected Total Cell Fluorescence (CTCF) and calculated using ImageJ for cells of five independent donors and for each time point. Each CTCF value is the average of five cells that is the integrated density minus the area of the selected cells multiplied by the mean fluorescence of the background readings.

Statistics

Data are presented as mean + standard error of the mean (SEM). Experiments were conducted at least in duplicate as indicated in the figure legends. Statistical analysis between two experimental groups was determined using two-tailed, unpaired Student's t-test. Normality was assessed by Shapiro-Wilk test and corrected if failed by using Mann-Whitney test. If unequal variances (F-test) were detected the t-test was adjusted with Welch's correction. For comparison of more than two groups one-way ANOVA analysis was used with Tuckey's posthoc test. P-values were considered significant if $p < 0.05$. Statistical analyses were performed using GraphPad Prism 9 (GraphPad).

Results

Microarray data of freshly purified skeletal lineage cell populations from day-10 mid-diaphyseal femoral fractures (Figures S1A, B) demonstrated that *Cox-2* but not *Cox-1* mRNA was abundantly expressed in freshly isolated mouse SSCs (CD45-Ter119-Tie2-Thy1-6c3-CD51+CD105-CD200+) and BCSPs (CD45-Ter119-Tie2-Thy1-6c3-CD51+CD105+) (Figures 1A, B). Additionally, primary mouse SSCs (mSSCs) cultured *in vitro* expressed high levels of COX2 (Figure 1C). When we seeded freshly sorted fracture mSSCs at clonal density and continuously treated expansion cultures with the common NSAIDs Ketorolac (Keto), Indomethacin (Indo), or Ibuprofen (Ibu) we did not observe any changes to the fibroblast colony forming unit (CFU-F) ability as well as the size of the colonies compared to controls (Figures 1D and S1C). This suggested that proliferation of mSSCs was most likely not affected by NSAID treatment. Next, we examined whether NSAIDs inhibited chondrogenic and osteogenic differentiation capacity of mSSCs *in vitro*. All three NSAIDs tested significantly inhibited chondrogenic differentiation in mSSC compared to controls as determined by Alcian Blue staining quantification (Figure 1E). Similarly, *in vitro* osteogenic mineralization was strongly diminished in the presence of Ketorolac and Indomethacin (Figure 1F). These results extend the previously reported inhibitory effect of Cox2-inhibition on bone biology in rodents to the purified skeletal stem cell level, indicating a direct role in perturbing endochondral bone formation processes.

Next, we examined whether COX enzymes played a functional role in human SSCs (hSSCs). We purified human hSSCs (CD45-CD235-CD31-TIE2-CD146-PDPN+CD164 +CD73+), as well as their downstream osteoprogenitors

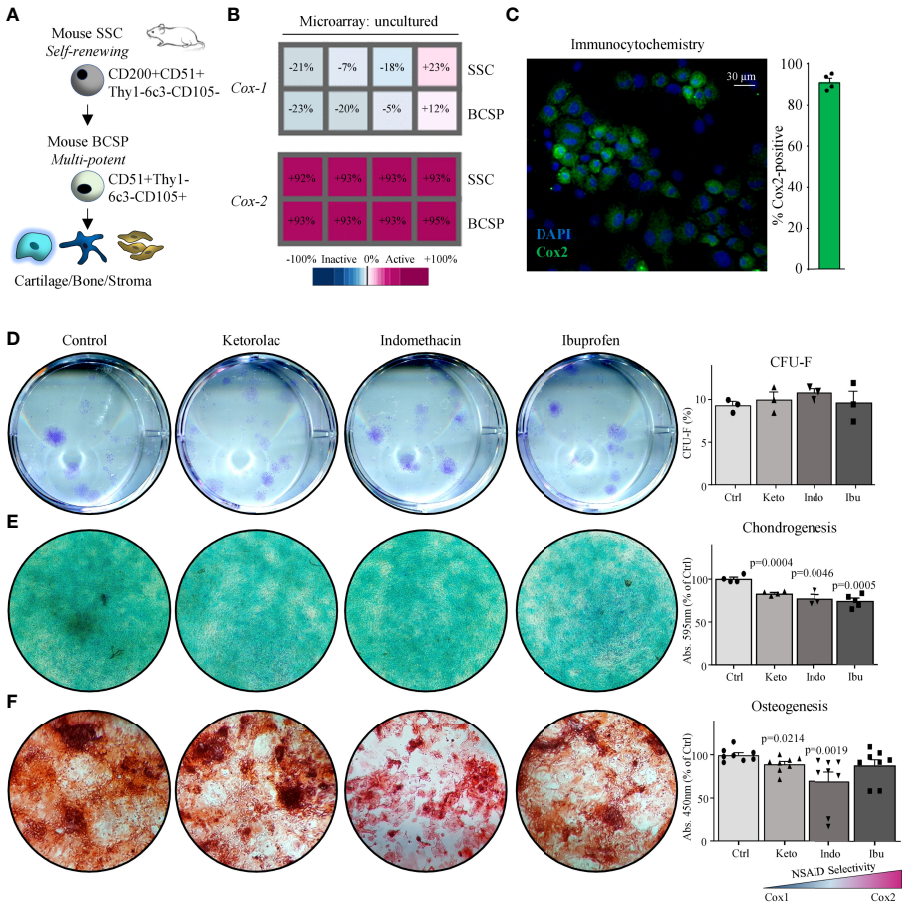

FIGURE 1
Mouse skeletal stem cells depend on Cox2 for functional osteochondrogenic differentiation. **(A)** The mouse skeletal stem cell (SSC) lineage tree as defined by surface marker expression profiles with the SSC at the apex and the downstream bone cartilage stroma progenitor (BCSP) which gives rise to committed bone, cartilage, and stroma progenitor cells. **(B)** Microarray analysis showing *Cox-1* and *Cox-2* expression of freshly purified SSCs and BCSPs from fracture calluses of four different mice. **(C)** Representative immunocytochemistry (ICC) staining of Cox2 of fracture-derived SSCs expanded in culture for five days. **(D)** Representative images of colony-forming unit assays of fracture-derived SSCs stained with Crystal Violet expanded in the absence or presence of NSAIDs (left; Ketorolac 0.3 µg/ml, Ibuprofen 3 µg/ml, or Indomethacin 0.3 µg/ml) and quantification thereof (right). Replicates from n=3 mice. **(E)** Representative images of chondrogenesis assays of fracture derived SSCs stained with Alican Blue differentiated in the absence or presence of NSAIDs (left) and quantification thereof (right). Replicates from n=4 mice. **(F)** Representative images of osteogenesis assays of fracture derived SSCs stained with Alizarin Red S differentiated in the absence or presence of NSAIDs (left) and quantification thereof (right). Replicates from n=4 mice. All data shown as mean + standard error of mean (SEM). Results from at least two independent experiments. Statistical testing versus control group by unpaired Student's t-test with Welch's correction for unequal variances and Mann-Whitney test for non-normality where necessary.

(hOPs) and chondroprogenitors (hCPs), from acute fractures at the time of surgical open reduction and internal fixation (Figure 2A and Figures S2A, B). Transcriptomic analysis revealed that *COX-1* mRNA was stably expressed in purified uncultured and differentiating patient-derived hSSCs (Figure 2B and Figure S2C). *COX-2* expression, on the other hand, was high in freshly isolated hSSCs but rapidly lost gene and protein expression upon early commitment towards the osteogenic lineage as shown by qPCR and immunocytochemistry time-course analyses (Figures 2B–E). In line with this observation, *COX-2* expression was not detectable in freshly isolated committed osteoprogenitors (hOPs; CD45-CD235-CD31-TIE2-CD146+PDPN-) (Figures S2D, E). Interestingly, early chondrocyte progenitor cells (hCPs) maintained high levels of *COX-1* and *COX-2* expression. To test the influence of the presence of *COX-2* in hSSCs during osteogenic differentiation we lentivirally overexpressed primary hSSCs with a *COX-2* construct and induced osteogenesis. Compared to GFP-transduced cells, hSSCs from three different patients showed strongly diminished *in vitro* mineralization when *COX-2* was continuously expressed (Figure 2F). Taken together, this data indicates that primary bona fide hSSCs express *COX-2* in an undifferentiated state but, in contrast to mSSCs, might depend on its downregulation for osteogenic differentiation.

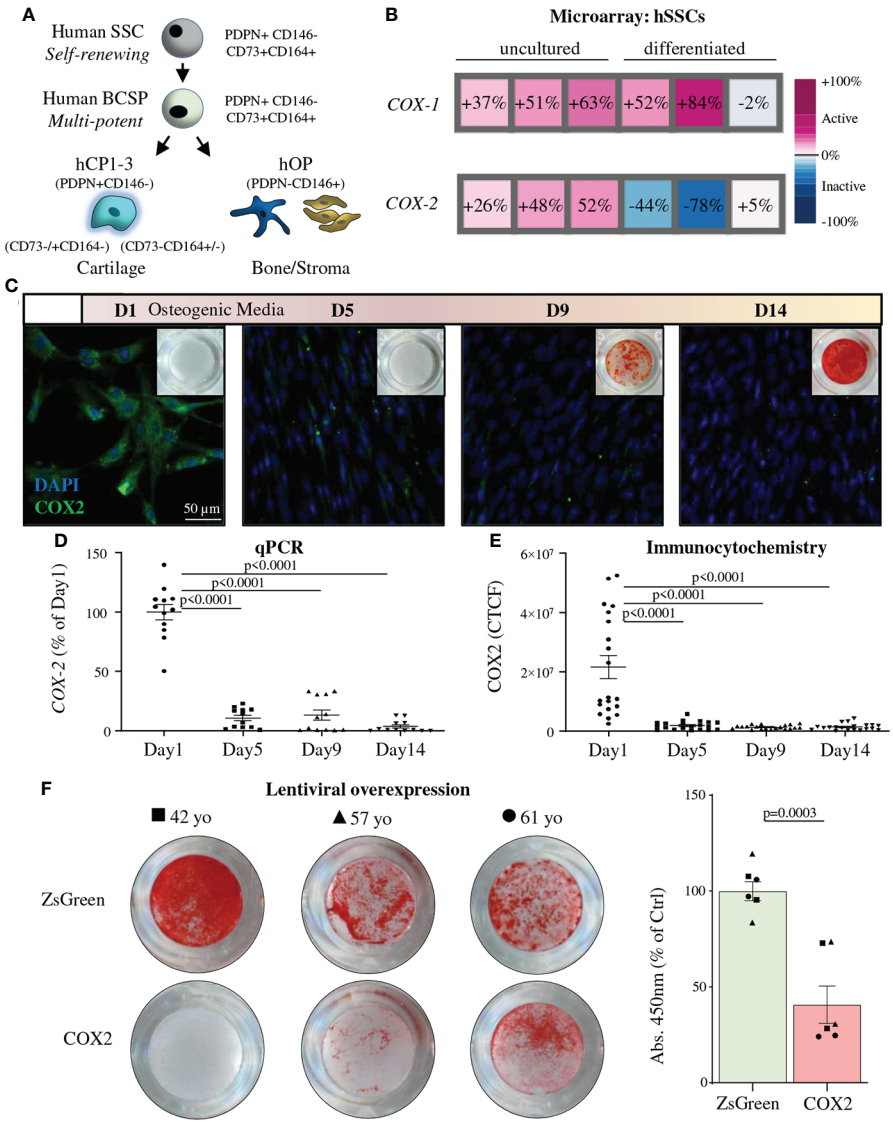

FIGURE 2
COX2 downregulation is necessary for osteogenic differentiation of human SSCs. **(A)** The human skeletal stem cell (hSSC) lineage tree as defined by surface marker expression profiles with the hSSC at the apex and the downstream bone cartilage stroma progenitor (hBCSP) which gives rise to committed bone (hOP) and cartilage (hCPs) progenitor cells. **(B)** Microarray analysis showing *COX-1* and *COX-2* expression of freshly purified (uncultured) hSSCs from human fracture callus tissue of three different patients as well as their expression after two-week osteogenic differentiation from hSSCs. **(C)** Representative IHC images of COX2 staining in freshly purified hSSCs at different timepoints during *in vitro* osteogenesis. **(D)** Related quantitative PCR of *COX-2* expression in the same experiment. n=12 independent replicates of hSSCs from four patients performed in triplicates. **(E)** Quantification of COX2 ICC staining by CTCF (corrected total cell fluorescence). n=20 independent replicates of hSSCs from two patients (n=10 each). Statistical testing between timepoints by one-way ANOVA with Tukey's posthoc test. **(F)** Alizarin Red staining and quantification of hSSCs (with patient age; yo: years old) of lentivirally overexpressed COX2 or ZsGreen controls during osteogenic differentiation. n=6 independent replicates of hSSCs from three patients performed in duplicate. Statistical testing by unpaired Student's t-test. All data shown as mean ± SEM. All results from at least two independent experiments.

Next, we surveyed reported peak plasma levels of common NSAIDs in human patients and treated colony-forming unit fibroblast assays with the average of these concentrations (Figure S3A) (19–21). Ketorolac (3 µg/ml), Indomethacin (3 µg/ml), or Ibuprofen (30 µg/ml) treatment did not alter clonogenicity of hSSCs compared to controls (Figure 3A). In contrast to mSSCs, chondrogenesis of hSSCs was also unaffected in the presence of these NSAIDs (Figure 3B). Using *in vitro* bone-forming assays we tested low and peak plasma concentration levels of NSAID and treated hSSC cultures either short-term (first three days) or continuously (throughout differentiation) with NSAIDs. Regardless of NSAID supplementation and duration of

treatment, there was no effect on osteogenic potential of hSSCs (Figure 3C and Figures S3B, C). Importantly, when we assayed the effect of the commonly used selective COX2-inhibitor Celecoxib at varying concentration, we could not observe any effect on osteogenic differentiation either (Figure 3D). Since NSAIDs could act downstream of the stem cell level or on a putative distinct SSC lineage, we also asked if short-term or continuous NSAID administration differentially affected osteogenic differentiation of CD146-positive osteoprogenitors (hOPs), previously described as a key source of bone formation in humans (22). We found that neither low nor high doses of NSAIDs added during differentiation, short-term or continuously, inhibited bone mineralization in hOPs (Figures S3D-F). This suggested a species-specific effect of COX-inhibition on bone-forming cell types between mice and humans.

Lastly, we sought to explore if exposure to NSAIDs affects *de novo* bone formation reflective of the fracture healing process *in vivo*. SSCs are able to recreate skeletal structures, if transplanted as purified single cell solution to ectopic sites, provided access to vascular ingress (13, 14, 23). Thus, we transplanted primary patient-derived hSSCs subcutaneously into immune-incompetent NSG mice that were treated intraperitoneally with Indomethacin or PBS as control daily for one week (Figure 4A). We reasoned that the lack of adaptive immunity in NSG mice would be well suited to assess a direct effect of NSAIDs on the hSSC function. As expected, patient hSSCs generated grafts complete with bone tissue at least in part

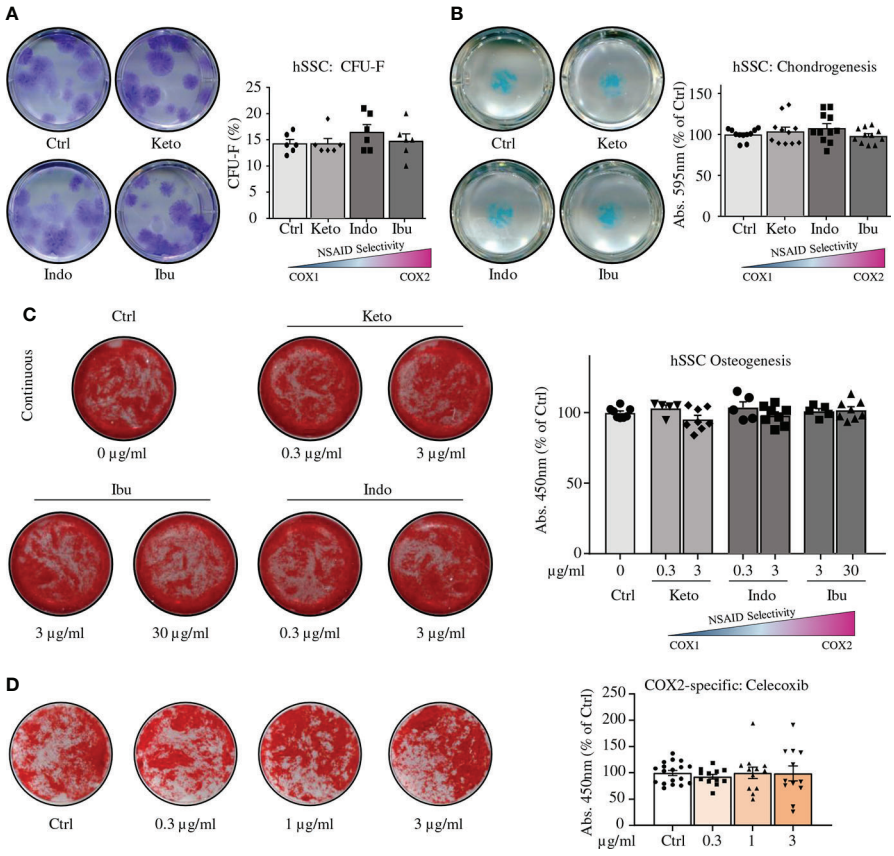

FIGURE 3
NSAIDs do not alter *in vitro* functionality of human SSCs. **(A)** Representative images of CFU-F assays of fracture derived hSSCs stained with Crystal Violet expanded in the absence or presence of NSAIDs (left; Ketorolac 3 µg/ml, Ibuprofen 30 µg/ml, or Indomethacin 3 µg/ml) and quantification thereof (right). n=6 independent replicates from hSSCs of two patients performed in triplicate. **(B)** Representative images of chondrogenesis assays of fracture derived hSSCs stained with Alican Blue differentiated in the absence or presence of NSAIDs (left) and quantification thereof (right). n=11 independent replicates from hSSCs of five patients performed at least in duplicate. **(C)** Continuous NSAID treatment of osteogenic differentiation assays from hSSCs. n=8 independent replicates from hSSCs of four patients performed in duplicate. **(D)** Osteogenic differentiation of hSSCs in the presence of COX2-specific inhibitor Celecoxib. n=12-18 independent replicates from hSSCs of six patients performed at least in duplicates. All data shown as mean ± standard error of mean (SEM). All results from at least two independent experiments. Statistical testing versus control group by unpaired Student's t-test with Welch's correction for unequal variances where necessary.

forming through a cartilage intermediate (Figures 4B–E and Figures S4A–C). At four and eight weeks, μCT analysis showed no differences in mineralization between hSSC-derived grafts from seven independent patients either transplanted into mice receiving NSAID doses or to patient-matched PBS controls (Figure 4C). Histomorphometric quantification of bone tissue in grafts confirmed these results. Importantly, immunostaining revealed that osteocalcin-expressing cells in grafts were of human origin and did not differ in frequency between groups (Figures 4F, G). In summary, osteochondrogenic differentiation of fracture-derived hSSC lineage populations is facilitated in the absence of COX2, providing a rationale for the discrepancy observed between animal experiments and human studies.

Discussion

The effects of NSAIDs on osteogenic stem cell differentiation and fracture healing remain controversial and appear to vary with investigated species and cell type. Here, we compared

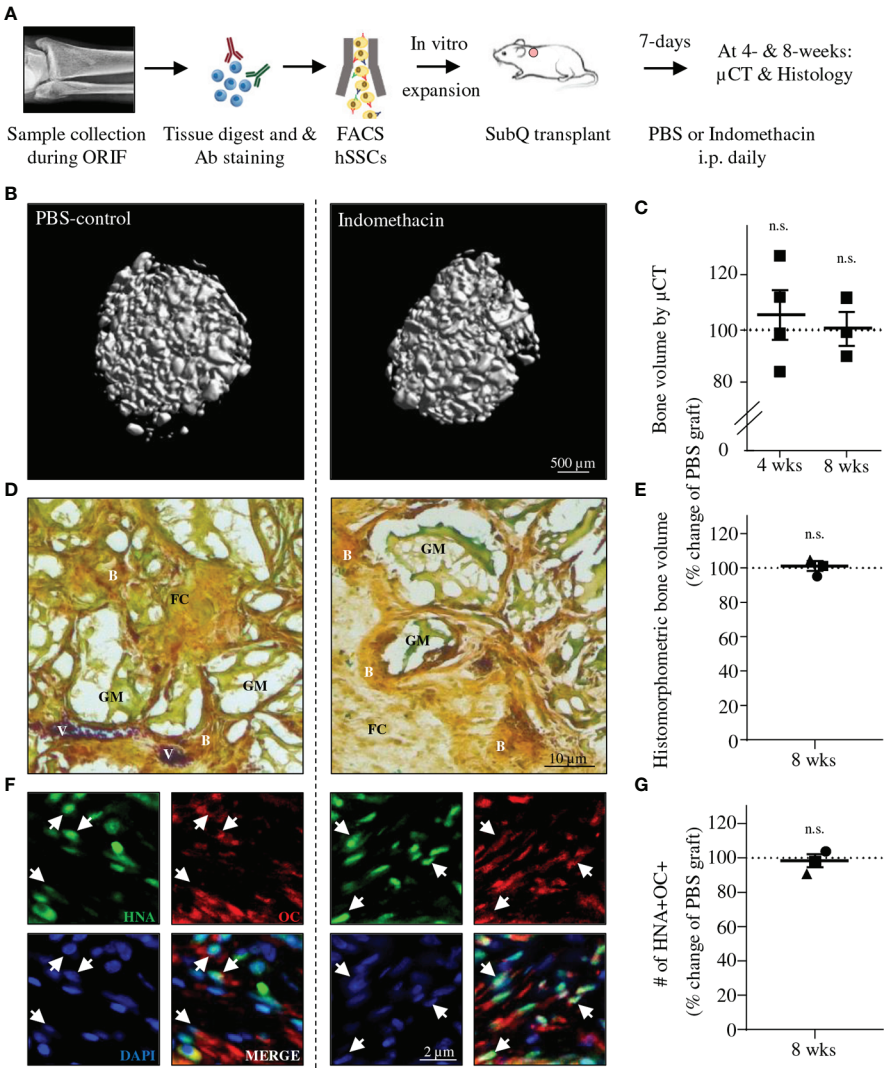

FIGURE 4
Indomethacin does not interfere with *in vivo* ossicle formation of human SSCs. **(A)** Experimental schematic for *in vivo* grafting of hSSCs and treatment of mice with Indomethacin. **(B)** Three-dimensional microCT reconstruction of mineralized graft tissue. **(C)** Quantification of mineralized graft tissues (total bone volume) at 4- (n=4) and 8-weeks (wks; n=3) post transplant between PBS and Indomethacin treated mice. Results from seven experiments with hSSCs from distinct patients. **(D)** Representative Movat Pentachrome staining of sectioned grafts (B, Bone; FC, Fibrocartilage; V, Blood vessel; GM, Graft material). **(E)** Histomorphometric quantification of graft bone volume (each data point represents average of three non-adjacent sections per patient hSSC-derived graft). **(F)** Immunohistochemistry showing graft derived osteogenic cells are of human origin. Human Nuclear Antigen (HNA; green), Osteocalcin (OCN; red), DAPI (blue). **(G)** Quantification of OCN-expressing cells of human origin based on IHC. Data shown as mean + SEM. Statistical testing by paired Student's t-test (n.s., not significant).

prospectively isolated, highly purified, homologous populations of skeletal stem cells from mice and humans and report that COX enzymes may be dispensable for chondrogenic and osteogenic differentiation in fracture-derived hSSCs but not mSSCs.

In mice we found that NSAIDs repressed chondrogenic and osteogenic differentiation of mSSCs from fractures. In general, NSAIDs appear to inhibit murine fracture healing based on previous evidence. Perhaps most convincingly, genetic *Cox-2* null mice demonstrate bone healing defects (5). From the perspective of bone marrow stromal cells, it has previously been reported that NSAIDs are inhibitory at the osteogenic differentiation level, although in a non-cell autonomous model (10). Although NSAIDs had no effect on serum markers of fracture healing or biomechanical properties of fracture callus in rat fractures (24), there is also evidence that in rat long bone fractures, prolonged NSAID administration inhibits BMSC differentiation and fracture callus formation (25). We have extended these observations by demonstrating an inhibitory effect of NSAIDs on osteochondrogenic differentiation in the highly purified and characterized mSSC, a bona fide skeletal stem cell, that has been shown to play an essential part in fracture healing (14–17, 26, 27). However, the limitations translating genetically homogenous mouse models to complex multi-factorial disease processes are well-documented (28, 29). Subsequently, we have also studied the homologous human cell population, the hSSC, and made distinct observations (13, 16).

We found no effect of NSAIDs on osteogenic and chondrogenic differentiation of hSSCs, which is not fully concordant with many previous human studies but is consistent with the strongest available clinical evidence. A previous analysis of human bone marrow stromal cells did find a specific inhibitory effect of multiple NSAIDs on chondrogenesis but not osteogenic differentiation (9), while another study demonstrated an inhibitory effect of NSAIDs on osteogenesis (30). These conflicting results might have several explanations, including the fact that cells were derived from uninjured tissue through bone marrow aspirates as well as prolonged selection and growth in culture. The present study used flow cytometrically purified defined skeletal progenitor cell types with minimal *in vitro* expansion. Our earlier work could show that fracture-derived SSCs behave differently than their steady-state counterparts (27) and that selection of heterogenous cell populations by plastic adherence leads to variations in experimental readout (11, 12, 31). Strikingly, in this study we also observed a lack of effect of NSAIDs on differentiation of lineage restricted osteoprogenitors (hOPs; CD146-positive), which contain a previously described populations of perivascular bone marrow stromal cells with stem cell-like features (22). It is feasible to assume that by initiating differentiation experiments at the hSSC level with cells undergoing maturation through more committed lineage progenitor stages before terminal osteochondral differentiation, our findings of a lack of effect of NSAIDs on experimental outcome can be extrapolated to human BMSCs, which contain a heterogeneous mixture of stem and progenitor cell types. While COX1/2 are expressed at time of isolation of hSSCs from fracture sites, COX2 expression becomes attenuated during differentiation, suggesting an alternate role, if any for this enzyme at sites of skeletal injury. We also observed that lentiviral overexpression of COX2 in hSSCs actually prevented *in vitro* mineralization. This could be a consequence of superphysiological COX2 levels. Moving forward this could be mitigated by using more specific transcriptional control with other genetic models. We will also have to test if the same results are obtained when a catalytically inactive COX2 variant is used as a control.

Our work might have not covered cell types highly enriched for "MSC"-like cells that have been shown to modulate local and systemic inflammatory responses (32), and may do so at sites of fracture as well. Future studies will have a closer look at NSAID effects on angiogenesis and immune cells during early fracture healing in humans. However, our *in vivo* results suggest that even in a monocyte/macrophage enriched environment, as present in NSG mice, which have been implicated in NSAID mediated suppression of osteogenesis, bone formation from SSCs is not impaired in the presence of NSAID drugs (10).

In the clinical setting, there remains a lack of convincing evidence, but not controversy, surrounding the use of NSAIDs in fracture healing (5–7, 33). A recent meta-analysis concluded that association of nonunion with NSAID use was predominantly found in studies with insufficient cohort sizes, unclear definition of outcomes and even fraud allegations, stating that there were a dearth of high quality studies in fracture literature (8). Another review cited lack of strong evidence against NSAID use in fracture healing (34).

In conclusion, there is great interest in safe post-operative analgesia, given the current opioid crisis, especially during fracture care in orthopaedic surgery. Currently, much of our understanding of the role of NSAIDs in fracture healing comes from rodent models. Here, we demonstrate that NSAIDs have disparate and species-specific effects on osteochondrogenic differentiation of homologous populations of murine and human fracture-derived SSCs, which are prospectively isolated and a highly purified cell population. In contradistinction to the mSSC, the hSSC is unaffected by NSAID administration. COX enzyme-specific mechanisms in SSCs likely evolved to synchronize priming of SSC-dependent regenerative responses with recruitment of inflammatory cell types that may also facilitate other aspects of the regenerative process. COX1 might be differentially regulated at the stem cell level in mice while, for instance, recent findings have also shown that there are

differences between humans and mice in their regulation of COX2 expression (18). Finally, the expression of COX1 versus COX2 in human versus mouse SSCs is a species-specific regulatory switch that might serve to maintain stem cell identity rather than promoting differentiation. Thus, caution should be used in extrapolating mechanistic data from experimental animal models to clinical practice. Our data provides evidence from a mechanistic perspective that NSAID does not appear to impair human skeletogenic stem and progenitor cells and contributes to the hypothesis that NSAID use might be safe after fractures in humans in some contexts. Additionally, hSSCs isolated from acute human fractures provide a model with which to study how common medications may influence fracture healing.

Data availability statement

The microarray data presented in the study haven been deposited in public repositories. All raw and processed data are available from the NCBI GEO database with accession number GSE211910. Data browsing is also available in the Gene Expression Commons depository (GEXC) at https://gexc.riken.jp/models/2551 and https://gexc.riken.jp/models/2552.

Ethics statement

The studies involving human participants were reviewed and approved by Stanford IRB. Written informed consent for participation was not required for this study in accordance with the national legislation and the institutional requirements. The animal study was reviewed and approved by Stanford's Administrative Panel on Laboratory Animal Care.

Author contributions

LG, TA, and CC conceived and designed the study. MGB, LG, TA, HS, and CC conducted experiments, analyzed and interpreted data, and wrote the manuscript. MH, HC, NR, MJB, JB, and MG collected samples and supported analysis. CC supervised the research. All authors contributed to the article and approved the submitted version.

Funding

This work was supported by NIH/NIA K99 R00 AG049958-01A1, 1S10OD028493-01A1, Heritage Medical Foundation, American Federation for Aging Research (AFAR)/Arthritis National Research Foundation (ANRF), Wu Tsai Human Performance Alliance and an endowment from the DiGenova Family to CC, the German Research Foundation (DFG-Fellowship) 399915929 and NIH/NIA 1K99AG066963 to TA. This work was also supported by CIRM Bridges 3.0 #EDUC2-12620 to MGB and the Young Investigator Research Award from the AO North America to LG. Additional support came from NIH S10 RR02933801 to Stanford University Stem Cell FACS core and NIH S10 1S10OD02349701 to Stanford University Clark Imaging Center (PI: Timothy Doyle).

Acknowledgments

We thank P. Lovelace, S. Weber, C. Carswell-Crumpton for FACS support. We also thank M.R. Eckart and the Stanford Gene Expression Facility (PAN Facility) as well as Stanford Human Immune Monitoring Center (HIMC) for technical support, assistance, and/or advice on this project. We also thank Dr. Pamela Robey for advice on bone grafts for in vivo experiments.

Conflict of interest

The authors declare that the research was conducted in the absence of any commercial or financial relationships that could be construed as a potential conflict of interest.

Publisher's note

Supplementary material

The Supplementary Material for this article can be found online at: https://www.frontiersin.org/articles/10.3389/fendo.2022.924927/full#supplementary-material

References

1. Goodman SB, Ma T, Genovese M, Smith RL. Cox-2 selective inhibitors and bone. *Int J Immunopathol Pharmacol* (2003) 16:201–5. doi: 10.1177/039463200301600303

2. Goodman SB, Ma T, Mitsunaga L, Miyanishi K, Genovese MC, Smith RL. Temporal effects of a COX-2-selective NSAID on bone ingrowth. *J BioMed Mater Res A* (2005) 72:279–87. doi: 10.1002/jbm.a.30231

3. Gerstenfeld LC, Thiede M, Seibert K, Mielke C, Phippard D, Svagr B, et al. Differential inhibition of fracture healing by non-selective and cyclooxygenase-2 selective non-steroidal anti-inflammatory drugs. *J Orthop Res* (2003) 21:670–5. doi: 10.1016/S0736-0266(03)00003-2

4. Zhang X, Schwarz EM, Young DA, Puzas JE, Rosier RN, O'Keefe RJ. Cyclooxygenase-2 regulates mesenchymal cell differentiation into the osteoblast lineage and is critically involved in bone repair. *J Clin Invest* (2002) 109:1405–15. doi: 10.1172/JCI15681

5. Butcher CK, Marsh DR. Nonsteroidal anti-inflammatory drugs delay tibial fracture union. *Injury* (1996) 27:375. doi: 10.1016/0020-1383(96)86874-4

6. Jeffcoach DR, Sams VG, Lawson CM, Enderson BL, Smith ST, Kline H, et al. Nonsteroidal anti-inflammatory drugs' impact on nonunion and infection rates in long-bone fractures. *J Trauma Acute Care Surg* (2014) 76:779–83. doi: 10.1097/TA.0b013e3182aafe0d

7. Fader L, Whitaker J, Lopez M, Vivace B, Parra M, Carlson J, et al. Tibia fractures and NSAIDs. does it make a difference? a multicenter retrospective study. *Injury* (2018) 49(12):2290–4. doi: 10.1016/j.injury.2018.09.024

8. Dodwell ER, Latorre JG, Parisini E, Zwettler E, Chandra D, Mulpuri K, et al. NSAID exposure and risk of nonunion: a meta-analysis of case-control and cohort studies. *Calcif Tissue Int* (2010) 87:193–202. doi: 10.1007/s00223-010-9379-7

9. Pountos I, Giannoudis PV, Jones E, English A, Churchman S, Field S, et al. NSAIDS inhibit *in vitro* MSC chondrogenesis but not osteogenesis: implications for mechanism of bone formation inhibition in man. *J Cell Mol Med* (2011) 15:525–34. doi: 10.1111/j.1582-4934.2010.01006.x

10. Lu LY, Loi F, Nathan K, Lin T, Pajarinen J, Gibon E, et al. Pro-inflammatory M1 macrophages promote osteogenesis by mesenchymal stem cells *via* the COX-2-Prostaglandin E2 pathway. *J Orthop Res* (2017) 35:2378–85. doi: 10.1002/jor.23553

11. Ambrosi TH, Longaker MT, Chan CKF. A revised perspective of skeletal stem cell biology. *Front Cell Dev Biol* (2019) 7:189. doi: 10.3389/fcell.2019.00189

12. Bianco P, Robey PG. Skeletal stem cells. *Development* (2015) 142:1023–7. doi: 10.1242/dev.102210

13. Chan CKF, Gulati GS, Sinha R, Tompkins JV, Lopez M, Carter AC, et al. Identification of the human skeletal stem cell. *Cell* (2018) 175:43–56.e21. doi: 10.1016/j.cell.2018.07.029

14. Chan CKF, Seo EY, Chen JY, Lo D, McArdle A, Sinha R, et al. Identification and specification of the mouse skeletal stem cell. *Cell* (2015) 160:285–98. doi: 10.1016/j.cell.2014.12.002

15. Ambrosi TH, Marecic O, McArdle A, Sinha R, Gulati GS, Tong X, et al. Aged skeletal stem cells generate an inflammatory degenerative niche. *Nature* (2021), 59(7875):256–62. doi: 10.1038/s41586-021-03795-7

16. Ambrosi TH, Goodnough LH, Steininger HM, Hoover MY, Kim E, Koepke LS, et al. Geriatric fragility fractures are associated with a human skeletal stem cell defect. *Aging Cell* (2020) 19:e13164. doi: 10.1111/acel.13164

17. Goodnough LH, Ambrosi TH, Steininger H, DeBaun MR, Abrams GD, McAdams TR, et al. Delayed union of a diaphyseal forearm fracture associated with impaired osteogenic differentiation of prospectively isolated human skeletal stem cells. *JBMR Plus*. (2020) 4(10):e10398. doi: 10.1002/jbm4.10398

18. Nguyen LK, Cavadas MAS, Kholodenko BN, Frank TD, Cheong A. Species differential regulation of COX2 can be described by an NFκB-dependent logic AND gate. *Cell Mol Life Sci* (2015) 72:2431–43. doi: 10.1007/s00018-015-1850-1

19. Rainsford KD. Ibuprofen: pharmacology, efficacy and safety. *Inflammopharmacology* (2009) 17:275–342. doi: 10.1007/s10787-009-0016-x

20. Brocks DR, Jamali F. Clinical pharmacokinetics of ketorolac tromethamine. *Clin Pharmacokinet* (1992) 23:415–27. doi: 10.2165/00003088-199223060-00003

21. Helleberg L. Clinical pharmacokinetics of indomethacin. *Clin Pharmacokinet* (1981) 6:245–58. doi: 10.2165/00003088-198106040-00001

22. Sacchetti B, Funari A, Michienzi S, Di Cesare S, Piersanti S, Saggio I, et al. Self-renewing osteoprogenitors in bone marrow sinusoids can organize a hematopoietic microenvironment. *Cell* (2007) 131:324–36. doi: 10.1016/j.cell.2007.08.025

23. Chan CKF, Chen C-C, Luppen CA, Kim J-B, DeBoer AT, Wei K, et al. Endochondral ossification is required for haematopoietic stem-cell niche formation. *Nature* (2009) 457:490–4. doi: 10.1038/nature07547

24. Huo MH, Troiano NW, Pelker RR, Gundberg CM, Friedlaender GE. The influence of ibuprofen on fracture repair: biomechanical, biochemical, histologic, and histomorphometric parameters in rats. *J Orthop Res* (1991) 9:383–90. doi: 10.1002/jor.1100090310

25. Gerstenfeld LC, Al-Ghawas M, Alkhiary YM, Cullinane DM, Krall EA, Fitch JL, et al. Selective and nonselective cyclooxygenase-2 inhibitors and experimental fracture-healing: Reversibility of effects after short-term treatment. *JBJS* (2007) 89:114–25. doi: 10.2106/JBJS.F.00495

26. Tevlin R, Seo EY, Marecic O, McArdle A, Tong X, Zimdahl B, et al. Pharmacological rescue of diabetic skeletal stem cell niches. *Sci Transl Med* (2017) 9(372):eaag2809. doi: 10.1126/scitranslmed.aag2809

27. Marecic O, Tevlin R, McArdle A, Seo EY, Wearda T, Duldulao C, et al. Identification and characterization of an injury-induced skeletal progenitor. *Proc Natl Acad Sci USA* (2015) 112:9920–5. doi: 10.1073/pnas.1513066112

28. Burkhardt AM, Zlotnik A. Translating translational research: mouse models of human disease. *Cell Mol Immunol* (2013) 10:373–4. doi: 10.1038/cmi.2013.19

29. Leenaars CHC, Kouwenaar C, Stafleu FR, Bleich A, Ritskes-Hoitinga M, De Vries RBM, et al. Animal to human translation: a systematic scoping review of reported concordance rates. *J Trans Med* (2019) 17:223. doi: 10.1186/s12967-019-1976-2

30. Yoon DS, Yoo JH, Kim YH, Paik S, Han CD, Lee JW. The effects of COX-2 inhibitor during osteogenic differentiation of bone marrow-derived human mesenchymal stem cells. *Stem Cells Dev* (2010) 19:1523–33. doi: 10.1089/scd.2009.0393

31. Via AG, Frizziero A, Oliva F. Biological properties of mesenchymal stem cells from different sources. *Muscles Ligaments Tendons J* (2012) 2:154–62.

32. Németh K, Leelahavanichkul A, Yuen PST, Mayer B, Parmelee A, Doi K, et al. Bone marrow stromal cells attenuate sepsis *via* prostaglandin E(2)-dependent reprogramming of host macrophages to increase their interleukin-10 production. *Nat Med* (2009) 15:42–9. doi: 10.1038/nm.1905

33. Giannoudis PV, MacDonald DA, Matthews SJ, Smith RM, Furlong AJ, De Boer P. Nonunion of the femoral diaphysis. the influence of reaming and non-steroidal anti-inflammatory drugs. *J Bone Joint Surg Br* (2000) 82:655–8. doi: 10.1302/0301-620x.82b5.9899

34. Kurmis AP, Kurmis TP, O'Brien JX, Dalén T. The effect of nonsteroidal anti-inflammatory drug administration on acute phase fracture-healing: A review. *J Bone Joint Surgery-American Volume* (2012) 94:815–23. doi: 10.2106/JBJS.J.01743

frontiers | Frontiers in Endocrinology

TYPE Original Research
PUBLISHED 12 September 2022
DOI 10.3389/fendo.2022.936159

OPEN ACCESS

EDITED BY
Michaela Tencerova,
Academy of Sciences of the Czech Republic (ASCR), Czechia

REVIEWED BY
Sundeep Khosla,
Mayo Clinic College of Medicine and Science, United States
Joe Varghese,
Christian Medical College & Hospital, India

*CORRESPONDENCE
Reina Armamento-Villareal
reina.villareal@bcm.edu

SPECIALTY SECTION
This article was submitted to Bone Research, a section of the journal Frontiers in Endocrinology

RECEIVED 04 May 2022
ACCEPTED 10 August 2022
PUBLISHED 12 September 2022

CITATION
Ballato E, Deepika F, Prado M, Russo V, Fuenmayor V, Bathina S, Villareal DT, Qualls C and Armamento-Villareal R (2022) Circulating osteogenic progenitors and osteoclast precursors are associated with long-term glycemic control, sex steroids, and visceral adipose tissue in men with type 2 diabetes mellitus. *Front. Endocrinol.* 13:936159. doi: 10.3389/fendo.2022.936159

Circulating osteogenic progenitors and osteoclast precursors are associated with long-term glycemic control, sex steroids, and visceral adipose tissue in men with type 2 diabetes mellitus

Elliot Ballato[1,2], Fnu Deepika[1,2], Mia Prado[1,2], Vittoria Russo[2], Virginia Fuenmayor[1,2], Siresha Bathina[1,2], Dennis T. Villareal[1,2], Clifford Qualls[3,4] and Reina Armamento-Villareal[1,2]*

[1]Division of Endocrinology, Diabetes and Metabolism, Department of Medicine, Baylor College of Medicine, Houston, TX, United States, [2]Center for Translational Research on Inflammatory Disease, Michael E DeBakey Veterans Affairs (VA) Medical Center, Houston, TX, United States, [3]Biomedical Research Institute of New Mexico, Albuquerque, NM, United States, [4]Research Service Line, New Mexico Veterans Affairs Health Care System, Albuquerque, NM, United States

Introduction: Type 2 diabetes mellitus (T2DM) is well-known to be associated with normal bone density but, concurrently, low bone turnover and increased risk for fracture. One of the proposed mechanisms is possible derangement in bone precursor cells, which could be represented by deficiencies in circulating osteogenic progenitor (COP) cells and osteoclast precursors (OCP). The objective of our study is to understand whether extent of glycemic control has an impact on these cells, and to identify other factors that may as well.

Methods: This was a secondary analysis of baseline data from 51 male participants, aged 37-65 in an ongoing clinical trial at Michael E. DeBakey VA Medical Center, Houston, Texas, USA. At study entry serum Hemoglobin A1c was measured by high-performance liquid chromatography osteocalcin (OCN) and C-terminal telopeptide of type 1 collagen (CTx) were measured by ELISA, and testosterone and estradiol by liquid-chromatography/mass-spectrometry. Areal bone mineral density (BMD), trabecular bone score and body composition were measured by dual energy x-ray absorptiometry, while COP and OCP were measured by flow cytometry.

Results: When adjusted for serum testosterone, parathyroid hormone, and 25-hydroxyvitamin D, those with poor long-term glycemic control had significantly higher percentage of COP ($p = 0.04$). COP correlated positively with visceral adipose tissue (VAT) volume ($r = 0.37$, $p = 0.01$) and negatively with free testosterone ($r = -0.28$, $p = 0.05$) and OCN ($r = -0.28$, $p = 0.07$), although only borderline for the latter. OCP correlated positively with age, FSH, lumbar

10.3389/fendo.2022.936159

spine BMD, and COP levels, and negatively with glucose, triglycerides, and free estradiol. Multivariable regression analyses revealed that, in addition to being predictors for each other, another independent predictor for COP was VAT volume while age, glucose, and vitamin D for OCP.

Conclusion: Our results suggest that high COP could be a marker of poor metabolic control. However, given the complex nature and the multitude of factors influencing osteoblastogenesis/adipogenesis, it is possible that the increase in COP is a physiologic response of the bone marrow to increased osteoblast apoptosis from poor glycemic control. Alternatively, it is also likely that a metabolically unhealthy profile may retard the development of osteogenic precursors to fully mature osteoblastic cells.

KEYWORDS

osteoblast (OB), osteoclast (OC), body composition, type 2 diabetes mellitus, circulating osteogenic progenitors

Introduction

A host of factors can lead to disorders of bone remodeling including but not limited to aging, menopause, hormonal imbalance, vitamin D deficiency, medications, immobilization, and chronic kidney disease, among others (1). Recently, type 2 diabetes mellitus (T2DM) has been added to this list. Our group previously reported that men with T2DM with or without hypogonadism had reduced bone turnover markers (2). This finding is in agreement with observations from other investigators suggesting impaired bone remodeling in these patients (3–6). Furthermore, our group also showed a differential effect of glycemic control on bone turnover. We recently reported that men with poor blood glucose control, defined as hemoglobin A1c (A1c) of ≥7% had suppressed bone turnover relative to men with good glycemic control (defined as A1c of <7%) (7). In fact, the bone turnover markers of the latter were comparable to patients without T2DM. These glycemia-associated differences in bone remodeling are in turn reflected by differences in bone microarchitecture and strength, with poor indices among those with poor control (8).

Diabetes mellitus is associated with accumulation of advanced glycation end products (AGE's) and non-enzymatic glycation products (NEG's) which can result in microstructural defects in bone (9, 10). Given the reduced bone remodeling in these patients, it is likely that repair of these microstructural damages and replacement of old with new bone is impaired, leading to skeletal fragility. The underlying mechanism for this observed reduction in bone remodeling in patients with T2DM is not well-established. Nevertheless, there are suggestions that low bone turnover in the context of T2DM is mostly a problem of bone formation since hyperglycemia impairs osteoblastogenesis (11, 12) and could be the initiating factor for reduced bone remodeling given the cross-talk between osteoblasts and osteoclasts. One study reported lower osteoblastic progenitors in patients with T2DM (13). However, it remains unclear if the degree of glycemic control affects the proliferation and differentiation of these cells *in-vivo*. The objective of this study is to evaluate the effect of glycemic control on circulating osteogenic progenitor (COP) cells and osteoclast precursors (OCP) in the circulation. Secondarily, we will also evaluate the effect of anthropometric, hormonal and metabolic factors on circulating COP and OCP.

We hypothesize that poor glycemic control (ie A1c>7%) is associated with fewer circulating COP and OCPs. Furthermore, we also hypothesize that other factors (hormonal and metabolic) will affect the flux of these cells in circulation resulting in alterations in bone parameters. To our knowledge, this is the first study of its kind examining the effect of glycemic control on COP and OCPs levels in adult males with T2DM.

Materials and methods

Patient population

This is a secondary analysis of baseline data from the study "Testosterone Therapy and Bone Quality in Men With Type 2 Diabetes Mellitus and Hypogonadism" which is ongoing at the Michael E DeBakey VA Medical Center since October 2019 (NCT03887936). The inclusion/exclusion criteria for this study are as described previously (14), but briefly, male veterans, 35 to 65 years old, with an average fasting morning total testosterone (T) level from 2 measurements of <300 ng/dL taken at least a day

apart and symptoms of hypogonadism as assessed by quantitative Androgen Deficiency in the Aging Male survey (qADAM) (15), having T2DM of <15 years duration with an A1c of <10.5% and body mass index (BMI) <35 kg/m^2. Diagnosis of T2DM was by chart review and A1c measurement at study entry, using widely-accepted diagnostic criteria of A1c≥6.5% and fasting plasma glucose>125mg/dL or use of antidiabetic medications (16). Excluded were those with 1) a history of prostate or breast cancer, 2) testicular disease, 3) untreated severe sleep apnea, 4) any illness that could prevent the subject from completing the study or diseases that interfere with bone metabolism 5) hematocrit of >50%, 6) prostate-related findings on digital rectal exam, 7) serum PSA of ≥4.0 ng/mL or ≥3.0 ng/mL for African-Americans, 8) International Prostate Symptom Score (IPSS) > 19, 9) on androgen therapy, or selective androgen receptor modulators, 10) on medications that affect bone metabolism, 11) current alcohol use of >3 drinks/day, 12) history of deep vein thrombosis, pulmonary embolism, stroke or recent diagnosis of coronary artery disease 13) a T-score ≤–2.5 assessed by dual-energy x-ray absorptiometry at the lumbar spine, total femur or femoral neck, or a history of fragility fractures (spine, hip or wrist), and/or 14) fasting total T less than 50 ng/dL.

Body mass index

Body weight and height were measured by standard weighing scale and stadiometer, respectively. BMI (kg/m^2) was calculated by dividing the weight (in kilograms) by height (in meters) squared.

Biochemical analyses

Blood was obtained in the morning after an overnight fast, processed, and samples were stored at -80°C until analysis. Serum total T and estradiol were measured by liquid chromatography/mass spectroscopy by LabCorp laboratory (Burlington, NC, USA), total T intra-assay CVs are 7.4%, 6.1%, 9.0%, 2.3%, and 0.9% at 0.65, 4.3, 48, 118, and 832 ng/dL, respectively. Inter-assay CVs are 8.9%, 6.9%, 4.0%, 3.6%, and 3.5% at 0.69, 4.3, 45, 117, and 841 ng/dL, respectively. The detection range is 0.5 to 2,000 ng/dL (17). Estradiol assay sensitivity is 0.23 to 405 pg/mL, intra-assay CV is 1.4% to 11.8% and inter-assay CV is 4.8% to 10.8% (2). SHBG was measured with electrochemiluminescence immunoassay by LabCorp laboratory (Burlington, NC, USA). The following were measured by the clinical laboratory at the Michael E. DeBakey VA Medical Center: A1c was measured by high-performance liquid chromatography using Tosoh Automated Glycohemoglobin Analyzer HLC-723G8. (Tosoh Bioscience, Inc. South San Francisco, CA, USA); triglycerides were measured by fluorometric assay and LDL and HDL were measured by colorimetric assay by UNICEL DxC (Beckman Coulter, Inc., 250 S. Kraemer Blvd., Brea, CA 92821 USA). Detection limits for these measurements are: 11–500 mg/dl for LDL, 5–135 mg/dL (0.13–3.5 nmol/L) for HDL, 10–1,000 mg/dL (0.1–11.3 mmol/L) for triglycerides; CVs <10% for all measurements (17). The free T index was calculated by using the formula previously described by Sowers et al. (18) i.e. 100×T (ng/dl)/28.84×SHBG (nM) which is unit free. The free E_2 index (FEI) was calculated as the molar ratio of total E_2 to SHBG (pmol/nmol) (19). Fasting glucose was measured using Unicel *DxC 800* Auto-analyzer (Beckman Coulter, Fullerton, CA, USA). The following were measured using enzyme-linked immunosorbent assay kits: CTx, marker of bone resorption (Crosslaps; Immunodiagnostic System Inc., Gaithersburg, MD); and OCN, marker of bone formation, (Metra OC; Quidel Corporation, San Diego, CA); and high-sensitivity C-reactive protein (hs-CRP) (Eagle Biosciences, Inc., Nashua, NH). The coefficients of variation (CVs) for the above assays in our laboratory are <10% and <3.5% for A1c.

Mean -12M A1c

Mean A1c was obtained from medical record review of each patient's chart using the Veterans Affairs Computerized Patient Record System, A1c values measured between 9 and 15 months prior to study enrollment. For each participant, the average of these A1c measurements was calculated to give a single 12-month average A1c value, the -12M A1c.

Flow cytometry

Identifying COP and OCP can and has been done by flow cytometry. OCP express several identifying proteins, chiefly among them M-CSF's receptor MCSFR. Gossiel et al. have previously described a staining protocol where dual CD14CD11b+, CD14MCSFR+, CD14CD120b+ cells are identified as OCPs (20). CD14 is a cell-surface receptor in monocytes that responds to lipopolysaccharides and serves as a pattern recognition receptor (21, 22), CD11b is an integrin protein found on many leukocytes of the macrophage lineage (23), and CD120b, also known as TNFR2, is a surface receptor for TNF-α. Osteoblasts and circulating COP are identified chiefly with anti-OCN antibodies as described by others (13, 24–26). To exclude B, T, and NK cells, the CD3-CD19-CD56- cell population can be gated. Finally, the fluorescence minus one

technique, as described by Perfetto et al. (27), can be useful in ruling out background noise to identify COP.

OCN positive COP were isolated from peripheral blood using a previously described method with modification (13, 24, 25, 28). Peripheral blood mononuclear cells (PBMC) were isolated *via* Ficoll-Paque density gradient. Fresh, whole blood, treated with anticoagulant, was diluted 1:1 with phosphate-buffered saline, then layered on top of Ficoll-Paque density gradient at a ratio of 4:3. This was centrifuged for 35 minutes at 400 x g. The pellet was then isolated and washed twice with PBS. PBMC were then stored on ice for the remainder of the experiment. They were stained with a) combination of CD3 (BD Pharmingen, San Diego, CA, USA), CD19 (Beckman Coulter, Indianapolis, IN, USA), CD56 (BD Horizon, San Diego, CA, USA), OCN (Santa Cruz Biotechnology, Dallas, TX, USA), and 4′,6-diamidino-2-phenylindole (DAPI, Beckman Coulter, Indianapolis, IN, USA) b) just CD3, CD19, CD56, and DAPI (reflecting the fluorescence minus one technique (27)) or c) just DAPI. Viable cells that were OCN+ and CD3CD19CD56- were considered COP (see Figure 1A).

OCPs were also isolated from peripheral blood. First, PBMC were extracted from whole blood as described above. These were then stained with a) combination of CD14 (BD Pharmingen, San Diego, CA, USA), CD11b (ThermoFisher Scientific, Waltham, MA, USA), and DAPI b) CD14, CD11b, MCSFR (Abcam, Waltham, MA, USA), and DAPI c) CD14, CD11b, CD120b (BD Pharmingen, San Diego, CA, USA), and DAPI or d) just DAPI. Viable cells that were dual CD14CD11b +, CD14MCSFR+, or CD14CD120b+ were considered OCPs (see Figure 1B). All flow cytometry data was collected on a CytoFlex LX Flow Cytometer (Beckman Coulter, Indianapolis,

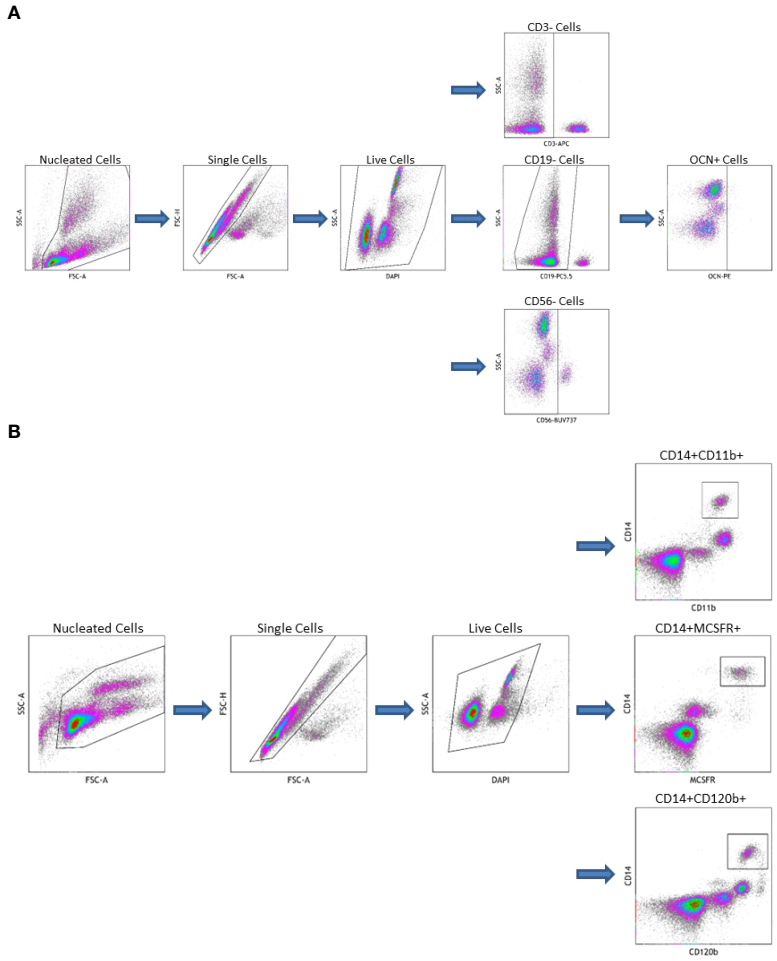

FIGURE 1
(A) Gating Strategy for Circulating Osteogenic Progenitor Cell Isolation. Cells are first sorted along forward/side scatter to identufy nucleated cells, then forward area and height to identify singlets, then DAPI-negative cells are identified as viable. Cells that are CD3-CD19-CD56-are gated from this population the OCN+ cells are identified as osteoblast progenitors. **(B)** Gating Strategy for Osteoclast Precursor Cell Isolation. Cells are first sorted along forward/side scatter to idfentify nucleated cells, then forward area and height to identify singlets, then DAPI-negative cells are identified as viable. Cells that are CD14+CD11b+, CD14+MCSFR+, or CD14+CD120b+ are identified as OC precursors.

IN, USA) and analyzed using Kaluza Analysis Software (Beckman Coulter, Indianapolis, IN, USA).

Imaging studies

Areal BMD, trabecular bone score and body composition

aBMD was assessed by dual energy X-ray absorptiometry (DXA) on the lumbar spine, left proximal femur (right femur if history of prior surgery) for total femur and femoral neck regions of interest, and whole body using Hologic Discovery (Hologic Inc, Bedford, MA, USA). The CVs at our center are ~1.1% for the lumbar spine and ~1.2% for the proximal femur (19, 29). TBS of the spine images (using L1-L4) obtained by DXA was assessed using the TBS Insight 2.2 software (Med-Imaps, Merignac, France). TBS is a gray-level textural assessment calculated from the standard DXA spine images which is considered a measure of skeletal microarchitecture at the spine (30).

Measurement of body composition was performed by DXA (Hologic-Discovery; Enhanced Whole Body 11.2 software version; Hologic Inc, Bedford, MA; USA). Images were analyzed according to manufacturer's instructions. The CV for fat mass and lean mass measurements in our center is 1.5% (19). Visceral adipose tissue (VAT) volume (g/cm^2) was calculated from the DXA body composition scan using APEX software (version 5.5.2; Hologic Inc., Bedford, MA) as previously described (29).

Statistical analyses

Results are presented as means ± standard deviation (SD) in the tables. A p-value <0.05 was considered significant, and <0.10 was considered borderline significant. Participants were grouped according to study entry and mean A1C levels, i.e. ≤7% and >7%. Group comparisons were performed by one-way analysis of covariance. The associations between COP and OCP cells with hormonal, metabolic and bone parameters were analyzed by simple correlation analysis. Independent predictors for each of these circulating cellular components were identified by multivariable regression analyses. This was performed by first identifying all variables that were significantly associated with the parameter of interest as candidate variables, then performing a backwards stepwise regression with all candidate variables included in the model. Significant predictors were identified and tabulated. Data were managed using Excel 2013 (Microsoft, Redmond, WA), and analyzed by Statgraphics Centurion XVI X64 (Statgraphics Technologies, Inc., The Plains, VA, USA).

Results

Demographics and medications

The data from 51 consecutive men who were able to provide the outcomes of interest were included in this analysis. Ages ranged from 37 to 65 with an average of 55.2 ± 6.3 years. Of the 51 men, 20 (39%) were African-American, 24 (47%) were non-Hispanic white, 6 (12%) were Hispanic, and 1 (2%) was Asian. Total T of the overall population was 265.0 ± 84.3 ng/dL, 43 participants were hypogonadal with an average Total T of 236.8 ± 44.4 while 8 were eugonadal with an average Total T of 328.4 ± 82.8 ng/dl. Average BMI was 31.7 ± 3.5. All participants had T2DM with average A1c 8.1 ± 1.4%. Mean duration of T2DM was 7.6 ± 5.7 years (see Table 1). Of the 51 participants, 42 were on medications for T2DM while 9 were not. Of the 42 participants on medications, 8 were on metformin alone, 2 on insulin alone, 4 on metformin and insulin in combination, and the other 28 were on different combinations of metformin, insulin, dipeptidyl peptidase 4 inhibitors, glucagon-like peptide-1 receptor agonists, sodium-glucose cotransporter-2 inhibitors, sulfonylureas, thiazolidinediones, and alpha-glucosidase inhibitors (see Supplemental Table 1).

Effect of glycemic control

To determine the effect of short- and long-term glycemic control, we divided our subjects according to A1c at study entry

TABLE 1 Demographic and clinical data of the study participants.

Parameter	Result (n = 51)
Age (years)	55.2 ± 6.3
BMI	31.7 ± 3.5
A1c at study entry (%)	8.1 ± 1.4
Testosterone (ng/dL)	265.0 ± 84.3
Duration of T2DM (years)	7.6 ± 5.7
Total Body Fat (%)	34.3 ± 4.3

Results are expressed as mean ± standard deviation. BMI, body mass index; A1c, glycated hemoglobin; T2DM, type 2 diabetes mellitus.

and the Mean (-12M) A1c into ≤ 7% (n = 15, good T2DM control) and >7% (n = 36, poor control), but only 46 subjects have data on COP and OCPs (good control N=15, poor control N=31). For clinical characteristics of subjects according to A1c at entry and Mean -12M A1c, please see Supplementary Tables 2, 3. Analysis according to A1c at study entry showed that poorly-controlled subjects had significantly longer duration of T2DM (9.0 ± 5.9 years vs 5.0 ± 4.5 years, p = 0.02), higher average A1c for the prior year (9.0 ± 1.9% vs 6.8 ± 1.0%, p < 0.001), lower 25-hydroxyvitamin D (23.8 ± 11.3 ng/mL vs 33.1 ± 14.7 ng/mL, p = 0.02), lower SHBG (22.0 ± 12.6 nmol/L vs 30.5 ± 11.3 nmol/L p = 0.02), and lower BMD at the total hip (1.062 ± 0.16 g/cm^2 vs 1.159 ± 0.16 g/cm^2, p = 0.05) (Supplementary Table 2). The significance of the latter disappears with adjustments for age and BMI (p = 0.14). Analysis according to Mean -12M A1c similarly showed that those with poor long-term glycemic control had significantly longer duration of T2DM (8.9 ± 5.9 years vs 4.7 ± 4.1 years p = 0.02). Furthermore, they had significantly lower total lean mass (63.1 ± 8.1 kg vs 68.2 ± 5.1 kg, p = 0.04) compared to those with good long-term glycemic control but significance was lost after adjustment for age and BMI, p = 0.20 (Supplementary Table 3). A separate analysis for BMD and body composition adjusted for age and BMI in both Supplementary Tables 1, 2 was done showing no significant between-group differences in any of these parameters in the short- or long-term glycemic control categories.

The average COP in the entire population was 0.41 ± 0.13% and within the reference range of normal for COP (OCN+) reported in a prior study (31). Analysis of precursor cells in Table 2 showed that those with long-term poor glycemic control had significantly increased percentage of COP when adjusted for factors that influence production, proliferation and differentiation of these cells such as PTH, 25-hydroxyvitamin D and free T levels (0.42 ± 0.12% vs 0.35 ± 0.11%, p = 0.04). However, when analysis was also adjusted for the duration of T2DM, the difference between the 2 groups became borderline (p=0.07). There were no significant differences in circulating OCP cells according to short- and long-term glycemic control.

Association between COP and OCPs with hormonal and metabolic factors

COP were inversely correlated with serum free T (r = -0.28, p = 0.05) and OCN (r = -0.28, p = 0.07), although significance for the latter was only borderline (Table 3). OCPs, CD14CD11b+, CD14MCSFR+, and CD14CD120b+ cells positively correlated with age and negatively correlated with plasma glucose, and triglycerides. FSH was positively correlated with all three of the OCP populations, but LH was not significantly associated with any of them. The CD14MCSFR+ negatively correlated with free estradiol (r = -0.34, p = 0.03). The CD14CD120b+ population was positively correlated with serum 25-hydroxyvitamin D (r = 0.33, p = 0.03), while significance was borderline for the other two. COP also positively correlated with all OCPs (r = 0.34, p = 0.02, r = 0.38, p = 0.01, r = 0.33, p = 0.03 for CD14CD11b+, CD14MCSFR+, and CD14CD120b+ respectively). There were no correlations between short- and long-term A1c and any cellular parameters.

Association between COP and OCPs with body composition

Average total body fat percentage was 34.3 ± 4.3%. COP increased significantly with increasing VAT (r = 0.37, p = 0.01, see Table 4 and Figure 2). There was no significant correlation between any of the OCPs with any parameter of body composition.

Other associations noted with body composition parameters are: VAT volume decreased significantly with increasing serum OCN levels (r = -0.46, p = 0.003, see Figure 3A) and negatively but weakly corelate with CTX (r = -0.31, p = 0.06). Appendicular lean mass, on the other hand, negatively correlated with CTX (r = -0.40,

TABLE 2 Circulating osteogenic progenitors and osteoclast precursors according to A1C at study entry and mean -12M A1c.

	A1c ≤ 7% (n = 15)	A1c >7% (n = 31)	P-value	Adjusted P*
A1C at study entry				
COP (%)	0.39 ± 0.15	0.42 ± 0.13	0.51	0.35
CD14CD11b+ (%)	4.20 ± 2.01	3.73 ± 1.91	0.45	0.77
CD14MCSFR+ (%)	3.95 ± 1.70	3.50 ± 1.87	0.44	0.81
CD14CD120b (%)	4.41 ± 2.15	3.83 ± 2.08	0.38	0.73
		Mean A1C		
COP (%)	0.35 ± 0.11	0.42 ± 0.12	0.10	**0.04**
CD14CD11b+ (%)	3.70 ± 2.35	3.93 ± 1.83	0.74	0.17
CD14MCSFR+ (%)	3.52 ± 2.03	3.69 ± 1.78	0.79	0.20
CD14CD120b (%)	3.80 ± 2.42	4.05 ± 2.02	0.73	0.12

Values are means ± SD, Bolded p-values are statistically significant. A1c, glycated hemoglobin; COP, circulating osteogenic progenitor. *Adjusted for free testosterone, 25-hydroxyvitamin D and parathyroid hormone.

TABLE 3 Correlation analysis of circulating osteogenic progenitors and osteoclast precursors on hormonal and metabolic parameters of interest.

Parameter	COP (n = 46)		CD14CD11b+(n = 46)		CD14MCSFR+(n = 45)		CD14CD120b (n = 46)	
	r	(p)	r	(p)	r	(p)	r	(p)
Age (years)	0.11	(0.47)	0.33	**(0.02)**	0.39	**(0.009)**	0.32	**(0.03)**
Glucose (mg/dL)	-0.08	(0.60)	-0.32	**(0.03)**	-0.35	**(0.02)**	-0.32	**(0.03)**
LDL (mg/dL)	0.09	(0.54)	-0.27	(0.07)	-0.26	(0.08)	-0.25	(0.10)
HDL (mg/dL)	-0.01	(0.97)	-0.20	(0.19)	-0.14	(0.37)	-0.20	(0.19)
Triglycerides (mg/dL)	-0.20	(0.19)	-0.32	**(0.03)**	-0.35	**(0.02)**	-0.29	**(0.05)**
25-OHD (ng/mL)	0.07	(0.63)	0.28	(0.06)	0.28	(0.06)	0.33	**(0.03)**
LH (mIU/mL)	-0.02	(0.89)	0.11	(0.46)	-0.03	(0.83)	0.11	(0.47)
FSH (mIU/mL)	0.13	(0.39)	0.31	**(0.03)**	0.29	**(0.05)**	0.31	**(0.03)**
Free T index	-0.28	**(0.05)**	-0.24	(0.10)	-0.22	(0.14)	-0.22	(0.14)
Free Estradiol (pmol/nmol)	-0.17	(0.27)	-0.28	(0.06)	-0.34	**(0.03)**	-0.21	(0.18)
PTH (pg/mL)	-0.24	(0.11)	0.01	(0.92)	-0.03	(0.83)	0.11	(0.47)
OCN (ng/mL)	-0.28	(0.07)	0.01	(0.93)	0.02	(0.92)	0.01	(0.95)
CTX (ng/mL)	-0.22	(0.17)	-0.09	(0.60)	-0.08	(0.63	-0.15	(0.37)
Hs-CRP (mg/L)	0.04	(0.78)	-0.03	(0.84)	0.01	(0.94)	-0.003	(0.98)
A1c at study entry (%)	-0.09	(0.56)	-0.22	(0.14)	-0.22	(0.14)	-0.24	(0.11)
Mean -12M A1c (%)	-0.07	(0.71)	-0.23	(0.13)	-0.22	(0.14)	-0.25	(0.098)
COP (%)	–	–	0.34	**(0.02)**	0.38	**(0.01)**	0.33	**(0.03)**

Bolded p-values are statistically significant. COP, circulating osteogenic progenitors; LDL, low-density lipoprotein; HDL, high-density lipoprotein; 25-OHD, 25-hydroxyvitamin D; LH, leutinizing hormone; FSH, follicle stimulating hormone; Free T, serum free testosterone; PTH, parathyroid hormone; OCN, osteocalcin; CTX, C-telopeptide of type I collagen; Mean -12M, average of all A1c measurements between 9 and 15 months prior to study entry; hs-CRP, high-sensitivity C-reactive protein.

p = 0.01, see Figure 3B). There was no significant association between VAT volume and hs-CRP (r=0.22, p=0.12).

Association between COP and OCPs with bone mineral density

There were no significant associations with bone density at the hip or femoral neck, but lumbar spine BMD was positively associated with all three OCP cell populations, though only the CD14CD11b+ reached statistical significance (r = 0.31, p = 0.04) (see Table 4).

Independent predictors of circulating bone progenitor/precursor cells

Multivariable regression analyses were performed to identify the significant predictors of COP and OCP concentration in peripheral blood (Table 5). VAT volume and OCP concentration were found to be independent predictors for the COP (R^2 = 33.1, p < 0.001 for the model). For each of the CD14+CD11b+, CD14+MCSFR+, and CD14+CD120b + cells, the independent predictors were found to be: age and COP; fasting plasma glucose and COP; 25-OH vitamin D and COP (R^2 = 20.7, p = 0.007, R^2 = 27.4, p = 0.002, R^2 = 19.9, p = 0.008, respectively).

TABLE 4 Correlation analysis of body composition parameters on circulating osteogenic progenitors and osteoclast precursors.

Parameter	COP (n = 45)		CD14CD11b+(n = 45)		CD14MCSFR+(n = 44)		CD14CD120b (n = 45)	
	r	(p)	r	(p)	r	(p)	r	(p)
VAT volume (cm^3)	0.37	**(0.01)**	0.01	(0.96)	-0.003	(0.98)	0.06	(0.69)
Body Fat (%)	-0.01	(0.95)	0.02	(0.89)	0.03	(0.86)	0.09	(0.57)
ALM (g)	0.19	(0.23)	0.22	(0.16)	0.18	(0.26)	0.27	(0.08)
Lean Mass (g)	0.18	(0.24)	0.18	(0.25)	0.15	(0.34)	0.22	(0.15)
L Spine BMD (g/cm^2)	0.02	(0.90)	0.31	**(0.04)**	0.27	(0.08)	0.28	(0.06)
Femoral Neck BMD (g/cm^2)	-0.06	(0.68)	0.03	(0.85)	0.05	(0.74)	0.03	(0.85)
Total body BMD (g/cm^2)	-0.22	(0.14)	0.08	(0.60)	0.10	(0.52)	0.05	(0.74)
TBS	-0.07	(0.63)	0.06	(0.68)	0.05	(0.73)	0.01	(0.93)

Bolded p-values are statistically significant. COP, circulating osteogenic progenitors; VAT, visceral adipose tissue; ALM, appendicular lean mass; L Spine, Lumbar spine; BMD, bone mineral density; TBS, trabecular bone score.

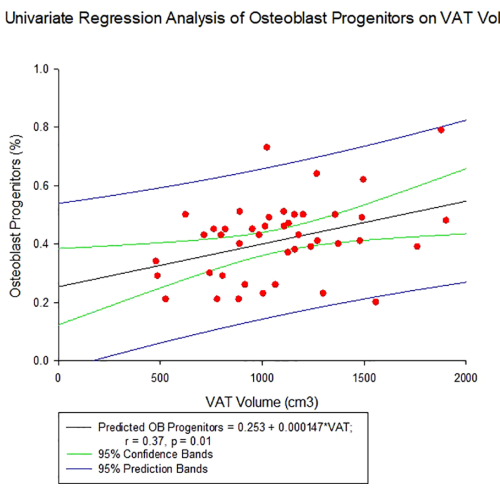

FIGURE 2
Regression of Circulating Osteogenic Progenitors (COP) with Visceral Adipose Tissue Volume. COP were identified as CD3-CD19-CD56-and OCN+ cells, and expressed as a percent of the nucleated, viable population.

Discussion

Our results show that in our population of mostly hypogonadal patients with T2DM, long-term poor glycemic control was associated with increased circulating COP compared to those with good long-term control. There were no significant differences in OCPs in either short- or long-term glycemic control status. COP positively correlated with VAT volume and negatively with free T. OCPs positively correlated with age, 25-hydroxyvitamin D, and FSH and negatively with plasma glucose, triglycerides, and free estradiol. Our results also showed that COP and OCP flux are positively correlated with each other as expected from the coupling mechanism. Further analysis revealed that VAT and OCPs are independent predictors of circulating COP; conversely, for OCPs independent predictors include COP for each, along with age; glucose; and 25-hydroxyvitamin D for the CD14CD11b+, CD14MCSFR+, and CD14CD120b+ cell populations respectively. Interestingly, we also found that OCN and CTX were inversely correlated with VAT and ALM respectively.

Osteoblasts are mononucleated cells whose primary function is to synthesize bone matrix. They derive from mesenchymal stem cells which are common progenitors for fibroblasts, chondrocytes, myoblasts, and adipocytes (32, 33). The process of differentiation into osteoblasts has been described in greater detail elsewhere (34–36), but briefly this common progenitor can be directed toward adipocytes by peroxisome proliferator-activated receptor gamma (PPARγ), myocytes by myoblast determination protein 1 (MyoD), chondrocytes by Sox-9, and osteoblasts by Runx-2. Upon Runx-2 activation, the cells undergo a 3-stage differentiation which results in a mature, osteocalcin (OCN)-secreting osteoblast (35).

Osteoclasts are multinucleated cells whose primary function in bone remodeling is to resorb bone. Mononuclear hematopoietic stem cells, in the presence of macrophage colony stimulating factor (M-CSF), differentiate into macrophage colony forming units, which are common precursors of both macrophages and osteoclasts. Receptor activator of nuclear factor κB (RANK) receptor activation by its ligand RANKL (among other downstream molecules) is then responsible for the differentiation of OCPs into mature osteoclasts (37–41). Multinucleation, stimulated by osteoclast stimulatory transmembrane protein (OC-STAMP) and

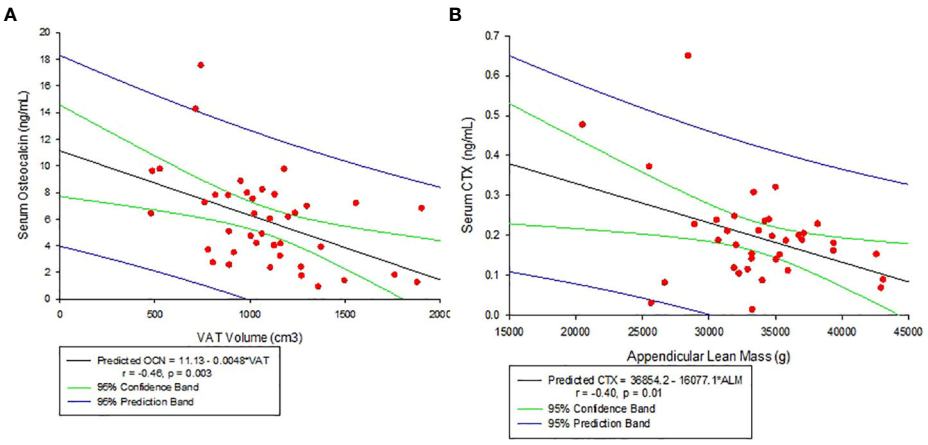

FIGURE 3
(A) Correlation between Serum Osteocalcin and Visceral Adipose Tissue Volume (VAT). **(B)** Correlation between Serum C-telopeptide (CTX) and Appendicular lean mass.

10.3389/fendo.2022.936159

TABLE 5 Multivariate regression analysis of circulating osteogenic progenitors and osteoclast precursors with variables of interest.

Parameter	R^2	β Estimate	SE	P	P (model)
COP	33.1				<0.001
CD14MCSFR+ (%)		0.031	0.010	0.005	
VAT Volume (cm^3)		1.8×10^{-4}	5.7×10^{-5}	0.003	
CD14CD11b+	20.7				0.007
Age (years)		0.093	0.042	0.03	
COP (%)		4.46	1.96	0.03	
CD14MCSFR+	27.4				0.002
Glucose (mg/dL)		-0.010	0.004	0.02	
COP (%)		4.951	1.810	0.009	
CD14CD120b+	19.9				0.008
D-25OH (ng/mL)		0.048	0.021	0.03	
COP (%)		4.718	2.133	0.03	

R^2 is expressed in percentage values; β Estimate is unitless. All significant variables from simple correlation analysis were included as candidate predictors. COP, circulating osteogenic progenitors; SE, standard error, VAT, visceral adipose tissue; D-25OH, 25-hydroxyvitamin D.

dendritic cell-specific transmembrane protein (DC-STAMP) (42, 43), is a complex process which appears to strongly enhance resorptive activity (44). Mature osteoclasts resorb bone at their ruffled surface through acid secretion and proteolysis to dissolve the inorganic and organic components of bone respectively (45–47).

That osteoblast and osteoclast activities are coupled has been recognized for decades (48, 49). Bone remodeling occurs in four phases: activation, during which osteoclasts are recruited; resorption when osteoclasts are active, reversal when osteoclasts undergo apoptosis, and formation where osteoblasts lay down new bone (50). This coupling process is delicately regulated by a number of cell-cell communication mechanisms, and mediators (51–57). The crosstalk between these 2 cells is well-illustrated in our study by the positive correlation between COP and OCPs, and one an independent predictor of the other.

The potential role of COP in health (for example, healing of fractures) and diseases such as vascular calcifications, heterotopic ossification, osteoporosis, and frailty is summarized in a recent review by Feehan and colleagues (58). A study in a population of 57 older adults demonstrated a positive correlation between BMD and bone mineral content of the whole body and femoral neck with levels of COP (59), Interestingly, the authors identified that a COP cut-off of 0.4% has 100% sensitivity and 79% specificity of predicting osteoporosis on the femoral neck. Furthermore, they also found COP to positively correlate with appendicular lean mass (59). Moreover, with the emerging body of evidence suggesting that diabetes is associated with low bone turnover (60–62) some investigators examined the role of COP as reflection of ongoing events in the bone of patients with T2DM. In a study by Manavalan et al. (13), circulating OCN+ cells or COP cells are significantly lower in patients with T2DM compared to those without diabetes. This observation was corroborated by findings of significantly reduced bone turnover markers in the serum and significantly lower bone formation rate, osteoblastic surface, and osteoid surface by histomorphometric analysis of iliac crest biopsy of patients with T2DM compared to those without diabetes. Unfortunately, they did not quantify circulating OCPs in this study, although parameters of osteoclast activity and number in the bone were examined. Given the cross-talk between osteoblasts and osteoclasts with reduced bone formation, it is expected that reduction in bone resorption follows with resultant low bone turnover. In previous studies, our group also reported that men with T2DM with or without hypogonadism (2) and obese men with T2DM have reduced bone turnover compared to those without T2DM (29). Furthermore, we demonstrated in another study that glycemic control could be an important determinant of this alteration in bone turnover in T2DM patients, with poor glycemic control associated with reduction in bone turnover as compared to those with good glycemic control (7).

However, in the current study, we found the opposite of what we anticipated initially. Those with poor long-term glycemic control in fact had higher COP compared to those with good long-term glycemic control. A previous study reported an increase in OCN+ cells in the circulation of subjects with A1c in the pre-diabetic and diabetic range compared to normal subjects. The authors speculated that this increase in OCN+ cells may initiate or account for increased vascular calcification in these patients (28). In fact, one study reported that OCN+ cells are associated with the severity of aortic calcification (63). Lineage plasticity of the mesenchymal stem cells is influenced by a variety of factors (64). It is possible that poor metabolic health alters the balance between osteoblastogenesis and adipogenesis favoring the former over the latter as compensatory response to osteoblast apoptosis from hyperglycemia (65, 66). On the other hand, a published report indicated that hyperglycemia also retards maturation of osteoblast progenitor cells in a dose-dependent manner (11) and may also contribute to the high COP in those with poor

glycemic control. The combined effect of hyperglycemia on the mature and differentiating osteoblastic cells is manifested clinically by dramatic reductions in bone formation indices histomorphometrically and on circulating COP followed by overall global reduction in bone turnover (13) (67–70). Although we did not find any concomitant increase in OCPs in our subjects, the segregation of the OCPs into different groups according to staining may have prevented us from finding a difference in these cells between the poor and good glycemic control groups.

As expected, there were significant negative correlations between the different OCPs with estradiol, and free T, deficiencies of which will result in increased bone turnover and bone loss (71–73). FSH receptors have been reported on the surface of osteoclasts (74), hence the finding of positive association between FSH and OCPs is not surprising. The negative relationship between OCPs and glucose, and triglycerides is likely a reflection of the suppression of bone remodeling that happens with T2DM and metabolic syndrome. However, we find an interesting positive correlation between COP and VAT, with the latter an independent predictor (in conjunction with OCPs) of the former in the multivariable regression analysis. One possible explanation for our observation could be the common progenitor shared by adipocytes and osteoblasts. Our cohort had average BMI of 31.7 and average total body fat of 34.3%, so they were more obese than the general population. It is possible that with more signals for this progenitor to differentiate into adipocytes, there was less signal to differentiate into osteoblasts. This is a possibility in patients with T2DM as hyperglycemia has been reported to divert OBP cells to an adipogenic pathway (75). Another possible explanation is VAT serving as a proxy for bone marrow adipose tissue (BMAT). Bredella et al. found a positive association between visceral fat and bone marrow fat, and additionally found an inverse correlation between marrow fat and trabecular BMD (76). Interestingly, when mesenchymal stem cell-derived osteoblasts are co-cultured with adipocytes, they show an increase in adipogenic and decrease in osteogenic markers (77). One study found that, compared to age-matched controls, people with osteoporosis have significantly more BMAT (78). Our findings also show that VAT is negatively associated with markers of bone formation (OCN), which in the presence of increased COP perhaps suggest that increased adipogenesis may suppress preosteoblast differentiation in our patient population, which would in turn decrease rate of bone remodeling and lead to poorer bone quality. Such findings have been suggested previously in the context of osteoporosis (79). We also found a negative association between CTX and ALM. One possible link between the bone homeostasis and muscle mass here could be RANKL's activation of the NF- κB pathway and concomitant inhibition of myogenic differentiation (80, 81). It has been reported that treatment with denosumab, a RANKL inhibitor, can improve muscle mass in osteoporotic, sarcopenic mice (82). Similar observations have also been noted in older, community-dwelling adults (83).

We were also interested in learning whether COP and OCPs concentrations would be associated with BMD. We found a positive association between OCPs and lumbar spine BMD. Excessive mature OC activity can result in decreased bone mass (84, 85). Accordingly, our result could be interpreted as higher bone density caused by reduced bone turnover, a product of fewer OCP's differentiating into mature osteoclasts. The positive correlation between OCPs and 25-hydroxyvitamin D, is consistent with the report from prior *in-vitro* studies showing that conversion of 25-hydroxyvitamin to 1,25-dihydroxyvitamin D occurs in macrophage lineage cells which results in increase in osteoclast transcription factors and regulation of osteoclastic differentiation (86, 87).

The strengths of this study include: 1) novelty, as this is the first study that examines the effect of glycemic control and other factors on the circulating bone precursor cells in T2DM and 2) the relatively good number participants for a flow cytometry study done on humans, which allows us to extrapolate a mechanistic understanding of previously observed trends in bone quality and geometry in patients with type 2 diabetes (2, 29). There are several limitations to our study. First, our patient population included mainly middle-aged men with T2DM, who for the most part are hypogonadal, and in the absence of normal controls and women, results from this study may not be applicable to the population of patients with T2DM in general. Second, although COP were higher in patients with Mean A1c>7%, the same trend was not observed for those with baseline A1c>7%, suggesting that the effect was either not strong, or that the effect of poor glycemic control on COP is a long-term relationship and may be difficult to capture at a single A1c timepoint. Finally, despite having significant p values, many of our correlation coefficients were somewhat weak.

In conclusion, findings from our study suggest high COP could be a marker for poor metabolic health with increased COP representing a potential compensatory response to the deleterious effect of hyperglycemia on osteoblasts (65, 66). However, there is also a possibility that poor metabolic health retards the maturation of COP cells to mature osteoblast (11). Given the different roles that COP may play in physiological and pathological conditions (58), future studies with larger sample size, longitudinal follow-up, and more demographically diverse patient population including women are needed to affirm results in this study.

Data availability statement

Restrictions apply to the availability of some or all data generated or analyzed during this study to preserve patient confidentiality or because they were used under license. The corresponding author will on request detail the restrictions and any conditions under which access to some data may be provided.

Ethics statement

This study involving human participants was conducted at the Michael E. DeBakey VA Medical Center in accordance with guidelines of the Declaration of Helsinki for the ethical treatment of human subjects. The protocol was approved by Baylor College of Medicine Internal Review Board. Each participant provided written informed consent to participate in this study.

Author contributions

Research concept was conceived and funding secured by RA-V and DV. Data collection and sample analysis were performed by EB, VR, VF, MP and SB. Data analysis was conducted by EB, FD, CQ, and RA-V. Manuscript was written by EB, FD, and RA-V, and was edited by EB, FD, CQ, and RA-V. All authors contributed to the article and approved the submitted version.

Funding

This work was supported by the US Department of Veterans Affairs Clinical Sciences Research and Development Merit Review Award 101CX001665 (to RAV) and National Institutes of Health (R01HD093047 to RAV).

Conflict of interest

The authors declare that the research was conducted in the absence of any commercial or financial relationships that could be construed as a potential conflict of interest.

Publisher's note

All claims expressed in this article are solely those of the authors and do not necessarily represent those of their affiliated organizations, or those of the publisher, the editors and the reviewers. Any product that may be evaluated in this article, or claim that may be made by its manufacturer, is not guaranteed or endorsed by the publisher.

Author Disclaimer

The contents do not represent the views of the U.S. Department of Veterans Affairs or the United States Government.

Supplementary material

The Supplementary Material for this article can be found online at: https://www.frontiersin.org/articles/10.3389/fendo.2022.936159/full#supplementary-material

References

1. Feng X, McDonald JM. Disorders of bone remodeling. *Annu Rev Pathol* (2011) 6:121–45. doi: 10.1146/annurev-pathol-011110-130203

2. Colleluori G, Aguirre L, Dorin R, Robbins D, Blevins D, Barnouin Y, et al. Hypogonadal men with type 2 diabetes mellitus have smaller bone size and lower bone turnover. *Bone* (2017) 99:14–9. doi: 10.1016/j.bone.2017.03.039

3. Shu A, Yin MT, Stein E, Cremers S, Dworakowski E, Ives R, et al. Bone structure and turnover in type 2 diabetes mellitus. *Osteoporos Int* (2012) 23(2):635–41. doi: 10.1007/s00198-011-1595-0

4. Sanches CP, Vianna AGD, Barreto F. The impact of type 2 diabetes on bone metabolism. *Diabetol Metab Syndrome* (2017) 9(1):85. doi: 10.1186/s13098-017-0278-1

5. Oz SG, Guven GS, Kilicarslan A, Calik N, Beyazit Y, Sozen T, et al. Evaluation of bone metabolism and bone mass in patients with type-2 diabetes mellitus. *J Natl Med Assoc* (2006) 98(10):1598–604. doi: 10.1186/s13098-017-0278-1

6. Rubin MR. Bone cells and bone turnover in diabetes mellitus. *Curr Osteoporos Rep* (2015) 13(3):186–91. doi: 10.1007/s11914-015-0265-0

7. Joad S, Ballato E, Deepika F, Gregori G, Fleires-Gutierrez AL, Colleluori G, et al. Hemoglobin A1c threshold for reduction in bone turnover in men with type 2 diabetes mellitus. *Front Endocrinol* (2021) 12.

8. Ballato E, Deepika F, Russo V, Fleires-Gutierrez A, Colleluori G, Fuenmayor V, et al. One-year mean A1c of > 7% is associated with poor bone microarchitecture and strength in men with type 2 diabetes mellitus. *Calcif Tissue Int* (2022). doi: 10.1007/s00223-022-00993-x

9. Karim L, Vashishth D. Heterogeneous glycation of cancellous bone and its association with bone quality and fragility. *PLoS One* (2012) 7(4):e35047. doi: 10.1371/journal.pone.0035047

10. Vashishth D, Gibson GJ, Khoury JI, Schaffler MB, Kimura J, Fyhrie DP, et al. Influence of nonenzymatic glycation on biomechanical properties of cortical bone. *Bone* (2001) 28(2):195–201. doi: 10.1016/S8756-3282(00)00434-8

11. Dienelt A, zur Nieden NI. Hyperglycemia impairs skeletogenesis from embryonic stem cells by affecting osteoblast and osteoclast differentiation. *Stem Cells Dev* (2011) 20(3):465–74. doi: 10.1089/scd.2010.0205

12. Huang K-C, Chuang P-Y, Yang T-Y, Huang T-W, Chang SF. Hyperglycemia inhibits osteoblastogenesis of rat bone marrow stromal cells via activation of the Notch2 signaling pathway. *Int J Med Sci* (2019) 16(5):696–703. doi: 10.7150/ijms.32707

13. Manavalan JS, Cremers S, Dempster DW, Zhou H, Dworakowski E, Kode A, et al. Circulating osteogenic precursor cells in type 2 diabetes mellitus. *J Clin Endocrinol Metab* (2012) 97(9):3240–50. doi: 10.1210/jc.2012-1546

14. Russo V, Colleluori G, Chen R, Mediwala S, Qualls C, Liebschnere M, et al. Testosterone therapy and bone quality in men with diabetes and hypogonadism: Study design and protocol. *Contemp Clin Trials Commun* (2021) 21:100723. doi: 10.1016/j.conctc.2021.100723

15. Mohamed O, Freundlich RE, Dakik HK, Grober ED, Najari B, Lipshultz LI, et al. The quantitative ADAM questionnaire: a new tool in quantifying the severity of hypogonadism. *Int J Impot Res* (2010) 22(1):20–4. doi: 10.1038/ijir.2009.35

16. Quattrocchi E, Goldberg T, Marzella N. Management of type 2 diabetes: consensus of diabetes organizations. *Drugs Context* (2020) 9:212607. doi: 10.7573/dic.212607

17. Colleluori G, Chen R, Turin CG, Vigevano F, Qualls C, Johnson B, et al. Aromatase inhibitors plus weight loss improves the hormonal profile of obese hypogonadal men without causing major side effects. *Front Endocrinol (Lausanne)* (2020) 11:277. doi: 10.3389/fendo.2020.00277

18. Sowers MR, Randolph J, Jannausch M, Lasley B, Jackson E, McConnell D., et al. Levels of sex steroid and cardiovascular disease measures in premenopausal and hormone-treated women at midlife: implications for the "timing hypothesis". *Arch.Intern.Med* (2008) 168(19):2146–53. doi: 10.1001/archinte.168.19.2146

19. Aguirre LE, Colleluori G, Fowler KE, Jan IZ, Villareal K, Qualls C, et al. High aromatase activity in hypogonadal men is associated with higher spine bone mineral density, increased truncal fat and reduced lean mass. *Eur.J.Endocrinol* (2015) 173(2):167–74. doi: 10.1530/EJE-14-1103

20. Gossiel F, Hoyle C, McCloskey EV, Naylor KE, Walsh J, Peel N, et al. The effect of bisphosphonate treatment on osteoclast precursor cells in postmenopausal osteoporosis: The TRIO study. *Bone* (2016) 92:94–9. doi: 10.1016/j.bone.2016.08.010

21. Ziegler-Heitbrock HWL, Ulevitch RJ. CD14: Cell surface receptor and differentiation marker. *Immunol Today* (1993) 14(3):121–5. doi: 10.1016/0167-5699(93)90212-4

22. Wright SD, Ramos RA, Tobias PS, Ulevitch RJ, Mathison JC. CD14, a receptor for complexes of lipopolysaccharide (LPS) and LPS binding protein. *Science* (1990) 249(4975):1431–3. doi: 10.1126/science.1698311

23. Schmid MC, Khan SQ, Kaneda MM, Pathria P, Shepard R, Louis TL, et al. Integrin CD11b activation drives anti-tumor innate immunity. *Nat Commun* (2018) 9(1):5379. doi: 10.1038/s41467-018-07387-4

24. Eghbali-Fatourechi GZ, Lamsam J, Fraser D, Nagel D, Riggs BL, Khosla S, et al. Circulating osteoblast-lineage cells in humans. *New Engl J Med* (2005) 352 (19):1959–66. doi: 10.1056/NEJMoa044264

25. Rubin MR, Manavalan JS, Dempster DW, Shah J, Cremers S, Kousteni S, et al. Parathyroid hormone stimulates circulating osteogenic cells in hypoparathyroidism. *J Clin Endocrinol Metab* (2011) 96(1):176–86. doi: 10.1210/jc.2009-2682

26. Cohen A, Kousteni S, Bisikirska B, Shah JG, Manavalan JS, Recker RR, et al. IGF-1 receptor expression on circulating osteoblast progenitor cells predicts tissue-based bone formation rate and response to teriparatide in premenopausal women with idiopathic osteoporosis. *J Bone Miner Res* (2017) 32(6):1267–73. doi: 10.1002/jbmr.3109

27. Perfetto SP, Chattopadhyay PK, Roederer M. Seventeen-colour flow cytometry: unravelling the immune system. *Nat Rev Immunol* (2004) 4(8):648–55. doi: 10.1038/nri1416

28. Flammer AJ, Gössl M, Li J, Matsuo Y, Reriani M, Loeffler D, et al. Patients with an HbA1c in the prediabetic and diabetic range have higher numbers of circulating cells with osteogenic and endothelial progenitor cell markers. *J Clin Endocrinol Metab* (2012) 97(12):4761–8. doi: 10.1210/jc.2012-2642

29. Vigevano F, Gregori G, Colleluori G, Chen R, Autemrongsawat V, Napoli N, et al. In men with obesity, T2DM is associated with poor trabecular microarchitecture and bone strength and low bone turnover. *J Clin Endocrinol Metab* (2021) 106(5):1362–76. doi: 10.1210/clinem/dgab061

30. Silva BC, Leslie WD, Resch H, Lamy O, Lesnyak O, Binkley N, et al. Trabecular bone score: A noninvasive analytical method based upon the DXA image. *J Bone Mineral Res* (2014) 29(3):518–30. doi: 10.1002/jbmr.2176

31. Gunawardene P, Bermeo S, Vidal C, Al-Saedi A, Chung P, Boersma D, et al. Age, gender, and percentage of circulating osteoprogenitor (COP) cells: The COP study. *Exp Gerontol* (2017) 96:68–72. doi: 10.1016/j.exger.2017.06.004

32. Friedenstein AJ, Chailakhyan RK, Gerasimov UV. Bone marrow osteogenic stem cells: in vitro cultivation and transplantation in diffusion chambers. *Cell Tissue Kinet* (1987) 20(3):263–72. doi: 10.1111/j.1365-2184.1987.tb01309.x

33. Yamaguchi A, Komori T, Suda T. Regulation of osteoblast differentiation mediated by bone morphogenetic proteins, hedgehogs, and Cbfa1. *Endocr Rev* (2000) 21(4):393–411. doi: 10.1210/edrv.21.4.0403

34. Neve A, Corrado A, Cantatore FP. Osteoblast physiology in normal and pathological conditions. *Cell Tissue Res* (2011) 343(2):289–302. doi: 10.1007/s00441-010-1086-1

35. Rutkovskiy A, Stensløkken KO, Vaage IJ. Osteoblast differentiation at a glance. *Med Sci Monit Basic Res* (2016) 22:95–106. doi: 10.12659/MSMBR.901142

36. Rosenberg N, Rosenberg O, Soudry M. Osteoblasts in bone physiology-mini review. *Rambam Maimonides Med J* (2012) 3(2):e0013. doi: 10.5041/RMMJ.10080

37. Boyle WJ, Simonet WS, Lacey DL. Osteoclast differentiation and activation. *Nature* (2003) 423(6937):337–42. doi: 10.1038/nature01658

38. Arai F, Miyamoto T, Ohneda O, Inada T, Sudo T, Brasel K, et al. Commitment and differentiation of osteoclast precursor cells by the sequential expression of c-fms and receptor activator of nuclear factor kappaB (RANK) receptors. *J Exp Med* (1999) 190(12):1741–54. doi: 10.1084/jem.190.12.1741

39. Masataka A, Hiroshi T. The molecular understanding of osteoclast differentiation. *Bone* (2007) 40(2):251–64. doi: 10.1016/j.bone.2006.09.023

40. Teitelbaum SL. Osteoclasts: what do they do and how do they do it? *Am J Pathol* (2007) 170(2):427–35. doi: 10.2353/ajpath.2007.060834

41. Xu F, Teitelbaum SL. Osteoclasts: New insights. *Bone Res* (2013) 1(1):11–26. doi: 10.4248/BR201301003

42. Yagi M, Miyamoto T, Sawatani Y, Iwamoto K, Hosogane N, Fujita N, et al. DC-STAMP is essential for cell-cell fusion in osteoclasts and foreign body giant cells. *J Exp Med* (2005) 202(3):345–51. doi: 10.1084/jem.20050645

43. Yang M, Birnbaum MJ, MacKay CA, Mason-Savas A, Thompson B, Odgren PR, et al. Osteoclast stimulatory transmembrane protein (OC-STAMP), a novel protein induced by RANKL that promotes osteoclast differentiation. *J Cell Physiol* (2008) 215(2):497–505. doi: 10.1002/jcp.21331

44. Kodama J, Kaito T. Osteoclast multinucleation: Review of current literature. *Int J Mol Sci* (2020) 21(16):5685. doi: 10.3390/ijms21165685

45. Roodman GD. Cell biology of the osteoclast. *Exp Hematol* (1999) 27 (8):1229–41. doi: 10.1016/S0301-472X(99)00061-2

46. Blair HC, et al. Isolated osteoclasts resorb the organic and inorganic components of bone. *J Cell Biol* (1986) 102(4):1164–72. doi: 10.1083/jcb.102.4.1164

47. Henriksen K, Kahn AJ, Crouch EC, Jeffrey JJ, Teitelbaum SL. Osteoclast activity and subtypes as a function of physiology and pathology–implications for future treatments of osteoporosis. *Endocrine Rev* (2011) 32(1):31–63. doi: 10.1210/er.2010-0006

48. Hattner R, Epker BN, Frost HM. Suggested sequential mode of control of changes in cell behaviour in adult bone remodelling. *Nature* (1965) 206(983):489–90. doi: 10.1038/206489a0

49. Takahashi H, Epker B, Frost HM. RESORPTION PRECEDES FORMATIVE ACTIVITY. *Surg Forum* (1964) 15:437–8.

50. Langdahl B, Ferrari S, Dempster DW. Bone modeling and remodeling: potential as therapeutic targets for the treatment of osteoporosis. *Ther Adv Musculoskeletal Dis* (2016) 8(6):225–35. doi: 10.1177/1759720X16670154

51. Cao X. Targeting osteoclast-osteoblast communication. *Nat Med* (2011) 17 (11):1344–6. doi: 10.1038/nm.2499

52. Kim J-M, Lin C, Stavre Z, Greenblatt MB, Shim JH. Osteoblast-osteoclast communication and bone homeostasis. *Cells* (2020) 9(9):2073. doi: 10.3390/cells9092073

53. Koichi M, Naoko I. Osteoclast–osteoblast communication. *Arch Biochem Biophysics* (2008) 473(2):201–9. doi: 10.1016/j.abb.2008.03.027

54. Chen X, Wang Z, Duan N, Zhu G, Schwarz EM, Xie C, et al. Osteoblast-osteoclast interactions. *Connect Tissue Res* (2018) 59(2):99–107. doi: 10.1080/03008207.2017.1290085

55. Clarke B. Normal bone anatomy and physiology. *Clin J Am Soc Nephrol* (2008) 3 Suppl 3(Suppl 3):S131–9. doi: 10.2215/CJN.04151206

56. Zaidi M. Skeletal remodeling in health and disease. *Nat Med* (2007) 13 (7):791–801. doi: 10.1038/nm1593

57. Kenkre J, Bassett J. The bone remodelling cycle. *Ann Clin Biochem* (2018) 55 (3):308–27. doi: 10.1177/0004563218759371

58. Feehan J, Kassem M, Pignolo RJ, Duque G. Bone from blood: Characteristics and clinical implications of circulating osteogenic progenitor (COP) cells. *J Bone Miner Res* (2021) 36(1):12–23. doi: 10.1002/jbmr.4204

59. Feehan J, Smith C, Tripodi N, Degabrielle E, Al Saedi A, Vogrin S, et al. Higher levels of circulating osteoprogenitor cells are associated with higher bone mineral density and lean mass in older adults: A cross-sectional study. *JBMR Plus* (2021) 5(11):e10561. doi: 10.1002/jbm4.10561

60. Napoli N, Chandran M, Pierroz DD, Abrahamsen B, Schwartz AV, Ferrari SL, et al. Mechanisms of diabetes mellitus-induced bone fragility. *Nat Rev Endocrinol* (2017) 13(4):208–19. doi: 10.1038/nrendo.2016.153

61. Farr JN, Khosla S. Determinants of bone strength and quality in diabetes mellitus in humans. *Bone* (2016) 82:28–34. doi: 10.1016/j.bone.2015.07.027

62. Compston J. Type 2 diabetes mellitus and bone. *J Intern Med* (2018) 283 (2):140–53. doi: 10.1111/joim.12725

63. Pal SN, Rush C, Parr A, Campenhout AV, Golledge J. Osteocalcin positive mononuclear cells are associated with the severity of aortic calcification. *Atherosclerosis* (2010) 210(1):88–93. doi: 10.1016/j.atherosclerosis.2009.11.001

64. Berendsen AD, Olsen BR. Osteoblast-adipocyte lineage plasticity in tissue development, maintenance and pathology. *Cell Mol Life Sci* (2014) 71(3):493–7. doi: 10.1007/s00018-013-1440-z

65. Zhen D, Chen Y, Tang X. Metformin reverses the deleterious effects of high glucose on osteoblast function. *J Diabetes its Complications* (2010) 24(5):334–44. doi: 10.1016/j.jdiacomp.2009.05.002

66. Zheng L, Shen X, Ye J, Xie Y, Yan S. Metformin alleviates hyperglycemia-induced apoptosis and differentiation suppression in osteoblasts through inhibiting the TLR4 signaling pathway. *Life Sci* (2019) 216:29–38. doi: 10.1016/j.lfs.2018.11.008

67. Hygum K, Starup-Linde J, Harsløf T, Vestergaard P, Langdahl BL. Mechanisms in endocrinology: Diabetes mellitus, a state of low bone turnover –

a systematic review and meta-analysis. *Eur J Endocrinol* (2017) 176(3):R137–57. doi: 10.1530/EJE-16-0652

68. Starup-Linde J. Diabetes, biochemical markers of bone turnover, diabetes control, and bone. *Front Endocrinol* (2013) 4:21–1. doi: 10.3389/fendo.2013.00021

69. Starup-Linde J, Lykkeboe S, Handberg A, Vestergaard P, Høyem P, Fleischer J, et al. Glucose variability and low bone turnover in people with type 2 diabetes. *Bone* (2021) 153:116159. doi: 10.1016/j.bone.2021.116159

70. Bilinski WJ, Szternel L, Siodmiak J, Krintus M, Paradowski PT, Domagalski K, et al. Effect of fasting hyperglycemia and insulin resistance on bone turnover markers in children aged 9–11 years. *J Diabetes its Complications* (2021) 35 (10):108000. doi: 10.1016/j.jdiacomp.2021.108000

71. Khosla S, Monroe DG. Regulation of bone metabolism by sex steroids. *Cold Spring Harbor Perspect Med* (2018) 8(1):a031211. doi: 10.1101/cshperspect.a031211

72. Compston JE. Sex steroids and bone. *Physiol Rev* (2001) 81(1):419–47. doi: 10.1152/physrev.2001.81.1.419

73. Schot LP, Schuurs AH. Sex steroids and osteoporosis: effects of deficiencies and substitutive treatments. *J Steroid Biochem Mol Biol* (1990) 37(2):167–82. doi: 10.1016/0960-0760(90)90325-F

74. Robinson LJ, Tourkova I, Wang Y, Sharrow AC, Landau MS, Yaroslavskiy BB, et al. FSH-receptor isoforms and FSH-dependent gene transcription in human monocytes and osteoclasts. *Biochem Biophys Res Commun* (2010) 394(1):12–7. doi: 10.1016/j.bbrc.2010.02.112

75. Wang A, Midura RJ, Vasanji A, Wang AJ, Hascall VC. Hyperglycemia diverts dividing osteoblastic precursor cells to an adipogenic pathway and induces synthesis of a hyaluronan matrix that is adhesive for monocytes. *J Biol Chem* (2014) 289(16):11410–20. doi: 10.1074/jbc.M113.541458

76. Bredella MA, Torriani M, Ghomi RH, Thomas BJ, Brick DJ, Gerweck AV, et al. Vertebral bone marrow fat is positively associated with visceral fat and inversely associated with IGF-1 in obese women. *Obes (Silver Spring)* (2011) 19 (1):49–53. doi: 10.1038/oby.2010.106

77. Clabaut A, Delplace S, Chauveau C, Hardouin P, Broux O. Human osteoblasts derived from mesenchymal stem cells express adipogenic markers upon coculture with bone marrow adipocytes. *Differentiation* (2010) 80(1):40–5. doi: 10.1016/j.diff.2010.04.004

78. Justesen J, Schols AM, Kelders MC, Wouters EF, Janssen-Heininger YM. Adipocyte tissue volume in bone marrow is increased with aging and in patients with osteoporosis. *Biogerontology* (2001) 2(3):165–71. doi: 10.1023/A:1011513223894

79. Rodríguez JP, Astudillo P, Ríos S, Pino AM. Involvement of adipogenic potential of human bone marrow mesenchymal stem cells (MSCs) in osteoporosis. *Curr Stem Cell Res Ther* (2008) 3(3):208–18. doi: 10.2174/157488808785740325

80. Lee D, Goldberg AL. Muscle wasting in fasting requires activation of NF-κB and inhibition of AKT/Mechanistic target of rapamycin (mTOR) by the protein acetylase, GCN5. *J Biol Chem* (2015) 290(51):30269–79. doi: 10.1074/jbc.M115.685164

81. Langen RC, Schols AM, Kelders MC, Wouters EF, Janssen-Heininger YM. Inflammatory cytokines inhibit myogenic differentiation through activation of nuclear factor-kappaB. *FASEB J* (2001) 15(7):1169–80. doi: 10.1096/fj.00-0463

82. Bonnet N, Bourgoin L, Biver E, Douni E, Ferrari S. RANKL inhibition improves muscle strength and insulin sensitivity and restores bone mass. *J Clin Invest* (2019) 129(8):3214–23. doi: 10.1172/JCI125915

83. Kirk B, Lieu N, Vogrin S, Sales M, Pasco JA, Duque G, et al. Serum levels of c-terminal telopeptide (CTX) are associated with muscle function in community-dwelling older adults. *Journals Gerontol: Ser A* (2022). doi: 10.1093/gerona/glac008

h84. Idris AI, van 't Hof RJ, Greig IR, Ridge SA, Baker D, Ross RA, et al. Regulation of bone mass, bone loss and osteoclast activity by cannabinoid receptors. *Nat Med* (2005) 11(7):774–9. doi: 10.1038/nm1255

85. Garbe AI, Roscher A, Schüler C, Lutter AH, Glösmann M, Bernhardt R, et al. Regulation of bone mass and osteoclast function depend on the f-actin modulator SWAP-70. *J Bone Mineral Res* (2012) 27(10):2085–96. doi: 10.1002/jbmr.1670

86. Kogawa M, Anderson PH, Findlay DM, Morris HA, Atkins GJ. The metabolism of 25-(OH)vitamin D3 by osteoclasts and their precursors regulates the differentiation of osteoclasts. *J Steroid Biochem Mol Biol* (2010) 121(1-2):277–80. doi: 10.1016/j.jsbmb.2010.03.048

87. Kogawa M, Findlay DM, Anderson PH, Ormsby R, Vincent C, Morris HA, et al. Osteoclastic metabolism of 25(OH)-vitamin D3: a potential mechanism for optimization of bone resorption. *Endocrinology* (2010) 151(10):4613–25. doi: 10.1210/en.2010-0334

frontiers | Frontiers in Endocrinology

TYPE Original Research
PUBLISHED 17 October 2022
DOI 10.3389/fendo.2022.913979

OPEN ACCESS

EDITED BY
Michaela Tencerova,
Academy of Sciences of the Czech Republic (ASCR), Czechia

REVIEWED BY
Hua Yue,
Shanghai Jiao Tong University, China
Marcela Buchtova,
Czech Academy of Sciences, Czechia

*CORRESPONDENCE
Fangfang Liu
lianpipi@fmmu.edu.cn
Yuanming Wu
wuym@fmmu.edu.cn
Yaoping Wu
horikawadavid@vip.Sina.com

†These authors have contributed equally to this work

SPECIALTY SECTION
This article was submitted to Bone Research, a section of the journal Frontiers in Endocrinology

RECEIVED 06 April 2022
ACCEPTED 28 September 2022
PUBLISHED 17 October 2022

CITATION
Chen Q, Yao Y, Chen K, Chen X, Li B, Li R, Mo L, Hu W, Zhang M, Wang Z, Wu Y, Wu Y and Liu F (2022) Aberrant activation of TGF-β1 induces high bone turnover *via* Rho GTPases-mediated cytoskeletal remodeling in Camurati-Engelmann disease. *Front. Endocrinol.* 13:913979. doi: 10.3389/fendo.2022.913979

Aberrant activation of TGF-β1 induces high bone turnover *via* Rho GTPases-mediated cytoskeletal remodeling in Camurati-Engelmann disease

Qi Chen[1,2†], Yan Yao[1,3†], Kun Chen[4†], Xihui Chen[1,2], Bowen Li[1,2], Rui Li[1,2], Lidangzhi Mo[1,2], Weihong Hu[3], Mengjie Zhang[3], Zhen Wang[5], Yaoping Wu[5*], Yuanming Wu[1,2*] and Fangfang Liu[6*]

[1]Department of Biochemistry and Molecular Biology, School of Basic Medicine, Air Force Medical University, Xi'an, China, [2]Shaanxi Provincial Key Laboratory of Clinic Genetics, Air Force Medical University, Xi'an, China, [3]Department of Cell Biology and Genetics, Medical College of Yan'an University, Yan'an, China, [4]Department of Anatomy, Histology and Embryology and K.K. Leung Brain Research Centre, School of Basic Medicine, Air Force Medical University, Xi'an, China, [5]Department of Orthopedics, The First Affiliated Hospital of Air Force Medical University, Xi'an, China, [6]Department of Neurobiology, School of Basic Medicine, Air Force Medical University, Xi'an, China

In the adult skeleton, the bone remodeling process involves a dynamic coordination between osteoblasts and osteoclasts, which is disrupted in diseases with high bone turnover rates and dysregulated transforming growth factor beta 1 (TGF-β1). However, little is known about how TGF-β1 signaling mediates bone resorption. Here, we described a pedigree with a heterozygous variant in TGF-β1 (R218C) that resulted in aberrant activation of TGF-β1 through an activating mechanism that caused Camurati-Engelmann disease (CED). We showed that CED patients have high levels of active Rho GTPases and the migration-related proteins Integrin β1 and Integrin β3 in their peripheral blood. HEK293T cells transfected with a plasmid encoding this mutant expressed high levels of TGF-β1 and active Rho GTPases. Furthermore, activation of Rho by TGF-β1 increased osteoclast formation and bone resorption, with increased migration of pre-osteoclasts, as well as cytoskeletal remodeling of pre-osteoclasts and mature osteoclasts. Importantly, pharmacological inhibition of Rho GTPases effectively rescued hyperactive TGF-β1-induced osteoclastogenesis *in vitro*. Overall, we propose that Rho GTPases mediate TGF-β1-induced osteoclastogenesis and suggest that Rho-TGF-β1 crosstalk is associated with high bone turnover in CED.

KEYWORDS

Camurati-Engelmann disease, osteoclast, TGF-β1, Rho GTPases, cytoskeletal remodeling

Introduction

Anomalies of the bone remodeling process are usually described in skeletal disorders, including Camurati-Engelmann disease (CED) (1). The disorder manifests with pain in early childhood, muscular weakness, and gait disturbances (2). Transforming growth factor beta 1 (TGF-β1) is involved in CED, and in healthy individuals, activated TGF-β1 stimulates bone deposition (3, 4). In CED, mutations cause inadequate activation of TGF-β1 and poor-quality bone formation (5); however, the role of TGF-β1 in CED remains unclear.

In skeletal tissues, TGF-β1 regulates the functions of osteoblasts and osteoclasts (1, 6–8). Specifically, TGF-β1 binds to cell surface receptors that activate receptor-regulated Smads (R-Smads), which are important proteins for regulating cell development and growth (9). In addition, TGF-β1 also acts through non-Smad effectors, including Rho GTPases, focal adhesion kinase (FAK) and mitogen-activated protein kinases (MAPKs) (10–13). Among them, Rho GTPases regulate the organization of the cytoskeleton (9), and once activated, they bind to protein kinases and actin-binding proteins that modulate F-actin dynamics, leading to morphological changes (9, 14). Recent studies found that the Rho GTPases and Rho-associated coiled-coil-containing protein kinases (ROCKs) were involved in cell growth, cell death and cytoskeletal reorganization in osteogenic cells. ROCK activity also triggered cartilage degradation and affected bone formation. In chondrocytes and osteoblasts, the inhibition of Rho GTPase/ROCK activity prevented cartilage degradation and promoted bone formation (15).

Osteoclasts maintain the balance of bone metabolism in the body by cooperating with osteoblasts. Excessive activity of osteoclasts leads to bone loss; thus, understanding the activities of osteoclasts is necessary for developing therapeutic strategies against osteoclast-related disorders (16). Although the relationship between Rho GTPases and bone metabolism is well-documented, the role of Rho GTPases in regulating TGF-β1-induced osteoclast production remains ambiguous.

Here, the clinical features of heterozygous patients with CED —with a mutation in the TGF-β1 propeptide—are described. We reported a CED pedigree that causes aberrant activation of TGF-β1 due to p.R218C mutation. Our study also confirmed that activated TGF-β1 promotes osteoclast fusion and maturation through Rho GTPase-mediated cytoskeletal remodeling and cell migration. We consider that Rho GTPases signaling is a possible therapeutic target for bone diseases with high bone turnover rates including CED.

Materials and methods

Genetics

Peripheral blood was obtained from individuals with CED and their relatives. The DNA extraction kit (QIAamp DNA Micro, Qiagen) was used to extract genomic DNA from white blood cells. Several sets of primers were designed to amplify segments of TGF-β1. The amplification was performed with PCR and the amplified products were analyzed by Sanger sequencing.

Cell treatments

Cells were purchased from the American Type Culture Collection (ATCC, TIB-71). The Dulbecco's modified Eagle's medium (DMEM) was used to culture RAW264.7 cells, along with 10% fetal bovine serum (FBS), streptomycin (100 μg/ml) and penicillin (100 units/ml). Then, they were seeded in a chamber at 37°C, supplemented with 5% CO_2. The ALK4/5/7 inhibitor SB431542 (MCE, 10 μM), ROCK inhibitor Y27632 (Selleck, 10 μM), or Rac GTPase inhibitor NSC23766 (Selleck, 50 μM) were used as treatments. Later, cells were exposed to recombinant sRANK Ligand (Peprotech, 30 ng/ml) and recombinant TGF-β1 (Peprotech, 10 ng/ml) and processed for further experiments.

Osteoclast differentiation

RAW264.7 cells were cultured with density at 2×10^4 cells/cm^2. At 12 hours, the cells attached to the wall were medicated with RANKL and TGF-β1 (0, 1, 5, 10, and 20 ng/ml) for 5 days. The inhibitors were added to the culture solution for 1 hour before adding RANKL and TGF-β1. Cells were harvested for protein, RNA, cell staining and SEM. We conducted osteoclast differentiation experiments at least three times.

TRAP staining assay

After washing with PBS, cells were fixed with 4% PFA. Then, 0.1% Triton X-100 permeabilized cells for 10 min. After washing, cells were stained with tartrate-resistant acid phosphatase (TRAP) solution (Sigma-Aldrich). After washing, cells were stained with hematoxylin to localize nuclei. TRAP positive cells (nuclei ≥ 3) were defined as differentiated osteoclasts. Bright-field images were captured using the inverted fluorescence microscope (Olympus IX73).

Western blot analysis

The RIPA buffer (Biotime Biotechnology, cat. #P0013B, China) was used to extract proteins. The total protein content was analyzed through a bicinchoninic acid (BCA) kit (Biovision, cat. #K813-2500). For denaturation, a metal bath was used to boil samples for 10 min after mixing with 6× loading buffer

(Tiangen, #RT201). The amount of 20 μg protein was moved into polyvinylidene difluoride (PVDF) membranes after separation using 10% SDS-PAGE. The blocking agent (5% skim milk) was then added. The PVDF was incubated with several primary monoclonal antibodies: rabbit anti-Smad2/3 (CST, #8685, 1:1000), rabbit anti-p-Smad2/3 (CST, #8828, 1:1000), rabbit anti-JNK (CST, #9552, 1:1000), rabbit anti-p-JNK (CST, #4668, 1:1000), rabbit anti-ERK1/2 (CST, #4695, 1:1000), rabbit anti-p-ERK1/2 (CST, #4370, 1:1000), rabbit anti-p38 (CST, #9212, 1:1000), rabbit anti-p-p38 (CST, #4631, 1:1000), rabbit anti-Tartrate Resistant Acid Phosphatase (Abcam, #ab191406, 1:2000), mouse anti-Smad4 (Santa, #sc-7966, 1:1000), rabbit anti-NFATc1 (CST, #8032, 1:1000), rabbit anti-RhoA (CST, #2117, 1:1000), rabbit anti-Cdc42 (CST, #2466, 1:1000) and mouse anti-β-actin (Sigma, 1:10000). Rabbit polyclonal antibodies anti-Rac1/2/3 (CST, #2465, 1:1000) were also used. The secondary antibodies used were horseradish peroxidase-conjugated goat anti-rabbit and goat anti-mouse (Sigma, 1:8000). The chemiluminescence was developed with ECL solution (Milllipore). Experimental procedures were performed three times in triplicate, independently.

Real time PCR

The AxypreTM Miniprep Kit (Axygen, cat. #365) extracted the RNA from RAW264.7 cells. The PrimeScript^{TM} RT Master Mix (Takara, cat. #RR036A) reverse-transcribed the RNA. The real-time quantitative polymerase chain reaction (PCR) was performed by SYBR Premix Ex Taq^{TM} II (Takara, #RR820A) and 7500 system (Applied Biosystems), followed by the operational steps: 95°C for 30 s, 40 cycles at 95°C for 3 s and 60°C for 30 s, then again 60°C for 30 s. The mRNA of GAPDH was the reference as standard control. The $2^{-\Delta\Delta Ct}$ method calculated the relative expression of target genes. The primers are described in Supplementary Table 1. The Primer 3 software (http://primer3.ut.ee/) designed oligonucleotides. We performed all PCR experiments three times in triplicate, independently.

Resorption pit formation assay

The assay was performed in accordance with a typical assay procedure of Bone Resorption Assay Kit (CSR-BRA-48KIT, Cosmo Bio Co., LTD). The kit contains 48-well plates pre-coated with carbonate apatite (CaP). Prior to cell seeding, each well in the plate was coated with fluoresceinamine-labelled chondroitin sulphate (FACS) for 2 h. RAW264.7 cells (1×10^4 cells per well) were used for the differentiation process with RANKL (30 ng/ml), TGF-β1 (10 ng/ml) and/or inhibitors. Plates were incubated at a humidity of 5% CO_2 for 5 days at 37°C. On day 5, the conditioned medium (100 μl) was moved into a 96-well black plates. For each well, the bone resorption assay buffer (50 μl) was later added. A plate shaker was used for mixing. The fluorescence was measured according to the previously set parameters. The media were aspirated on day 5 to analyze pit formation. 5% sodium hypochlorite (100 μl) was added for 5 min. The wells dried at room temperature from 3 to 5 h after washing with distilled water. The pit areas were visualized under bright-field using a microscope. The Image J software analyzed the images. A microplate reader (Tecan Spark, Switzerland) was used to read the fluorescence signal produced.

Transwell migration assay

The migratory response of RAW 264.7 cells was analyzed through transwell inserts (8 um, Costar, Corning, NY). RAW 264.7 cells were seeded in the upper chamber (1×10^5 cells/well), with RANKL (30 ng/ml), TGF-β1 (10 ng/ml) and/or inhibitors. The inhibitors were used as pre-treatment for 1 h for 2 days. Methanol fixed migrated cells, then crystal violet stained cells. The transwell membrane was photographed through three independent views and the migrated cells were counted.

FITC-phalloidin staining

After washing two times with PBS, 3.7% formaldehyde fixed cells and 0.1% Triton X-100 permeabilized cells for 10 min, respectively. Monolayers were blocked with 2% BSA for 30 min and seeded with 10 μg/ml of FITC-phalloidin (P5282, Sigma-Aldrich) at 37°C for 1 h. Then, the nucleus were labelled with DAPI (D9542, Sigma Aldrich, 1 μg/ml) for 5 min. After another washing with PBS, cells were visualized through a laser confocal microscope (Olympus, Japan). For each sample, random fields evaluating intracellular F-actin intensity and the formation of F-actin ring with a specific software.

Electron microscopy

RAW264.7 cells on the plastic coverslip were treated as described. 1% osmium tetroxide and 2.5% glutaldehyde were used to fix mock and inhibitor-treated cells, followed by ethanol dehydration. After drying, silver paste was used to mount slides. Osteoclasts were imaged under ×1,000 and ×3,000 magnification using a Hitachi S-3400N SEM. In addition, for pre-osteoclasts, the magnifications were ×2,000 and ×7,000, respectively.

Rho GTPase activation assay

The assay was implemented through a GTPase G-LISA activation assay kit (BK135, Cytoskeleton, Inc.). After washing with PBS, RAW264.7 or HEK293T cells were treated with a cold

lysis buffer for 20 min. After centrifugation at 4°C, the samples were analyzed through a bicinchoninic acid (BCA) protein assay kit (Biovision, cat. #K813-2500). Around 25 µg of total proteins were loaded in GTPases binding wells for detecting the active form of Rho GTPases (RhoA, Rac1 and Cdc42). The active forms were immobilized, then primary antibodies for Rho GTPases and HRP-conjugated secondary antibodies were added. After PBS washing HRP detection substrates were added and a microplate reader (Tecan Spark, Switzerland) was used to measure the intensity by luminometric methods. Detection of lysates from peripheral blood mononuclear cells (PBMCs) was also performed according to the procedure described above.

TGF-β1 mutants and cell transfection

Human cDNA was cloned from TGF-β1 in pCDNA 3.1 vectors. Plasmids constructed by Hunan FengHui Biotechnology Co., Ltd include pcDNA3.1-T2A-EGFP (control), TGF-β1-WT-pcDNA3.1-T2A-EGFP (WT) and TGF-β1 (C652T)-pcDNA3.1-T2A-EGFP (mutation). Medium or cell lysates were obtained for expression of mutant and WT TGF-β1 after transfection. The protein expression was quantified by enzyme-linked immunosorbent assay (ELISA), GLISA, western blotting and cell staining as described.

Conditioned medium culture

Forty-eight hours after we transfected HEK293T cells with the above plasmids, the conditioned medium was collected and concentrated with a centrifugal filter device (3 kDa cut-off; Amicon Ultra-15, Millipore). The resulting medium (approximately 50-fold concentrated) was assayed for active TGFB1 levels by ELISA assays and preserved in aliquots at −80°C until use. When preparing to start the experiment, add concentrated conditioned medium was added to RAW264.7 cells cultured in 12-well and 24-well plates to induce osteoclasts for 5 days. We set up the following experimental groups: concentrate of untransfected HEK293T cells (293-U, with RANKL), concentrate transfected with NC plasmid (NC, with RANKL), wild-type plasmid (WT, with RANKL), mutant plasmid (MUT, with RANKL), blank control group (CON, RANKL only) and positive control group (PC, RANKL and TGF-β1 combined); the final concentration of TGF-β1 in the medium of the mutant group was 10ng/ml. Cells were then collected for western blot analysis and TRAP staining.

ELISA test

TGF-β1 was properly quantified by the enzyme-linked immunosorbent assay (ELISA, Novus, USA) in serum and supernatants.

Molecular structure

Human TGF-β1 was obtained from the Protein Data Bank (https://www.uniprot.org) code P01137. Graphics were generated using Swiss-Model (https://swissmodel.expasy.org).

TGF-β1 conservation analysis

A phylogenetic tree was generated and evolutionary conservation analysis was done using the ConSurf server. Bayesian calculation method was used to calculate conservation score from the protein sequence. Here the ConSurf Server (vConSurf-2016) evaluated the conservation of TGF-β1 across species. The multiple sequence alignment is displayed in Figure 8. Supplementary Figure 4 shows the residue variety for R218 variant in TGF-β1. Human wild-type TGF-β1 residues are indicated in blue and human TGF-β1 variant in red (17, 18).

Statistical analysis

Data are presented as mean ± standard deviation (SD). Independent groups were compared using the two-tailed *t*-test. GraphPad Prism software (San Diego, CA) was used. A *p*-value below 0.05 was set as statistically significant.

Results

Clinical features and biochemical findings

Five individuals across two generations were covered by the pedigree (Figure 1A). The proband (patient 1, female) and her sister (patient 2, female) exhibited bone abnormalities. Computed tomography (CT) imaging showed periosteal thickening and sclerosis of facial bones and skulls (Figures 1B, C). Both patients suffered pain in the extremities and reported gait disturbances, protruding eyeballs and muscle weakness. They also exhibited hepatosplenomegaly, dizziness, blurred vision, and hearing loss, and patient 1 had anemia, which was absent in patient 2; however, patient 2 had changes in secondary sexual characteristics. Notably, patient 1 developed left ventricular dilation and deterioration of cardiac function, which were rarely detected in previous cases (Supplementary Figure 1A, Supplementary Table 2).

Biochemical results are displayed in Table 1. Serum alkaline phosphatase (ALP) and phosphorus (P) were significantly elevated in both patients (reference range: ALP, 53–141 U/L; P, 0.9–1.34 mmol/L). The thyroid hormone was in the normal range in both patients. Still, the serum thyroid-stimulating

hormone (TSH) of patient 1 was significantly higher than the normal value, and her calcium level was lower than normal (reference range: 2.00–2.50 mmol/L). In addition, both patients had abnormally high activated partial thromboplastin time (APTT) and prothrombin time (PT).

Sequencing analysis identified a heterozygous transition (c.652C > T) [p.Arg218Cys] in exon 4 of TGF-β1 in the proband of each patient (Figure 1D). No mutation was found in their parents or siblings (Supplementary Figure 1B).

A high level of active TGF-β1 in peripheral blood of CED patients is associated with bone remodeling

Radiographs demonstrated sclerosis of the calvarium and the skull base; bilaterally (Figure 2A). Imaging revealed elevated bilateral hyperostosis and endostosis of several long bone diaphysis (Figures 2B, C). In addition, patient 1 had severe scoliosis (Figure 2D). Bone scintigraphy found diffuse uptake in the skull and the upper and lower extremities, consistent with the sclerosing dysplasia lesions on radiographs (Figure 2E). Reduced bone densitometry values were reported for patient 1 (Supplementary Figure 1C). Increases in active TGF-β1 expression (Figure 2F) and mRNA expression of the osteoclasts marker acid phosphatase type 5 (*ACP5*) (Figure 2G) were described in peripheral blood and PBMCs of patients, respectively.

TGF-β1 enhances RANKL-induced osteoclast formation

Excessive osteoclast activity leads to bone loss and osteoporosis (16). Osteoclasts were used to assess the regulatory function of TGF-β1 because of the lower bone mineral density in CED patients and the high expression of osteoclast marker ACP5 in their peripheral blood. We differentiated RAW264.7 cells in osteoclasts. The effects of different concentrations of receptor activators of nuclear factor-κB ligand (RANKL, 30 and 50 ng/ml) were first evaluated. TRAP staining showed that the effects of 30 and 50 ng/ml RANKL were similar (Supplementary Figure 2A); therefore, 30 ng/ml was used to induce osteoclasts in further experiments. During osteoclast formation, we administered 0, 1, 5, and 10 ng/ml of TGF-β1, which increased RANKL-induced osteoclast formation in a dose-dependent manner. Therefore, 10 ng/ml was used in the following experiments. When used alone, TGF-β1 had no osteoclast-inducing effect *in vitro*, even at a high concentration (Figures 3A, B).

Next, we varied the duration of exposure to these two cytokines and analyzed the osteoclast-inducing effects of TGF-β1. TGF-β1 was administered in RAW264.7 cells for different periods (Figures 3C, D). When RANKL was administered, exposure to TGF-β1 throughout the culture caused a time-dependent increase in the level of the osteoclast marker TRAP. Nuclear factor of activated T cells c1 (NFATc1) was significantly increased in the early stages (1–3 days). SB431542 is a potent and specific inhibitor of transforming growth factor-beta superfamily type I activin receptor-like kinase (ALK) receptors ALK4, ALK5, and ALK7. We found that treatment with SB431542 inhibited osteoclast differentiation (Figures 3E, F). In addition, exposure to a high concentration of TGF-β1 (20 ng/ml) reduced the number and area of multinucleated osteoclasts, and this inhibitory effect was not rescued by the addition of SB431542 (Figures 3G, H). These results indicate that 1–10 ng/ml of TGF-β1 could enhance RANKL-induced osteoclast formation, while a high concentration (20 ng/ml) of TGF-β1 had the opposite effect.

The Smad and MAPK pathways regulate TGF-β1-mediated osteoclast formation

To assess the effects of TGF-β1 treatment on the classical TGF-β1/Smad and non-Smad pathways during osteoclastogenesis, we analyzed the levels of mRNAs and proteins during RANKL-induced osteoclast differentiation when TGF-β1 was present. Expression of Smad4 and Smad2/3 did not significantly change, while expression of p-Smad2/3 increased in the early stage, decreased in the intermediate stage, and increased again in the late stage (Figure 4A). Consistent with the findings regarding osteoclastogenesis, TGF-β1 significantly increased the expression of osteoclast-associated genes induced by RANKL, including *Acp5* (also known as *Trap*), cathepsin K (*Ctsk*), and osteoclast stimulatory transmembrane protein (*Oc-stamp*) (Figure 4B). In addition, we investigated other effects of TGF-β1. The phosphorylation of p38, ERK, and JNK was inhibited by TGF-β1 in the early stages and stimulated in the late stages (Figure 4C). SB431542 inhibited phosphorylation of Smad2/3, p38, and ERK, indicating that it inhibits TGF-β1 induced Smad and MAPK activation in osteoclasts (Figures 4D, E). In the presence of SB431542, expression of transforming growth factor beta-activated kinase 1 (*Tak1*) was inhibited, confirming the effect of the inhibitor. The expression levels of *Acp5, Ctsk, Oc-stamp*, and osteoclast-associated receptor (*Oscar*) were significantly reduced. The enhancement of osteoclast differentiation by TGF-β1 was blocked (Figure 4F).

To investigate the effect of the p.R218C mutation on TGF-β1 activity *in vitro*, we constructed WT and mutant vectors investigating the effects of the p.R218C mutation on TGF-β1 activity *in vitro*. We measured the TGF-β1 protein in the supernatants of HEK293T cells transfected with these vectors using the ELISA test. TGF-β1 was higher in the supernatants of transfected cells (Figure 4G). Expression of the constitutively active TGF-β1 variant in HEK293T cells increased the

phosphorylation of Smad2/3 and p38, but not in cells expressing WT TGF-β1 (Figure 4H). The TGF-β1 variant in the patients enhanced well-defined TGF-β1 receptor-mediated Smad and p38/MAPK signaling pathways and augmented osteoclast differentiation mediated by these pathways.

Rho GTPases regulate TGF-β1-mediated pre-osteoclast migration and fusion

How TGF-β1 regulates Rho GTPases to participate in osteoclast formation remains an important question in the field. To assess TGF-β1 effects on Rho signaling during osteoclast differentiation, the levels of Rho GTPases during RANKL-induced osteoclast differentiation were investigated. Expression of Rho GTPases did not significantly change overall, but the levels of GTP-bound Rho GTPases were augmented. Their levels were decreased to varying extents in the presence of SB431542 (Figures 5A, B), and mRNA expression of *Rock1* and *Rock2* downstream of RhoA was also reduced by SB431542 administration (Supplementary Figure 2B). Expression of the constitutively active TGF-β1 variant in HEK293T cells increased the levels of active Rho GTPases but not in WT TGF-β1 cells (Figure 5C), which was consistent with the results concerning osteoclasts.

To determine the effect of the p.R218C mutation on osteoclasts, we collected conditioned medium from HEK293T cells transfected with the plasmids to stimulate RAW264.7 cells. The results showed that the p.R218C mutant HEK293T cells-

TABLE 1 Overview of patients' clinical data.

Characteristic	Patient 1	Patient 2
Gender	Female	Female
Pain in extremities	+	+
Waddling gait	+	+
Muscle weakness	+	+
Hepatosplenomegaly	+	+
Easy fatigability	+	+
Headache and dizziness	+	+
Exophthalmos	+	+
Anemia	+	–
Bone mineral density	Osteoporosis	Osteoporosis
ALP	384 U/L[1]	422 U/L[1]
P	2.14 mmol/L[1]	1.46 mmol/L[1]
Ca	1.53 mmol/L[1]	2.33 mmol/L
TG	25.31 ng/ml	12.8 ng/ml
T3	1.68 nmol/L	2.04 nmol/L
T4	99.61 nmol/L	121 nmol/L
FT3	4.51 pmol/L	4.37 pmol/L
FT4	14.86 pmol/L	17.5 pmol/L
TSH	35.09 mIU/L[1]	3.44 mIU/L
PT	13.8s[1]	14.3s[1]
APTT	43.10s[1]	52.4s[1]

[1]abnormal value. ALP, serum alkaline phosphatase; P, phosphorus; Ca, calcium; TG, thyroglobulin; T3, triiodothyronine; T4, thyroxine; FT3, free triiodothyronine; FT4, free thyroxine; TSH, thyroid-stimulating hormone; PT, prothrombin time; APTT, activated partial thromboplastin time.

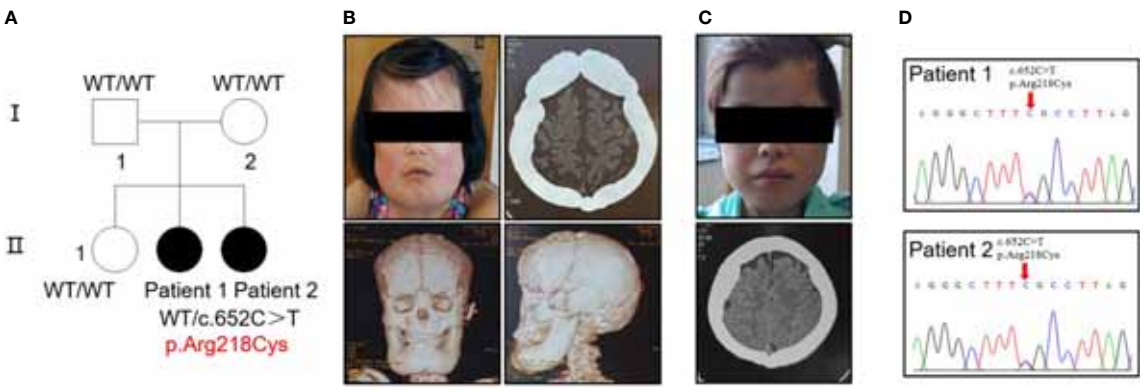

FIGURE 1
Identification of a heterozygous p.R218C mutation in patients with CED. **(A)** The pedigree covered two generations and five individuals. Patients 1 and 2 had a *de novo* mutation (p.R218C). Black-filled symbols indicate affected individuals. Patient 1 was the proband. **(B)** Clinical photograph of patient 1. A CT scan showed bilateral sclerotic thickening of the base of the skull. Images based on a reconstructed CT scan showed more pronounced symptoms. **(C)** Clinical photograph of patient 2. A CT scan showed the same symptom as patient 1. Written permission from the patients was obtained for the reproduction of these photographs. **(D)** Electropherograms of Sanger sequencing show that the TGF-β1 mutation (c.652C > T) was heterozygous in the affected individuals in this family.

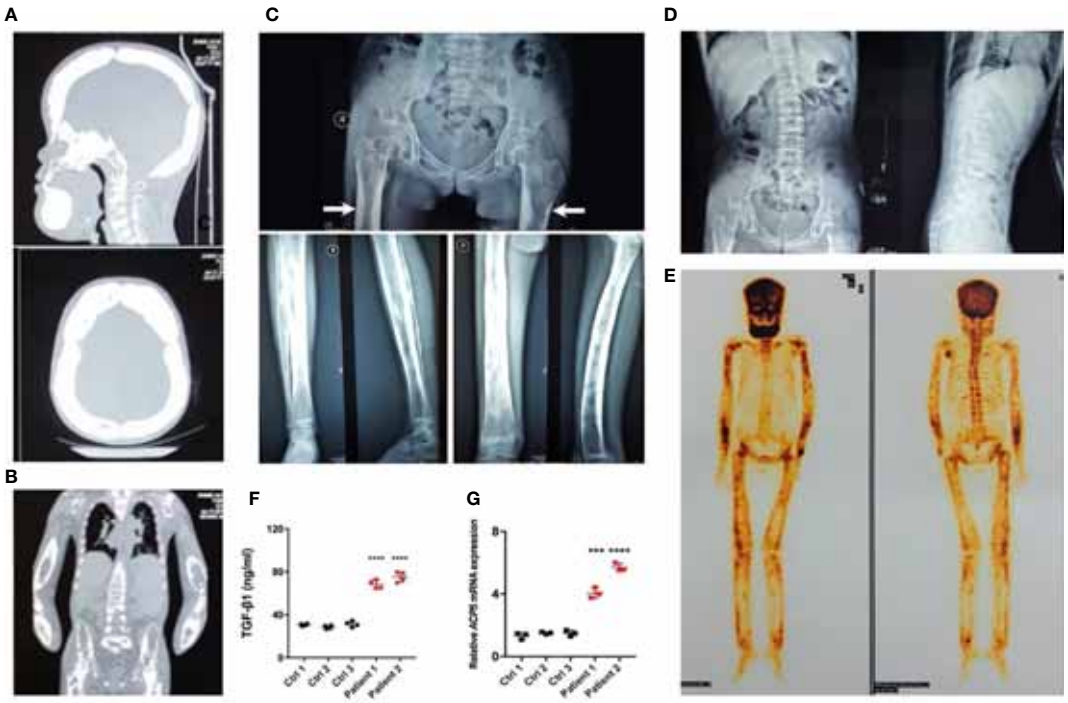

FIGURE 2
Typical osteosclerotic lesions of CED patients. **(A)** Skull radiographs of patient 1 showing bilateral sclerotic bony enlargement in the skull base and calvarium. **(B)** Thickening and irregularity of endosteal and periosteal sides of diaphyses of all long bones, including the radius and ulna. **(C)** Anteroposterior radiograph of the pelvis showing bilateral chronic femoral diaphyseal cortical thickening and sclerosis with severe degenerative changes of the hips (arrows). Lower-extremity radiographs showed bilateral symmetrical hyperostosis and endostosis of the diaphysis in both femurs, tibias, and fibulas. **(D)** Radiographs from patient 1 show severe scoliosis of the spine with osteopenia. **(E)** Whole-body bone scintigraphy of patient 1 shows the symmetrical distribution of the disease. Increased tracer uptake is visible in the diaphyseal portion of the long bones of the femora, lower legs, humeri, forearms, clavicles, and frontal bones, consistent with the radiographic findings. **(F)** The levels of active TGF-β1 were higher in peripheral blood of patients 1 and 2 than in the peripheral blood of normal controls. **(G)** The mRNA levels of *ACP5* were higher in the PBMCs of patients 1 and 2 than in normal controls. ***$p < 0.001$; ****$p < 0.0001$.

conditioned medium promoted the formation of osteoclasts differentiated from RAW264.7 cells (Supplementary Figures 2C, D) and activated the Smad and MAPK signaling pathways (Supplementary Figures 2E, F).

To further validate the role of Rho GTPases in TGF-β1-mediated osteoclastogenesis, we examined the formation of mature osteoclasts. The formation of mature osteoclasts decreased when a RhoA inhibitor (Y27632) and a Rac1 inhibitor (NSC23766) were administered. The suppressive effects of Rac1 inhibition on mature osteoclast formation (Figures 5D, E) and bone resorption (Figures 5F, G) were much greater than those of RhoA inhibition.

Spatiotemporally coordinated activation of RhoA, Rac1 and Cdc42 is required for effective cell migration. Therefore, we examined how TGF-β1 regulates osteoclast migration by activating RhoA, Rac1, and Cdc42. Transwell-based migration assays demonstrated that TGF-β1 enhanced RANKL-induced migration of pre-osteoclasts. SB431542, Y27632, and NSC23766 inhibited this migration to varying extents (Figures 5H, I). We determined how RhoA and Rac1 contributed to the expression of FAK and integrins involved in TGF-β1-induced osteoclast migration using Y27632 and NSC23766. Inhibition of RhoA and Rac1 downregulated RANKL- and TGF-β1-induced protein expression of p-FAK (Figures 5J, K) and mRNA expression of *Integrin β1* and *Integrin β3* (Figure 5L) according to western blotting and qRT-PCR, respectively.

To fully assess the functional consequences of the p.R218C substitution, we transfected HEK293T cells as described earlier. Transwell-based migration assay showed that the constitutively active TGF-β1 variant of HEK293T cells migrated more substantially than WT (Supplementary Figures 2G, H), which was consistent with the results for pre-osteoclasts. The TGF-β1 variant in the patients enhances the well-defined TGF-β1 receptor-mediated Rho signaling pathway and augments cell migration mediated by this pathway.

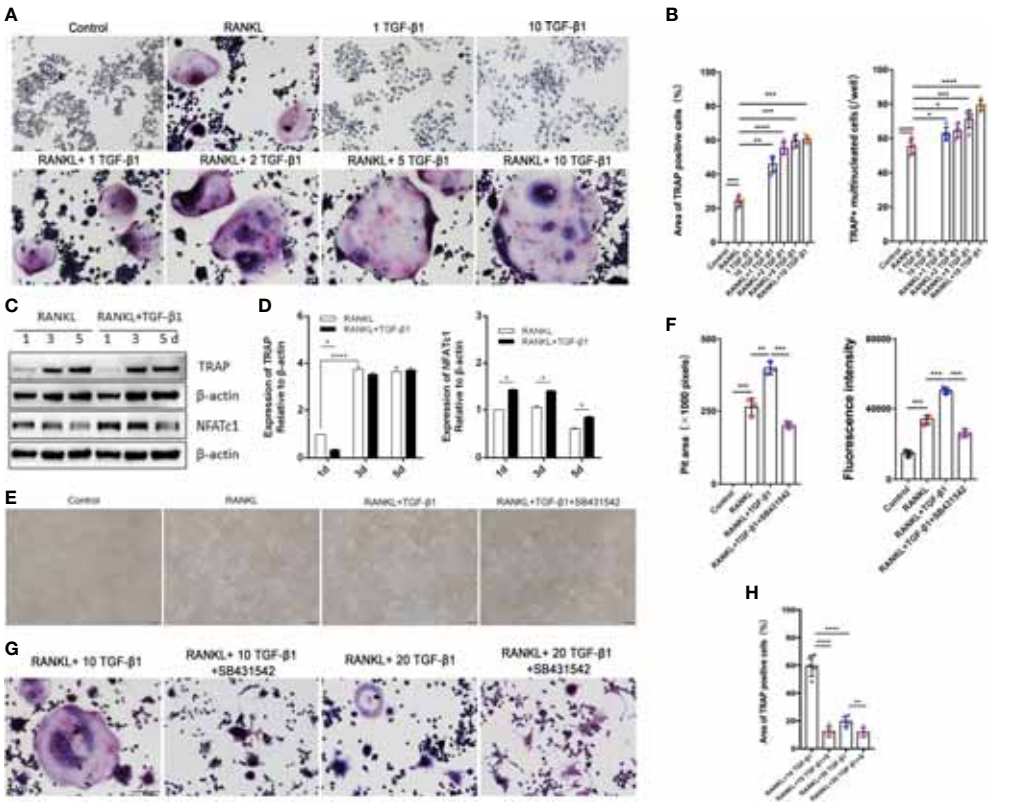

FIGURE 3
Effects of treatment of RAW264.7 cells with various concentrations of TGF-β1 for 1, 3, or 5 days in the presence or absence of RANKL. **(A)** Multinucleated cells cultured for 5 days were viewed by light microscopy and stained for TRAP. Bar: 100 μm. **(B)** The formation of multinucleated osteoclastic cells upon treatment with various concentrations of TGF-β1 was quantified by counting the number of TRAP-positive multinucleated cells and measuring the TRAP-positive cell area (n = 5). **(C, D)** Protein levels of TRAP and NFATc1 in cells cultured for 1, 3, or 5 days were determined by western blotting. **(E)** RAW264.7 cells were cultured on OsteoAssay plates for 5 days with RANKL and TGF-β1 in the presence or absence of SB431542. Resorption lacunae were visualized by bright-field microscopy. Bar: 100 μm. **(F)** Areas of resorption pits were measured. Data represent means ± SD (n = 3). **(G, H)** Cells were treated with RANKL and 10 or 20 ng/ml TGF-β1 in the presence or absence of SB431542 and then stained for TRAP. The TRAP-positive area was determined (n = 5). Bar: 100 μm. *$p < 0.05$; **$p < 0.01$; ***$p < 0.001$; ****$p < 0.0001$.

Rho GTPases mediate TGF-β1-induced migration of pre-osteoclasts through cytoskeletal remodeling

Actin dynamics are inextricably linked to osteoclast differentiation (19, 20). We hypothesized that Rho GTPases regulate pre-osteoclasts migration through the cytoskeleton reorganization. TGF-β1 significantly promoted the formation of intracellular F-actin and filopodia in RAW264.7 cells, and SB431542, Y27632, and NSC23766 inhibited this effect. Treatment with these inhibitors, especially the Rac1 inhibitor, increased the roundness of RAW264.7 cells. These cells had fewer filopodia and lamellipodia, which is likely not conducive to migration and fusion of pre-osteoclasts (Figures 6A, B). These findings were validated in RAW264.7 cells by scanning electron microscopy (Figure 6C). Then, using the previously described plasmids, we expressed the constitutively active TGF-β1 variant that promoted actin recombination in HEK293T cells, as revealed by pre-osteoclasts, but to a lesser extent in WT TGF-β1 (Figures 6D–F. Complete information is in Supplementary Figure 3A). Rho signaling mediated TGF-β1-induced pre-osteoclast migration through cytoskeletal remodeling, with Rac1, in particular, playing a more important role.

Rho GTPases are associated with cytoskeletal remodelling during TGF-β1-induced osteoclastogenesis

RAW264.7 cells showed increased cell-cell fusion and formed large multinucleated TRAP-positive osteoclasts during RANKL-induced differentiation. RANKL activation produced an actin ring in close proximity to osteoclasts. In addition, TGF-β1 promoted the formation of a larger actin ring and more

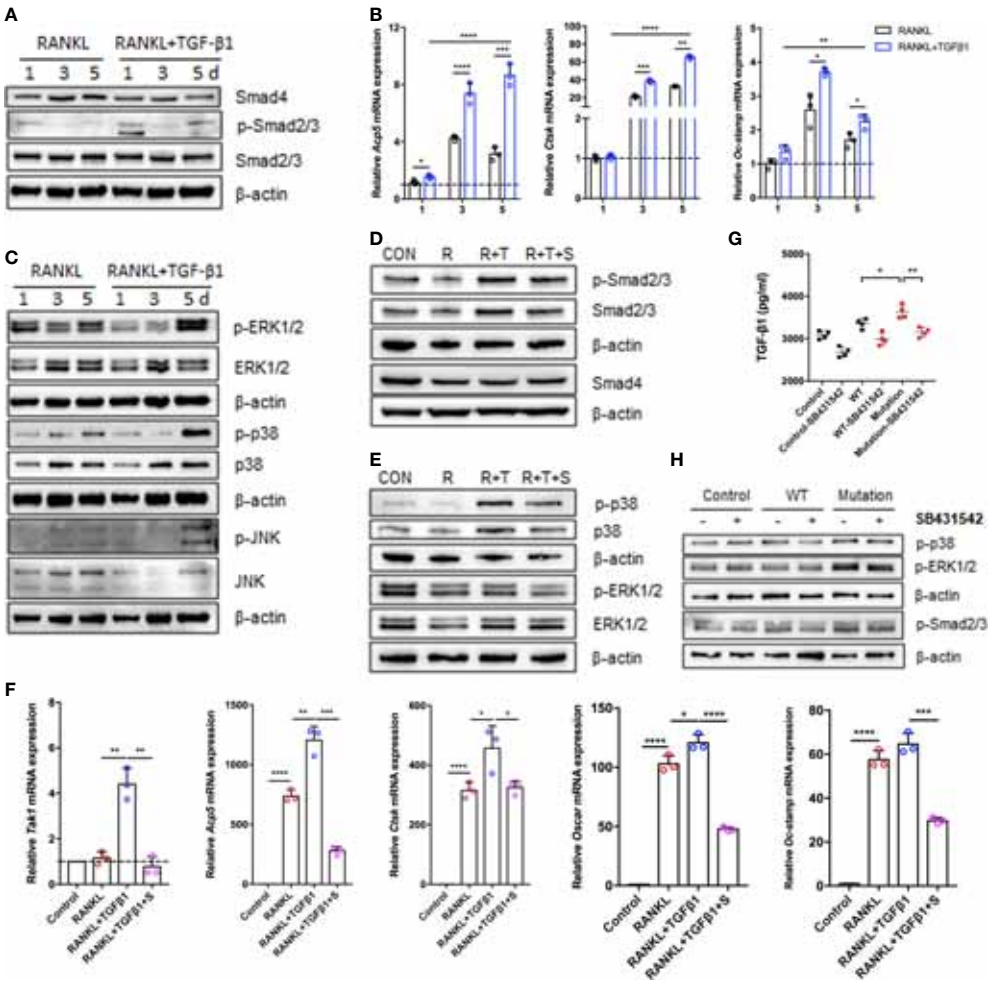

FIGURE 4
Expression of Smad and MAPK signaling pathway molecules during TGF-β1-induced osteoclastogenesis. **(A, C)** Protein levels of Smad2/3, p-Smad2/3, Smad4, ERK1/2, p-ERK1/2, p38, p-p38, JNK, and p-JNK were determined by western blotting in cells cultured with RANKL and TGF-β1 for 1, 3, or 5 days (n = 3). **(B)** Relative mRNA expression of *Acp5, Cstk*, and *Oc-stamp* was determined by qRT-PCR and normalized to that of *Gapdh* (n = 3). **(D, E)** RAW264.7 cells were cultured for 5 days with TGF-β1 and RANKL in the presence or absence of SB431542. Protein levels of Smad2/3, p-Smad2/3, Smad4, ERK1/2, p-ERK1/2, p38, and p-p38 were determined by western blotting. Representative blots are shown (n = 3). **(F)** Effects of SB431542 treatment on relative mRNA expression of *Acp5, Cstk, Oc-stamp, Oscar*, and *Tak1* were determined by qRT-PCR. These levels were normalized to that of *Gapdh* (n = 3). **(G)** HEK293T cells were transfected with the WT TGF-β1 or p.R218C mutant plasmid for 48 h. Cell supernatants were collected for an enzyme-linked immunosorbent assay (ELISA) of TGF-β1 levels (n = 4). **(H)** Western blotting of HEK293T cells transfected with the WT or mutant plasmid described above in the presence or absence of SB431542 was performed. Data represent means ± SD. *$p < 0.05$; **$p < 0.01$; ***$p < 0.001$; ****$p < 0.0001$.

abundant intracellular F-actin. Treatment with SB431542 led to osteoclasts forming smaller and contracted actin rings, while cells treated with Y27632 or NSC23766 lacked abundant F-actin in the cytoplasm, despite having larger actin rings (Figures 7A, B). Next, the formation of membrane folds and changes to filopodia and pseudopods were confirmed by scanning electron microscopy. The activation of TGF-β1 led to the formation of membrane ruffles and filopodia in mature osteoclasts—both actin-based structures are required for cell migration. Treatment with the aforementioned inhibitors, especially the Rac1 inhibitor, significantly reduced the formation of these structures (Figure 7C). TRAP staining of osteoclasts treated with these inhibitors yielded consistent results (Supplementary Figure 3B).

The TGF-β1 variant demonstrates a gain of function

Twelve TGF-β1 mutations that cause CED have been reported based on OMIM (https://omim.org/) data. These mutations are divided into three main categories according to

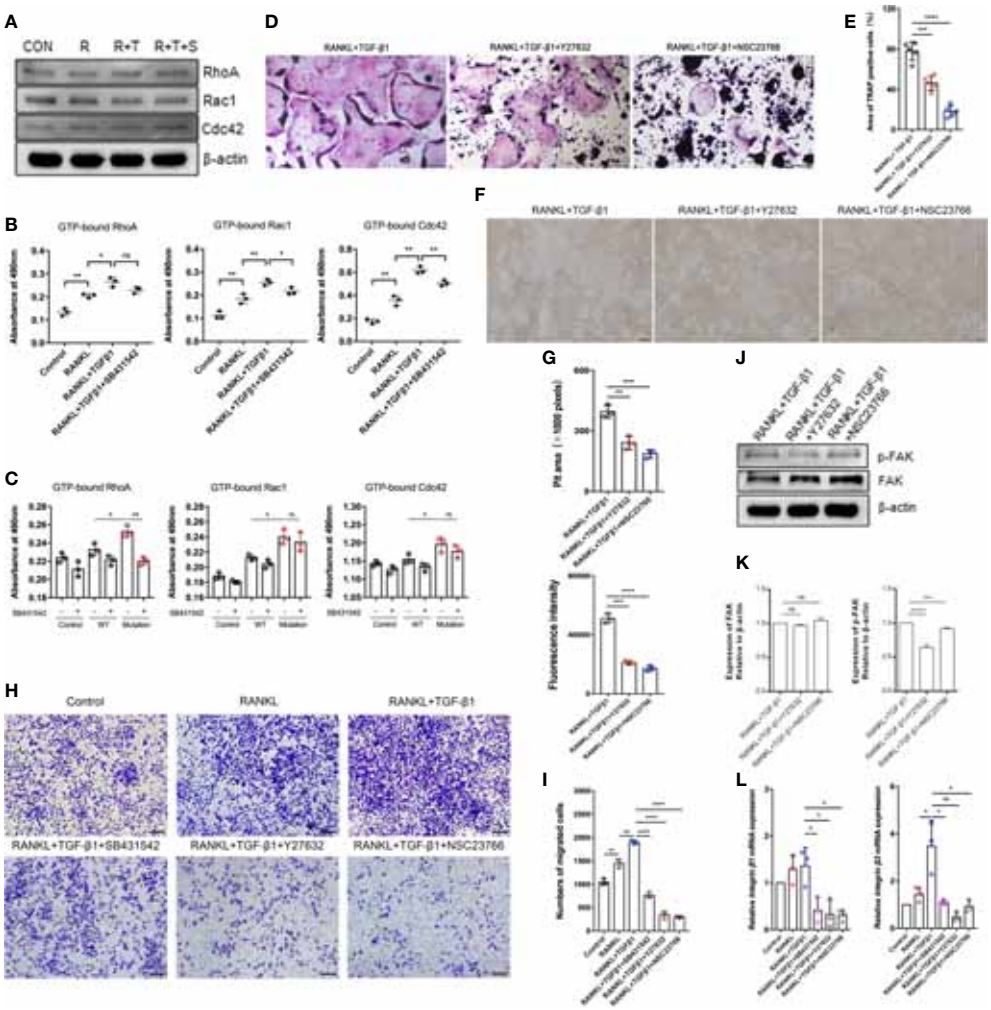

FIGURE 5
Effect of the Rho signaling pathway on TGF-β1-induced osteoclastogenesis. **(A)** RAW264.7 cells were cultured for 5 days with TGF-β1 and RANKL in the presence or absence of SB431542. Protein levels of total RhoA, Rac1, and Cdc42 were determined by western blotting. **(B)** The levels of GTP-bound RhoA, Rac1, and Cdc42 were detected by GLISAs (n = 3). **(C)** HEK293T cells were transfected with the WT TGF-β1 or p.R218C mutant plasmid for 48 h. Cell lysates were collected for GLISAs of GTP-bound RhoA, Rac1, and Cdc42 levels (n = 3). **(D, E)** Representative images of TRAP staining **(D)** (bar: 200 μm) and areas of TRAP-positive multinucleated (≥ 3 nuclei) RAW264.7 cells **(E)** after 5 days of culture. Cells were cultured with RANKL and TGF-β1 in the presence or absence of a Rho GTPase inhibitor (Y27632 or NSC23766) (n = 5). **(F, G)** RAW264.7 cells were cultured on OsteoAssay plates for 5 days with RANKL and TGF-β1 in the presence or absence of a Rho GTPase inhibitor (Y27632 or NSC23766). Resorption lacunae were visualized by bright-field microscopy (n = 3). Bar: 100 μm. **(H, I)** Representative images of Raw264.7 cells (stained with crystal violet) on the lower surface of a Transwell membrane **(H)** and quantitative analysis of cell migration by cell counting **(I)** after 2 days of culture. Cells were cultured alone (control), with RANKL, with RANKL plus TGF-β1, or with RANKL plus TGF-β1 plus an inhibitor (SB431542, Y27632, or NSC23766) (n = 3). Bar: 100 μm. **(J, K)** Protein levels of FAK and p-FAK were determined by western blotting, and the gray values were statistically analyzed. **(L)** the mRNA levels of *Integrin β1* and *Integrin β3* were determined by quantitative RT-PCR in RAW264.7 cells cultured for 5 days (n = 3). Data represent means ± SD. *$p < 0.05$; **$p < 0.01$; ***$p < 0.001$; ****$p < 0.0001$; *ns: no significance*.

the effect on the protein, namely, mutations located in exon 1, including leucine insertion in the signal peptide region (p.L10_L12dup and p.L10_L13dup) and a missense mutation at the N-terminus of LAP (p.Y81H) (21); mutations located in exon 2 including two missense mutations at the N-terminus of LAP (p.R156C and p.E169K) (22); and mutations located in exon 4, i.e., C-terminal missense mutations of LAP (p.R218C, p.R218H, p.H222D, p.C223R, p.C223S, p.C223G, and p.C225R) (23) (Figures 8A, B). All pathogenic mutations eventually increase the proportion of TGF-β1 in the circulation and bone, causing bone hyperplasia, accelerated bone turnover, inhibition of normal bone mineralization and decreased bone density. The mutation (p.R218C) reported here accounts for more than 60% of all mutations and is considered a hotspot mutation for CED (24). Given that TGF-β1 mutants are involved in the initiation of CED, we assessed the evolutionary

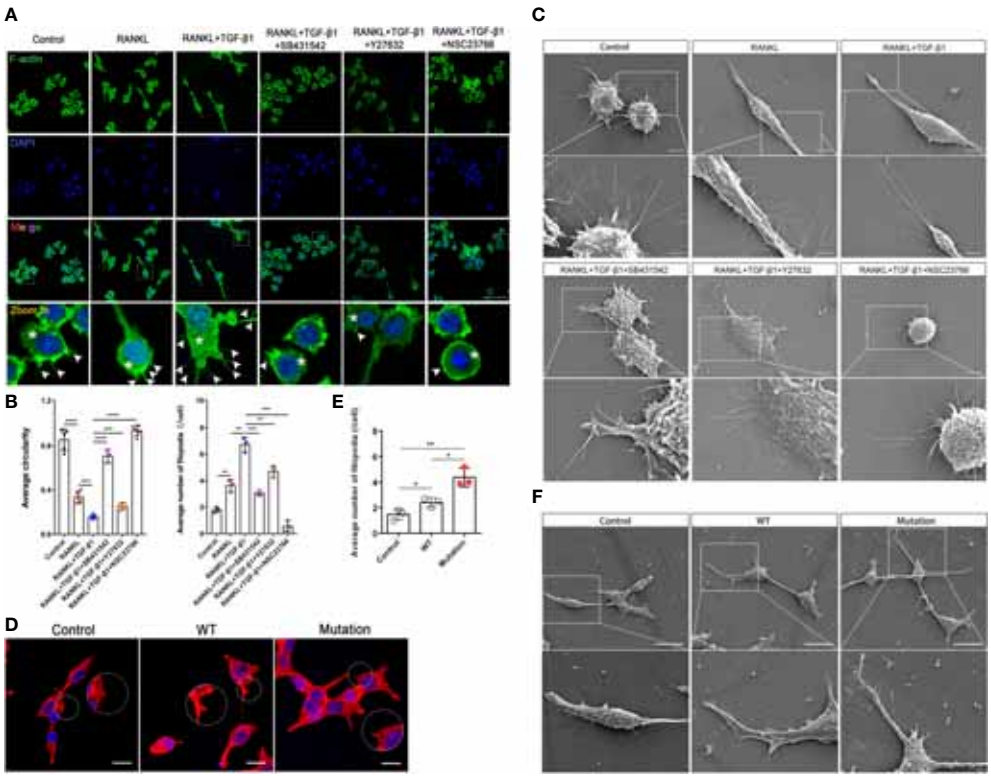

FIGURE 6
Inhibition of Rho GTPases suppresses migration of RAW264.7 cells by disrupting the actin cytoskeleton. **(A)** RAW264.7 cells were pretreated with an inhibitor (SB431542, Y27632, or NSC23766) for 24 h, treated with RANKL plus TGF-β1 for 10 min, fixed, permeabilized, and stained with phalloidin to visualize F-actin. TGF-β1-treated cells had well-defined intracellular F-actin (white asterisks) and filopodia (white arrows). Cells treated with inhibitors had less intracellular F-actin and fine aggregates of F-actin. The inhibitors caused marked morphological changes and reduced cell size, especially during treatment with NSC23766, following which cells contained little intracellular F-actin and tended to be round. **(B)** Formation of filopodia and average roundness of the different groups of cells in A (n = 3). Data represent means ± SD. $^{**}p < 0.01$; $^{***}p < 0.001$; $^{****}p < 0.0001$. **(C)** Scanning electron microscopy showed that the inhibitors suppressed the formation of filopodia and membrane ruffles. Images (2000× and 7000× magnification) were captured using a Hitachi S-4800 FEG scanning electron microscope. NSC23766 treatment disrupted the actin cytoskeleton and caused shrinkage of RAW264.7 cells. Bar: 5 μm (2000×), 2 μm (7000×). **(D, E)** HEK293T cells were cultured for 16 h, transfected with different plasmids for 48 h, fixed, permeabilized, and stained with phalloidin to visualize F-actin. Cells transfected with the mutant plasmid had well-defined intracellular F-actin and more filopodia. Bar: 50 μm. **(F)** HEK293T cells were cultured for 16 h and transfected with different plasmids for 48 h, and then pseudopod expression was analyzed using scanning electron microscopy. Bar: 20 μm (1500×).

conservation of the mutant acid interface. From the ConSurf server results, it was found that, all the reported pathogenic TGF-β1 variants were located in highly conserved regions, signifying that they have a critical role (Figure 8C). For R218, none of the missense amino acids were reported in the TGF-β1 homologs (Supplementary Figure 4).

To determine the functional consequences of the TGF-β1 mutation in patients regarding Rho GTPases, we examined their activation. The GTP-bound Rho GTPases were higher in PBMCs from CED patients than in healthy adults (Figure 8D). Likewise, the mRNA of *TAK1*, *Integrin β1*, and *Integrin β2* were augmented in the peripheral blood of the CED patients (Figure 8E). These data indicated that the TGF-β1 R218C variant induces actin remodeling by activating downstream signals. This variant led to constitutive Rho GTPases activation, consistent with the effects in osteoclasts and HEK293T cells.

We propose that in pathological conditions resulting from a gain-of-function mutation of TGF-β1 [p.Arg218Cys], well-defined TGF-β1 receptor-mediated Rho signaling in precursor cells is hyperactivated, leading to cytoskeletal remodeling. These actin-based activities lead to increased migration of precursor cells that more readily aggregate and fuse into large osteoclasts to perform their functions, leading to excessive bone resorption and disturbances in bone coupling (Figure 8F).

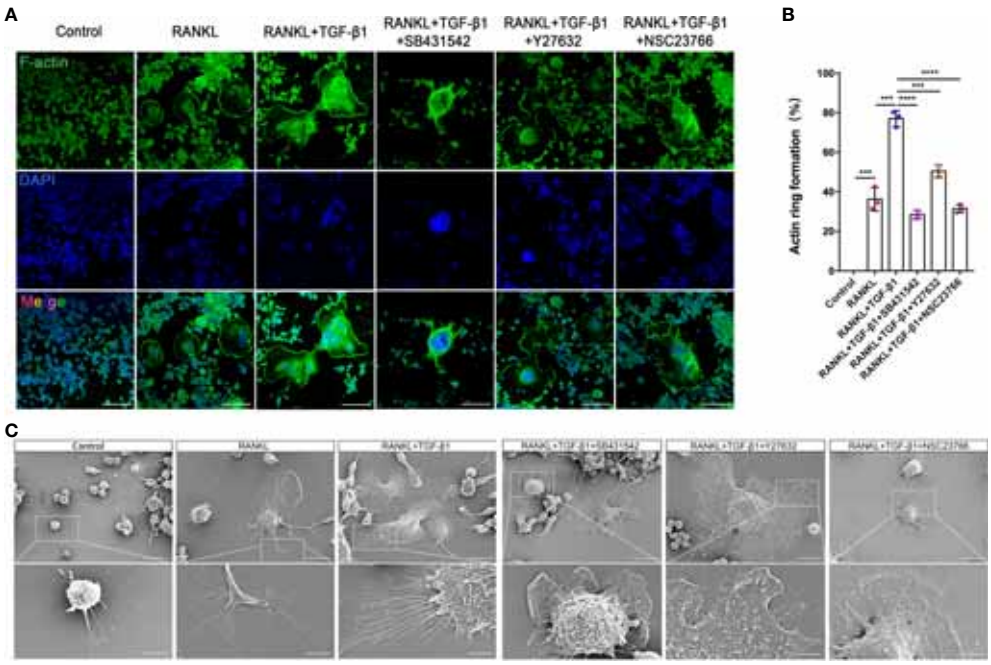

FIGURE 7
Inhibition of Rho GTPases suppresses the formation of osteoclasts from RAW264.7 cells by disrupting the actin cytoskeleton. **(A)** Actin (green) and nuclei (blue) were stained in osteoclasts cultured with RANKL, RANKL plus TGF-β1, or RANKL plus TGF-β1 plus an inhibitor (SB431542, Y27632, or NSC23766). Bar: 100 μm. **(B)** The percentage of osteoclasts with closed actin rings at the cell periphery (n = 3). Data represent means ± SD. ***$p < 0.001$; ****$p < 0.0001$. **(C)** Scanning electron microscopy demonstrated that the inhibitors suppressed the formation of filopodia and membrane ruffles. Images (1000× and 3000× magnification) were captured using a Hitachi S-4800 FEG scanning electron microscope. Treatment with SB431542 or NSC23766 disrupted the actin cytoskeleton and inhibited the formation of larger osteoclasts from RAW264.7 cells. Bar: 20 μm (1000×), 5 μm (3000×).

Discussion

In this study, we described two patients with CED, usually characterized by pain at the extremities, gait disturbances, fatigue, muscle weakness, headaches, ophthalmopathy, and otological symptoms (25, 26). Our patients had these symptoms, although the incidence of hearing disturbances in CED is only 18% (5). Mutations of TGF-β1 are the genetic cause of CED (27); thus the diagnosis was performed by genetic testing of TGF-β1 in our patients. Both patients were heterozygous for c.652C > T [p.Arg218Cys] in the TGF-β1 gene. Furthermore, patient 1 exhibited left ventricular dilatation and decreased cardiac function, which were rarely reported previously. The TGF-β1 gene polymorphisms might predispose individuals to heart conditions, and several cardiomyopathies are associated with elevated TGF-β1 (28, 29). The aforementioned reports led to speculation that the predisposition might be related to aberrant activation of TGF-β1 caused by the TGF-β1 mutation in CED patients.

Twelve TGF-β1 mutations that cause CED have been identified based on OMIM (https://omim.org/), which might lead to an increased expression of pro-inflammatory cytokines (30). Studies of the influences of TGF-β1 on osteoblasts and osteoclasts have yielded contradictory effects (31); however, our study suggests that TGF-β1 maintains a biphasic effect on the differentiation of osteoclasts. Specifically, osteoclast differentiation is enhanced by low TGF-β1 and inhibited by high TGF-β1, consistent with a previous report (32). This highlights the influences of TGF-β1 on bone biology. More importantly, the latent TGF-β1 level was 68–75 ng/ml in peripheral blood cells, which was more than two times higher than that in normal controls (~30 ng/ml). In a previous study, PBMCs from CED patients contributed to the formation of more osteoclasts than healthy controls in the presence of a range of RANKL concentrations (2). We described that treatment with 10 ng/ml TGF-β1 increased the formation of osteoclasts from RAW264.7 cells substantially, but RAW264.7 cells did not form osteoclasts in the absence of RANKL, indicating that TGF-β1 cannot replace RANKL for the stimulation of osteoclast differentiation and function.

It has been reported that HEK293T cells transfected with p.R218C exhibit activated Smad signaling and secrete an increased amount of active TGF-β1 into the culture medium (21). Our observations complement the results of this previous

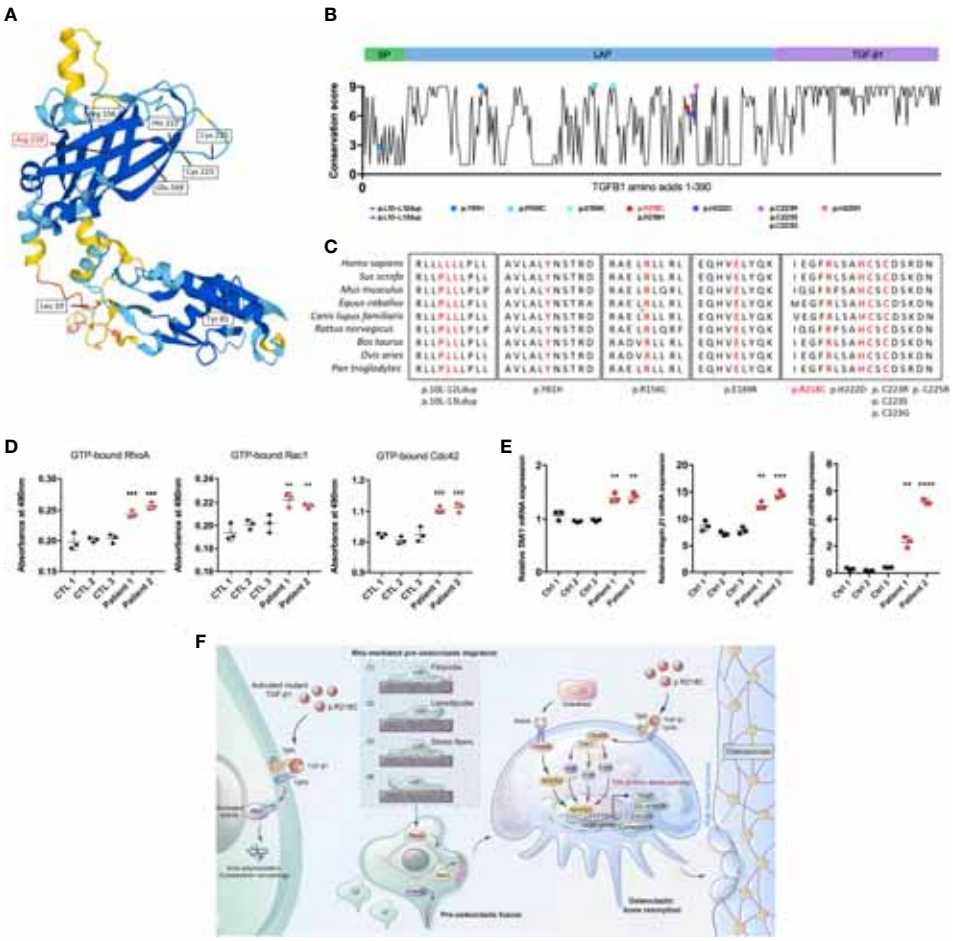

FIGURE 8
TGF-β1 variants in CED demonstrate a gain of function. **(A)** Structural model of WT human TGF-β1, highlighting the sites of TGF-β1 gain-of-function variants. **(B)** A graphical illustration of TGF-β1 sequence conservation (black line) based on the ConSurf conservation score (see Methods). The TGF-β1 domain structure and positions of the variants identified in patients are indicated, including those reported in this study (red symbols). **(C)** Multiple species alignment of TGF-β1 protein sequences at all the mutant amino acid positions reported in CED patients. Amino acids p.L10, p.L11, p.L12, p.L13, p.Y81, p.R156, p.E169, p.R218, p.H222, p.C223, and p.C225 of TGF-β1 all show species conservation. Red indicates the mutation site in the patients in this study. The red label is the variant we reported. **(D)** Levels of GTP-bound RhoA, Rac1, and Cdc42 in PBMCs from patients 1 and 2 were determined by GLISAs. **(E)** mRNA expression of *Integrin β1*, *Integrin β3*, and *TAK1* in PBMCs from patients 1 and 2 was determined by qRT-PCR (n = 3). Data represent means ± SD. $^{**}p < 0.01$; $^{***}p < 0.001$; $^{****}p < 0.0001$. **(F)** TGF-β1 variants in CED patients lead to increased Rho GTPase activity through aberrant activation, resulting in Rho GTPase-mediated remodeling of the cytoskeleton: (1) sensing of the motogenic signal by filopodia, (2) formation and protrusion of lamellipodia and pseudopodia-like forward extension, (3) attachment of protrusions to the extracellular matrix, (4) F-actin-mediated contraction of the cell body to allow forward progress, and rear release. It promotes pre-osteoclast migration, fusion, osteoclast formation, and bone resorption, ultimately leading to osteoporosis.

study. We found that not only TGF-β1/Smad signaling, but also TGF-β1/non-Smad signaling, was activated in HEK293T cells transfected with the mutant plasmid and osteoclasts induced with exogenous TGF-β1, including MAPK and Rho GTPase signaling. Rho GTPases are regulators of cytoskeletal organization (33). Here, we reported that active Rho GTPases are higher in the peripheral blood of CED patients than in that of healthy controls. Consistent results were obtained with transfected HEK293T cells with a mutant plasmid. Furthermore, the levels of active Rho GTPases and mRNA expression of *Rock1* and *Rock2* were augmented in osteoclasts treated with TGF-β1. The TGF-β1 R218C mutation in CED patients presumably activates the Rho signaling pathway.

Small GTPases and ROCKs participate in cytoskeletal reorganization and differentiation toward osteogenic cells (15). These findings support the idea that RhoA/ROCK are indispensable for skeletal metabolism. We confirmed that the TGF-β1 receptor inhibitor SB431542 inhibited the activation of Rho GTPases in RAW264.7 cell-induced osteoclasts and HEK293T cells, while Rho GTPase inhibitors, including Y27632 and NSC23766, significantly reduced bone effects induced by TGF-β1. In addition, the mRNA levels of the cell

migration-related molecules *Integrin β1* and *Integrin β3* were increased in the peripheral blood of CED patients. Our study further confirmed the promoting role of Rho signaling in TGF-β1-mediated osteoclastogenesis.

Excessive bone degradation by osteoclasts leads to characteristic diseases such as CED; however, how Rho GTPases are regulated by TGF-β1 in osteoclast formation remains elusive. Osteoclasts use podosomes, structures composed of F-actin and integrins, to attach to bone surfaces. The binding of integrins to ligands promote osteoclast adhesion, migration and bone resorption (34, 35). We found that TGF-β1 promoted cytoskeletal remodeling in precursor and mature osteoclasts, as manifested by an increased number of filopodia and abundant intracellular F-actin, and SB431542, Y27632, and NSC23766 partially inhibit this phenomenon. Active osteoclasts form a stable actin ring (36), and our results confirmed that TGF-β1 contributes to its formation. However, results with Rho inhibitors indicated an abolishment of the proper actin cytoskeletal network.

Meanwhile, increased migration of precursor cells, elevated expression of osteoclast-related molecules (ACP5, OSCAR, TRAP, OC-STAMP, and Ctsk), and increased bone resorption pits revealed the increased formation of mature osteoclasts. HEK293T cells transfected with the TGF-β1 mutant plasmid also exhibited changes to their cytoskeleton and migration. Therefore, we propose that the pathogenic mechanism underlying CED involves the acceleration of osteoclastogenesis and bone resorption by TGF-β1 through Rho GTPase-mediated cell migration and cytoskeletal remodeling, resulting in accelerated bone turnover, decreased bone density and osteoporosis.

There is no definitive treatment for CED. The most common treatments are corticosteroids, nonsteroidal anti-inflammatory drugs (NSAIDs) and bisphosphonates to reduce limb pain. Corticosteroids may counteract the increased activity of TGF-β1 and relieve some symptoms (37); however, they can also cause a reduction in bone density and inhibition of TGF-β1-induced transcription (38). The administration of NSAIDs does not usually elicit an efficient response (39), and the use of bisphosphonates is also disputed (37, 40). Losartan has recently been used to treat patients with CED; however, there were some limitations in terms of safety and efficacy (5, 38). In addition to CED, enhanced TGF-β1 has been documented in several connective tissue disorders (8, 41–43). It might be crucial to attenuate the effects of TGF-β1 signaling for these disorders.

In the future, a treatment approach that modulates the TGF-β1 signaling pathway might be effective in patients with CED (5). In a recent study, the inhibition of RhoA/ROCK prevented aging-associated bone loss (44). Similarly, our findings raise the possibility of a treatment for diseases in which TGF-β1 is abnormally activated, including CED. Moreover, the inhibition of Rho GTPases rescues the imbalance in bone coupling and excessive bone resorption.

In summary, we provided new clues for the pathogenesis of CED, highlighting the role of Rho GTPases in osteoclast differentiation and function and proposing their potential as targets for treating osteoporosis pathology. It is important to explore how the activation of TGF-β1/Rho GTPases leads to more specific manifestations of CED and whether inhibition of Rho GTPases improves therapeutic effects using animal models. Our new understanding of how the TGF-β1 mutation-triggered overactivation of Rho GTPases in CED leads to high bone turnover will help address the specific mechanisms of decreased bone density or osteoporosis due to aberrant TGF-β1 signaling in related diseases and inform the development of new therapeutic approaches.

Data availability statement

The original contributions presented in the study are publicly available. This data can be found here: GenBank, 2631956.

Ethics statement

The studies involving human participants were reviewed and approved by The Ethics Committee of Air Force Medical University. The patients/participants provided their written informed consent to participate in this study. Written informed consent was obtained from the individual(s) for the publication of any potentially identifiable images or data included in this article.

Author contributions

YuW initiated the project and discovered the genetic variant. QC contributed to the idealization of the project, experimental design, data curation and collection, drafting the manuscript and statistical analysis. YY contributed to cell experiments and data analysis, KC contributed to the idealization and administration of the project and editing of the manuscript. XC contributed to clinical data and editing of the manuscript. BL and RL contributed to the methodology, collection of data and structural analysis. LM, WH, MZ, and ZW contributed to manuscript writing. YW, YuW, and FL contributed to the research concept, idealization of the project and drafting the manuscript. All authors approved the current version of the study.

Funding

This study was supported by grant/award in Shaanxi (Grant/Award Number: 2019SF-059 and 2020SF-204), the Key Innovative Project in Shaanxi (Grant/Award Number:

2021ZDLSF02-02) and the National Natural Science Foundation of China (Grant/Award Number: 81671476 and 31570906).

Acknowledgments

We thank all study participants and their family for their contribution to the study. I (FL) want to thank my newborn son (Chufan Chen) for his great support.

Conflict of interest

The authors declare that the research was conducted in the absence of any commercial or financial relationships that could be construed as a potential conflict of interest.

Publisher's note

Supplementary material

The Supplementary Material for this article can be found online at: https://www.frontiersin.org/articles/10.3389/fendo.2022.913979/full#supplementary-material

References

1. Tang Y, Wu X, Lei W, Pang L, Wan C, Shi Z, et al. Tgf-β1–induced migration of bone mesenchymal stem cells couples bone resorption with formation. *Nat Med* (2009) 15(7):757–65. doi: 10.1038/nm.1979

2. McGowan NWA, MacPherson H, Janssens K, Van Hul W, Frith JC, Fraser WD, et al. A mutation affecting the latency-associated peptide of Tgfβ1 in camurati-engelmann disease enhances osteoclast formation *in vitro*. *J Clin Endocrinol Metab* (2003) 88(7):3321–6. doi: 10.1210/jc.2002-020564

3. Janssens K G-BR, Guañabens N, Migone N, Ralston S, Bonduelle M, Lissens W, et al. Mutations in the gene encoding the latency-associated peptide of tgf-β1 cause camurati-engelmann disease. *Nat Genet* (2000) 26(3):273–5. doi: 10.1038/81563

4. Iqbal J, Sun L, Zaidi M. Coupling bone degradation to formation. *Nat Med* (2009) 15(7):729–31. doi: 10.1038/nm0709-729

5. Kim Y-M, Kang E, Choi J-H, Kim G-H, Yoo H-W, Lee BH. Clinical characteristics and treatment outcomes in camurati–engelmann disease. *Medicine* (2018) 97(14):e0309. doi: 10.1097/md.0000000000010309

6. Crane JL, Cao X. Bone marrow mesenchymal stem cells and tgf-β signaling in bone remodeling. *J Clin Invest* (2014) 124(2):466–72. doi: 10.1172/jci70050

7. Dallas SL, Rosser JL, Mundy GR, Bonewald LF. Proteolysis of latent transforming growth factor-β (Tgf-β)-Binding protein-1 by osteoclasts. *J Biol Chem* (2002) 277(24):21352–60. doi: 10.1074/jbc.M111663200

8. Satoki Ichimura SS, Murata T, Fukumura R, Gondo Y, Ikegawa S, Furuichi T. An enu-induced P.C225s missense mutation in the mouse Tgfb1 gene does not cause camurati-engelmann disease-like skeletal phenotypes. *Exp Anim* (2017) 66 (2):137–44. doi: 10.1538/expanim.16-0085

9. Wang Y, Lei R, Zhuang X, Zhang N, Pan H, Li G, et al. Dlc1-dependent parathyroid hormone–like hormone inhibition suppresses breast cancer bone metastasis. *J Clin Invest* (2014) 124(4):1646–59. doi: 10.1172/jci71812

10. Fabregat I, Caballero-Díaz D. Transforming growth factor-β-Induced cell plasticity in liver fibrosis and hepatocarcinogenesis. *Front Oncol* (2018) 8:357. doi: 10.3389/fonc.2018.00357

11. Pardali E, Goumans M-J, ten Dijke P. Signaling by members of the tgf-β family in vascular morphogenesis and disease. *Trends Cell Biol* (2010) 20(9):556–67. doi: 10.1016/j.tcb.2010.06.006

12. Mu Y, Gudey SK, Landström M. Non-smad signaling pathways. *Cell Tissue Res* (2011) 347(1):11–20. doi: 10.1007/s00441-011-1201-y

13. Tu S, Huang W, Huang C, Luo Z, Yan X. Contextual regulation of tgf-β signaling in liver cancer. *Cells* (2019) 8(10):1235. doi: 10.3390/cells8101235

14. Jeong KJ, Park SY, Cho KH, Sohn JS, Lee J, Kim YK, et al. The Rho/Rock pathway for lysophosphatidic acid-induced proteolytic enzyme expression and ovarian cancer cell invasion. *Oncogene* (2012) 31(39):4279–89. doi: 10.1038/onc.2011.595

15. Strzelecka-Kiliszek A, Mebarek S, Roszkowska M, Buchet R, Magne D, Pikula S. Functions of rho family of small gtpases and rho-associated coiled-coil kinases in bone cells during differentiation and mineralization. *Biochim Biophys Acta (BBA) - Gen Subj* (2017) 1861(5):1009–23. doi: 10.1016/j.bbagen.2017.02.005

16. Das A, Wang X, Kang J, Coulter A, Shetty AC, Bachu M, et al. Monocyte subsets with high osteoclastogenic potential and their epigenetic regulation orchestrated by Irf8. *J Bone Mineral Res* (2020) 36(1):199–214. doi: 10.1002/jbmr.4165

17. Wang L, Aschenbrenner D, Zeng Z, Cao X, Mayr D, Mehta M, et al. Gain-of-Function variants in syk cause immune dysregulation and systemic inflammation in humans and mice. *Nat Genet* (2021) 53(4):500–10. doi: 10.1038/s41588-021-00803-4

18. Mandage R, Kamath P, Wakle M, Momin A. Discovery of β-lactam antibiotic resistance specific functional residues: a bioinformatics approach. *Electron J Biol* (2012) 8(1):15–8.

19. Wang G, Beier F. Rac1/Cdc42 and rhoa gtpases antagonistically regulate chondrocyte proliferation, hypertrophy, and apoptosis. *J Bone Mineral Res* (2005) 20(6):1022–31. doi: 10.1359/jbmr.050113

20. Goggs R, Williams Christopher M, Mellor H, Poole Alastair W. Platelet rho gtpases–a focus on novel players, roles and relationships. *Biochem J* (2015) 466 (3):431–42. doi: 10.1042/bj20141404

21. Janssens K, ten Dijke P, Ralston SH, Bergmann C, Van Hul W. Transforming growth factor-β1 mutations in camurati-engelmann disease lead to increased signaling by altering either activation or secretion of the mutant protein. *J Biol Chem* (2003) 278(9):7718–24. doi: 10.1074/jbc.M208857200

22. Wu S, Liang S, Yan Y, Wang Y, Li F, Deng Y, et al. A novel mutation of Tgfβ1 in a Chinese family with camurati–engelmann disease. *Bone* (2007) 40 (6):1630–4. doi: 10.1016/j.bone.2007.02.025

23. Walton KL, Makanji Y, Chen J, Wilce MC, Chan KL, Robertson DM, et al. Two distinct regions of latency-associated peptide coordinate stability of the latent transforming growth factor-β1 complex. *J Biol Chem* (2010) 285(22):17029–37. doi: 10.1074/jbc.M110.110288

24. Campos-Xavier A, Saraiva JM, Savarirayan R, Verloes A, Feingold J, Faivre L, et al. Phenotypic variability at the tgf-β1 locus in camurati-engelmann disease. *Hum Genet* (2001) 109(6):653–8. doi: 10.1007/s00439-001-0644-8

25. Janssens K. Camurati-engelmann disease: Review of the clinical, radiological, and molecular data of 24 families and implications for diagnosis and treatment. *J Med Genet* (2005) 43(1):1–11. doi: 10.1136/jmg.2005.033522

26. Carlson ML BC, Neff BA, Link MJ, Driscoll CL. Skull base manifestations of camurati-engelmann disease. *Arch Otolaryngol Head Neck Surg* (2010) 136(6):566–75. doi: 10.1001/archoto.2010.68

27. Kinoshita TS A, Tomita H, Makita Y, Yoshida K, Ghadami M, Yamada K, et al. Domain-specific mutations in Tgfb1 result in camurati-engelmann disease. *Nat Genet* (2000) 26(1):19–20. doi: 10.1038/79128

28. Tania C, Araujo-Jorge MCW, Alejandro M, Hasslocher-Moreno, Seírgio S, Xavier, et al. Implication of transforming growth factor–B1 in chagas disease myocardiopathy. *J Infect Dis* (2002) 186:1823–8. doi: 10.1086/345882

29. Khan R, Sheppard R. Fibrosis in heart disease: Understanding the role of transforming growth factor-Beta1 in cardiomyopathy, valvular disease and

arrhythmia. *Immunology* (2006) 118(1):10–24. doi: 10.1111/j.1365-2567.2006.02336.x

30. Chen Y, Xie W, Hu F, Chen J, Zheng H, Zhou H, et al. Clinical diagnosis and mutation analysis of a Chinese family with camurati-engelmann disease. *Mol Med Rep* (2017) 15(1):235–9. doi: 10.3892/mmr.2016.6024

31. Van Hul W, Janssens S, ten Dijke P, Janssens K. Transforming growth factor-β1 to the bone. *Endocr Rev* (2005) 26(6):743–74. doi: 10.1210/er.2004-0001

32. Oursler MJ, Khosla S, Westendorf JJ, Pederson L, Ruan M, Quint P, et al. Tgf-β induces Wnt10b in osteoclasts from female mice to enhance coupling to osteoblasts. *Endocrinology* (2013) 154(10):3745–52. doi: 10.1210/en.2013-1272

33. Shao J-S, Cai J, Towler DA. Molecular mechanisms of vascular calcification. *Arterioscler Thromb Vasc Biol* (2006) 26(7):1423–30. doi: 10.1161/01.atv.0000220441.42041.20

34. Freídeíric Saltel OD, Bard Fídeíric, Eichert D, Jurdic P. Apatite-mediated actin dynamics in resorbing osteoclasts. *Mol Biol Cell* (2004) 15(12):5231–41. doi: 10.1091/mbc.E04

35. Kim J-M, Kim MY, Lee K, Jeong D. Distinctive and selective route of Pi3k/Pkcα-Pkcδ/Rhoa-Rac1 signaling in osteoclastic cell migration. *Mol Cell Endocrinol* (2016) 437:261–7. doi: 10.1016/j.mce.2016.08.042

36. Faccio R, Novack DV, Zallone A, Ross FP, Teitelbaum SL. Dynamic changes in the osteoclast cytoskeleton in response to growth factors and cell attachment are controlled by β3 integrin. *J Cell Biol* (2003) 162(3):499–509. doi: 10.1083/jcb.200212082

37. Combier A, Palazzo E, Forien M, Gardette A, Dieudé P, Ottaviani S. Failure of conventional treatment and losartan in camurati-engelmann disease: A case report. *Joint Bone Spine* (2018) 85(5):649–50. doi: 10.1016/j.jbspin.2018.01.015

38. Simsek-Kiper PO, Dikoglu E, Campos-Xavier B, Utine GE, Bonafe L, Unger S, et al. Positive effects of an angiotensin ii type 1 receptor antagonist in camurati-engelmann disease: A single case observation. *Am J Med Genet Part A* (2014) 164 (10):2667–71. doi: 10.1002/ajmg.a.36692

39. Castro GRW, Appenzeller S, Marques-Neto JF, Bértolo MB, Samara AM, Coimbra I. Camurati-engelmann disease: Failure of response to bisphosphonates: Report of two cases. *Clin Rheumatol* (2005) 24(4):398–401. doi: 10.1007/s10067-004-1056-7

40. Iba K, Takada J, Kamasaki H, Oda T, Hatakeyama N, Wada T, et al. A significant improvement in lower limb pain after treatment with alendronate in two cases of camurati–engelmann disease. *J Bone Mineral Metab* (2008) 26(1):107–9. doi: 10.1007/s00774-007-0783-7

41. Verstraeten A, Alaerts M, Van Laer L, Loeys B. Marfan syndrome and related disorders: 25 years of gene discovery. *Hum Mutat* (2016) 37(6):524–31. doi: 10.1002/humu.22977

42. Gori I, George R, Purkiss AG, Strohbuecker S, Randall RA, Ogrodowicz R, et al. Mutations in ski in shprintzen–Goldberg syndrome lead to attenuated tgf-β responses through ski stabilization. *eLife* (2021) 10. doi: 10.7554/eLife.63545

43. Almpani K, Liberton DK, Jani P, Keyvanfar C, Mishra R, Curry N, et al. Loeys-Dietz and shprintzen-Goldberg syndromes: Analysis of tgf-β-Opathies with craniofacial manifestations using an innovative multimodality method. *J Med Genet* (2021), jmedgenet–2021-107695. doi: 10.1136/jmedgenet-2021-107695

44. Shi W, Xu C, Gong Y, Wang J, Ren Q, Yan Z, et al. Rhoa/Rock activation represents a new mechanism for inactivating Wnt/β-catenin signaling in the aging-associated bone loss. *Cell Regen* (2021) 10(1). doi: 10.1186/s13619-020-00071-3

Frontiers in Endocrinology

Explores the endocrine system to find new therapies for key health issues

The second most-cited endocrinology and metabolism journal, which advances our understanding of the endocrine system. It uncovers new therapies for prevalent health issues such as obesity, diabetes, reproduction, and aging.

Discover the latest Research Topics

See more →

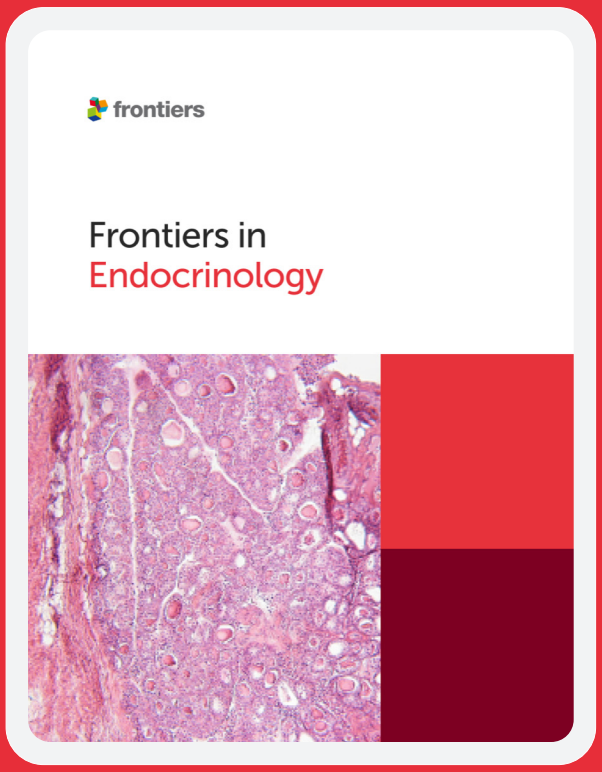

Frontiers

Avenue du Tribunal-Fédéral 34
1005 Lausanne, Switzerland
frontiersin.org

Contact us

+41 (0)21 510 17 00
frontiersin.org/about/contact